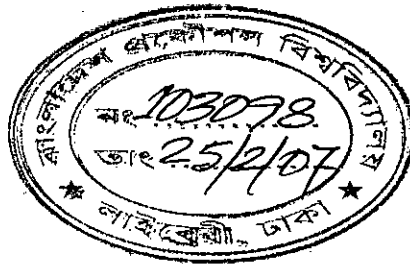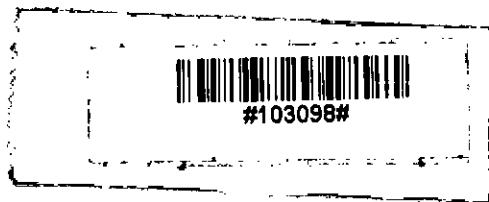**Effect of Sonic Vibration on Vapour Deposited Coating**

by

Syed Md. Ihsanul Karim

DOCTOR OF PHILOSOPHY

Mechanical Engineering

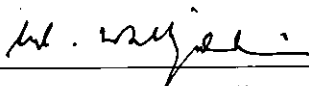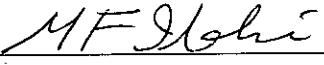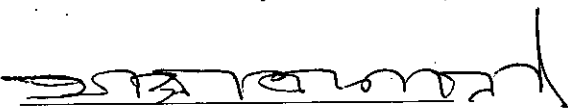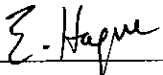BANGLADESH UNIVERSITY OF ENGINEERING AND TECHNOLOGY

2006

The thesis titled "Effect of Sonic Vibration on Vapour Deposited Coating" Submitted by Syed Md. Ihsanul Karim Roll No: 001/10/98F Session: 1995-96-97 has been accepted as satisfactory in partial fulfillment of the requirements for the degree of Doctor of Philosophy in Mechanical Engineering.

BOARD OF EXAMINERS

1. _____

Dr. Md. Maksud Helali
Professor and Head
Department of ME, BUET, Dhaka
(Supervisor)

Chairman

2. _____

Dr. Md. Wahhaj Uddin
Professor (Retired)
Department of ME, BUET, Dhaka

Member

3. _____

Prof. Dr. Md. Fazli Ilahi
Vice-Chancellor
Islamic University of Technology

Member

4. _____

Dr. A.S.W. Kurny
Professor
Department of MME, BUET, Dhaka

Member

5. _____

Dr. M. A. Taher Ali
Professor
Department of ME, BUET, Dhaka

Member

6. _____

Prof. Dr. Ehsanul Haque
Member
University Grants Commission of Bangladesh, Dhaka

Member (External)

i

CANDIDATE'S DECLARATION

It is hereby declared that this thesis or any part of it has not been submitted elsewhere for the award of any degree or diploma.

Signature of the Candidate

SYED MD. IHSANUL KARIM

DEDICATED TO
MY MOTHER,
WIFE & CHILDREN

CONTENTS

LIST OF FIGURES

ix

LIST OF TABLE

List of Abbreviations of Symbols and Terms

ρ	Mass density
u	Flow density
x	Distance from inlet in flow direction
μ	Viscosity
Re	Reynolds number
a	Amplitude
n	Frequency
V	Velocity
P	Pressure
T	Temperature
γ	Specific heat
T_{sub}	Substrate heater temperature
T_{act}	Activation heater temperature
d	Distance between substrate and activation heater
P_{ch}	Pressure of the reactor chamber
θ	Diffraction Angle
PVD	Physical Vapor Deposition
CVD	Chemical Vapor Deposition
SEM	Scanning Electron Microscope
EDX	Energy Dispersive X-ray Spectrometry
XRD	X-ray Diffraction
MME	Department of Materials & Metallurgical Engineering
IAT	Institute of Appropriate Technology
BITAC	Bangladesh Industrial Technical Assistance Center
TICI	Training Institute for Chemical Industries

ACKNOWLEDGEMENTS

ABSTRACT

This work examines how vapor deposited coating of carbon (partially diamond) on stainless steel 304 substrate is affected by the sound vibration. For this a specially designed chemical vapor deposition (thermal CVD, hot filament) apparatus having facility of generating sound vibration at different frequency is fabricated. A coating of carbon (partially diamond) has been deposited on the substrate, and the characterization of the coating has been done by SEM including EDX and XRD. The coating of carbon is identified by EDX, and the allotropic forms of graphite and diamond peaks of carbon are found by XRD analysis. By SEM analysis, it is found that the microstructures of deposited coatings are more compact and smoother under vibration than that in absence of vibration. The experiments were conducted under different ranges of vibration including sonic and ultra sonic range. Studies have shown that the growth rate of deposited coating on a unit area is higher under vibration than that in absence of vibration. It is found that deposition rate varies with the distance between substrate and activation (tungsten) heater and frequency of vibration. The deposition rate does not vary significantly with the change of frequency in the sonic range.

The amount of deposition under ultrasonic vibration increases significantly with the frequency of vibration upto 5 - 6 mm distance between substrate and activation heater. Within this distance, the difference of deposition rate under vibration and without vibration conditions increases almost linearly with the increase of frequency of vibration. Beyond this distance, the effect of frequency on deposition rate becomes almost constant. In addition, the higher the distance the less is the effectiveness of frequency of vibration on the deposition rate in that range. The deposition rate increases due to the extra vibration of sound added to the system which may enhance the activation energy by increasing its kinetic energy. During experiments the effects of pressure, temperature and duration on deposition rate under vibration and absence of vibration are also investigated.

The experimental results are compared with those available in the literature and physical explanations are provided.

CHAPTER 1
INTRODUCTION
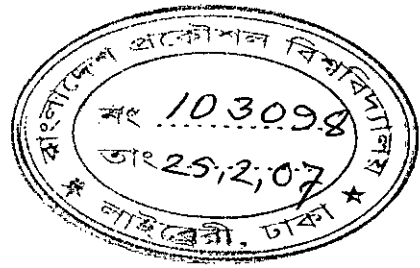
1.1 INTRODUCTION

Chemical vapor deposition (CVD) is a process in which a solid material formed from a vapor phase by chemical reaction, is deposited on a heated substrate. The deposited material is obtained as a coating of multicrystal layer. The controlling parameters in CVD process are surface kinetics, mass transport in the vapor, thermodynamics of the system, chemistry of the reaction and processing parameters like temperature, pressure, etc. The deposition rate which is the prime limiting factor in a CVD process is mainly controlled by the formation of required species to be deposited and its transportation in the vapor and surface kinetics [1-3]. Several authors [4-9] observed that the quality and the rate of deposition depend on temperature of the substrate and filament, gas flow rate, gas composition (reactants) and chamber pressure. Different arrangements and techniques such as centrifugation, vertical vibration of the substrate, hydrogen and argon inclusion, change of gas injecting location and formation of plasma has been studied by different authors [10-14]. The effects of operating parameters on the deposition rate were also investigated for these techniques. The effect of ultrasonic vibration in the formation of thin film produced by thermal vaporization process is investigated in [15]. A study is carried out to observe the effect of ultrasonic vibration on electrochemical deposition [16]. However, the effect of sound vibration on CVD process is yet to be investigated. Kinetic energy increases by adding extra energy of sound which may increase the deposition rate. This extra kinetic energy enhances the chemical activity by overcoming the potential barrier and increases the mass transport of the species.

The effect of sound vibration increases with the increase of density of media, through which it travels. Therefore, the CVD process has been selected, as CVD does not usually require very low pressure, which is necessary for PVD system. Consequently, the vacuum system in CVD is simpler and less costly. Comparing with other CVD process, thermal CVD (hot filament) is relatively inexpensive and experiments are readily carried out. Therefore, in this study an attempt is made to investigate the effect of sound vibration in particular, the frequency of vibration on the deposition rate. In addition to deposition rate the quality of deposited coating is also investigated. Deposition in absence of vibration

was investigated first and then the results were compared with the results obtained under different frequency of vibrations. Some parameters that affect the deposition were also inspected.

1.2 OBJECTIVES OF THE PRESENT STUDY

The following objectives have been considered in the present study:

(a) Design and fabrication of a Chemical Vapor Deposition (CVD) set-up incorporating sound vibration system. This setup has the ability to change the following parameters:

        (i)   reactor chamber pressure

        (ii)   substrate temperature

        (iii)   reactant gas activation temperature

        (iv)   gas flow

        (v)   sound with different frequency

        (vi)   location of sound source

        (vii)   distance between substrate and activation heater

        (viii)   cooling of the chamber.

(b) Deposit of carbon coating (partially diamond).

(c) Study of the effect of sound vibration on deposition rate and coating quality.

(d) Characterization of the deposited coating.

(e) Observe of the effect of pressure of the reactor chamber, temperature of the activation heater and distance between substrate and activation heater on deposition rate.

CHAPTER 2
LITERATURE REVIEW

become physically or chemically adsorbed to the surface. In addition, the whole texture of the surface layer has a series of irregularities with different amplitudes and frequencies of occurrences [18-19].

2.3 SOME IMPORTANT PHYSIO-CHEMICAL PARAMETERS OF SURFACE LAYERS

2.3.1 Adsorption

Adsorption is manifest in changes of concentration of a substance in the boundary layer between two neighboring phases and depends both on the properties of adsorbing body (adsorbent), as well as the adsorbed body (adsorbate). Greater adsorption is exhibited by bodies with a developed surface (rough and porous) than by bodies with smooth surfaces [20-24].

One of the most common types of surface interaction that can take place with a clear surface is the physical adsorption (physisorption) of species on the solid surface. By this process molecules are attracted to the surface because of Van der Waals type electrostatic force. This adsorption process is relatively weak and very small amount of energy is required to remove the physisorbed atoms. The result of physisorption is the reduction of the modulus and yield stress of the metals as well as nonmetals in the presence of adsorbed films [25]. As a result of this effect, lower stress is developed when asperities collide.

Chemisorption is a much stronger bonding than that associated with physisorption. Chemisorption occurs when the individual gaseous atoms interact with a solid surface and the atomic species become bonded to the solid surface. The higher the surface energy of the solid surface, the stronger is the tendency to chemisorption. Bond strength is also a function of chemical activity of the solid surface, reactivity of the adsorbing species and its structure. Due to the chemisorption, the adhesion behavior of the surface changes significantly. The quality of the adsorbed species on a solid surface

and its concentration change the adhesion properties of the surface. The naturally occurring oxides present on metals prevent their destruction during rubbing. Physisorption and Chemisorption are shown in figure 2.2.

The potential energy at the metal surface varies approximately like a sine curve (fig. 2.3) [17]. The energy of bonding of an absorbed molecule attains maximum values at sites corresponding to the minimum of the sine wave. The height of the potential barrier, limiting the mobility of adsorbed molecules (molecules, atoms and radicals) between adsorption sites, is small in comparison with bonding energy of the molecule at any given site.

2.3.2 Diffusion

Diffusion in the most general case consists of relative changes in the locations of atoms or particles in the stationary system, driven by thermal excitation [26].

In a solid crystalline material there are two basic diffusion mechanisms (figure 2.4) [26-34].

Vacancy occurs mainly in substitution type solutions, when the displacement of atoms takes place by way of vacancies, i.e., point defects of the lattice, created by the absence of an atom in the lattice node.

Interstitial occurs mainly in interstitial solutions, when, by means of jumps, atoms smaller than those of the matrix move from one interstitial (interatomic) void to the next. Such voids occur always, even in lattices with closest packing and their size depends on the type of lattice.

2.3.3 Friction

Friction is the resistance to relative motion of the contacting bodies which results in a serious cause of energy dissipation. Friction experienced during a sliding condition is known as sliding friction and that during a rolling condition is known as rolling friction. The degree of friction is expressed as the coefficient of friction. Friction originates from

complicated molecular-mechanical interactions between contacting bodies and these interactions differ from one application to another.

The frictional forces have different components such as adhesion, ploughing and deformation component. The adhesion component of friction is due to the formation and rupture of interfacial bonds. These bonds are the results of interfacial interatomic forces that depend on the degree of penetration of asperities. In the case of rolling of metals, the adhesion component is not the dominating factor for determining the order of coefficient of friction. When one of the contacting surfaces is harder than the other, the asperities of the harder surface may penetrate and plough into the softer surface. If there is any tangential motion, the ploughing resistance is added to the friction forces. Thus ploughing component of friction depends not only on the material properties but also on geometric properties of the asperities, penetrated wear particles and direction of motion. When the asperities of two sliding surfaces come into contact with each other they have to deform in such a way that the resulting displacement field is compatible with the sliding direction. Major part of the energy dissipation due to friction is associated with the plastic deformation of the contacting materials. Although energy is required to deform a metal elastically, however most of the energy is recoverable. Friction force can also arise when the wear debris is a viscoelastic or plastic substance that sticks to the sliding interface and undergoes repeated deformation resulting in consumption of energy. In short, friction is a serious cause of energy dissipation.

2.3.4 Wear

Wear is a surface damage or removal of material from one or both of two solid surfaces in a sliding, rolling, or impact motion relative to one another. In most cases, wear occurs through surface interactions at asperities. During relative motion, first, material on the contacting surface may be displaced so that properties of the solid body, at least at or near the surface, are altered, but little or no material is actually lost. Later, material may be removed from a surface and may result in the transfer to the mating surface or

may break loose as a wear particle. In the case of transfer from one surface to another, net volume or mass loss of the interface is zero, although one of the surfaces is worn (with a net volume or mass loss). Wear damage precedes actual loss of material, and it may also occur independently. It is very steady and continuous process. Wear is classified into many categories, which are based on quite distinct and independent phenomena.

2.4 COATING

There are two alternative means to reduce the deterioration of surface in service, a change of service condition to offer a less destructive environment and a selection of more resistant materials for the surfaces of a component [35].

The achievement of desirable surface properties involves either modification of the surface properties or the properties of the bulk materials to meet the surface demands. In the past it had been the practice to manufacture components from a single material and to impart specific properties to the surface, the component is treated and its microstructure and/or chemical composition is changed. These processes are called surface treatment techniques. The other methods of achieving desirable surface properties are surface coatings.

The act of building a deposit on a substrate is called coating. The conventional way of applying coating is the wet processes in which coating is applied in the form of liquid or solution. The advanced way of applying coating is dominated by the dry process which means that the coating is deposited to a substrate in the vapor (gaseous) or molten or semi-molten state. The term deposition is related with two terms: diffusion and overlay (figure 2.5). Diffused coatings are applied by complete inter-diffusion of material applied to the substrate into the bulk of the substrate material. Examples of these are the diffusion of oxygen into metals to form various sub-oxide and oxide layers. An overlay coating is an add-on to the surface of the part. Depending upon

the process parameters an inter-diffusion layer between the substrate and the overlay coating may or may not be present [36].

The physical dimension of the thickness of thick and thin film is not quite distinct. A thickness of 1 micron is often accepted as the boundary between thick and thin film [37]. A recent view point is that a film can be considered thick or thin depending on the application and discipline. According to this idea, a coating used for improving the surface properties is a thin film whereas that used for bulk properties is a thick film.

2.4.1 Properties of the Coating

The performance of the coating does not only depend on the type of coating but also on the coating-substrate combination. The first consideration is that the substrate must be able to support the coating without causing strain to the coating to failure. As such, the coating-substrate complex systems act together to perform the desired performance. There are a large number of process parameters such as gas flow rates, gas composition, pressure, environment, substrate temperature and geometry, which determine the quality of coating. The application area is another factor affecting the process variables. Therefore, understanding the relationship between these process variables is required, to select an optimum coating-substrate composite system towards a definite application. Figure 2.6 shows the relationship of coating process variables and their applications.

Physical properties of the coating vary widely depending on the coating processes and the process parameters. The large numbers of variables involved have limited the number of fundamental investigations of the process property relationship. The microstructure of coating dictates many of the physical properties of the coating. Some of the important properties of the coating and their probable variation are highlighted below.

2.4.2 Bonding

Adhesion and adhesive strength are macroscopic properties that depend on the bonding within the deposited particles or atoms and bonding across the interfacial region and the local stresses generated during deposition. The bonding and local stresses are determined by the environment, the chemical and thermal properties of the coating and substrate materials, coating morphology, mechanical property, defected morphology of the interfacial region and external stresses [38]. Bonding depends on the processes and their mode of growth of coating from source material.

In case of atomistically deposited coating, the nature and condition of the substrate surface determine many of the factors which control nucleation, interface formation and film growth. These in turn control the interfacial properties. When atoms impinge on the surface, they lose energy to the surface and finally condense by forming stable nuclei. A strong surface atom interaction will give a high density of nuclei and a weak interaction will result in widely spaced nuclei and nucleate by collision with absorbed atoms or other atoms migrate on the surface. It has been proposed that the nuclei density and the nuclei growth mode determine the effective interfacial contact area and the development of voids in the interfacial region [39]. Nuclei density and orientation formed during deposition can be affected by ion bombardment, electric fields, gaseous environment, contaminant layers, surface impurities, surface defects and deposition techniques. In addition to the effective contact area the mode of growth of the nuclei will determine the defect morphology in the interfacial region and the amount of diffusion and reaction between the depositing atoms and the substrate material [40].

Interface may be classified into different types mechanical, monolayer-to-monolayer (abrupt), compound, diffusion or pseudo-diffusion and combinations thereof. Formation of different types of interface depends on the substrate surface morphology, contamination, chemical interactions, the energy available during interface formation and the nucleation behavior of the depositing atoms.

The mechanical interface is characterized by mechanical interlocking and the strength of this interface will depend on the mechanical properties of the materials and surface roughness. The monolayer to monolayer type interface is characterized by an abrupt change of coating material to substrate material. This type of interface may be formed because of no diffusion, lack of solubility between materials, little reaction energy available, or the presence of contaminant layers.

A compound interface may be formed either by an intermetallic compound or some other chemical compound such as an oxide. In this type of interface, there may be abrupt physical and chemical discontinuities associated with the abrupt phase boundaries. Often during compound formation there is segregation of impurities at the phase boundaries and stress could be generated due to lattice mismatching. Porosity may develop in the interfacial region [37].

In the diffusion type of interface there is gradual change in composition, intrinsic stress and lattice parameters across the interface region. Diffusion process may be important in the defect structure of the interface region.

A combination of several types of interfacial regions is possible by controlling the environment or film composition during the initial phase of the film deposition as well as heating during and after film deposition.

As the nuclei join together, the film begins to form. The properties of the coating are determined by the manner in which a film develops. In the vapor deposited process, spit or small droplets of source material may be ejected with the vapor which land on the substrate and incorporate with the coating [37]. The composition of the droplet is different and therefore can be the initiator of corrosion. The spit may also fall leaving the pinhole behind which can be stress raiser and sit for fatigue crack initiation. Spit and foreign particles can induce preferential growth of the deposit termed as flake, which can lead to crack formation or nucleation of corrosive attack.

2.4.3 Residual Stresses

Deposited coatings almost always create residual stress [37]. It appears at the interfacial region in a very complex manner due to geometric effects, variation in the physical properties of the material and usually non-homogeneous nature of the film and interfacial material. The presence of pores and voids in the interfacial region will create stress concentration and alter the value of the tensile and shear components of the interfacial stress. The total stresses are composed of a thermal stress due to the difference in the coefficient of thermal expansion of the coating and substrate materials and an intrinsic stress which arises from the accumulation effect of crystallographic flaws and incorporate into the film during deposition. The intrinsic stress is a function of the deposition process. It may be affected by a number of processing and growth parameters, film deposition rate, angle of incidence, presence of residual gas, deposition temperature and gas incorporation. [41]. Residual stress in evaporated metal films is tensile and on the other hand residual stress in the sputtered metal films can be either tensile or compressive, depending on the deposition parameters [42].

2.4.4 Hardness of Coating

The process parameters such as deposition rate, pressure, temperature and ion bombardment can cause considerable change in microstructure resulting in change of hardness. An increase in substrate temperature commonly increases the coating hardness for refractory compounds in contrast to the behavior of the metal films. Other factors affecting the hardness are interatomic forces, stress level, adhesion of the coating, impurity content and film texture [36-37].

2.4.5 Applications of Coatings

The performance and life of the component that is subjected to friction, wear, high temperature and corrosion can be considerably improved by the selection of suitable materials with a suitable coating. Such coating provides a greater flexibility in the design and selection of materials for a particular component. For giving protection and providing decoration, the majority of manufactured goods and architectural and industrial structures are coated. A few uses of coating are described below.

2.4.5a Coating for Tribological Applications

In general, the standard requirements for multifunctional optimization of tribological surfaces are score resistance, conformability, embeddability, compressive strength, fatigue strength, thermal conductivity, wear resistance, corrosion resistance and cost.

Hard coatings of oxides, carbides, nitrides, borides and silicates deposited by vacuum and other deposition processes are successfully used in various bearing applications. Various coating has been developed for application in high vacuum and high temperature.

(i) Coating for Gears, Cams Tappets and Piston Rings

Gears, cams and tappets are extensively employed in machines to transform motion. Wear of these components can be reduced by applying a coating. The types of coating include chemically deposited oxide coatings on ferrous metal, electrochemically deposited Sn and Al, and TiN and TiC coatings applied by PVD and CVD.

(ii) Coating for cutting tools

Coatings of various ceramic materials, such as TiC, TiN, Al_2O_3, ZrC, HfN, on high speed steel and cemented carbide substrate have been deposited by various deposition

techniques. The low deposition temperatures of evaporation, ion plating, and sputtering are well suited for coating tools. Coating shows an improvement in tool life by a factor of 2 to 10 depending on the type of cutting tool and the coating.

(iii) Other Application of Coatings

Abradable coatings are used as rub-tolerant seals in compressor and turbine section of aircraft gas turbine engines. Thermal-barrier coatings of zirconia, which has insulating properties and hot corrosion resistance, are used in hot sections of turbine engines. These coatings are applied by plasma spraying. Hard coatings of TiC-N deposited by CVD, SiC deposited by sputtering have been found to enhance resistance to erosion of gas turbine blades. The performance of various forming dies, punches and moulds can be improved by putting hard coating on the surfaces.

2.5 CLASSIFICATION OF COATING PROCESSES

A coating process can be divided into three steps: 1) Synthesis or creation of depositing species, 2) Transport of species, and 3) Accumulation or growth of coating on the substrate. These steps can be completely separated from each other or be super-imposed on each other depending upon the process under consideration [36]. The synthesis or creation and transport of the depositing species can be done in three distinct phase viz. Vapor (gaseous) phase, Liquid phase, and molten or semi-molten phase. Some of the different coating processes are described below [19].

2.6 VAPOR DEPOSITION

This is one of the oldest techniques used for depositing thin films. In this process, vapor is generated by boiling or subliming a source material, then the vapor is transported from the source to substrate where it condenses to a solid film. Vapor deposition process has the ability to produce thin coatings with high purity, high adhesion, and

unusual microstructure at high deposition rates. Most nongassing substrate materials which can withstand the deposition temperature can be coated by this process. Coatings deposited by this method generally do not require post finishing. A major disadvantage of vapor deposition process is the high capital cost (processing cost associated with vacuum system) and the low deposition rate.

There are three classes of vapor deposition techniques: physical vapor deposition (PVD), chemical vapor deposition (CVD), and physical chemical vapor deposition (P-CVD).

2.7 PHYSICAL VAPOR DEPOSITION

Physical vapor deposition is used to apply coatings by condensation of vapors in vacuum (10^{-6} to 10 Pa) atomistically at the substrate surface. This technology is versatile, enabling one to deposit virtually every type of inorganic materials (metals, alloys, compounds, and mixtures) as well as some organic materials. There are three physical vapor deposition processes namely evaporation, ion plating and sputtering.

2.8 CHEMICAL VAPOR DEPOSITION

Chemical vapor deposition is a synthesis process in which the chemical constituents react in the vapor phase near or on a heated substrate to form a solid deposit. The CVD technology combines several scientific and engineering disciplines including thermodynamics, plasma physics, kinetics, fluid dynamics, and of course chemistry.

The number of chemical reactions used in CVD is considerable and include thermal decomposition (pyrolysis), reduction, hydrolysis, disproportionation, oxidation, carburization, and nitridation. They can be used either singly or in combination. These reactions can be activated by several methods which are mainly thermal activation, plasma activation and photon activation, etc. The most important are the followings:

- Thermal activation which typically takes place at high temperatures, [>900 °C], although the temperature can also be lowered considerably if metallo-organic precursors are used (MOCVD).

- Plasma activation which typically takes place at much lower temperatures, [<500°C].

- Photon activation, usually with shortwave ultraviolet radiation, which can occur by the direct activation of a reactant.

Most CVD operations can be readily optimized experimentally by changing the reaction chemistry, the activation method, or the deposition variables until a satisfactory deposit is achieved.

2.8.1 Thermodynamics of CVD

A CVD reaction is governed by thermodynamics, that is the driving force which indicates the direction the reaction is going to proceed, and by kinetics, which defines the transport process and determines the rate control mechanism, in other words, how fast it is going.

Reaction thermodynamics is concerned with the interrelation of various forms of energy and the transfer of energy from one chemical system to another in accordance with the first and second laws of thermodynamics. In the case of CVD, this transfer occurs when the gaseous compounds, introduced in the deposition chamber, react to form the solid deposit and by-product gases.

The first step of a theoretical analysis is to ensure that the desired CVD reaction will take place. This will happen if the thermodynamics is favorable, that is, if the transfer of energy, the free energy changes of the reaction known as ΔG_r, is negative. To calculate the ΔG_r, it is necessary to know the thermodynamic properties of each component, specifically their free energies of formation (also known as Gibbs free energy), ΔG_f. The relationship is expressed by the following equation:

$$\Delta G_r^o = \sum \Delta G_f^o \ products - \sum G_f^o \ reacants \qquad (2.1)$$

The energy of formation is not fixed but varies as a function of several parameters which include the type of reactants, the molar ratio of these reactants, the process temperature, and the process pressure.

2.8.2 Kinetics and mass transport mechanism

The sequence of events taking place during a CVD reaction is shown graphically in Figure 2.7 and can be summarized as follows [43]:

- Reactant gases enter the reactor by forced flow.
- Gases diffuse through the boundary layer.
- Gases come in contact with surface of substrate.
- Deposition reaction takes place on surface of substrate.
- Gaseous by-products of the reaction are diffused away from the surface, through the boundary layer.

These steps occur in the sequence shown and the slowest step determines the deposition rate. The rules of boundary layer apply in most CVD deposition in the viscous flow range where pressure is relatively high. In cases where very low pressure is used (in the mTorr range), the rule are no longer applicable.

2.8.3 Boundary Layer

The behavior of the gas as it flows down the tube is controlled by fluid mechanics. In the case of laminar flow, the velocity of the gas at the deposition surface is zero. The boundary is that region in which the flow velocity changes from zero at the wall to essentially that of bulk gas away from the wall. This boundary layer starts at the inlet of

the tube and increases in thickness until the flow becomes stabilized as shown in figure 2.8.The reactant gases flowing above the boundary layer have to diffuse through this layer to reach the deposition surface as is shown in figure 2.7.

The thickness of the boundary layer Δ is inversely proportional to the square root of the Reynolds number as follows:

$$\Delta = \sqrt{\frac{x}{R_e}} \tag{2.2}$$

Where; $R_e = \frac{\rho u_x}{\mu}$

ρ = mass density

u = flow density

x = distance from inlet measured along the flow direction

μ = viscosity

This means that the thickness of the boundary layer increases with lower gas-flow velocity and with increased distance from the tube inlet [44].

2.8.4 Rate-Limiting Steps

The rate –limiting step is generally determined by either the surface reaction kinetics or by mass transport.

2.8.4a Surface-Reaction Kinetics

In the case of control by surface reaction kinetics, the rate is dependent on the amount of reactant gases available. As an example, one can visualize a CVD system where the temperature and the pressure are low. This means that the reaction occurs slowly because of the low temperature and there is a surplus of reactants at the surface since, because of the low pressure, the boundary layer is thin, the diffusion coefficients are large, and the reactants reach the deposition surface with ease as shown in figure 2.9.

2.8.4b Mass Transport

When the process is limited by mass-transport phenomena, the controlling factors are the diffusion rate of the reactant through the boundary layer and the diffusion out through this layer of the gaseous by-products. This usually happens when pressure and temperature are high. As a result, the gas velocity is low, and the boundary layer is thicker, making it more difficult for the reactants to reach the deposition surface. Furthermore, the decomposition reaction occurs more rapidly since the temperature is higher and any molecule that reaches the surface reacts instantly. The diffusion rate through the boundary layer then becomes the rate limiting step as shown in figure 2.10.

2.8.4c Pressure as Rate Limiting Factor

Pressure is similar to temperature as a rate limiting factor since the infusibility of a gas is inversely related to its pressure. For instance, lowering the pressure 760 Torr to 1 Torr increases the gas-phase transfer of reactants to the deposition surface and the diffusion out of the by-product by more than 100 times. Clearly, at low pressure, the effect of mass-transfer variables is far less critical than at higher pressure.

2.8.5 Important Factors that Control the Nature and Properties of Growth Mechanism and Structure of the Deposit

2.8.5a Epitaxy

Epitaxy can be defined as the growth of a crystalline film on a crystalline substrate, with the substrate acting as a seed crystal. When both substrate and deposit are of the same material or when their crystalline structures are identical or close, the phenomena is known as homoepitaxy. When the lattice parameters are different, it is heteroepitaxy. Epitaxial growth cannot occur if these structure differences are too great. Then a solution is to use an intermediate buffer layer of common parameter.

2.8.5b Gas Phase Precipitation

A CVD reaction may occur in the gas phase instead of at the substrate surface if the super saturation of the reactive gases and the temperature are sufficiently high. This is generally detrimental because gas-phase precipitated particles, in the form of soot, become incorporated in the deposit, causing nonuniformity in the structure, surface roughness, and poor adhesion. In some cases, gas-phase precipitation is used purposely, such as in the production of extremely fine powders.

2.8.5c Thermal Expansion

Large stresses can be generated in a CVD coating during the cooling period from deposition temperature to room temperature, if there is a substantial difference between coefficient of thermal expansion (CTE) of the deposit and that of the substrate. These stresses may cause cracking and spalling of the coating. If differences are large, it may be necessary to use a buffer coating with an intermediate CTE or with high ductility. Deposition processes which do not require high temperatures, such as MOCVD or plasma CVD, should also be considered.

2.8.6 Structure and Morphology of CVD Material

The properties of a CVD material are directly related to the nature of its structure which is in turn controlled by deposition conditions. The structure of a CVD material can be classified into three major types which are shown schematically in figure 2.11 [45]. In zone (A), the structure consists of columnar grains which are capped by a domelike top. In zone (B), the structure is also columnar but more faceted and angular. In zone (C), it consists of fine grains.

2.8.6a Control of CVD Microstructure

It is possible to control the nature of a CVD structure by the proper manipulation of the deposition parameters such as temperature, pressure, supersaturation, and the selection of the CVD reaction.

Pressure controls the thickness of the boundary layer and consequently the degree of diffusion. By operating at low pressure, the diffusion process can be minimized and surface kinetics becomes rate controlling. Under these conditions, deposited structures tend to be fine-grained, which is usually a desirable condition (figure 2.11c). Fine grained structures can also be obtained at low temperature and high supersaturation as well as low pressure.

At higher temperature, deposits tend to be columnar (figure 2.11a, b) as a result of uninterrupted grain growth toward the reactant source. The structure is also often dependent on the thickness of the deposit. For instance, grain size will increase as the thickness increases.

2.8.7 The chemistry of CVD

CVD processes frequently proceed by complicated chemical reaction scheme. However, use of overall CVD reactions enables a classification to be made.

Thermal decomposition reactions or pyrolytic reactions means, a gaseous compound AX is thermally dissociated into A (a solid material) and X (a gaseous reaction product),

$$AX (g) \rightarrow A (s) + X (g)$$
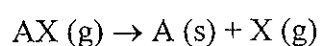
Use of thermal decomposition reactions normally results in relatively pure coatings. Examples of some thermal decomposition reactions are given below:

$$CH_4 (g) \rightarrow C (s) + 2H_2 (g)$$

$$SiH_4 (g) \rightarrow Si (s) + 2H_2 (g)$$
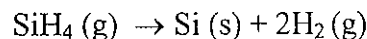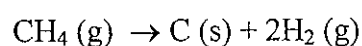
Reduction reactions, where hydrogen acts as a reducing agent, are frequently used,

$$2AX (g) + H_2 (g) \rightarrow 2A (s) + 2HX (g)$$

As for example,

$$WF_6 (g) + 3H_2 (g) \rightarrow W (s) + 6HF (g)$$

$$2BCl_3 (g) + 3H_2 (g) \rightarrow B (s) + 6HCl (g)$$
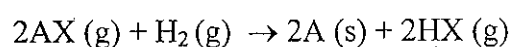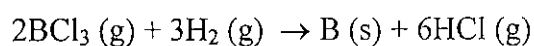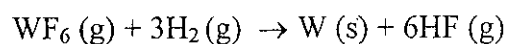
Exchange reactions means that an element E replaces another element, for instance X, in the molecule AX according to

$$AX (g) + E (g) \rightarrow AE (s) + X (g)$$
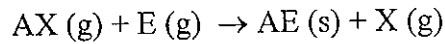
Examples of exchange reactions are:

$$Zn (g) + H_2S (g) \rightarrow ZnS (s) + H_2 (g)$$

$$SiCl_4 (g) + CH_4 (g) \rightarrow SiC (s) + 4HCl (g)$$
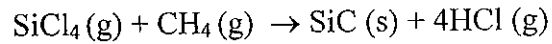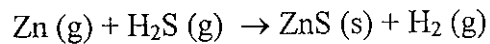
Disproportionation reactions are rarely used in CVD. Disproportionation means a reaction where the oxidation number of an element both increases and decreases through the formation of two new species. CVD of A from AX can be obtained in disproportionation like

$$2AX (g) \rightarrow A (s) + A X_2 (g)$$

$$3AX (g) \rightarrow 2A (s) + A X_3 (g)$$
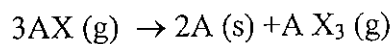
Examples of disproportionation reactions are

$$2GeI_2 (g) \rightarrow Ge (s) + GeI_4 (g)$$

$$2TiCl_2 (g) \rightarrow Ti (s) + TiCl_4 (g)$$
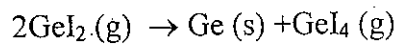
2.8.8 CVD Precursors

The choice of the proper reactants (the precursors) is very important. These precursors fall into several general groups which are the halides, carbonyls and hydrides. The choice of a precursor is governed by certain general characteristics which can be summarized as follows:

- Stability at room temperature.
- Ability to react cleanly in the reaction zone.
- Sufficient volatility at low temperature so that it can be easily transported to the reaction zone without condensing in the lines.
- Capability of being produced in a very high degree of purity.
- Ability to react without producing side reactions.

2.8.9 CVD Processes and Equipment

The various CVD processes comprise what is generally known as thermal CVD, which is the original process, laser and photo CVD, and more importantly plasma CVD, which has many advantages. The difference between these processes is the method of applying the energy required for the CVD reaction to take place.

2.8.9a Thermal CVD: Deposition System and Reactor Design

Thermal CVD requires high temperature, generally (800 to 2000°C), which can be generated by resistance heating, high frequency induction, radiant heating, hot plate heating, or any combination of these. Thermal CVD can be divided into two basic systems known as hot wall reactor and cold-wall reactor.

(i) Hot-Wall Reactors:

A hot wall reactor is often heated by resistance elements. The parts to be coated are loaded in the reactor, the temperature is raised to the desired level, and the reaction gases are introduced. Figure 2.12 shows such a furnace which is used for the coating of cutting tools with TiC, TiN, and Ti(CN). Hot wall reactors have the advantage of close temperature control. A disadvantage is that deposition occurs everywhere, on the part as well as on the walls of the reactor, which require periodic cleaning or the use of a disposable liner.

(ii) Cold-Wall Reactors:

In a cold wall reactor, the substrate to be coated is heated directly either by induction or by radiant heating while the rest of the reactor remains cool or at least cooler. Most CVD reactions are endothermic, that is., they absorb heat and deposition takes place preferentially on the surfaces where the temperature is the highest, in this case the substrate. The walls of the reactor, which are cooler, remain uncoated. A simple laboratory type reactor is shown in figure 2.13. It is used for the deposition of tungsten on a graphite substrate using in situ chlorination. It is heated by high-frequency induction and operates at low pressure.

(iii) Typical Reactor Design:

CVD production reactors which include cold-wall and hot-wall reactors operating at low or atmospheric pressures. The decision to use a given system should be made after giving due consideration to all the factors of cost, efficiency, production rate, ease of operation, and quality.

2.8.9b Laser and Photo CVD

Two methods based on photon activation are as follows:

(i) Laser CVD

A laser produces a coherent, monochromatic high-energy beam of photons, which can be used effectively to activate a CVD reaction. Laser CVD occurs as a result of the thermal energy from the laser coming in contact with and heating an absorbing substrate. The wavelength of the laser is such that little or no energy is absorbed by the gas molecules. The substrate is locally heated in a manner analogous to the local heating in a cold-wall reactor and deposition is restricted to the heated area as shown in figure 2.14, which illustrates the deposition of a thin stripe.

Laser CVD involves essentially the same deposition mechanism and chemistry as conventional thermal CVD and theoretically the same range of materials can be deposited.

(ii) Photo CVD

In photo CVD, the chemical reaction is activated by the action of photons, specifically ultraviolet (UV) radiation, which have sufficient energy to break the chemical bonds in the reactant molecules.

2.8.9c Plasma CVD

Thermal CVD relies on thermal energy to activate the reaction, and deposition temperatures are usually high. In plasma CVD, also known as plasma-enhanced CVD (PECVD) or plasma assisted CVD (PACVD), the reaction is activated by plasma and the deposition temperature is substantially lower.

(i) Principles of plasma deposition

If a diatomic gas, for instance hydrogen, is heated above a given temperature, all the molecules (i.e., H_2) are dissociated into atoms ($H_2 \rightarrow 2H$) and eventually most if not all these atoms become ionized, that is they are stripped of their electrons and a plasma is formed which consists of ions (with positive charge), electrons (with negative charge), and atoms that have not been ionized (neutral) [46]. However, since ionization temperatures are usually extremely high (>5000K), a large amount of thermal energy is required.

A more convenient way to achieve plasma is with electrical energy, such as a low frequency discharge. By increasing the electrical energy in a fixed amount of gas, all molecules are eventually dissociated and complete ionization is achieved.

(ii) Types of plasma

Two types of plasma are currently used in CVD; glow-discharge plasma and arc plasma.

(iii) Glow-Discharge (Microwave) plasma

A glow-discharge plasma is generated in a gas by a high-frequency electric field, such as microwave, at relatively low pressure [47].In such a plasma, the following events occur:

- In a high-frequency electric field, the gases are ionized into electrons and ions. The electrons, with their extremely small mass, are quickly accelerated to high-energy levels corresponding to 5000K or higher.
- The heavier ions with their much greater inertia cannot respond to the rapid changes in field direction. As a result, their temperature and that of the plasma

remain low, as opposed to the electron temperature (hence the name non-isothermal plasma).

- The high-energy electrons collide with the gas molecules resulting dissociation and generation of reactive chemical species and the initiation of the chemical reaction.

The most common frequencies in use for CVD are microwave (MW) and radio frequency (RF). A microwave-plasma deposition apparatus (for the deposition of polycrystalline diamond) is shown schematically in figure 2.15.

(iv) Advantage of Plasma CVD:

As shown in table 2.1, with plasma CVD, a deposit is obtained at temperatures where no reaction whatsoever would take place in thermal CVD. This is its major advantage since it permits the coating of low-temperature substrates, such as aluminum, organic polymers or of metals or metal alloys which experience structural changes at high temperature.

2.8.10 The CVD of the Allotropes of Carbon

Each carbon atom has six electrons, with two electrons in the first shell and four electrons in its second and outer shell. The planer structure of a carbon atom can adopt three different bonding configurations (figure 2.16).

- sp^3: Each of the carbon's four valence electrons is assigned to a tetrahedrally directed sp^3 hybrid orbital, which then forms a strong σ (covalent) bond with an adjacent atom. This structure exists in diamond, and strong bonding results in exceptionally high hardness and high thermal conductivity.

- sp^2: Three of the four electrons are assigned to trigonally directed sp^2 hybrid orbital, which form σ bonds; the fourth unhybridized electron lies in a p_z orbital lying normally to the σ bonding plane. The p_z orbital forms the weaker π bond of the van der Waals type between planes, accounting for the layered structure of graphite.

- sp^1: Only two electrons form strong σ bonds along $\pm O_y$, and the remaining two electrons are left in orthogonal p_x and p_z orbitals to form weak π bonds. This structure exists in hydrocarbons and in certain polymers.

Such a configuration allows the ready formation of several allotropic forms: graphite, microcrystalline carbon, diamond, lonsdaleite (a form detected in meteorites). These allotropes (polymorphs) have the same building block, the carbon atom, but their physical form – the way the building blocks are put together, that is., their crystalline structure is different. The two major allotropes of carbon, Graphite and diamond, which are both produced extensively by CVD, are discussed.

2.8.11 The CVD of Graphite

The CVD of graphite is theoretically simple and is based on the thermal decomposition (pyrolysis) of a hydrocarbon gas. The most common precursor is methane (CH_4), which is generally pyrolyzed at 1100°C or above, over a wide range of pressure from about 100 Pa (0.001 atm) to 10^5 Pa (1 atm). The reaction in a simplified form is as follows: [52- 53].

$$CH_4 \rightarrow C + 2H_2$$
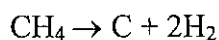
2.8.11a Structure of Graphite

The carbon atoms of graphite form continuous hexagons in stacked basal planes (ab direction). Within each basal plane, the carbon atom is strongly bonded to its three neighbors with a covalent bond. This atomic bonding is threefold coordinated and is known as sp^2. The hybridized fourth valence electron is bonded to an electron of the adjacent plane by a much weaker metal-like bond. Graphite is commonly produced by CVD and is often referred to as pyrolytic graphite.

2.8.11b Properties of CVD Graphite

The properties of CVD graphite are similar to single crystal graphite. It is a highly refractory material, which is practically unaffected by thermal shock. It is very inert to most chemical environments except oxygen and it oxidizes readily above 500^0C [48-51].

2.8.12 The CVD of Diamond

To deposit diamond by CVD, the carbon species must be activated since, at low pressure, graphite is thermodynamically stable and without activation only graphite would be formed. Activation is obtained by two energy-intensive methods: high temperature and plasma

A basic reaction in the CVD of diamond is based on the decomposition of a hydrocarbon, such as methane, as follows:

$$CH_4\,(g) \;\rightarrow\; C\,(diamond) + 2H_2\,(g)$$
$$activation$$
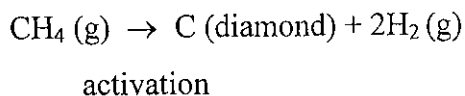
In the deposition process, two conditions seem necessary: (a) activation of the carbon species and (b) the action of atomic hydrogen.

2.8.12a The structure of Diamond

The hybridization of the carbon atom from the ground state to the hybrid sp^3 (or tetragonal) orbital state accounts for the tetrahedral symmetry and the valence state of four with four $2sp^3$ orbitals found in the diamond structure. These orbitals are bonded to the orbitals of four other carbon atoms with a strong covalent bond (i.e., the atoms share a pair of electrons) to form a regular tetrahedron with equal angles to each other. Each diamond tetrahedron combines with four other tetrahedra to form a strongly bonded, three dimensional and entirely covalent crystalline structure [54-55].

2.8.12b Characteristics and Properties of Diamond

The compact structure of diamond accounts for its outstanding properties. It is the hardest of all materials with the highest thermal conductivity. It is the most perfectly transparent material and has one of the highest electrical resistivities [56-59].

Diamond is obtained as a polycrystalline material by CVD with properties similar to these of natural diamond. Efforts to produce single crystal thin films have so far been largely unsuccessful

2.8.12c Role of atomic hydrogen

The stable hydrogen diatomic molecule (H_2) dissociates at high temperature or in a high current-density arc to form atomic hydrogen. The rate of dissociation increases rapidly above 2000°C. It also increases with decreasing pressure [60]. Atomic hydrogen plays an essential role in the surface and plasma chemistry of diamond deposition as it contributes to the stabilization of the sp^3 dangling bonds found on the diamond surface plane. Without this stabilizing effect, these bonds would not be maintained and the diamond plane would collapse (flatten out) to the graphite structure.

The other function of atomic hydrogen is to remove graphite selectively. Unlike molecular hydrogen, atomic hydrogen is extremely reactive. It etches graphite

twenty times as fast as it etches diamond and, when graphite and diamond are deposited simultaneously, graphite is preferentially removed while most of the diamond remains [61]. These two effects of atomic hydrogen, graphite removal, and sp^3 bond stabilization, are believed essential to the growth of CVD diamond.

2.8.13 Thermal CVD (Hot Filament)

Plasma can be generated by high temperature which, in the case of diamond deposition, is obtained by a resistance-heated wire or tube made of tungsten or tantalum heated to 2000°C or slightly higher. [62-63].A schematic diagram of the set-up is shown in figure 2.17. Atomic hydrogen is formed and the carbon species become activated in the vicinity of the hot metal. The deposition rate and composition and morphology of the deposit are functions of the temperature and the distance between the hot metal and the substrate. This distance is usually 10 mm or less. Much beyond that, most of the atomic hydrogen recombines and no diamond is formed. The substrate temperature should be kept between 800 and 1000°C and cooling may be necessary. The gas combination and pressure are generally mixture of methane and hydrogen and 0.1 to 40 Torr respectively.

A disadvantage of the hot-filament process is the short life of the metallic heater, which tends to carburize and embrittle rapidly. The heated metal may also evaporate and contaminate the diamond film.

2.8.14 The chemistry of CVD Diamond Growth

The complex chemical and physical processes which occur during diamond CVD comprise several different but interrelated features, and are illustrated in figure 2.18. The process gases first mix in the chamber before diffusing toward the substrate surface. En route, they pass through an activation region (a hot filament or electric discharge), which provides energy to the gaseous species. This activation causes molecules to fragment into reactive radicals and atoms, creates ions and electrons, and

heats the gas up to temperatures approaching a few thousand kelvins. Beyond the activation region, these reactive fragments continue to mix and undergo a complex set of chemical reactions until they strike the substrate surface. At this point the species can either adsorb and react with the surface, desorb again back into the gas phase, or diffuse around close to the surface until an appropriate reaction site is found. If a surface reaction occurs, one possible outcome, if all the conditions are suitable, is diamond.

2.8.15 The Substrate Material

Most of the CVD diamond films reported to date have been grown on single-crystal Si wafers, mainly due to the availability, low cost, and favourable properties of Si wafers. However, this is by no means the only possible substrate material, although any candidates for diamond growth must satisfy a number of important criteria. One requirement is obvious: the substrate must have a melting point (at the process pressure) higher than the temperature required for diamond growth (normally greater than 700 °C). This precludes the use of existing CVD techniques to coat low-melting point materials, like plastics, aluminum, some glasses, and electronic materials such as GaAs. Another criterion is that the substrate material should have a thermal expansion coefficient comparable with that of diamond. This is because at the high growth temperatures currently used, a substrate will tend to expand, and thus the diamond coating will be grown upon and bonded directly to an expanded substrate. Upon cooling, the substrate will contract back to its room temperature size, whereas the diamond coating, with its very small expansion coefficient will be relatively unaffected by the temperature change. Thus, the diamond film will experience significant compressive stresses from the shrinking substrate, leading to bowing of the sample, and/or cracking, flaking or even delamination of the entire film.

In order to form adherent films, it is a requirement that the substrate material be capable of forming a carbide layer to a certain extent. This is because diamond CVD on non-diamond substrates usually involves the formation of a thin carbide interfacial layer, upon which the diamond then grows. The carbide layer can be pictured as the

'glue' which promotes growth of diamond and aids its adhesion by (partial) relief of stresses at the interface (caused by lattice mismatch or substrate contraction).

2.8.16 Application of CVD Diamond

Some actual and potential applications of CVD diamond are summarized in the Table 2.2 [57-58].

2.8.17 The CVD of Diamond Like Carbon

A new form of carbon coating is now available which is neither diamond nor graphite and is known as diamond-like carbon (DLC) [41]. DLC can be considered as a metastable carbon produced as a thin coating with a broad range of structure and composition [64-65].

DLC has properties similar to CVD diamond and it is easier to process without the high- temperature substrate requirements and with little restriction of size. However, it has several disadvantages: low deposition rate, high internal stress, and availability only in thin coatings.

The differences between graphite, diamond, and DLC are summarized in Table 2.3.

The structure and composition of DLC may vary considerably and, as a result, so do some of its properties. This is not necessarily a disadvantage since it is often possible to control and tailor these properties to fit specific applications. Its properties are generally similar to those of diamond, such as high hardness and chemical inertness, but different in some key areas. As opposed to diamond, DLC has a variable index of refraction and variable electrical conductivity, both a function of hydrogen content.

2.9 THE NATURE OF A SOUND WAVE

2.9.1 Sound is a Mechanical Wave

Sound is a wave which is created by vibrating objects and propagated through a medium from one location to another. A wave can be described as a disturbance that travels through a medium, transporting energy from one location to another location. The medium is simply the material through which the disturbance is moving; it can be thought of as a series of interacting particles. The example of a slinky wave is often used to illustrate the nature of a wave. A disturbance is typically created within the slinky by the back and forth movement of the first coil of the slinky. The first coil becomes disturbed and begins to push or pull on the second coil; this push or pull on the second coil will displace the second coil from its equilibrium position. As the second coil becomes displaced, it begins to push or pull on the third coil; the push or pull on the third coil displaces it from its equilibrium position. As the third coil becomes displaced, it begins to push or pull on the fourth coil. This process continues in consecutive fashion, each individual particle acting to displace the adjacent particle; subsequently the disturbance travels through the slinky. As the disturbance moves from coil to coil, the energy which was originally introduced into the first coil is transported along the medium from one location to another.

A sound wave is similar in nature to a slinky wave for a variety of reasons. First, there is a medium which carries the disturbance from one location to another. Typically, this medium is air; though it could be any material such as water or steel. The medium is simply a series of interconnected and interacting particles. Second, there is an original source of the wave, some vibrating object capable of disturbing the first particle of the medium. The vibrating object which creates the disturbance could be the vocal chords of a person, the vibrating string and sound board of a guitar or violin, the vibrating tines of a tuning fork, or the vibrating diaphragm of a radio speaker. Third, the sound wave is transported from one location to another by means of the particle interaction. If the sound wave is moving through air, then as one air particle is displaced

from its equilibrium position, it exerts a push or pull on its nearest neighbors, causing them to be displaced from their equilibrium position. This particle interaction continues throughout the entire medium, with each particle interacting and causing a disturbance of its nearest neighbors. Since a sound wave is a disturbance which is transported through a medium via the mechanism of particle interaction, a sound wave is characterized as a mechanical wave.

2.9.2 Sound is a Pressure Wave

Sound is a mechanical wave which results from the longitudinal motion of the particles of the medium through which the sound wave is moving. If a sound wave is moving from left to right through air, then particles of air will be displaced both rightward and leftward as the energy of the sound wave passes through it. The motion of the particles parallel (and anti-parallel) to the direction of the energy transport is what characterizes sound as a longitudinal wave.

A vibrating tuning fork is capable of creating such a longitudinal wave. As the tines of the fork vibrate back and forth, they push on neighboring air particles. The forward motion of a tine pushes air molecules horizontally to the right and the backward retraction of the tine creates a low pressure area allowing the air particles to move back to the left. Because of the longitudinal motion of the air particles, there are regions in the air where the air particles are compressed together and other regions where the air particles are spread apart. These regions are known as compressions and rarefactions respectively. The compressions are regions of high air pressure while the rarefactions are regions of low air pressure. The figure 2.19 depicts a sound wave created by a tuning fork and propagated through the air in an open tube. The compressions and rarefactions are labeled.

The wavelength of a wave is merely the distance which a disturbance travels along the medium in one complete wave cycle. Since a wave repeats its pattern once every wave cycle, the wavelength is sometimes referred to as the length of the repeating

pattern, the length of one complete wave. For a transverse wave, this length is commonly measured from one wave crest to the next adjacent wave crest, or from one wave trough to the next adjacent wave trough. Since a longitudinal wave does not contain crests and troughs, its wavelength must be measured differently. A longitudinal wave consists of a repeating pattern of compressions and rarefactions. Thus, the wavelength is commonly measured as the distance from one compression to the next adjacent compression or the distance from one rarefaction to the next adjacent rarefaction.

Since a sound wave consists of a repeating pattern of high pressure and low pressure regions moving through a medium, it is sometimes referred to as a pressure wave. If a detector, whether it is the human ear or a man-made instrument, is used to detect a sound wave, it would detect fluctuations in pressure as the sound wave impinges upon the detecting device. At one instant in time, the detector would detect a high pressure; this would correspond to the arrival of a compression at the detector site. At the next instant in time, the detector might detect normal pressure and then finally a low pressure would be detected, corresponding to the arrival of a rarefaction at the detector site. Since the fluctuations in pressure as detected by the detector occur at periodic and regular time intervals, a plot of pressure vs. time would appear as a sine curve. The crests of the sine curve correspond to compressions; the troughs correspond to rarefactions; and the "zero point" corresponds to the pressure which the air would have if there were no disturbance moving through it. The figure 2.20 depicts the correspondence between the longitudinal nature of a sound wave and the pressure-time fluctuations which it creates.

2.9.3 Intensity and the Decibel Scale

Sound waves are introduced into a medium by the vibration of an object. For example, a vibrating guitar string forces surrounding air molecules to be compressed and expanded, creating a pressure disturbance consisting of an alternating pattern of compressions and rarefactions. The disturbance then travels from particle to particle through the medium,

transporting energy as it moves. The energy which is carried by the disturbance was originally imparted to the medium by the vibrating string. The amount of energy which is transferred to the medium is dependent upon the amplitude of vibrations of the guitar string. If the more energy is put into the plucking of the string (that is, more work is done to displace the string a greater amount from its rest position), then the string vibrates with a wider amplitude. The greater amplitude of vibration of the guitar string thus imparts more energy to the medium, causing air particles to be displaced a greater distance from their rest position. Subsequently, the amplitude of vibration of the particles of the medium is increased, corresponding to an increased amount of energy being carried by the particles.

The amount of energy which is transported past a given area of the medium per unit time is known as the intensity of the sound wave. The greater the amplitude of vibrations of the particles of the medium, the greater the rate at which energy is transported through it, and the more intense that the sound wave is. Intensity is the energy/time/area; and since the energy/time ratio is equivalent to the quantity power, intensity is simply the power/area.

$$Intensity = \frac{Energy}{Time \times Area}$$

$$or\ Intensity = \frac{Power}{Area}$$

$$= 2\rho\,\pi^2\,a^2\,n^2\,V \times 10^{-7}\,watt\,/\,cm^2 \qquad (2.3)$$

Where ρ = density of the media,

a = amplitude,

n = frequency, and

V = velocity of sound

It is known that,

$$\frac{P}{\rho} = cons\tan t,$$ *where P is the pressure of media*   (2.4)

$$V = \sqrt{\frac{\gamma P}{\rho}},$$ *where γ is specific heat ratio of the media*   (2.5)

$$V \alpha \sqrt{T},$$ *where T is the temperature of the media, and*   (2.6)

$$V \alpha \frac{1}{\sqrt{\rho}}$$ (2.7)

As sound wave carries energy through a two-dimensional or three-dimensional medium, the intensity of the sound wave decreases with increasing distance from the source. The decrease in intensity with increasing distance is explained by the fact that the wave is spreading out over a circular (2 dimensions) or spherical (3 dimensions) surface and thus the energy of the sound wave is being distributed over a greater surface area. The figure 2.21 shows that the sound wave in a 2-dimensional medium is spreading out in space over a circular pattern. Since energy is conserved and the area through which this energy is transported is increasing, the power (being a quantity which is measured on a per unit area basis) must decrease. The mathematical relationship between intensity and distance is sometimes referred to as an inverse square relationship. As the intensity varies inversely with the square of the distance from the source. So if the distance from the source is doubled (increased by a factor of 2), then the intensity is quartered (decreased by a factor of 4).

Humans are equipped with very sensitive ears capable of detecting sound waves of extremely low intensity. The faintest sound which the typical human ear can detect has an intensity of 1×10^{-12} W/m^2. The scale for measuring intensity is the decibel scale. The intensity of 1×10^{-12} W/m^2 is assigned a sound level of 0 decibels (abbreviated, 0 dB). A sound which is 10 times more intense (1×10^{-11} W/m^2) is assigned a sound level of 10 dB [66-69].

2.10 REASONS FOR SELECTION OF SOUND AS AN INFLUENCING FACTOR ON CVD

Introduction of sound in the process of CVD may overcome or reduce the potential barrier [17] during the chemical activity by adding some extra energy. This extra sound energy may work on the deposition process by the following ways:

As media particles vibrate back and forth, they create the region of compression and rarefaction. The compressions are the region of high pressure while the rarefactions are the region of the low pressure. According to the potential energy as a function of interatomic distance between two charged atoms or ions curve (figure 2.22) [70], some energy is added to the system due to addition of extra vibration because the amount of energy added in the system during compression for a certain movement of the molecules is not compensated by rarefaction for the same movement. In addition the media particles are moving already towards the substrate get extra push on its way in the compression region. In the rarefaction region, due to low pressure, particles from all sides experienced attraction towards the region, but as the density of carbon particles is less at the vicinity of the substrate due to adsorption and diffusion of carbon particles during deposition of coating on the substrate by heterogeneous reaction, more particles of carbon are pulled from out side having higher density of carbon towards the direction of substrate. As a result, the wave of the sound towards the direction of substrate might create some extra pushes on the on going particles, accelerating the speed of the depositing species towards the substrate surface which might increases the availability of the reactant species for higher deposition at the substrate surface.

For constant temperature the amount of adsorption depends on pressure (figure 2.23) [71-73]. Starting from a certain boundary pressure, sometimes difficult to determine, further rise in pressure does not affect the amount of the absorbed substance. The absorbent appears as if it were saturated. This case occurs seldom in physical adsorption but takes place mainly in chemical adsorption. The wave of the sound

towards the direction of substrate might create some extra pushes which increases pressure on the on going particles. In addition, as velocity increases, the momentum of the species increases during strike upon the substrate, which might increases the adsorption.

Due to the sound vibration within the media, the movement of the particles increases the concentration of diffusing carbon element, which might decrease the diffusion layer [74-75]. As a result the diffusion rate of the coating may increase. In addition, the substrate also vibrates itself due to sound effect, might cause the surface layer turbulent, as a result the diffusion layer might be reduced or weaker, which might increase the diffusion rate.

Atoms repeatedly vibrate about their positions within the molecules or crystal [70]. Extra vibration of sound may increase the momentum difference of carbon and hydrogen due to their atomic mass difference in methane (CH_4) molecule. This momentum difference might enhance the dissociation of the methane during the chemical reaction in CVD process, and ultimately the deposition rate may increase.

2.11 RECENT RESEARCHES RELATED TO THE EFFECT OF PROCESS CONDITIONS OF CHEMICAL VAPOR DEPOSITED COATING

Effects of process conditions on hot-wire chemical vapor deposition of Silicon from Silane (SiH_4) were investigated [4]. They have examined the deposition of uniform polycrystalline silicon films over large surface area for application in flat panel displays. Depositions were conducted using a commercially available hot-wire chemical vapor deposition chamber. They investigated the effect of silane flow rate, filament temperature, total pressure, substrate temperature and hydrogen dilution on the exit gas phase composition, film growth rate, and film crystalline fraction.

Experiments show that the growth rate increases with silane flowrate and is independent of the substrate temperature. The growth rate variation with pressure and filament temperature is observed. A transition from amorphous to polycrystalline silicon films is observed with increasing total pressure, filament temperature and

substrate temperature and decreasing silane flowrate. The effect of hydrogen dilution is found to be equivalent to the effect of increasing gas pressure using pure silane. The experiments suggest that interaction of atomic hydrogen with the growing surface leads to the growth of crystalline phase in the silicon films.

Effects of substrate temperature (TSS) and deposition profile for $Cu(InGa)Se_2$ films deposited by multi source elemental evaporation on film structure and solar cell performance were investigated [6].. The $Cu(InGa)Se_2$ morphology including quantitative analysis of the grain size distributions, and the performance of completed solar cells are compared at TSS = 400 and 550°C. The higher TSS gives larger grains and better device performance with the best devices obtained in this work having efficiency = 16.4% for 550°C and 14.1% for 400°C. At 550°C, Cu-rich film growth gives bigger grains than a uniform flux process, but there is no difference in the device performance. With TSS = 400°C, there is no significant difference in the grain size with the different flux profiles, but the Cu-rich growth is needed for improved devices.

Effects of temperature and flow rate on silicon-nitride layers deposited by the hot-wire chemical vapor deposition technique were investigated [5]. Therefore, the source gases silane (SiH_4) and ammonia (NH_3) are decomposed at hot tantalum filaments (~1800°C). They present the structural, optical and electrical properties as characterized by different techniques. Silicon-nitride layers on crystalline silicon wafers and glass substrates have a hydrogen content as low as 1%. They exhibit a high electrical resistivity. By varying the source-gas ratio, materials with a wide range of composition were made with a refractive index varying from 1.8 to 2.5. The substrate temperature could be decreased from 475°C to 300°C with only slightly diminishing material quality. Thus, hot-wire CVD is a promising technique for large-area and low-temperature deposition of silicon nitride.

2.12 RECENT RESEARCHES RELATED TO THE DIFFERENT ACTIVATION METHODS OF CHEMICAL VAPOR DEPOSITED COATING

Influence of the frequency of Radio Frequency (rf) on the deposition of microcrystalline silicon thin film were investigated [11]. To deposit this thin film 2% silane in hydrogen at 0.5 Torr pressure was used with 13.56 to 50 MHz rf frequency. The increase of frequency of rf lead to a decrease of the rf field and a marked increase of the electron density were observed. By this method the amount of power consumption by electron also increases. Thus, there is a significant increase in the hydrogen flux toward surfaces, which can be explained as the beneficial effect of frequency to the crystallinity of thin films. At the same time, SiH_4 electron impact enhanced dissociation mainly due to the increase of electron density.

Effects of very high frequency (100 MHz) on the deposition rate of diamond like carbon (DLC) film in a plasma enhanced vapor deposition system (PECVD) were investigated [14]. DLC films were grown using 13.56 and 100 MHz plasma as excitation frequencies in the same PECVD system. Deposition rate, stress, hardness, optical band gap, refractive index, electrical conductivity, and hydrogen content of these films have been measured. It was found that just by changing the excitation frequency from 13.56 to 100 MHz, deposition rates of DLC films were enhanced about five times. Thus, very high frequency (100 MHz) PECVD process, with imposed dc bias, is capable of producing reasonably hard DLC films at high growth rates.

Effects of introduction of Nitrogen in CH_4/ H_2 gas mixture during the growth of Crystalline Silicone Carbonitride using microwave plasma enhanced chemical vapor deposition (MW-PECVD) were investigated [9]. In this study, it is tried to synthesize crystalline carbon nitride film using MW-PECVD by gradually increasing the content of nitrogen into H_2/CH_4 gas mixture. Well- faceted crystalline diamond film could be synthesized with a H_2/CH_4 gas ratio of 198:2. With the gradual increase of nitrogen the diamond film gradually transformed into Crystalline Silicone Carbonitride. Nitogen content upto 3% in the gas mixture film quality deteriorates seriously and the

morphological crystal size and growth rate of diamond coatings decreased significantly. With the nitrogen gas content increased to approximately 6-22%, a lot of separated round diamond-like particles formed on the surface rather than a continuous film. Only with the nitrogen content increased above 72%, could some tiny crystals with a type of hexagonal facet form on the silicon surface, together with many large, round particles. With the further increase of nitrogen gas content about 90%, many large, well-faceted hexagonal crystals formed on silicon surface.

The ratio of H_2 to Ar in the reactant gas plays an important role in control of the grain size of diamonds and the growth of the nanocrystalline diamonds was observed [12]. Nanocrystalline diamond thin films have been prepared using hot filament CVD technique with a mixture of $CH_4/H_2/Ar$ as the reactant gas. They have also investigated the growth of carbon nanotubes from catalytic CVD using a hydrocarbon as the reactant gas. Furthermore, focused ion beam technique has been developed to control the growth of carbon nanotubes individually.

Dependence of the gas composition in a microwave plasma-assisted diamond chemical vapor deposition reactor on the inlet carbon source (CH_4 versus H_2) was investigated [8]. Molecular beam mass spectrometry was used to measure the gas-phase composition near a growing diamond surface in a microwave plasma-assisted chemical vapor deposition reactor. The dependencies of the gas composition on changes in the identity of the inlet carbon source and the surface temperature were studied. Unlike the hot-filament case, the gas composition was independent of the identity of the inlet hydrocarbon source Films grown using either hydrocarbon exhibited similar growth rates, morphology and Raman spectra. The gas composition was also generally insensitive to changes in surface temperature suggesting that reported temperature sensitivities of film growth properties are primarily due to changes in the kinetics of surface processes rather than changes in the gas composition near the surface.

Relationship between Diamond Growth Rate and Hydrocarbon Injector Location in Direct-Current Arc jet Reactors was investigated [13]. A series of detailed calculations have been carried out using a stagnation flow model to examine the dependence of diamond growth rate on hydrocarbon injection location in dc arcjet

reactors. It is predicted that, for methane feed, growth rate can be increased by as much as 75% by relocating the injector from a position near the plasma torch exit to one near the diamond surface, but outside the boundary layer. As the injector is moved towards the surface from the plasma torch, the concentration of C and CH_3 present at the surface increase. When the injector is located within the boundary layer, the lower atomic hydrogen concentration and short residence time leave most of the injected CH_4 unreacted, causing growth rates to drop.

The influences of centrifugation on this deposition of diamond on graphite and carbon felt from graphite heated in hydrogen at low-pressure were investigated [10]. They described a simple new technique for deposition of diamond on a wide variety of surfaces, with and without centrifugation to accelerate deposition. A graphite rod is heated electrically to approximately 2000°C in the presence of H_2 at >50 Torr in a closed chamber. The desired substrate is placed nearby, and is heated by the graphite rod. This investigation deals with deposition of diamond on graphite and carbon felt without any prior contact with diamond powder with faceted diamond crystals randomly distributed over the graphite. Tape adhesion tests removed neither the diamonds nor any graphite. Without centrifugation, the diamond crystals were on about 50% of the 3 cm² surface of the graphite substrate, while crystals were on about 90% with centrifugation. The size of the crystals was about 55% larger when deposition was carried out under the same conditions as without centrifugation. Longer deposition times should yield complete coverage of graphite by polycrystalline diamond.

2.13 RECENT RESEARCHES RELATED TO THE DIFFERENT EFFECTS OF VIBRATION ON COATING PROCESSES

Effects of ultrasonic vibrations on the formation and structure of thin films produced by thermal vaporization were investigated [15]. Ultrasonic vibrations perpendicular to the deposition plane improved the uniformity of vapor-deposited Al and Ag films by intensifying diffusion. The effect increased with increasing intensity. Ultrasonic vibration parallel to the substrate surface enables control of the film thickness.

Ultrasonic vibrations normal to the deposition surface increased the film thickness. The higher the wave intensity, the larger is the film grain size.

The effects of ultrasonic vibrations on the localized electrochemical deposition (LECD) process were studied [16]. Nickel micro-columns were locally electrodeposited onto a copper substrate from a nickel sulphamate solution using a non-soluble platinum counter electrode, both with and without ultrasonic vibrations. Three output parameters were investigated in the experiments: rate of deposition, concentricity and porosity of the micro-columns. Results showed that generally, ultrasonic vibrations increased the rate of deposition and improved the concentricity of the fabricated micro-columns. On the other hand, it gives rise to structures with higher porosity as compared to those deposited in the absence of ultrasound. The application of ultrasonic vibrations in the LECD process is a novel effort to utilize a well-studied phenomenon to enhance the capability of a new micro fabrication process.
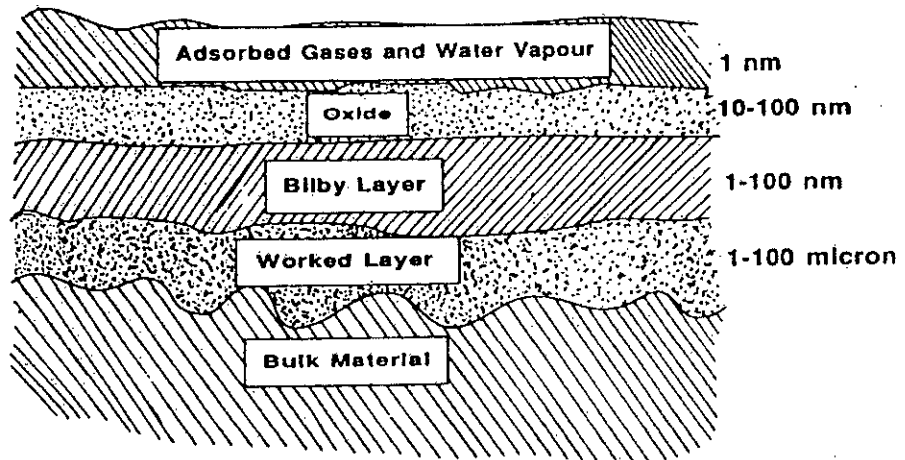
Fig. 2.1. Schematic representation of metal surface [19].
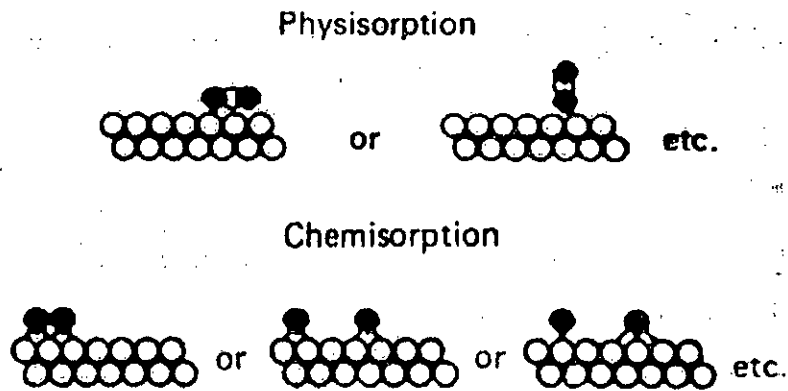
Fig. 2.2. Schematic diagrams of various surface interactions [70].
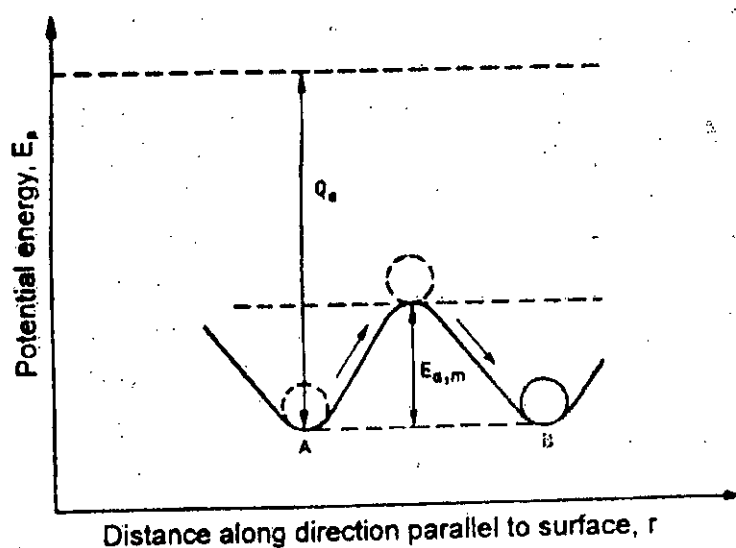
Fig. 2.3. Potential energy curve in plane perpendicular to ideal metal surface [17].
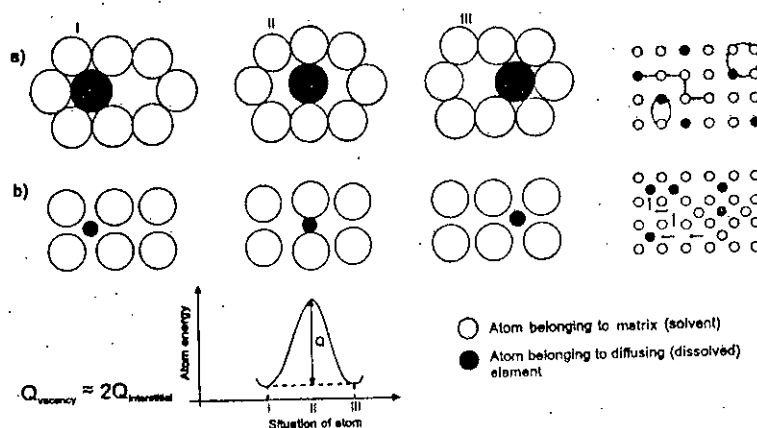
Fig. 2.4. Diagrams showing mechanisms of diffusion: a) vacancy, b) interstitial; I-atom in initial position; II-atom in activated position; III-atom in final position [26]-[34].
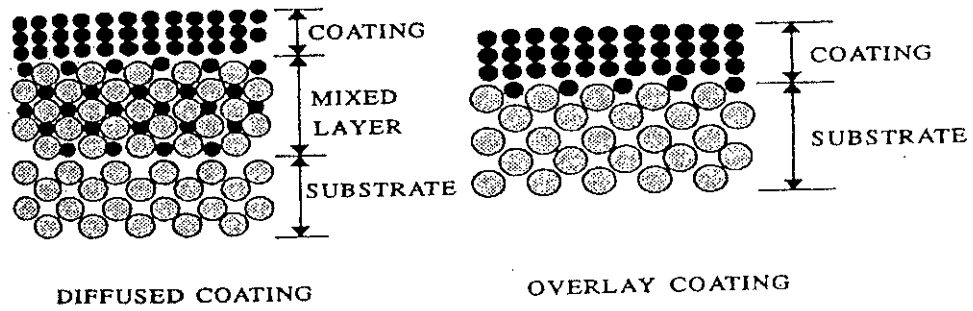
Fig. 2.5. Schematic illustration of the diffused coating and overlay coating [19].
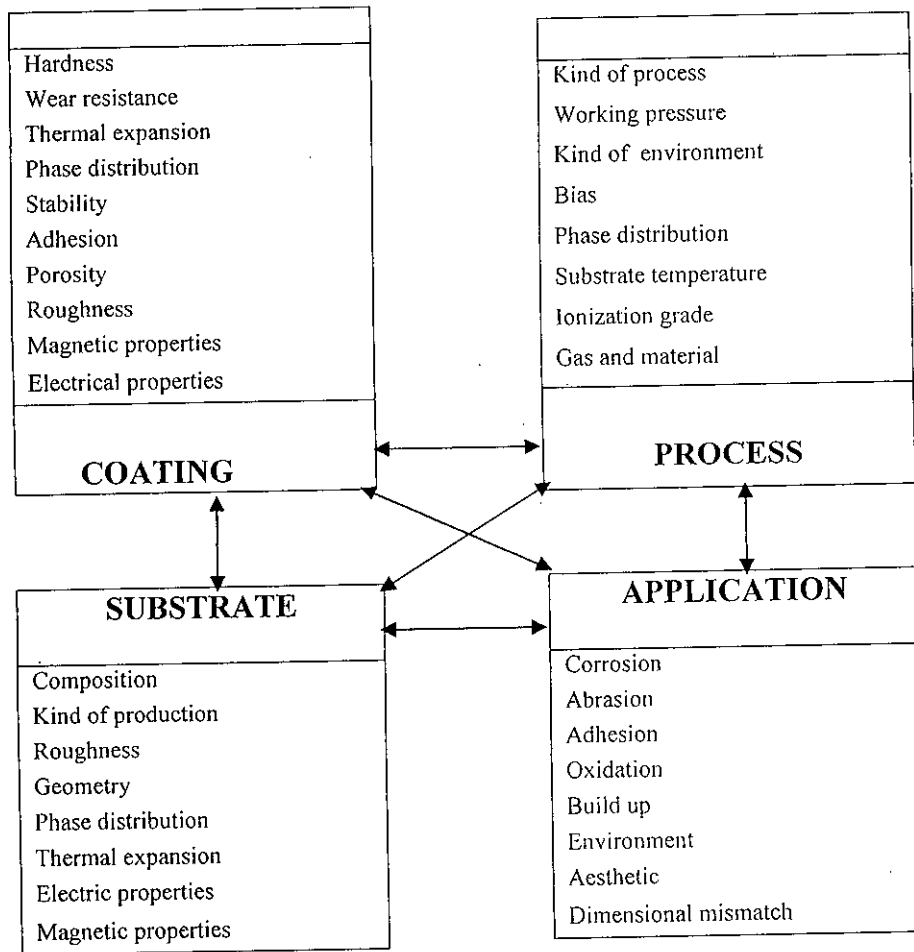
Fig. 2.6. The inter-relationship of coating, substrate, process and application [19].

Main flow of reactant gases

Gaseous
by-products

Boundary
layer

Interface (negligible
thickness)
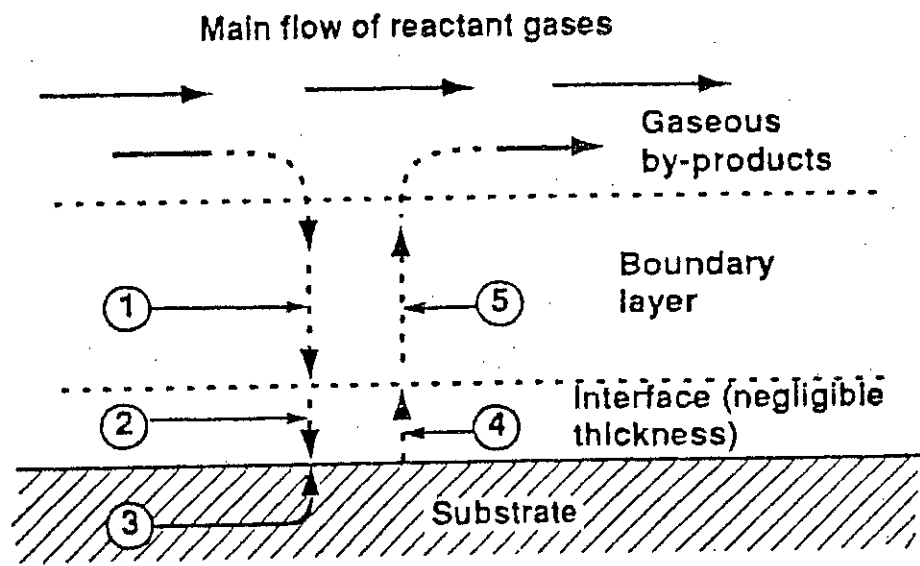
Substrate

1. Diffusion in of reactants through boundary layer
2. Adsorption of reactants on substrate
3. Chemical reaction takes place
4. Desorption of adsorbed species
5. Diffusion out of by-products

Fig. 2.7. Sequence of events during deposition [43].
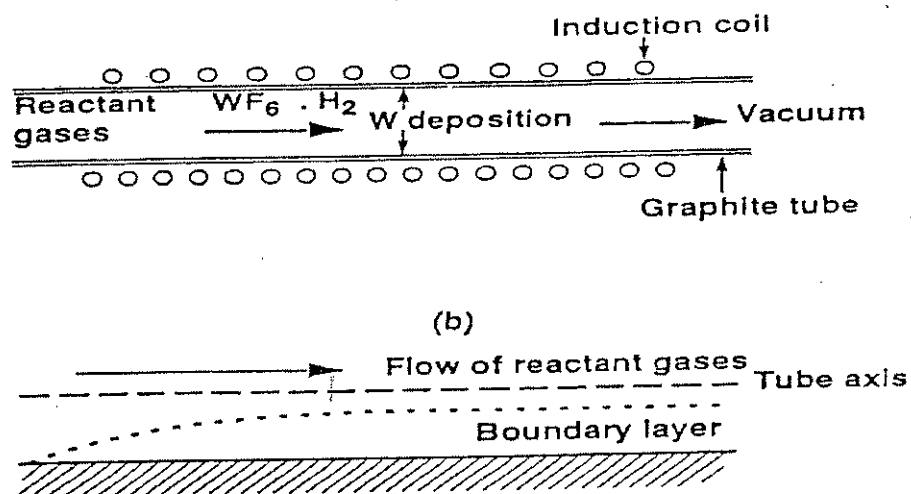
Fig. 2.8. (a) Tungsten deposition in a tubular reactor, (b) boundary layer condition [44].
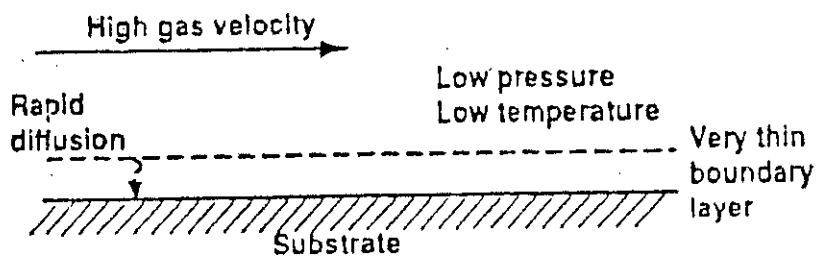
Fig. 2.9. Rate-limiting steps in a CVD reaction; surface reaction kinetics control [1].
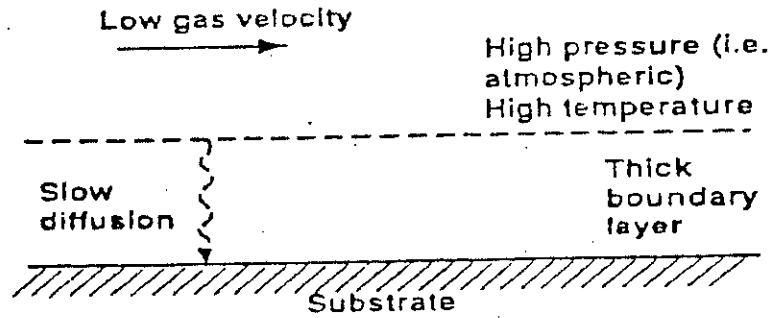
Fig. 2.10. Rate-limiting steps in a CVD reaction; diffusion control [1].

(a)   (b)   (c)
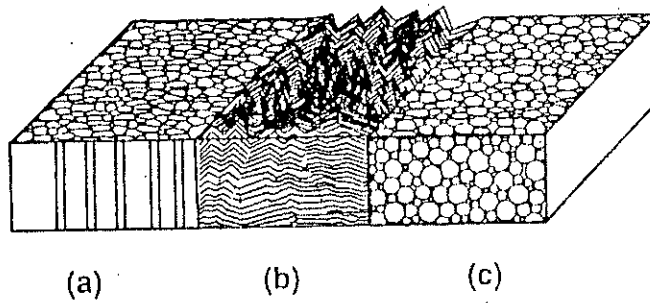
Fig. 2.11. Schematic of structures obtained by CVD: (a) columnar grains with domed tops, (b) faceted columnar grains, (c) equiaxed fine grains [45].
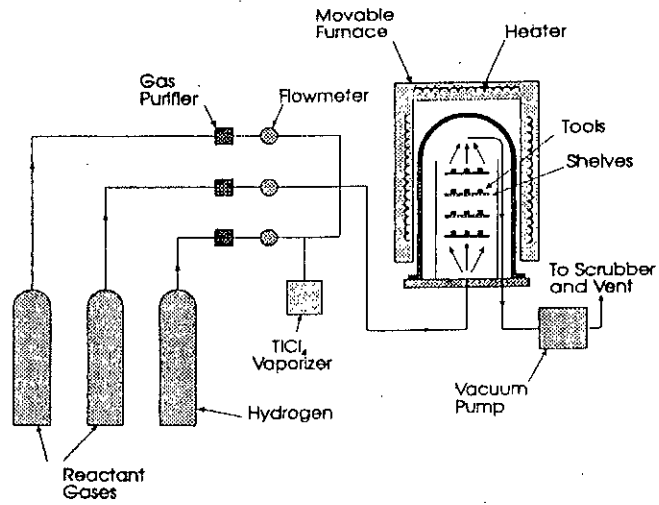
Fig. 2.12. Production CVD reactor for the coating of cutting tools [1].
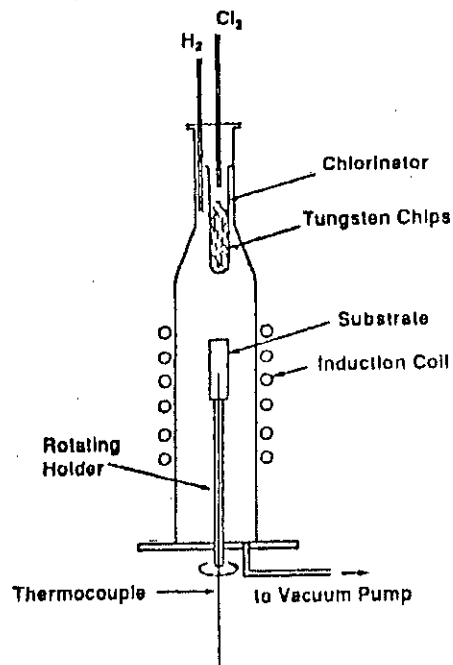
Fig. 2.13. Cold-wall laboratory reactor for tungsten deposition [1].
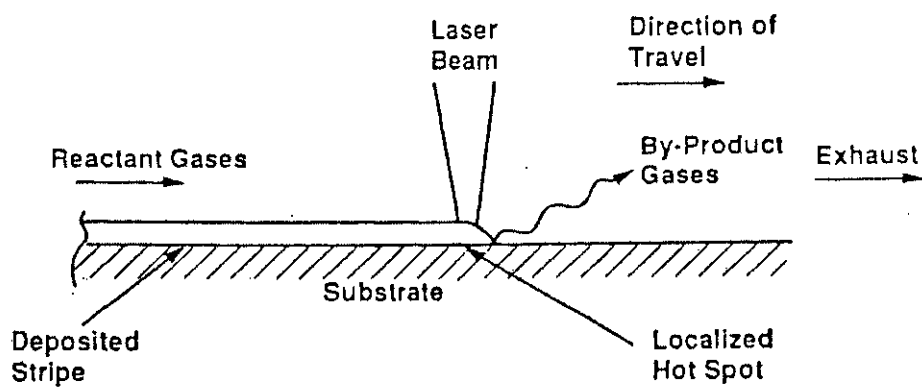
Fig. 2.14. Schematic of laser CVD growth mechanism [1].
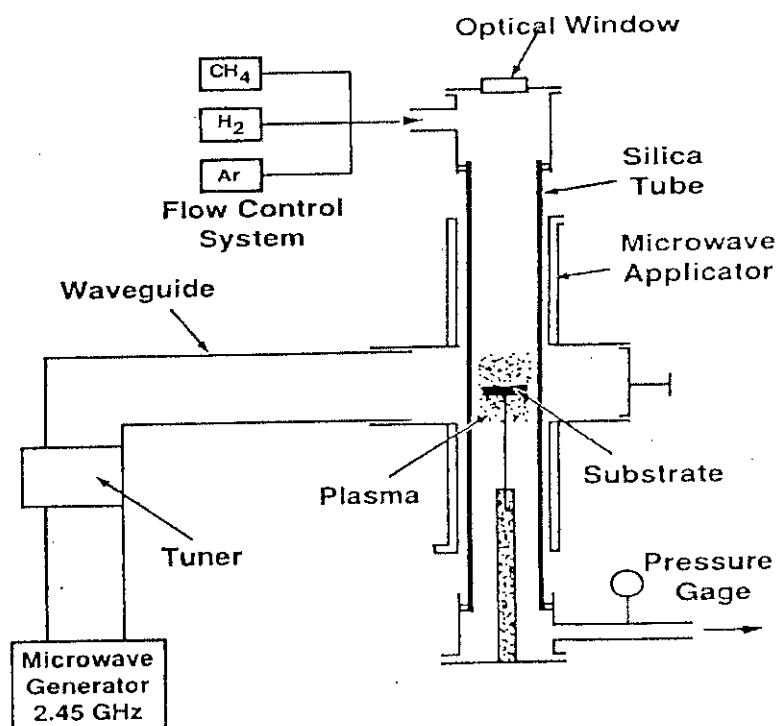
Fig. 2.15. Microwave plasma apparatus for the deposition of diamond [1].
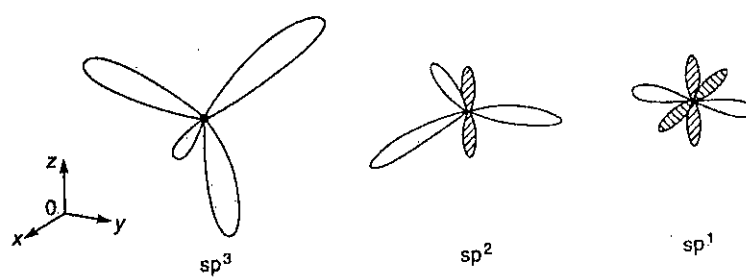
Fig. 2.16. Schematic representation of sp^3 (diamond), sp^2 (graphite), sp^1 (hydrocarbon and certain polymers) bonding types of carbon atoms [70].

Gas Manifold
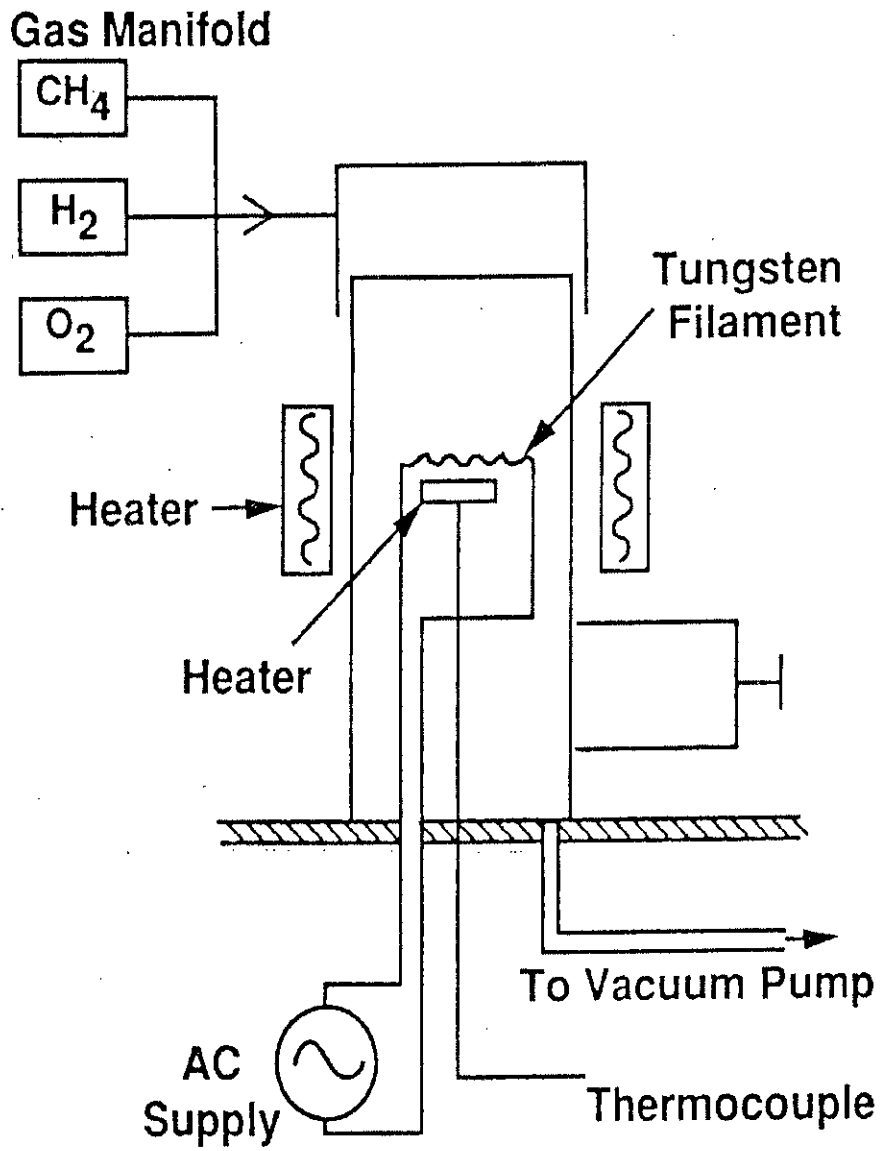
Fig. 2.17. Schematic diagram of hot-filament apparatus for the deposition of diamond [1].
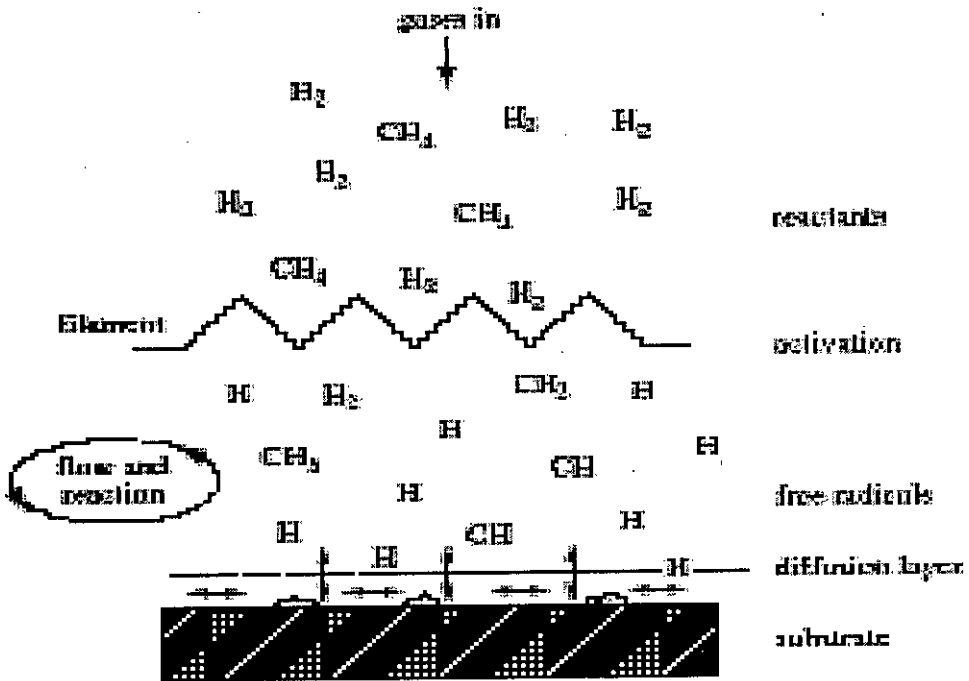
Fig. 2.18. Schematic diagram of the physical and chemical processes occurring during diamond CVD [76].
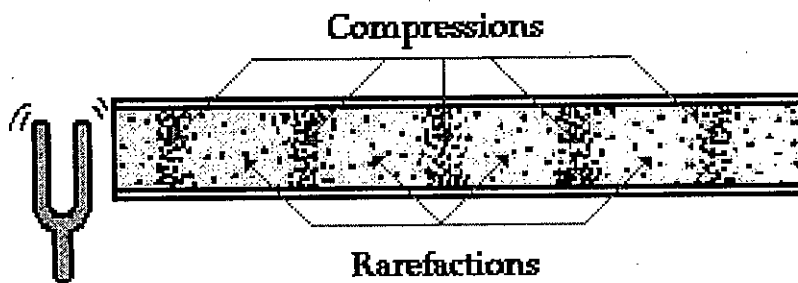
Fig. 2.19. Sound wave created by a tuning fork and propagated through the air in an open tube [67].

Sound is a Pressure Wave

NOTE: "C" stands for compression and "R" stands for rarefaction
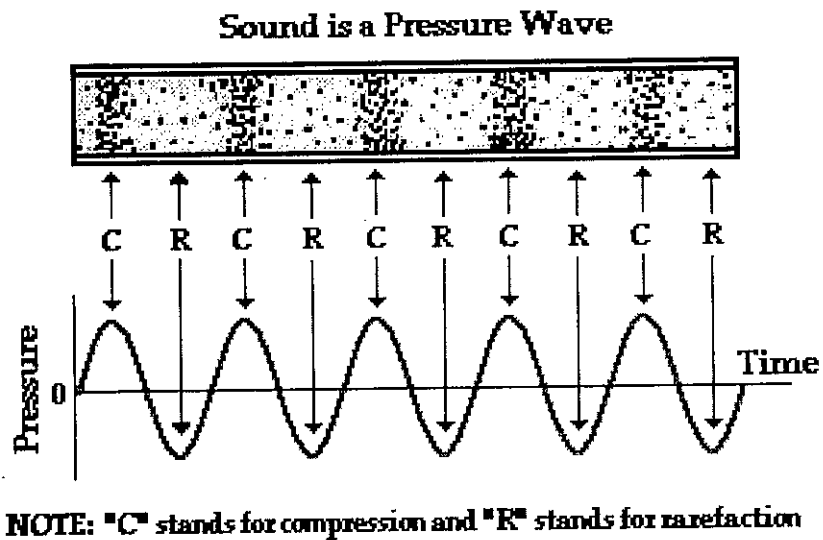
Fig. 2.20: the correspondence between the longitudinal nature of a sound wave and the pressure-time fluctuations which it creates [67].
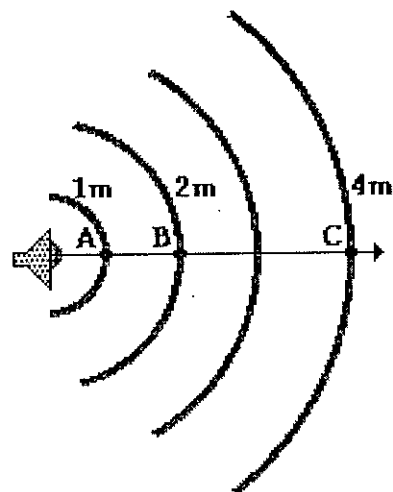
Fig. 2.21: The sound wave in a 2-dimensional medium is spreading out in space over a circular pattern [68].
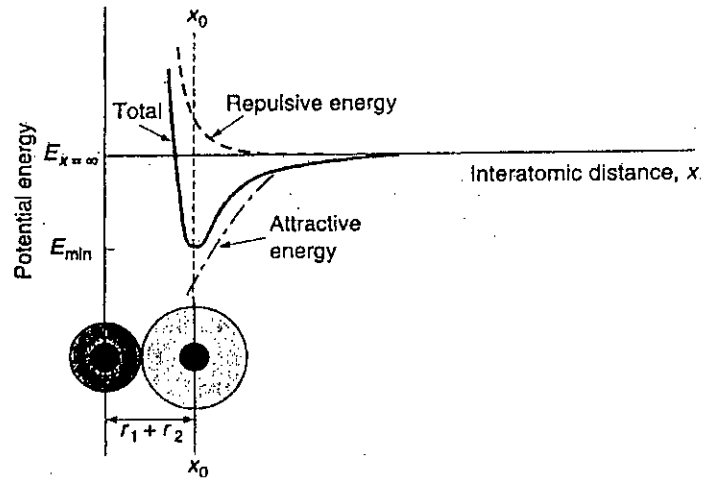
Fig. 2.22: Potential energy as a function of interatomic distance between two charged atoms or ions [70].

Type I : Typical curve for chemical adsorption
Type II-V : Various curves for physical adsorption
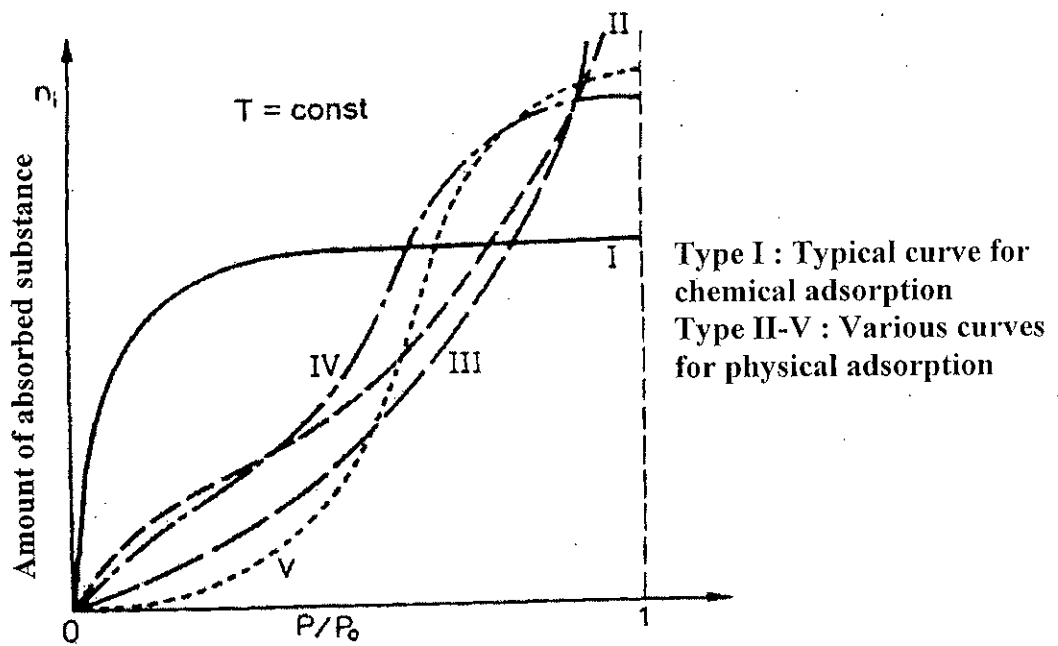
Fig. 2.23: Amount of adsorbed substance as a function of pressure [71]-[73].

Table 2.1: Typical deposition temperatures for thermal and plasma CVD [1].

Material	Deposition Temperature (°C)	
	Thermal CVD	Plasma CVD
Epitaxial silicon	1000–1250	750
Polysilicon	650	200–400
Silicon nitride	900	300
Silicon dioxide	800–1100	300
Titanium carbide	900–1100	500
Titanium nitride	900–1100	500
Tungsten carbide	1000	325–525

Table 2.2: Actual and potential applications of CVD diamond [57]-[58].

Grinding, cutting:	Inserts Twist drills Whetstones Industrial knives Circuit-board drills	Oil-drilling tools Slitter blades Surgical scalpels Saws
Wear parts:	Bearings Jet-nozzle coatings Slurry valves Extrusion dies Abrasive pump seals Computer disk coatings	Engine parts Medical implants Ball bearings Drawing dies Textile machinery
Acoustical:	Speaker diaphragms	
Diffusion, corrosion:	Crucibles Ion barriers (sodium)	Fiber coatings Reaction vessels
Optical coatings:	Laser protection Fiber optics Scanners Lenses	Antireflection UV to IR windows X-ray windows Radomes
Photonic devices:	Radiation detectors	Switches
Thermal management:	Heat-sink diodes Heat-sink PC boards	Thermal printers Target heat-sinks
Semiconductor:	High-power transistors High-power microwave Photovoltaic elements	Field-effect transistors UV sensors

Table 2.3: Comparison of graphite, diamond and DLC [1].

	Graphite	Diamond	DLC
Composition	Pure carbon carbon (<1 atm % hydrogen)	Essentially	Up to 50 atm % hydrogen
Microstructure	Crystalline	Crystalline	Amorphous
Atom-bonding state	sp^2 only	sp^3 only	sp^2, sp^3, sp^1 (variable ratio)
Stability	Stable	Stable	Metastable
Raman spectrum	Sharp peak at 1580cm	Sharp peak at 1332 cm	Broad humps at 1330 & 1550 cm
Electrical conductivity	Conductor (ab dir.)	Insulator	Insulator

CHAPTER 3
EXPERIMENTATION

3.1 INTRODUCTION

Thermal chemical vapor deposition (hot filament) process has been selected to observe the effect of sound vibration on coating.

The effect of sound vibration on coating increases with the increase of density of media, through which it travels. The CVD process has been selected as CVD does not usually require the low pressure which is necessary with PVD system. Consequently, the vacuum system in CVD is simpler and less costly. Comparing with other CVD process, thermal CVD (hot filament) is relatively inexpensive and experiments can be readily carried out. Specially, plasma generation by high temperature, which is obtained by resistant heating, is relatively easy and less costly. On the other hand, a disadvantage of the hot-filament process is the short life of the metallic resistant heater, which tends to carburize and embrittle rapidly.

To observe the effect of sound vibration by applying the specially arranged vibration of different frequencies on the CVD process, a CVD setup has been designed and constructed. The photograph of hot filament chemical vapor deposition setup including related measuring instruments is shown in figure 3.1 and reactor chamber with inside arrangement is shown in figure 3.2. Natural gas is used as reactant gas for CVD process. The composition of used natural gas is given in Table 3.1.

Figures 3.3 shows the sound generator with oscilloscope. Detailed Specification of the Accessories and measuring apparatus used in the experiment are shown in table 3.2.

3.2 DESCRIPTION OF THE EXPERIMENTAL SETUP

Detailed schematic diagrams of the setup including different sub-assemblies and related part drawings of the components are shown in figures 3.4.

Mainly, the CVD system comprises of a reactor chamber supported by some sub-systems shown in figure 3.5 to figure 3.10.

3.2.1 Reactor Chamber

Cylindrical shaped main reactor chamber sub-assembly including related part drawings of the components are shown in figure 3.4.1. It is made of stainless steel 304 and the outside diameter of the cylinder, height and wall thickness are 304 mm 457 mm and 3 mm respectively. Stainless steel is used as a reactor material due to its advantageous properties such as non-corrosiveness, high temperature resistant and relatively less reactive than other materials, which is suitable for CVD reaction. The chemical reactions of CVD process occur in this chamber. This reactor chamber consists of a cylindrical body with top end closed by a plate and a lower replaceable plate. Inside the chamber there are substrate heater and activation (Tungsten) heater connectors. Outside of the chamber, there are cooling copper tube around the circumference and a water sump at the top. A sound vibration generating chamber is installed by a hollow shaft at the top of the reactor chamber. The lower flange of the cylinder is placed on the lower plate. Between this plate and flange there is a rubber seal which can withstand high temperature having leak proof quality. During extraction of the gases from inside, the parts press together due to vacuum, the rubber seal is being squeezed and the leak proof quality increases as vacuum increases. The upper cylindrical body and the lower plate are to be dismantled for setting the substrate. Therefore, there is a provision for lifting the upper cylindrical body by a mechanical lifter.

The substrate and activation heaters are mounted inside the reactor chamber at the bottom plate by the connectors. To install the sound generating system, the hollow shaft is connected at the center of the top surface of the upper cylindrical body by welding, where the water sump is located. It is submersed in water to certain level during operation. A chamber, where vibration generating system is being installed, is bolted with this hollow shaft in such a way that the high vacuum in the chamber is ensured. This sump is made of a piece of mild steel pipe. This pipe is clamped at the top surface of the reactor chamber by tightening of six clamping bolts between collars, equally spaced at the circumference of the pipe, and circular flange collar at the top of the cylindrical body. Rubber seal is used in the

joint to make it water proof. Copper tube is used around the circumferential surface of the reactor chamber for cooling.

The upper cylindrical main body (figure 3.4.1a.) has collar at bottom end. A rectangular groove is machined at the lower surface of the collar. A rubber seal is being fixed by high temperature resistant glue.

The lower bottom plate of the reactor chamber is shown in figure 3.4.1d. All the connections of heater, gas outlet and gas inlet, vacuum gauge outlet are provided through this lower plate with proper insulation and leak proof quality. The lower plate is being fixed with structure. There is a tap hole at the center for gas extraction line by vacuum pump. Six holes are machined in the lower plate of which two holes 45 mm equally apart from the center of the plate through the center line for substrate heater connector, two tap holes of same size, 150 mm apart in same line, for activation heater connector, and another two holes of same size, 150 mm apart in transverse direction of the heater line, one for vacuum gauge connector and the other for inlet gas connector.

The hollow shaft is shown in figure 3.4.5d. The purpose of the hollow shaft is to connect the reactor chamber with the sound vibration generating chamber, ensuring leak proof quality by the hollow nut. The hollow shaft is made of stainless steel. To transmit sound vibration, there is a hole inside the shaft, partly threaded at the top, and the remaining length is a taper hole up to the bottom. Depending on the type of functions, the reactor chamber can be divided into the following sub assemblies:

1. Heater
2. Sound vibration generating unit
3. Connector
4. Cooling line

3.2.1a Heater

Activation (Tungsten) heater is used for gas dissociation as well as activation. Substrate (Nicrom) heater is used for substrate heating.

Substrate heater assembly is shown in figure 3.4.3. Nicrom heater coil of coil diameter 4 mm, wire diameter 0.5 mm, and 20 coils per inch pass through T-shaped slots within the high heat resistant clay blocks shown in figure 3.4.3e. Five numbers of clay blocks are used to make a block of rectangular shape with opened upper side. The T-slot side of the blocks is kept towards inside direction, so that heat generated by coils remains towards the inside space. This integrated heater block is placed within a stainless steel box on a stainless steel plate in such a way that, the top surface of the block is placed at 5 mm down from the top of the stainless steel box. Another stainless steel rectangular plate is placed at the top of the block, inside the stainless steel box. A same size mica sheet of 1 mm thickness is also placed on stainless steel rectangular plate. Mica is used to make this cover plate insulated and reduce the chance of deposition of C on this plate. There is a rectangular opening through the mica and stainless plate at the center. The substrate is placed on this opening so that radiative heat generated from Nicrom heater is transferred through the opening and heat up the substrate as required. Below the rectangular plate, a gap of 20 mm is created by block spacer, to accommodate the connector screw.

Five heater coils placed in five clay blocks are connected in parallel. Ceramic connectors are used for every junction point of the heater coil. Nicrom wires of 1 mm in diameter are used as an extension wire to connect the junction points; these wires are covered with small ceramic washer blocks as insulator. The two ends of wires from heater passes through the side passage between the stainless steel box and the clay block, where the connector screws are located.

Two connector screws are fixed into the stainless steel box through the bottom side with insulated material in such a way that it will not touch the body. The schematic diagram of connecting screw arrangement is shown in figure 3.4.3f. The substrate heater gets the electrical power from these connectors within the vacuum chamber through connection between heater and connector by insulated extension wire. The wire clamping nut is used as a connection wire clamping nut as well as the holding device of the stainless steel box on the connector stainless steel rod.

The schematic diagram of activation heater sub-assembly is shown in figure 3.4.4. There are two connecting rods which have 70 mm threaded portion of M8 at the top end, are introduced vertically through the bottom surface of the main

reactor chamber. There are two adjustable horizontally placed extension rods of which one is for each vertical rod, screwed at the threaded portion of connector rod.. These two extension rods are used to hold as well as to supply electrical power to the activation heater. A connector is clamped at one side with the extension rod by the screw, and at other side, it is clamped with another connector by the screw. Finally the activation heater is mounted through the connector by tightening the screw. This activation heater is placed slightly above the substrate, and the gap between substrate and activation heater can be adjusted within the range of 0 to 50 mm by moving the extension rods at the threaded portion of the supporting rods by the two adjusting nuts.

3.2.1b Sound Generating Unit

The sound vibration generating unit sub-assembly is shown in figure 3.4.5. This vibration generating unit has upper and lower parts. The sound generating system is fixed with the lower part. The upper part is only a leak proof cover so that, no sound can go outside the chamber and at the same time it will ensure the vacuum of the chamber.

The lower part is clamped with the hollow shaft fixed at the top of the reactor chamber, at its internal thread, located at the upper side, by a hollow bolt. The hollow shaft having the same outside diameter of counter bore in the lower part are assembled together in such a way that, it goes inside of the counter bore up to 6 mm, and a rubber seal is placed there. Another rubber seal is placed under the collar of the bolt. There are six equally spaced holes in lower part, for fixing upper and lower part together by six bolts. A rubber seal is used between the two parts. There are two connectors at the bottom part. The piezoelectric horn body is clamped on the bottom part at its lower plastic collar by four numbers of bolts, there is also a rubber seal of 6 mm thick between the lower plate and plastic collar of the piezoelectric horn. A stainless steel washer plate is used at the top of the plastic flat portion of the horn body as a support of the plastic body to fix it with lower part by horn clamping bolt. There are two metallic connectors for electric connection at the head of the

horn; flexible wires are used for electrical connection between metallic connector of piezoelectric horn and the connectors inside the sound vibration generation chamber.

The upper part, shown in figures 3.4.5a,b, is made of a piece of pipe, with one end closed by a plate. To make a collar having 6 equally spaced threaded holes, a ring plate is welded at outer circumference of the pipe piece for fixing it with lower part.

The lower bottom part is shown in figure 3.4.5c. It is a circular plate. It has a hole at the center of diameter 40 mm; with a counter bore of 50 mm for fixing it with hollow shaft at the top surface of the reactor chamber. There are six equally spaced holes in lower part, for fixing upper and lower part together. There are two threaded holes at 125 mm apart, through the center line of the plate for fixing the connectors. And there are four threaded blind holes up to the depth of 8 mm from the top surface of the bottom part at 75 mm diagonal distance for fixing the piezoelectric horn body.

The hollow bolt is shown in figure 3.4.5e. It is used for clamping the bottom part of the vibration generating chamber and the hollow shaft, located at the top of the reactor chamber. To facilitate the transmission of sound through it, there is slightly tapered hole of 30 mm diameter at the end.

The piezoelectric horn is shown in figure 3.4.5 and 3.11. It is chosen because of its capability to transmit high frequency, also it has the advantage over magnetic horn, not to create any disturbance during heating due to the effect of heat on the magnetic field. The piezoelectric horn consists of a cylindrical shape plastic head, and an asymmetric shape body at head side, rectangular at other side, with a flat collar. In the flat collar, there are four holes at four corners. There is a domelike structure inside the body of the horn.

3.2.1c Connector used for power supply

Figure 3.17 shows the detailed view of connector used for power supply. This connector is manufactured specially in such a way that it can maintain the required insulation and leak proof quality when it is screwed with the metallic body. All connectors are placed at the lower surface of the main reactor chamber. A hollow

bolt (6) of Polytetrafluoroethylene (PTFE, commercially known as Teflon) is screwed with the bottom plate of the main reactor chamber from outside of the chamber. A stainless steel rod ensures tight fit through the hollow Teflon bolt which is used to transport the electricity from outside to inside of the reactor chamber. The detail schematic drawing of the steel rod and Teflon bolt are shown in figure 3.4.5f. There is a taper portion of steel rod located at the upper part of the Teflon bolt. This taper portion of the movable connector stainless steel rod is being locked gradually to ensure leak proof quality with the fixed Teflon bolt by tightening the nut. Due to internal outward pressure towards the circumference, the Teflon bolt is being flattened slightly, as a result it become more locked at thread portion with the bottom plate of the reactor chamber, which ensures leak proof quality more. There are two types of metallic washer, one is bush washer at the tightening bolt side, and another is flat washer at the Teflon side. These washers are used to facilitate the rod pulling mechanism. Rubber seal is used between Teflon bolt head and bottom plate of the reactor chamber. For wire connection, one pair nut for both the upper and lower side of the connection rod is used.

3.2.1d Connector for gas extraction and supply

There is another type of connector for extraction and supply of gases inside the reactor chamber. It needs only the leak proof quality. A schematic diagram of the connector sub-assembly is shown in figure 3.4.8. A specially made connector bolt is screwed at the middle of the bottom plate of the reactor chamber, a rubber seal washer is used between the matching parts. Another end of the special connector bolt is clamped with the welded flanged collar at one end of the supply pipe by the tightening the nut. A rubber washer is also used between the matching parts to ensure the leak proof quality.

3.2.1e Cooling Line

Figure 3.5 and 3.7 show the total cooling line of reactor chamber. The top plate of the reactor chamber is the most heated area since the heat generated from the heaters

goes upward to the plate directly, at the same time, the most heat sensitive piezoelectric horn of sound generating system is installed there. Therefore, a water sump is made at the top of the reactor chamber to cool the top portion most effectively and directly by water. In the sump a considerable level of water is maintained by placing the outlet of water at that level for higher cooling efficiency.

Bottom portion of the reactor chamber also needs very effective cooling because there are many rubbers and Teflon sealing elements. Therefore, the outer surface of reactor chamber is covered by cooling coils made of copper tube.

The maximum operating temperature of vacuum gauge sensor is 40^0C. To maintain the temperature within this limit, the gauge sensor is connected through a copper tube coil which is connected with bottom plate at one end by a connector and another end is connected with the gauge sensor. The length of the copper tube is adjusted such that hot gases of reactor chamber passing through the copper coil tube lose the heat and the temperature goes down to the tolerable limit.

3.3 SUB SYSTEMS WITHIN CVD PROCESS

During CVD process, the following sub-systems are working:

1. Gas evacuation system
2. Electric supply system
3. Heating system
4. Cooling system
5. Gas supplying system
6. Sound generating system
7. Substrate cleaning system
8. Measuring system of process parameters
9. Structure and handling system of reactor chamber

3.3.1 Gas Evacuation System

The gases inside the reaction chamber and by-product gases of the chemical reactions are evacuated through stainless steel tube by a rotary vacuum pump. In this

system leak proof connectors are used at both the ends of the tube, one end with the pump and another end with the reactor chamber bottom plate. The outlet pipe from the pump of the evacuation system is submersed into the water to consume the harmful particles in the exhaust gases on its way to environment through the water.

3.3.2 Electric Supply System

In this system, power from 220V is supplied to the different components of the CVD setup through properly designed flexible wire. The circuit diagram of CVD system is shown in figure 3.10. Power enters into the main distribution box through the cable and circuit breaker Sp-63A, which have the capability to carry 50 ampere, since the total system load is approximately 50 ampere. The variacs are also selected on the basis of the power consumption of the heaters. The required voltages of the heater are adjusted through variac. Since, vacuum pump, vacuum gauge, sound generator and oscilloscope consume very low ampere, normal available wires are used for their connection.

3.3.3 Heating System

The heating system is shown in figure 3.6. Thermal CVD to deposit diamond requires high temperature, generally from 800 to 2000^0 C, which can be generated by resistance heating, high frequency induction, radiant heating, hot plate heating, or any combination of these. Resistance heating is used here to obtain the required temperature. In substrate heating; there is a rectangular opening at the top of the substrate heater box. The substrate is placed on this opening, so that heat generated from Nicrom heater, inside the rectangular box is transferred through the opening to the substrate as required by adjusting the supply voltage to the heater by variac. Activation heater operates directly by supplying voltage from variac and the temperature can be adjusted by varying the variac voltage also.

It is a cold wall reactor system, since the substrate to be coated is heated directly by resistance heater while the rest of the reactor remains cool, or at least cooler. The CVD reaction is endothermic, that is: it absorb heat and deposition takes

place on the substrate surfaces, where the temperature is the highest. The walls of the reactor, which are cooler, remain uncoated.

3.3.4 Cooling system

In this system, water from external water source enters into the copper cooling tube from the upper side of the reactor chamber. This water passes through the copper coils and comes out from the lower side of the reactor chamber. After absorbing the generated heat from the outer surface of the reactor chamber during CVD process, water through flexible tube goes to the water sump placed at the top surface of the main reactor chamber and drains out.

A forced cooling by extra fan can be applied if necessary to cool the hot gases passing through the copper tube coil to the sensor of the vacuum gauge, to maintain the temperature at the sensor within the safe limit of 40^0C. The total cooling system is shown in figure 3.7.

3.3.5 Gas Supplying System

The available natural gas of pressure approximately 15 psi from the supply gas pipe line enters into the inlet line through the flow meters. Another flow control valve is connected for better control before the flow meter. Flow meter supply controls amount of gas to the reactor chamber through stainless steel tube and leak proof connector. Another stainless steel tube is connected vertically upto 150 mm above the substrate position inside the reactor chamber from the bottom inlet port of the reactant gases, 75 mm apart from the center of the bottom plate of the reactor chamber is fixed in such a way that the reactant gases can flow from the top of the substrate, and hence an asymmetric flow of gas on substrate is generated during the CVD process shown in figure 3.8.

3.3.6 Sound Generating System

The signal of sound vibration is generated by signal generator. After amplification by an amplifier, this signal of sound vibration passes through the wire to the piezoelectric horn, placed inside the vibration generating chamber. There are two insulated leak proof connectors in the vibration generating chamber, facilitate to pass the sound signal from outside to inside. The sound is generated in the piezoelectric horn since it gets the sound generating signal from signal generator, and passes through hollow pipe towards the substrate. There is a provision to monitor the frequency and amplitude of the generated sound vibration by an oscilloscope, connected parallel with the input wire. The schematic diagram of sound generating system is shown in figure 3.9.

3.3.7 Structure and Handling System

The reactor chamber is supported on a metallic structure. The metallic structure consists of a bottom rectangular structure and upper structure shown in figure 3.4. The reactor chamber is placed on the top of the bottom rectangular structure at its center. Upper structure is made of three pipes, two vertical and one horizontal. The two vertical pipes are at a distance 800 mm apart from each other. At the top end of these two pipes, the horizontal pipe is placed through the holes in the two vertical pieces of pipe, each welded horizontally at the top of the vertical pipes. The upper structure can be disassembled easily for transportation. This upper structure is constructed for holding the mechanical weight pulling mechanism. When the upper part of the reactor chamber is required to assemble and disassemble, the pulling mechanism is used to pull the reactor chamber.

3.3.8 Substrate Cleaning System

In addition to the prior polishing and cleaning by emery paper and acetone respectively, ultrasonic sound is generated inside the reactor chamber towards the substrate from the top for ultrasonic cleaning, before experiment. This ultrasonic

sound is generated in the air medium by the same set up which is made to observe the effect of sound vibration on CVD process. Before the start of the coating process, vacuum cleaning (up to $4X10^1$ Torr) is performed by the extraction of existing gases.

3.3.9 Measuring System

During CVD process, it is necessary to measure the following parameters:

1. Process pressure
2. Temperature of substrate and activation heater
3. Flow of gas
4. Frequency and amplitude of sound vibration

The process pressure during CVD process is continuously measured by a digital vacuum gauge meter. The sensor of the gauge is connected with a copper coil tube by a plastic connector at one end, and the other end of the copper coil tube is connected with the reactor chamber by a metallic connector.

During CVD process, the temperature of the substrate and the temperature of the activation tungsten heater are measured by optical pyrometer looking through the glass window of the reactor chamber. A mounting system is developed to hold the pyrometer properly at the height of the looking window.

Gas flow inside the reactor chamber during CVD process is measured by the gas flow meter from the range of 0 to 1.5 liter per minute. This flow meter is connected to the supply line of the gas, in the reactor chamber.

The frequency and the amplitude of the sound vibration, generated in the reactor chamber during the CVD process, are measured by the oscilloscope, connecting it in parallel with the input line of sound signal towards piezoelectric horn.

3.4 TEST SAMPLE PREPARATION

The test samples used in this investigation is stainless steel 304; its spectro analysis of composition is shown in table 3.3. Test samples of two shapes size are used, one

circular and the other rectangular. Both are manufactured from stainless steel sheet. For circular shapes, metallic die-punch shear cutting machine and for rectangular shaped, conventional shearing machine were used. The dimension of round test sample is 30mm X 2mm and the dimension of rectangular test sample is 14 mm X 22mm X 1.15 mm. Test samples are polished by different grades of emery papers and cleaned with Acetone. Finally, the sample substrate is cleaned by ultrasonic sound and vacuum during the experiment

3.5 EXPERIMENTAL CONDITIONS

A CVD coating system has been designed and fabricated with a view to coat a substrate by carbon from methane gas by high temperature hot filament activation.

The system has the facilities to vary the following process parameters. The process parameters are: reactor chamber pressure, substrate heater temperature, reactant gas activation temperature, gas flow, sound with different frequency, location of sound source and distance between substrate and activation heating coil.

The ranges of these parameters that can be adjusted by this equipment are as follows:

Vacuum of the reactor chamber: atmospheric pressure to 10^{-1} Torr

Substrate heater temperature: approximately 2000^{0}C maximum

Activation temperature: approximately 2000^{0}C maximum

Gas flow: 0.1 - 1.5 liter/minute

Frequency of sound: 0 - 1 MHz

Location of the sound source: Top and side of the chamber

Gap between substrate and activation heater: 3 mm to 50 mm maximum

The process parameters of coating were selected on the basis of the principles of thermal CVD (hot filament) process [1], [76-81]: According to these references, the process parameters are as follows:

Activation heater temperature: 2000^0C or slightly higher,

Distance between the hot metal and substrate: about 1 cm

Substrate temperature: 800 and 1000^0C

Deposition pressure: 0.5 - 40 Torr

Reactant gas: Methane (CH_4)

The substrate material and its size were chosen according to the reference [76], [79], [82] for convenience of heating, fixing and further analysis.

During the initial experiments, the following values of the process parameter were used:

Initial vacuum of the reactor chamber: 10^{-1} Torr

Purging by methane gas: up to atm pressure

Pressure during coating: 15 Torr

Substrate temperature: 1000^0C

Activation temperature: 2000^0C

Methane gas flow rate: 1.5 litre/minute

Substrate used: Stainless steel 304

Size of the substrate: diameter 30 X thickness 3 mm

Reactant gas: CH_4 (methane)

The coating of carbon was deposited on the substrate and these coated samples were used for further characterization.

3.6 PROBLEMS ENCOUNTERED DURING CONSTRUCTION EXPERIMENTATION

Initially, the desired vacuum of 10^{-1} Torr could not be attained even after long time of operation of the vacuum pump. To find out the cause of this problem, micro crack in welding region, leakage in the sealing points were tested. To ensure these, hydro-tests were performed. This hydro-test was done by introducing air at high pressure (10 bars) into the reactor chamber, and then the total reactor chamber was

submerged into the water, and found that some air bubbles through the micro cracks in welding and sealing points. To rectify these problems, re-welding at the points of micro cracks were done, and proper sealing were ensured by tightening at different location. Finally the total system again was retested to find the leakage and was found alright.

After evacuating several times, it was observed that, time required to attain 10^{-1} Torr was about 3 hours all the times. It needs 8 to 9 minutes to attain 1 Torr, then it needs another 20 minutes to attain 4×10^{-1} Torr. But after that, due to high vacuum, the evacuating rate was slow for a rotary pump.

After installing substrate heater inside the reactor chamber, the problem of non-attaining the desired vacuum arose again. In this case, after 2 hours of continuous running of vacuum pump it was impossible to reduce pressure below 1 Torr. To sort-out the cause of this problem, again hydro tests were done to re-examine the crack in welding region and leakage in sealing points but no leakage was detected. Since the vacuum level was satisfactory before introduction of the substrate heater, again vacuum was checked without the heater and the vacuum level was found satisfactory as before. It thus indicated that, the problem lied with the heater. Then the behavior of each components of the substrate heating system in vacuum were studied and analyzed. It was found that the asbestos which was used as top plate of the heater evaporates at this level of vacuum and temperature which restrained the chamber to become highly evacuated. To avoid the problem, the asbestos plate was replaced by a very thin sheet of mica.

After attaining the required (4×10^{-1} Torr) vacuum, the substrate heating was started. Due to heating, pressure in the chamber raised upto 8×10^{-1} Torr. As the vacuum pump was on, the pressure inside the chamber again came down to 4×10^{-1} Torr. After heating for 30 minutes, the substrate was gradually becoming reddish color and within next 20 minutes, the temperature of substrate rose to about 1000^0C

In some cases the substrate heater was fused during the operation. After examined, it was found that Nicrom filament of substrate heater was fused at the point of sharp bends, at the point of loose connections and some of the clamping screws were damaged due to high temperature. The substrate heater was constructed again maintaining tight connections and avoiding all kinds of sharp bends.

Initially, tungsten wire of diameter 1 mm was chosen to make activation heater. It was in the form of straight wire. As the tungsten wire is brittle, it was not possible to make a proper heating coil. As the substrate size was 30 mm in diameter, it was needed to make a heater coil approximately of the following sizes: coil diameter 10 to 15 mm, and length 30 mm to 40 mm. Therefore a coil with minimum sharp bend and almost uniform diameter was fabricated.

The experiment was carried out by using the above heater. The temperature was gradually increased by increasing the voltage up to 7V, corresponding current was about 30A (temperature was approximately 1400-1500^{0}C). During this operation, the heater was fused after 7 to 8 minutes due to sharp bend. After this incomplete test, the substrate was studied and found slight coating deposited on it.

Again another experiment was carried out under similar conditions, after making the heater coil more uniform. But during operation of approximately 7 minutes the heater again got fused and at the same time the looking glass of the reactor chamber also were broke. After through examination, some rubber seal elements used in connectors were found slightly melted. The looking glass and rubber seal found damaged due to the high temperature.

To solve the problem of improper cooling of the vacuum chamber, two decisions were taken: 1) An extra cooling system was to be incorporated, 2) redesign the looking system to keep it far apart from heat source.

The looking glass location was shifted apart, by modifying the design of reactor chamber. Initially the shape of the looking glass was 10 inch X 4 inch at the circumference of the reactor chamber. Due to over heating problem, this window was closed by stainless steel plate keeping a hole of diameter 4 inch at the middle of the plate. A pipe (length 125 mm and inside diameter 90 mm) was welded at one end with the circumference of the hole and a looking glass was clamped at the other end.

To solve the fusing problem of the activation heater, another filament (of dimension 0.2 mm diameter, coil diameter 4 mm, length 40 mm) was selected. This filament also provided the advantage of low ampere requirement at high temperature. To install this heater, the clamping system was modified.

The shape and size of the substrate was modified from round to rectangular. This modification was done for easy mounting in XRD machine for characterization. This modification also lowered the substrate heating time from 50 minutes to 25 minutes because of reduction of the size and thickness of the substrate.

According to our initial target to achieve the vacuum level of 10^{-1} Torr to extract the existing gases in the reactor chamber at the beginning of the experiment, time needed were about 3 hours. But within 27 minutes vacuum level of 4×10^{-1} Torr was attained. Several experiments were performed at different level of vacuum to obtain the optimum vacuum with respect to time required for evacuation. It was found that there were no trace of O_2 & N_2 in the deposited coating by XRD analysis up to the vacuum level of 4×10^{-1} Torr, which is the evidence that in the residual gas of the reactor chamber no trace of O_2 & N_2 is present up to the vacuum level of 4×10^{-1} Torr, so that instead of 10^{-1} Torr (as the initial process parameter), 4×10^{-1} Torr was used for initial extraction of reaction chamber gas to reduce the experimental time considerably.

Similarly to optimize the level of vacuum for purging, several experiments were done by varying the vacuum level. Vacuum level of 1.5 Torr was found as the optimum level for purging.

There was another problem due to which no deposition were found even though the gauge was perfectly calibrated. After investigation, it was found that, current passed through the activation heater decreased considerably, which lowered down the activation temperature. Examining the heater thoroughly, some micro crack or partial break of filament wire was identified.

Sometimes, malfunction of vacuum gauge was found. This might have been due do the high temperature of the gases in the reactor chamber, which come in contact with the vacuum gauge sensor whose maximum operating temperature was 40^0 C. This high temperature was lowered down within the tolerable limits by increasing the cooling of the vacuum chamber. The cooling effect was increased by increasing the flow rate of cooling water into the reactor chamber.

Sometimes deposition was not found after experiment. The readings of vacuum gauge heater temperature were examined several times. No problem was

identified. Then calibration of vacuum gauge was tested. The calibration of the vacuum gauge was made by mercury manometer. Some calibration problem was found and rectified. After that, occasionally, the calibration of vacuum gauge was done.

Experiments were done with different level of gaps between substrate and activation heater. It was found that when the gap is very low (approximately 3 mm) the over-load current supply lines tripped as a result of touching the heater filament with substrate due to sagging. Examining the activation tungsten heater, it was found that, the tungsten heater filament loses its strength with heating time, which might increase sagging problem.

Adjusting all the above parameters, successful coating was done on the substrate, which was further analyzed.

3.7 DESCRIPTION OF THE EXPERIMENTAL PROCEDURE

The experimental conditions are shown in table 3.4.

The setup handles two distinct groups of test. They are:

(a) Experiment without vibration,

(b) Experiment with vibration

The sequences of experimental procedure are as follows:

1. Before conducting deposition, the substrate is prepared by cleaning and polishing.

2. Initial weight is taken by a weighing machine.

3. Upper portion of the main reactor chamber is pulled out by manual lifter from the lower portion of it

4. The substrate is placed on the opening of the substrate heater.

5. The upper portion of the main reactor chamber is pulled down on the bottom plate.

6. Provide ultrasonic sound vibration of 100 kHz, for further cleaning.

7. The vacuum pump is switched on to pump out inside gases. The

vacuum is maintained at 4.0×10^{-1} torr.

8. The methane gas is introduced inside the reactor chamber up to the vacuum level 1.5 torr for purging

9. After 1.5 torr vacuum level, the methane gas supply is closed.

10. The substrate heater is switched on after attaining vacuum level of 4.0×10^{-1} torr.

11. The substrate heating is carried out until the substrate is being heated to 1000^0C.

12. In the mean time cooling is started to maintain the required temperature of the reactor chamber.

13. The main reactant gas methane is allowed to flow through the flow meter. The flow rate was 1.5 l/min.

14. During the supply of methane gas, the vacuum pump is closed at a vacuum level of 1.5 torr.

15. The gas flow is closed up to the required vacuum level.

16. The activation heater is switched on and adjusted up to the temperature $1800-2000^0$C.

17. Immediately after switch on the activation heater, the sound generator is also switched on. For without vibration only the temperature of activation heater is maintained to the required time. For vibration both the temperature of activation heater and vibration supplied are maintained up to the required time. The chemical vapor deposition is performed during this time.

18. Cooling is continued so that the temperature of the reactor chamber comes down to the room temperature.

19. After cooling, the substrate is collected from the chamber after lifting the upper part of the chamber.

20. Characterization of the coating is performed.

The total time required for one experiment for deposition is approximately 4 hours.

The test samples before and after deposition are shown in figure 3.12.

3.8 CHARACTERIZATION OF THE DEPOSITED COATINGS

Characterizations of the deposited coatings are performed as follows:

Following instruments are used:

1. Weighing machine
2. Optical Microscope
3. Scanning Electron Microscope (SEM) attached with energy dispersive X-ray spectrometry (EDX)
4. X-ray diffraction (XRD)
5. Spectrometer

The weight difference is obtained by taking weights of specimen before and after deposition by digital electronic balance of 0.0001 gm accuracy. The deposition rates of the coating in gram per unit area per unit time were calculated from the weight difference of substrate before and after deposition. The microstructure of X-sectional side view of deposited specimen is studied under Optical Microscope and Scanning Electron Microscope (SEM). The surface morphologies of the deposited coatings were investigated by SEM attached with energy dispersive X-ray spectrometry (EDX) X-ray diffraction (XRD) with target of Mo (Zr), 30 kV/20 mA and an incident angle of 1^0, is used to study the composition of coated material. The substrate material and coated material composition are also examined by Spectrometer.
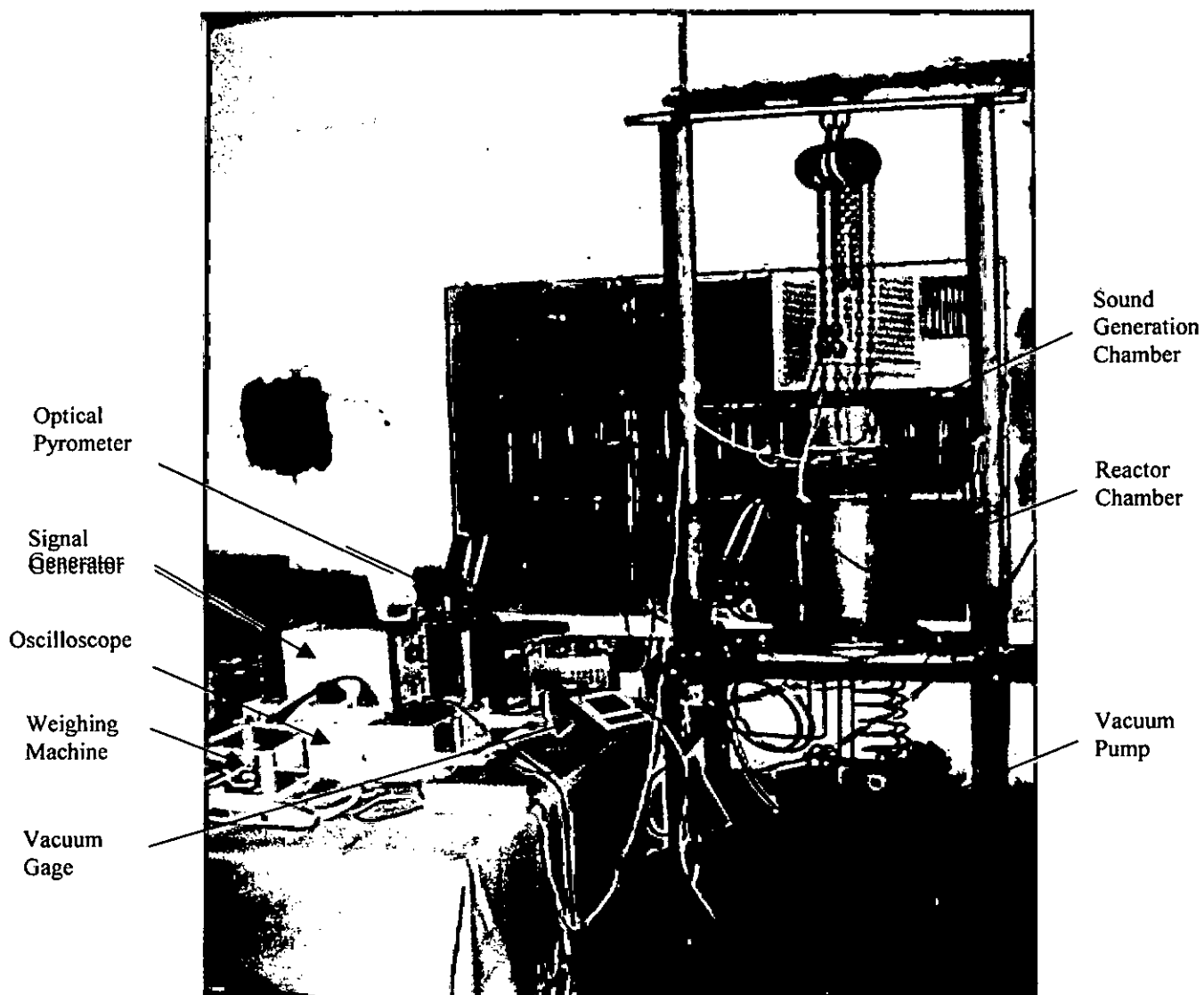
Fig. 3.1 Hot filament chemical vapor deposition setup including related measuring instruments

Water Sump

Upper Cylindrical Body

Looking Glass

Copper Tube

Substrate Heater

Connector For Heater

Lower Plate
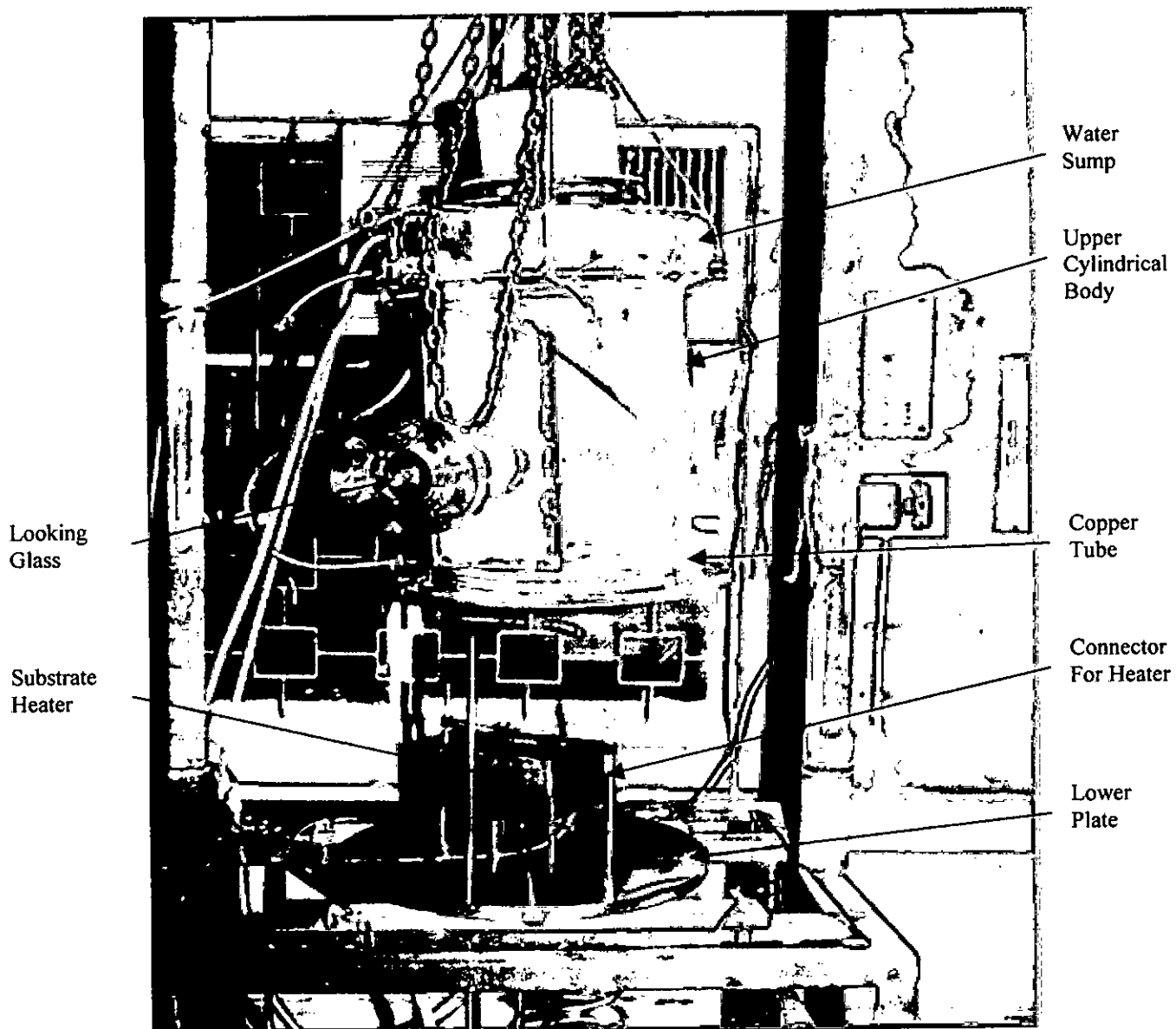
Fig. 3.2 Reactor chamber with inside arrangement
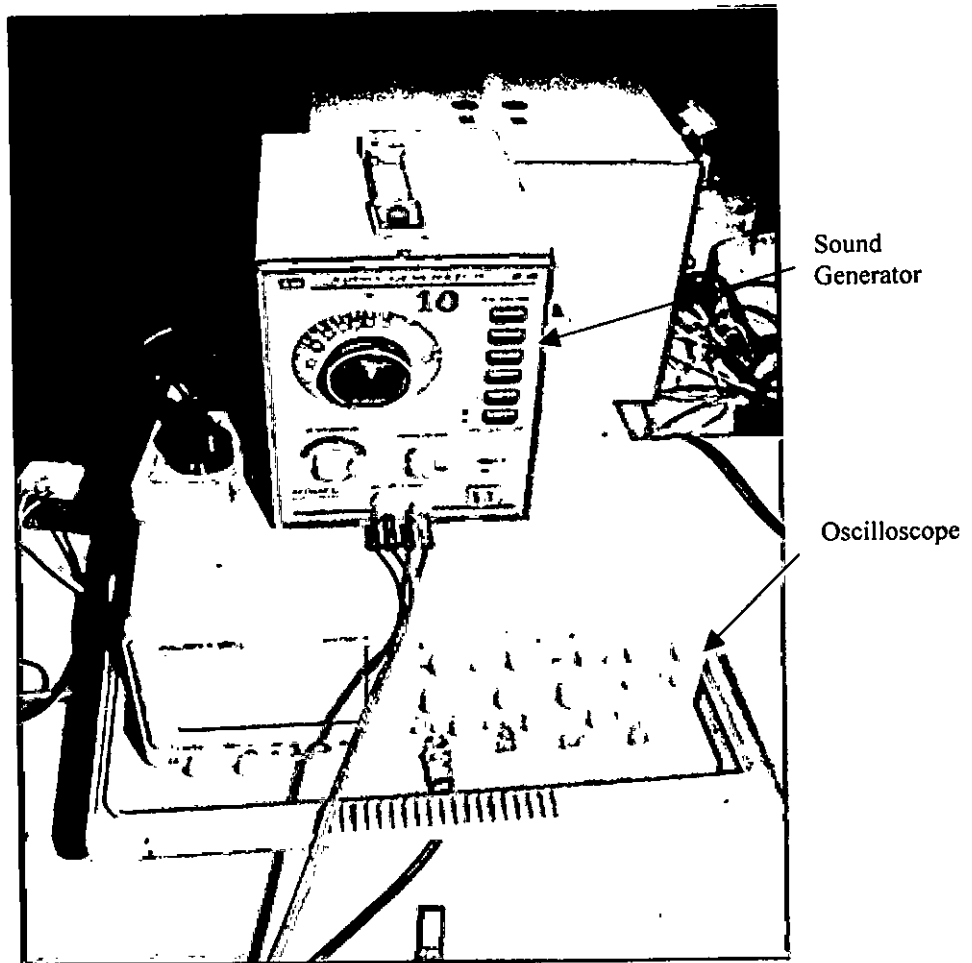
Fig. 3.3: Sound generator and oscilloscope

1. Reactor Chamber
2. Water Sump
3. Substrate Heater
4. Activation Heater
5. Sound Generating Chamber
6. Connector for Activatation Heater
7. Connector for Substrate Heater
8. Connector for Vacaum Pump
9. Connector for Gas Inlet
10. Gas Regulator
11. Gas Inlet Pipe
12. Vacuam Gauge Sensor
13. Water Pot
14. Vacuum Pump
15. Looking Glass
16. Connector for Vacuum Gauge
17. Copper Tube

VACUUME CHAMBER
BASE PLATE VIEW

86

FRONT VIEW

SIDE VIEW
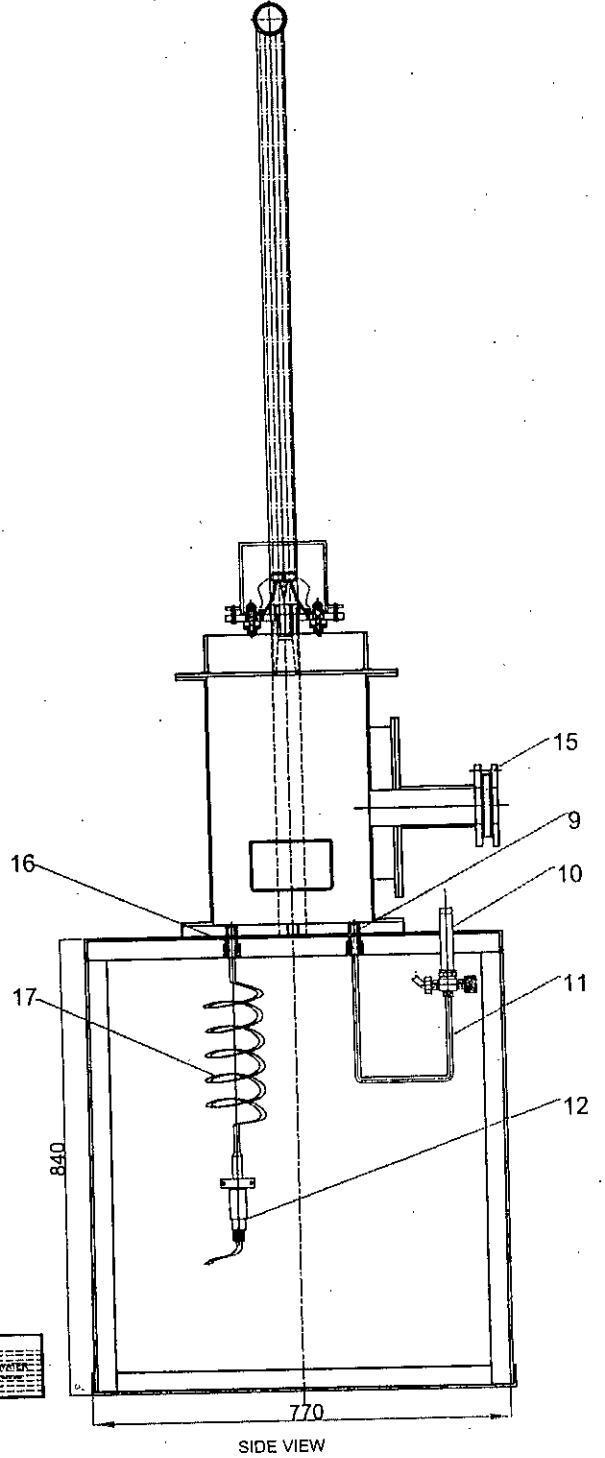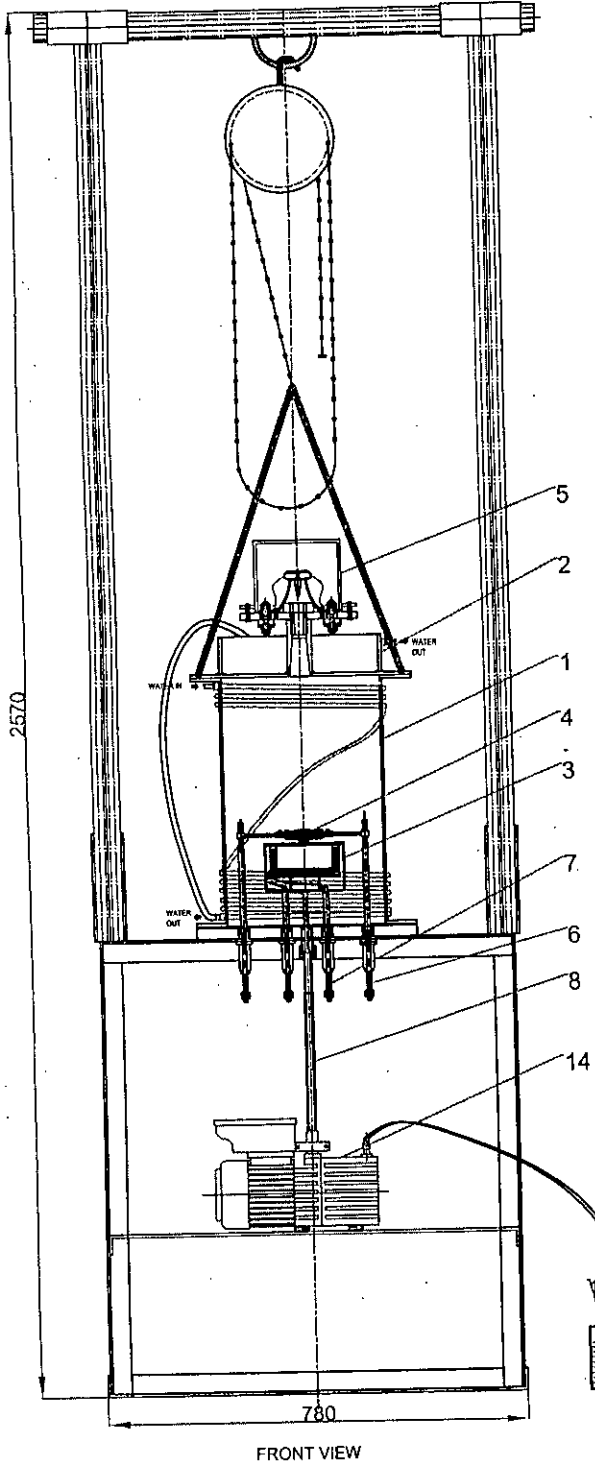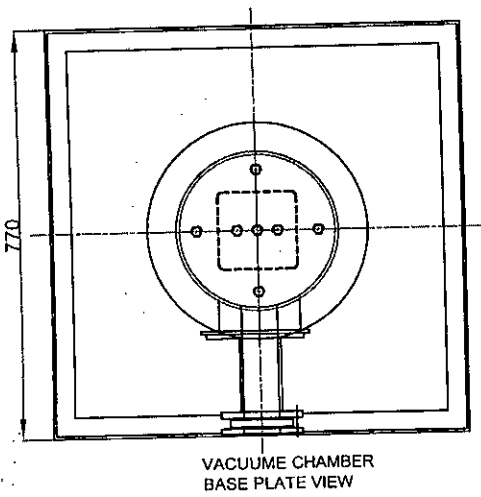
Fig 3.4 Schematic Diagram of Different Views of CVD Setup
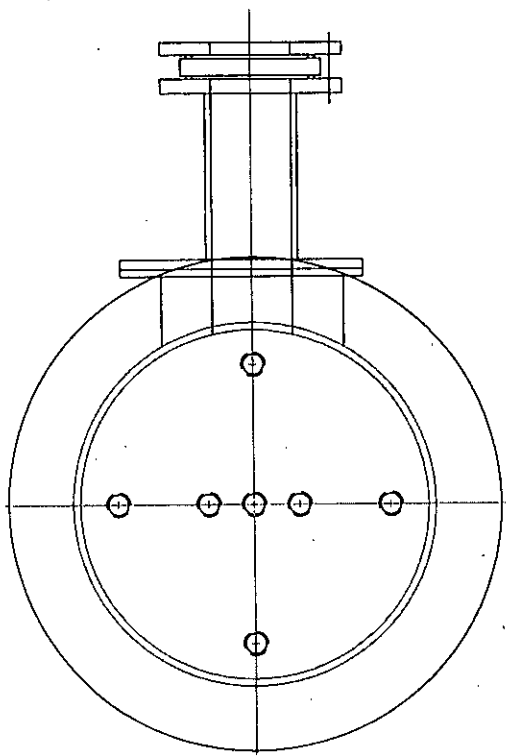
a) Main Body

b) Looking box

c) Looking Flange

d) Bottom Plate

Ø408

483

a

d

b

c
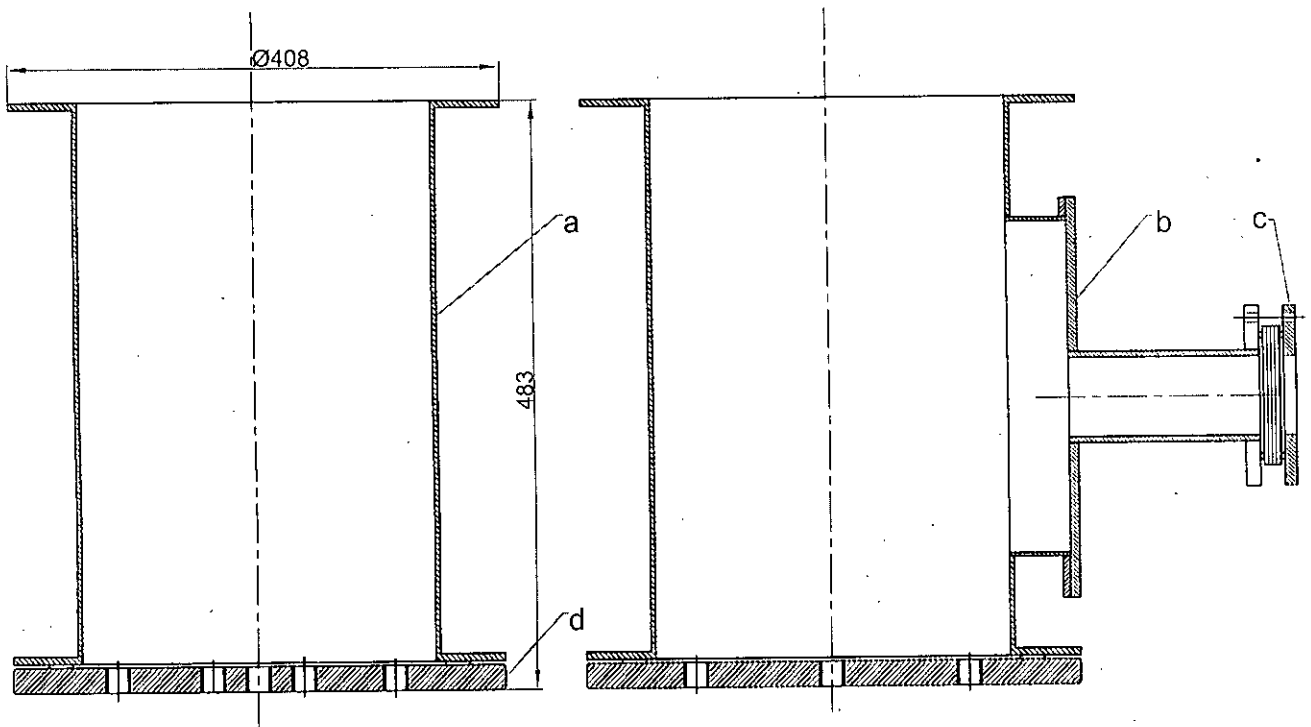
Fig. 3.4.1. Sub-Assembly of Reactor Chamber
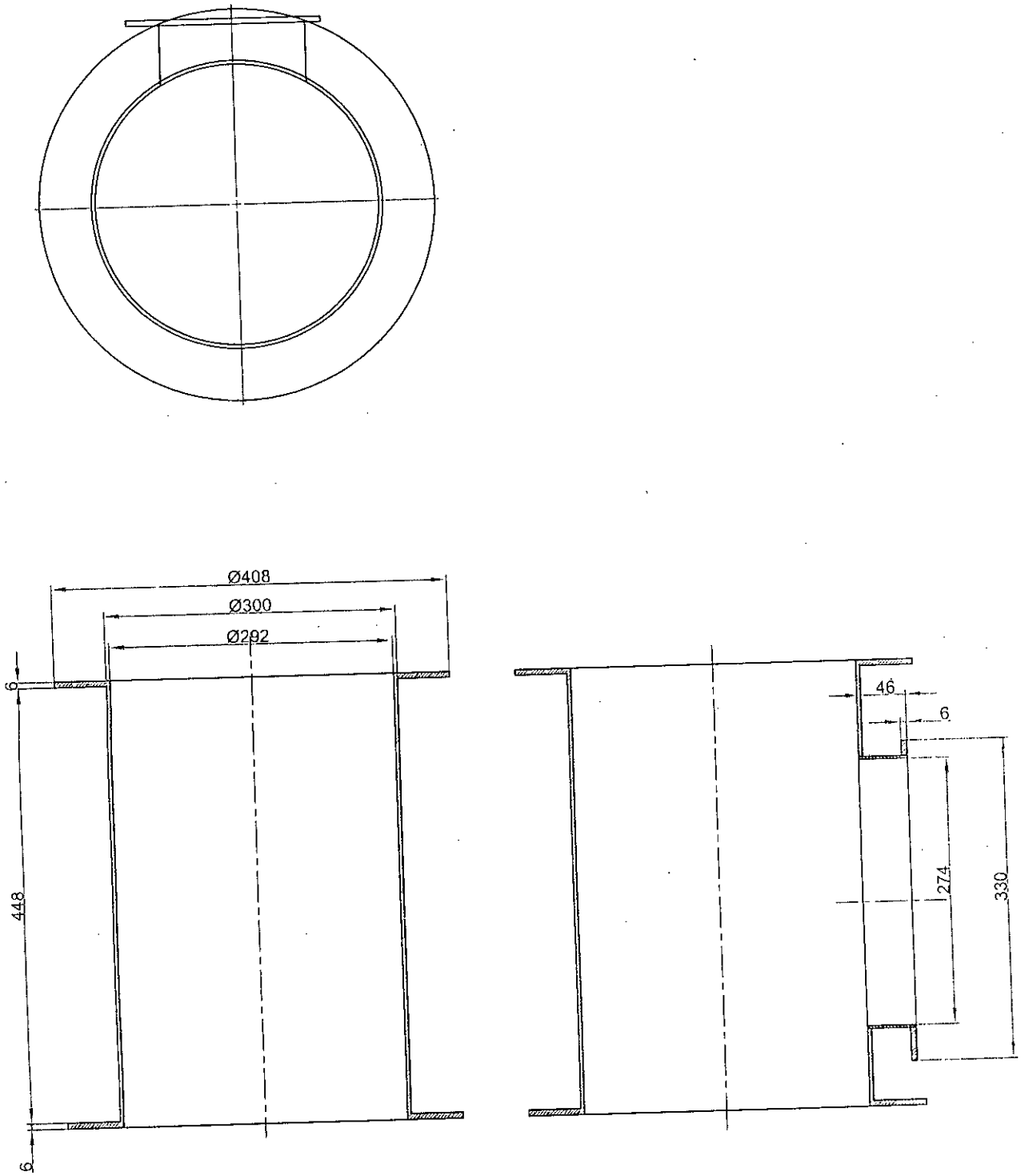
Fig. 3.4.1a. Main Body
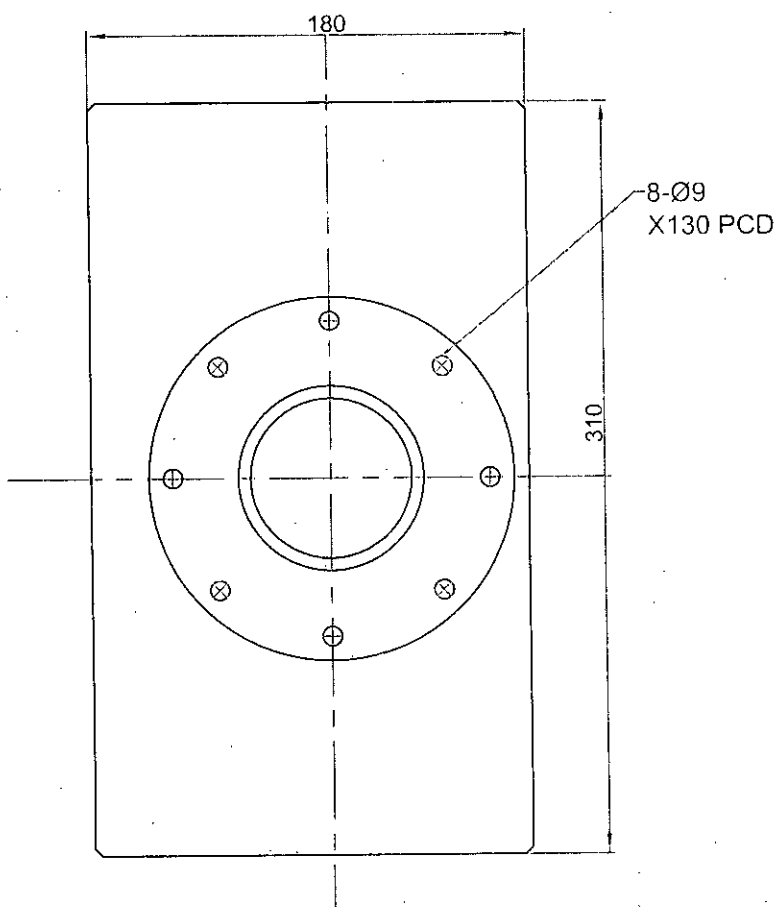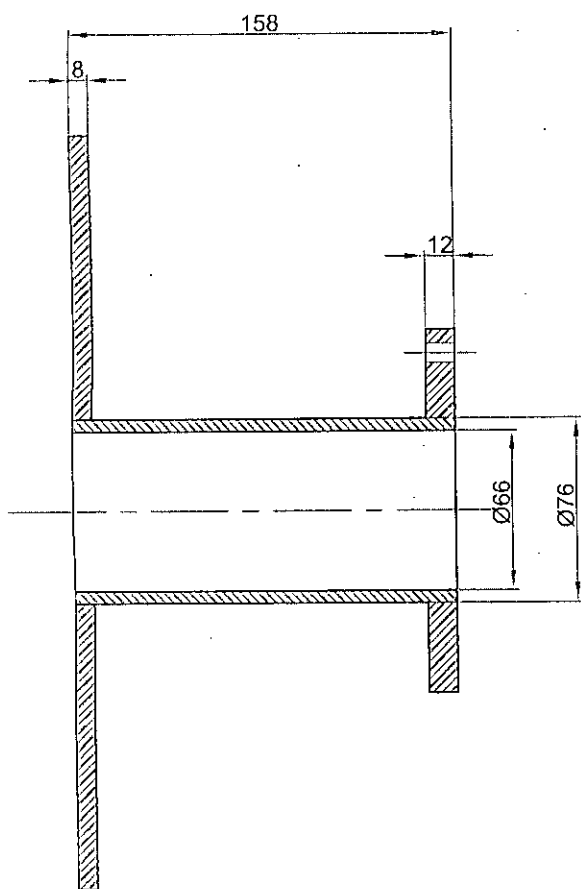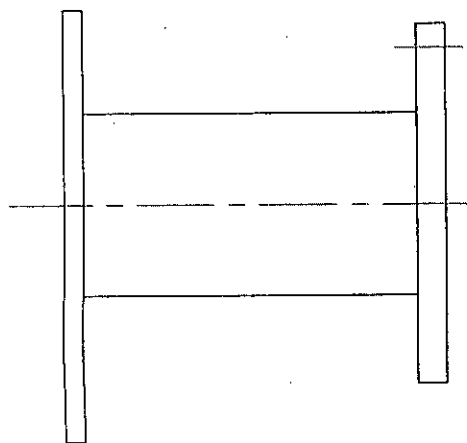
Fig. 3.4.1b. Looking box

8-Ø9
x130 PCD

Ø150

Ø66

10

Fig. 3.4.1c. Looking Flange

4-M20x230 PCD

2-M20x75 PCD

Ø408

20
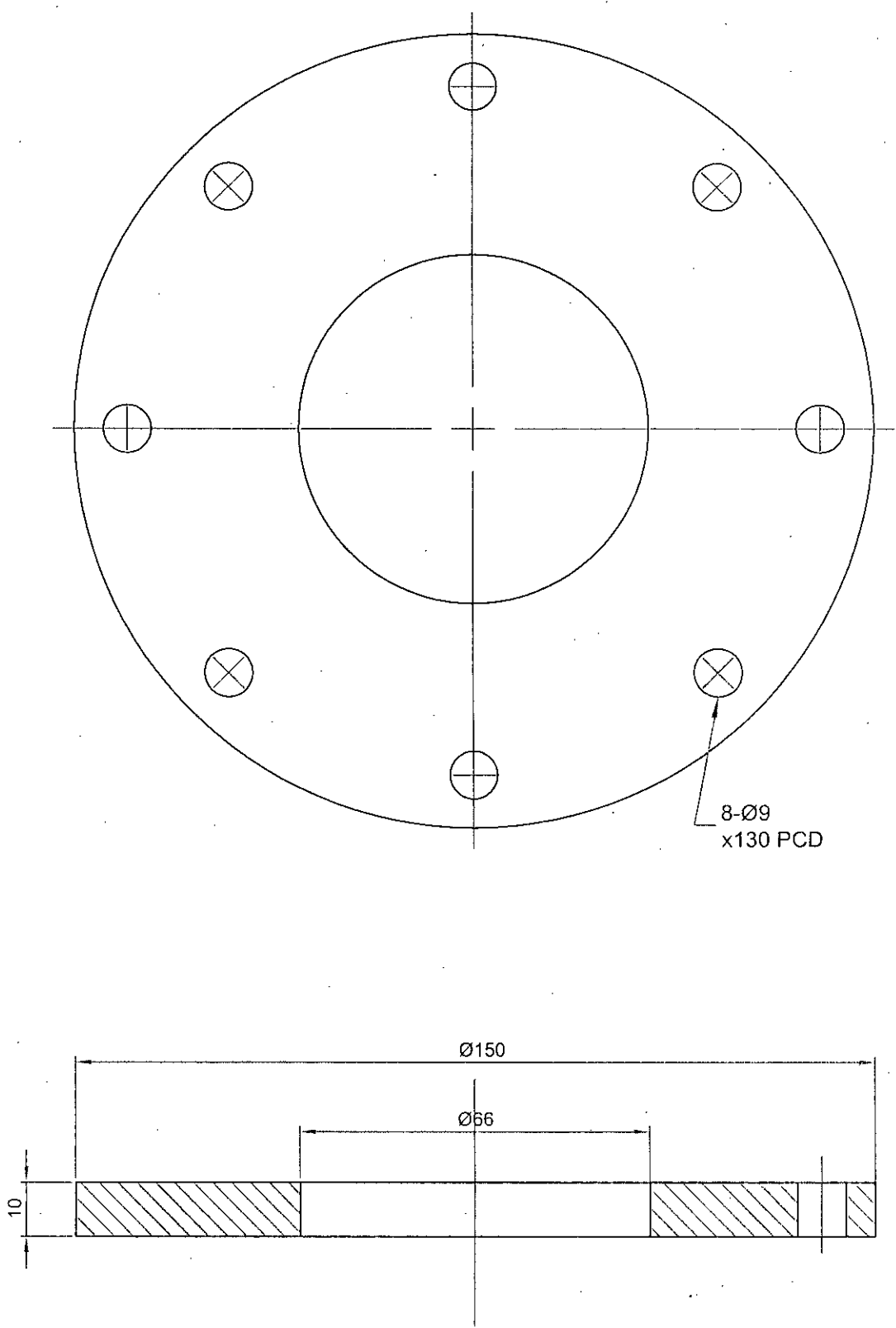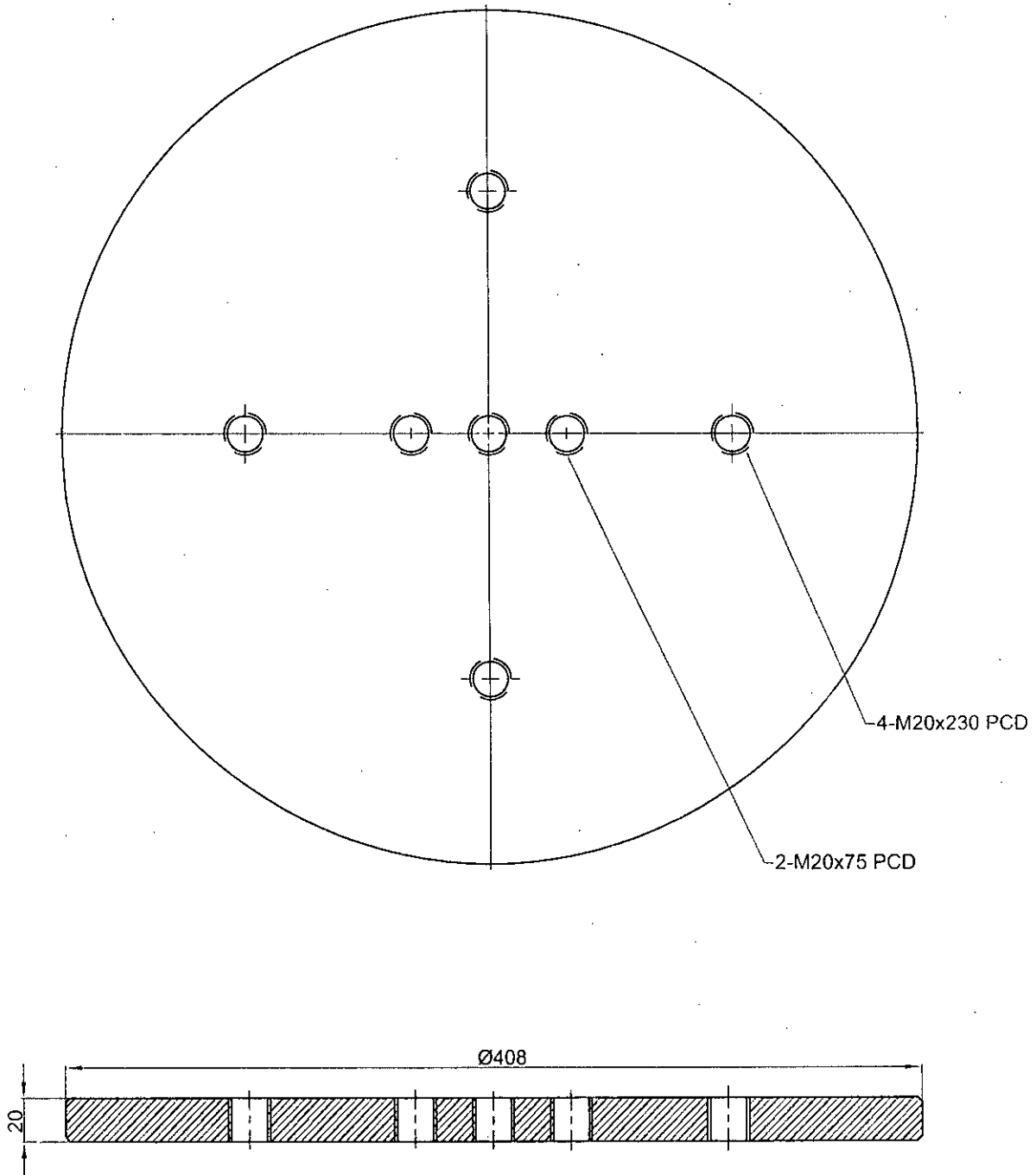
Fig. 3.4.1d. Bottom Plate

a) Water Sump Body

b) Back Plate

a

b
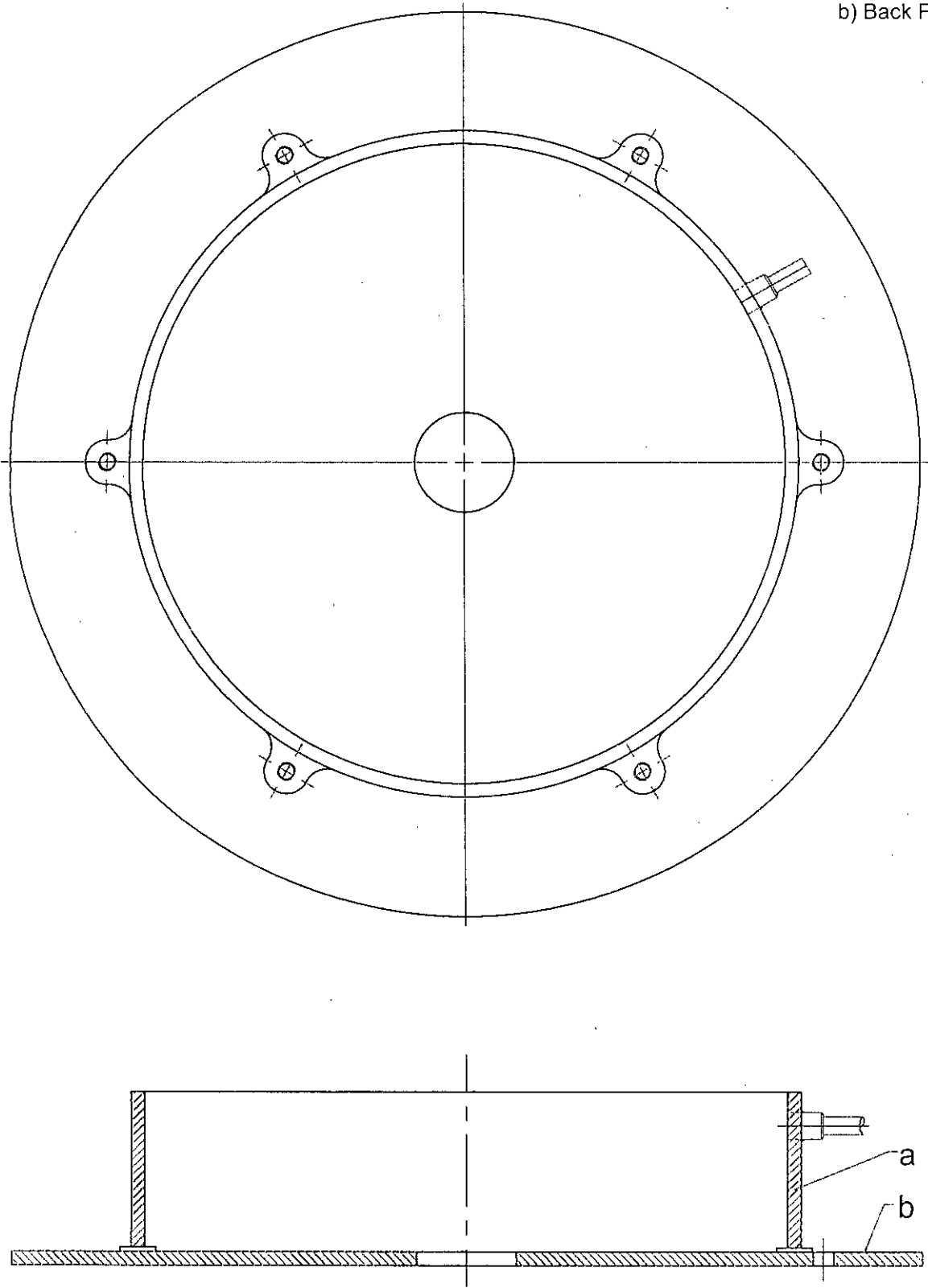
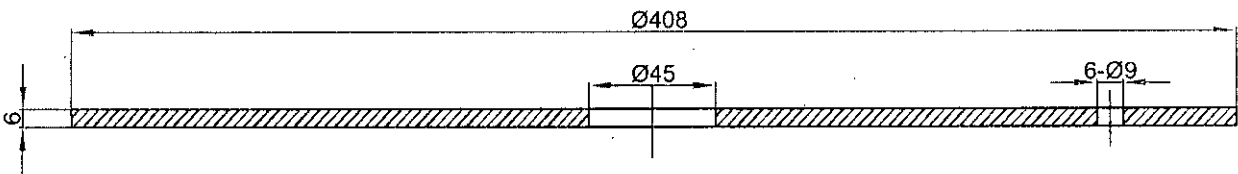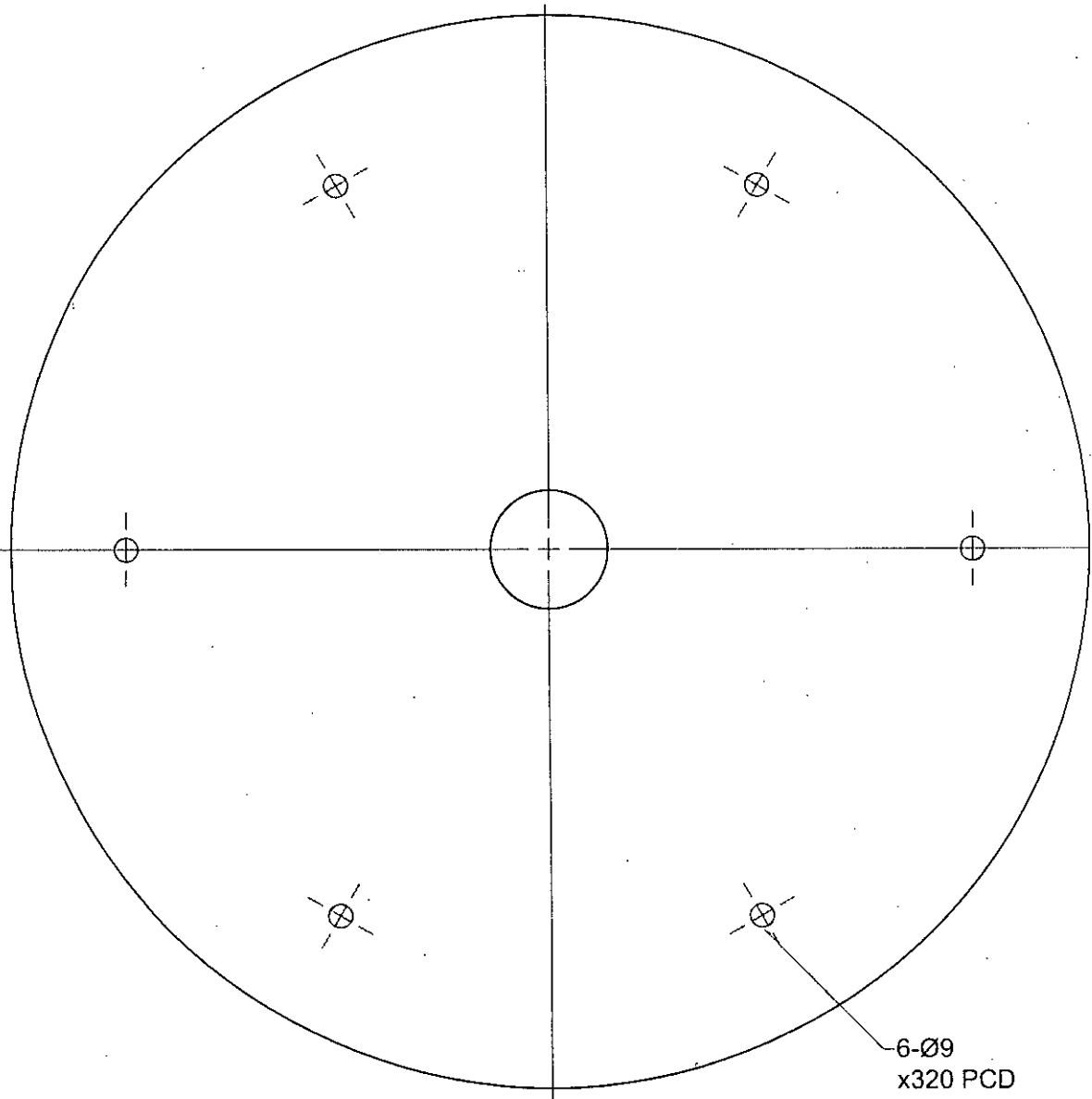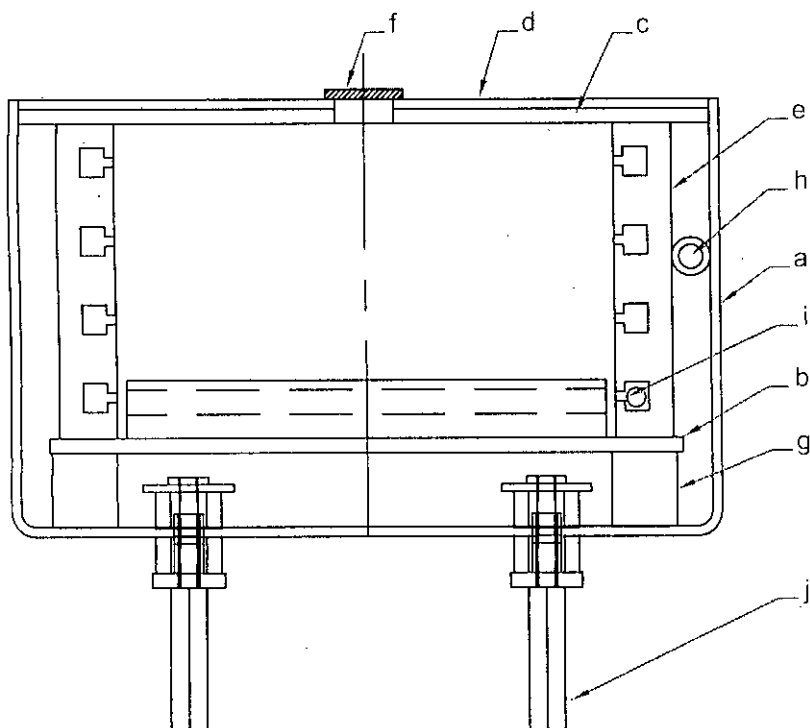**Fig. 3.4.2. Sub-Assembly of Water Sump**
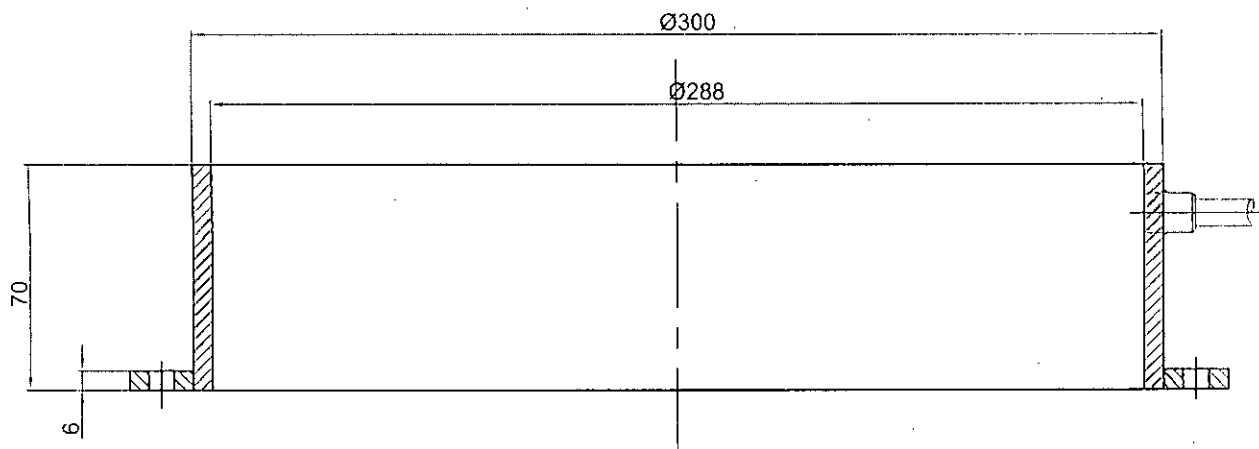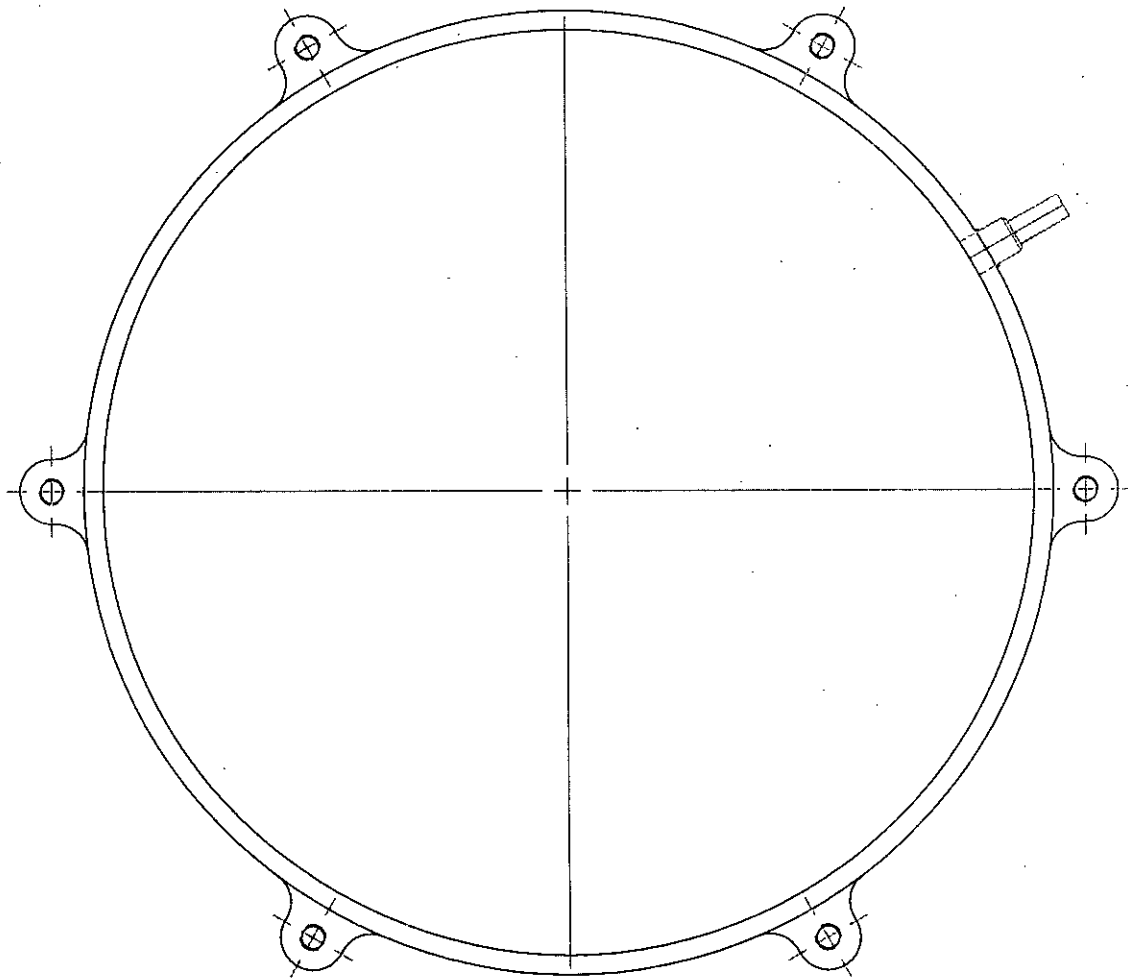
Fig. 3.4.2a. Water Sump Body

Fig. 3.4.2b. Back Plate
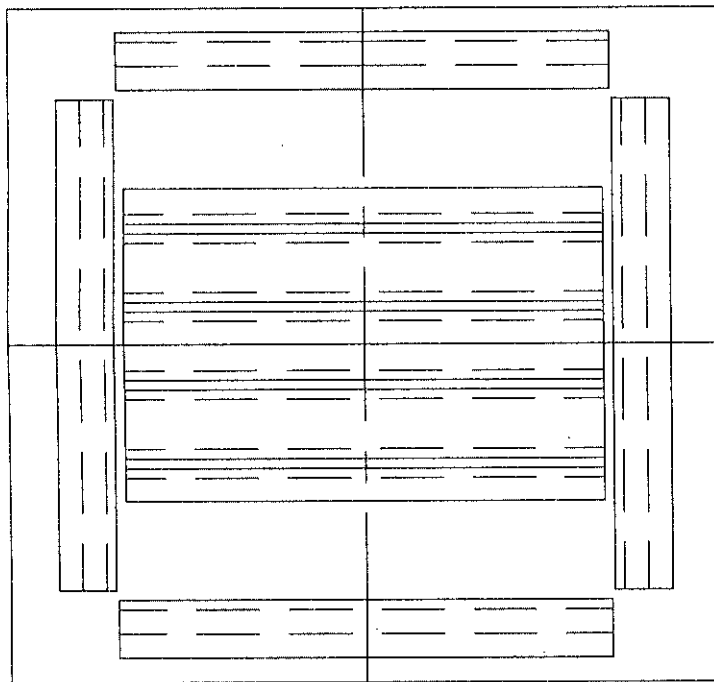
a) SS Heater Box

b) SS Base Plate

c) SS Top Plate

d) Mica Sheet

e) Heat Resistant Clay Block

f) Substrate

g) Ceramic Block

h) Separator Ceramic Washer

i) Nichrome Heater Coil

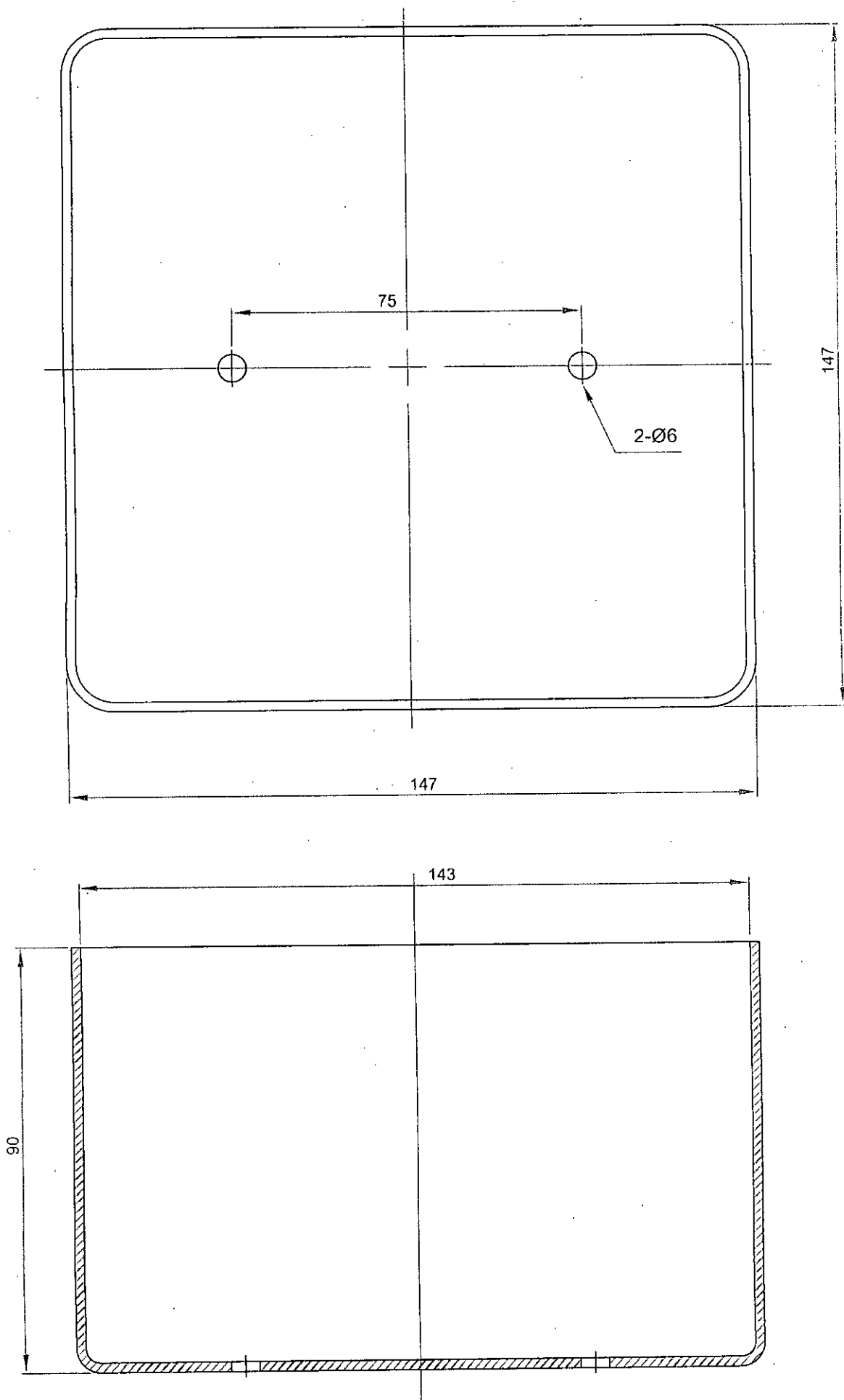j) Connector

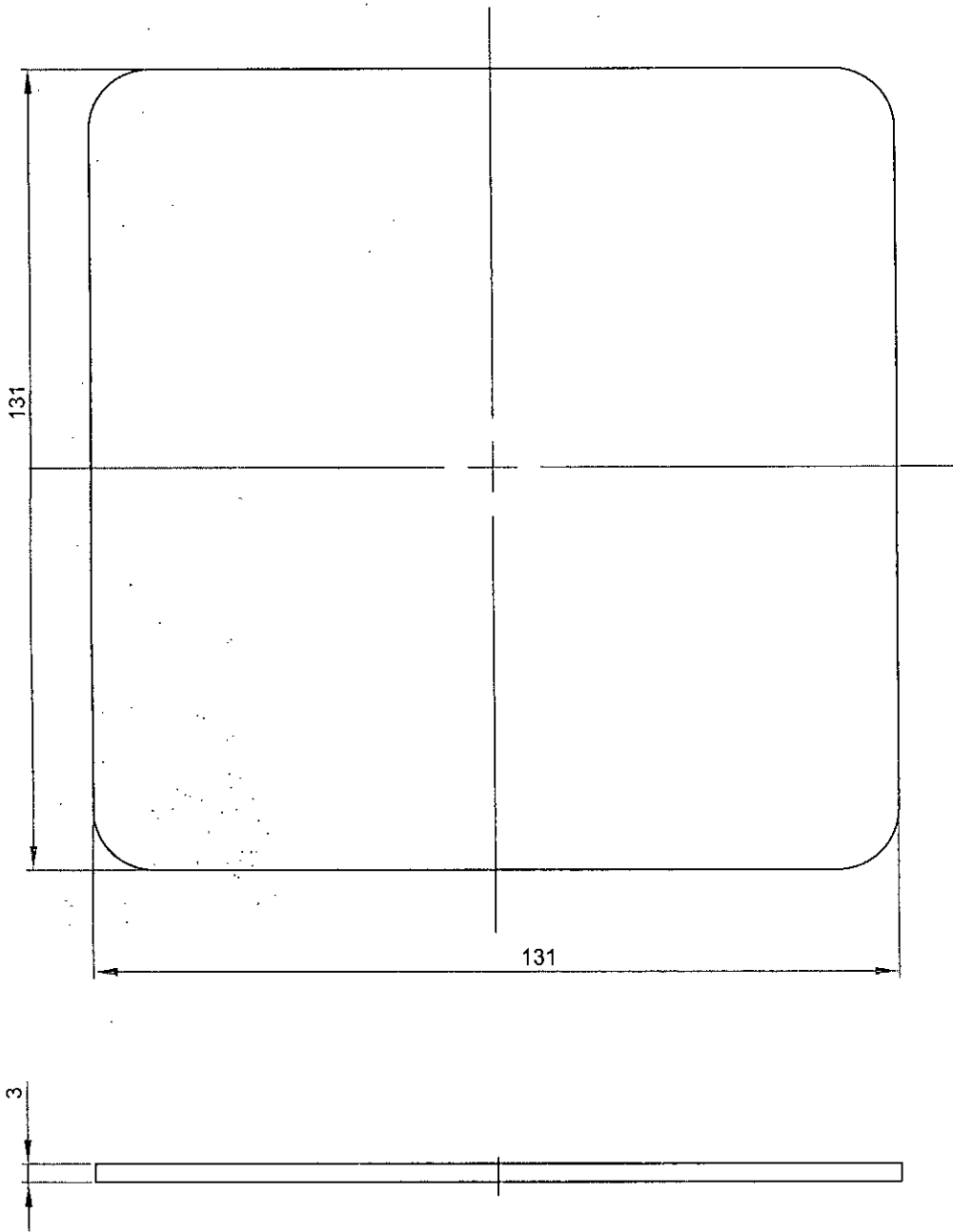**Fig. 3.4.3. Sub-Assembly of Substrate Heater**
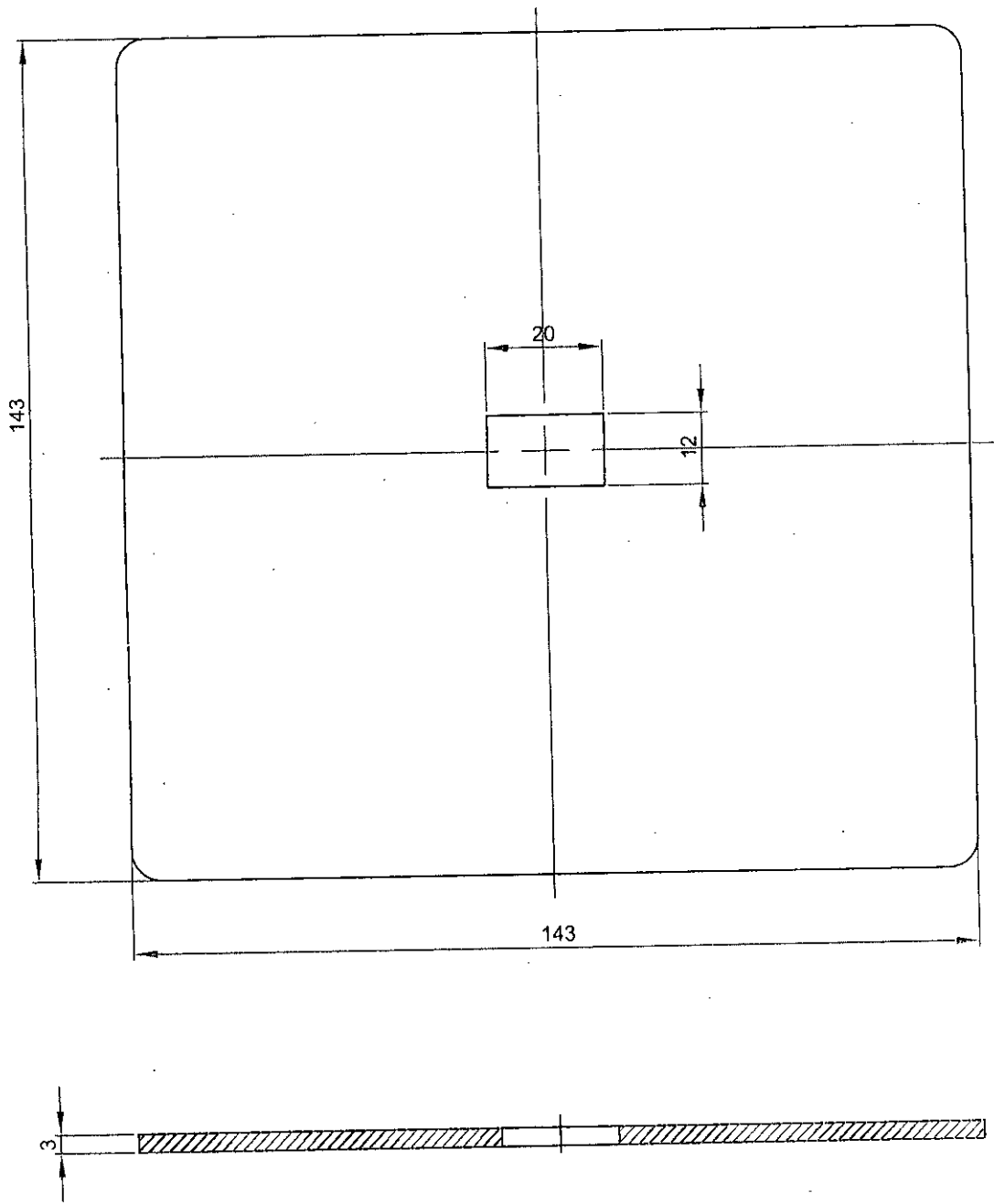
Fig. 3.4.3a. SS Heater Box

131

131

3

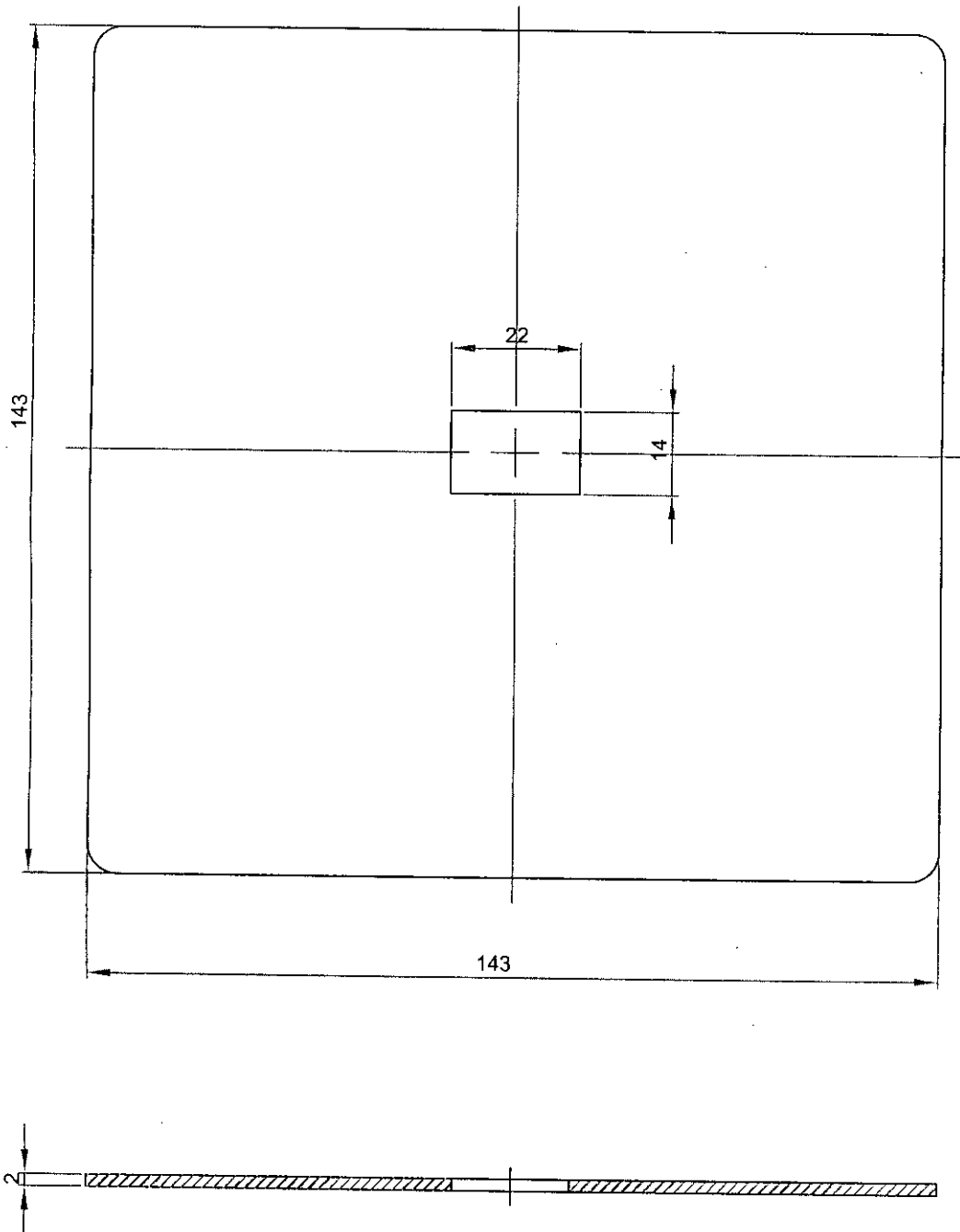**Fig. 3.4.3b. SS Base Plate**

Fig. 3.4.3c. SS Top Plate

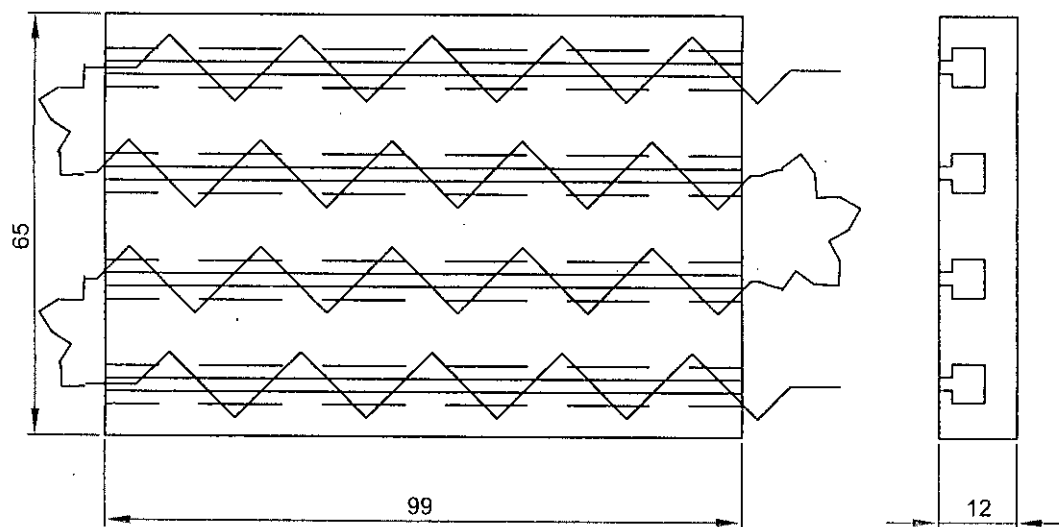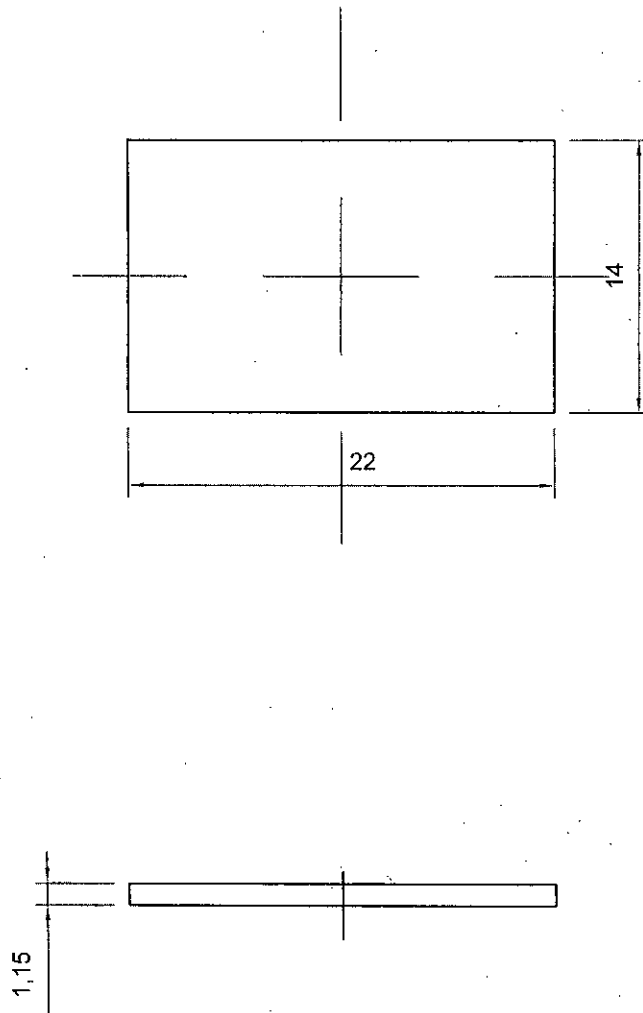**Fig. 3.4.3d. Mica Sheet**

Fig. 3.4.3e. Heat Resistant Clay Block

Fig. 3.4.3f. Substrate

1. Connector Rod

2. Metalic Washer

3. Ceramic Inside Washer

4. Ceramic Washer

5. SS Box Bottom Plate

6. Ceramic Washer

7. SS Washer

8. Clamping Nut
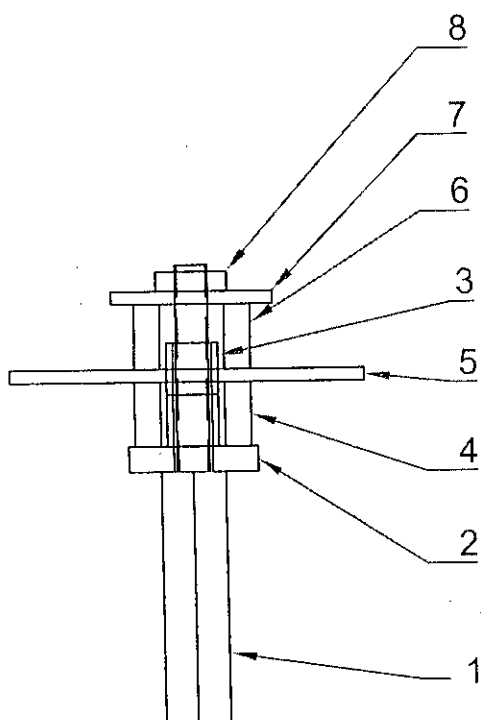
Fig. 3.4.3j. Sub Assembly of Connector.

a) Connector and Support Rod

b) Extension Rod

c) Holder with Extension Rod

d) Extension Rod Holder Screw

e) Heater Element Holder Screw

f) Holder with Heater Element

g) Heater Element Holder Screw

h) Tungsten Heater Element
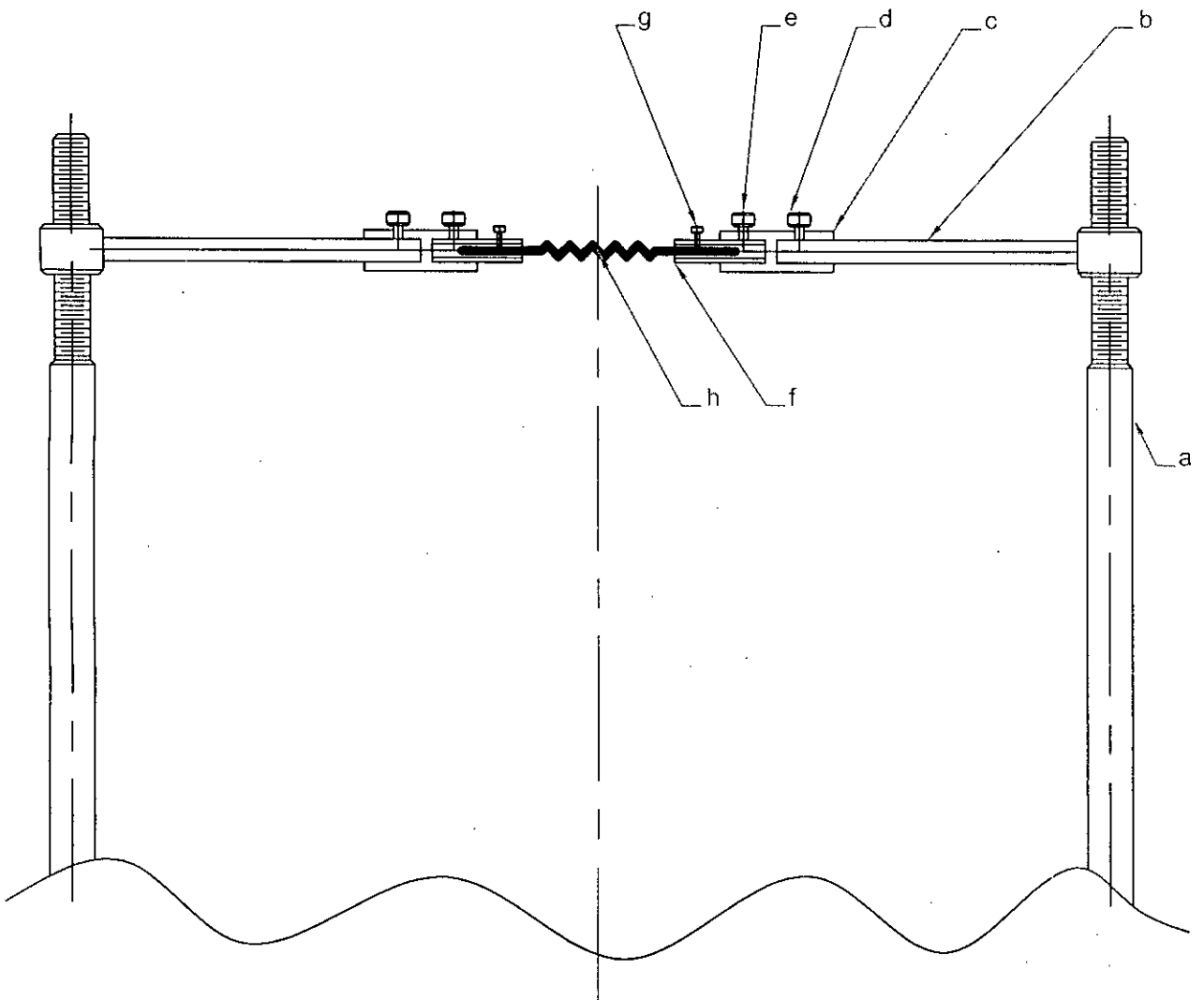
Fig. 3.4.4. Sub-Assembly of Activation Heater
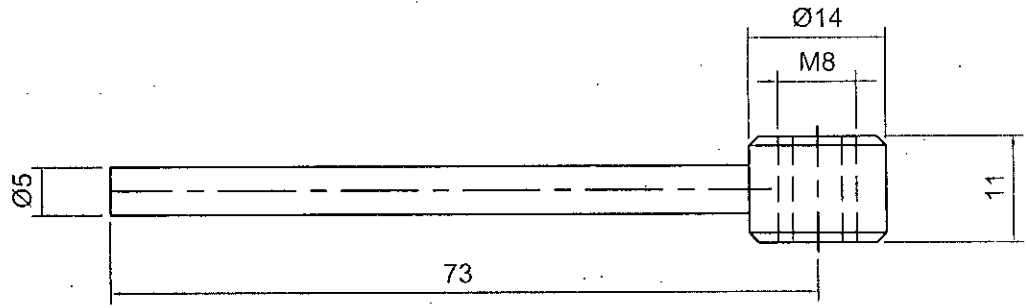
Fig. 3.4.4b. Extension Rod
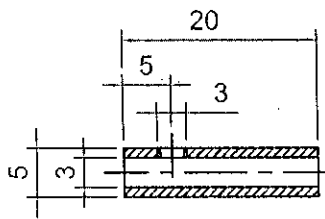
Fig. 3.4.4c. Holder with Extension Rod
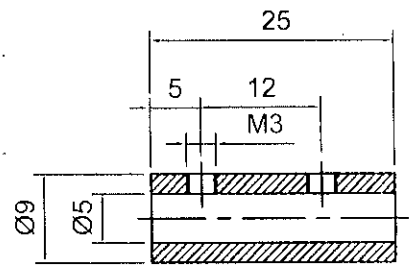
Fig. 3.4.4f. Holder with Heater Element

a) Sound Generating Chamber

b) Chamber Flange

c) Bottom Plate

d) Internally Threaded Hollow Pipe

e) Hollow Bolt

f) Teflon Bolt

g) Connector Rod

h) Metalic Washer

i) Horn
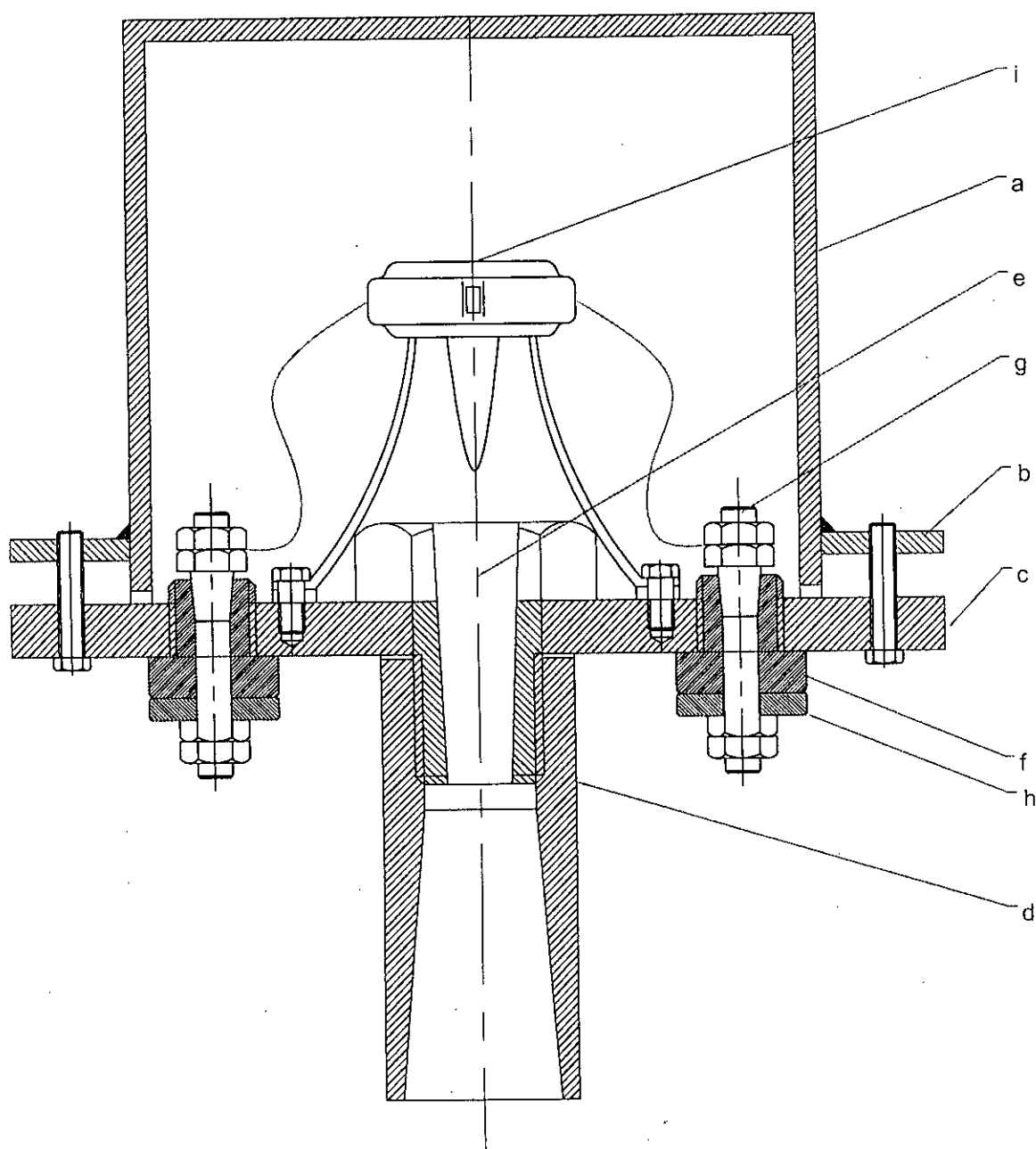
Fig. 3.4.5. Sound Generating Chamber
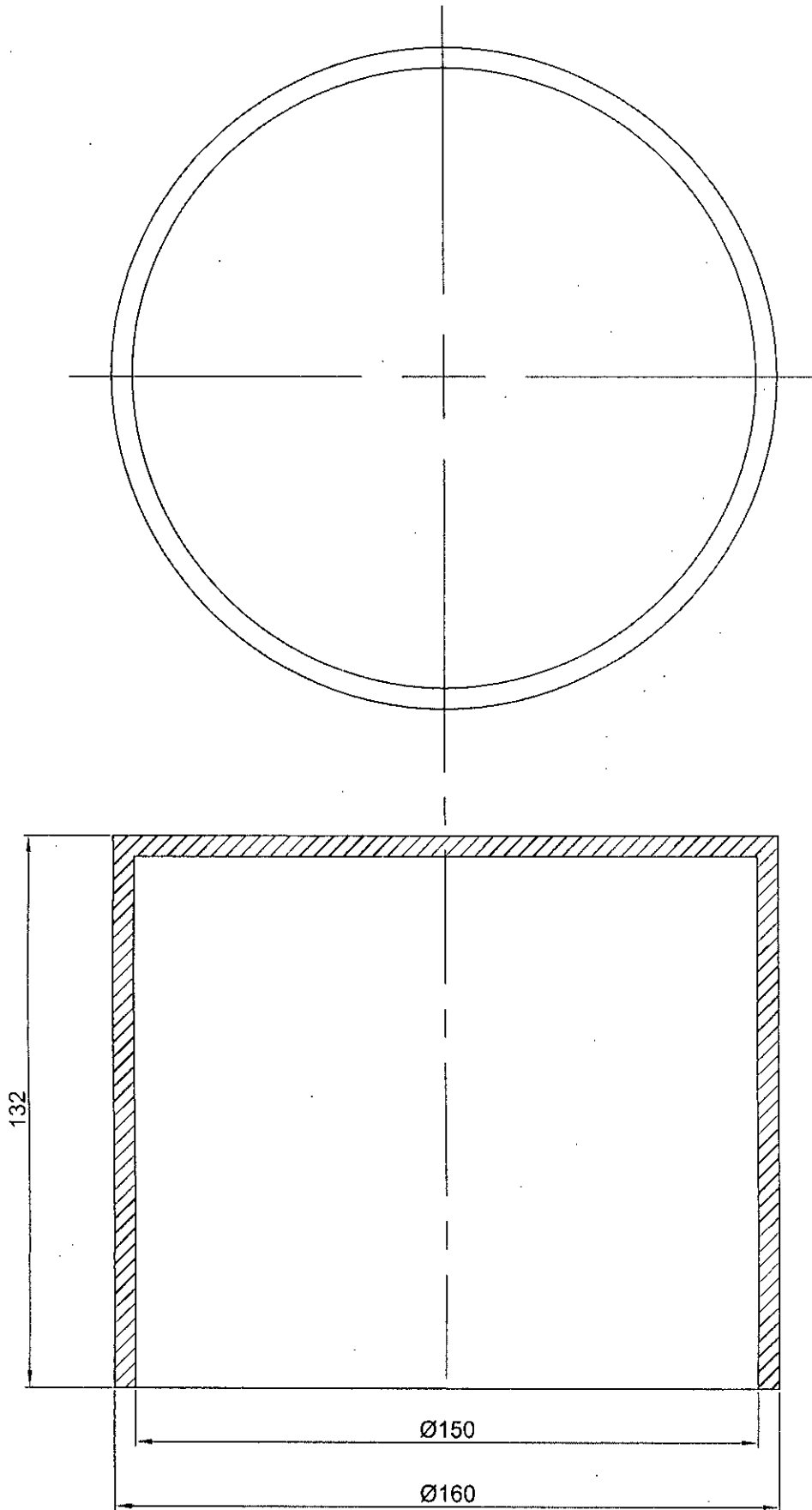
Fig. 3.4.5a. Sound Generating Chamber

12-M6x188 PCD

Ø216

Ø160

5

Fig. 3.4.5b. Chamber Flange

12-M6x188 PCD

12-M6x188 PCD

12-M6x188 PCD

M30

12

Ø216
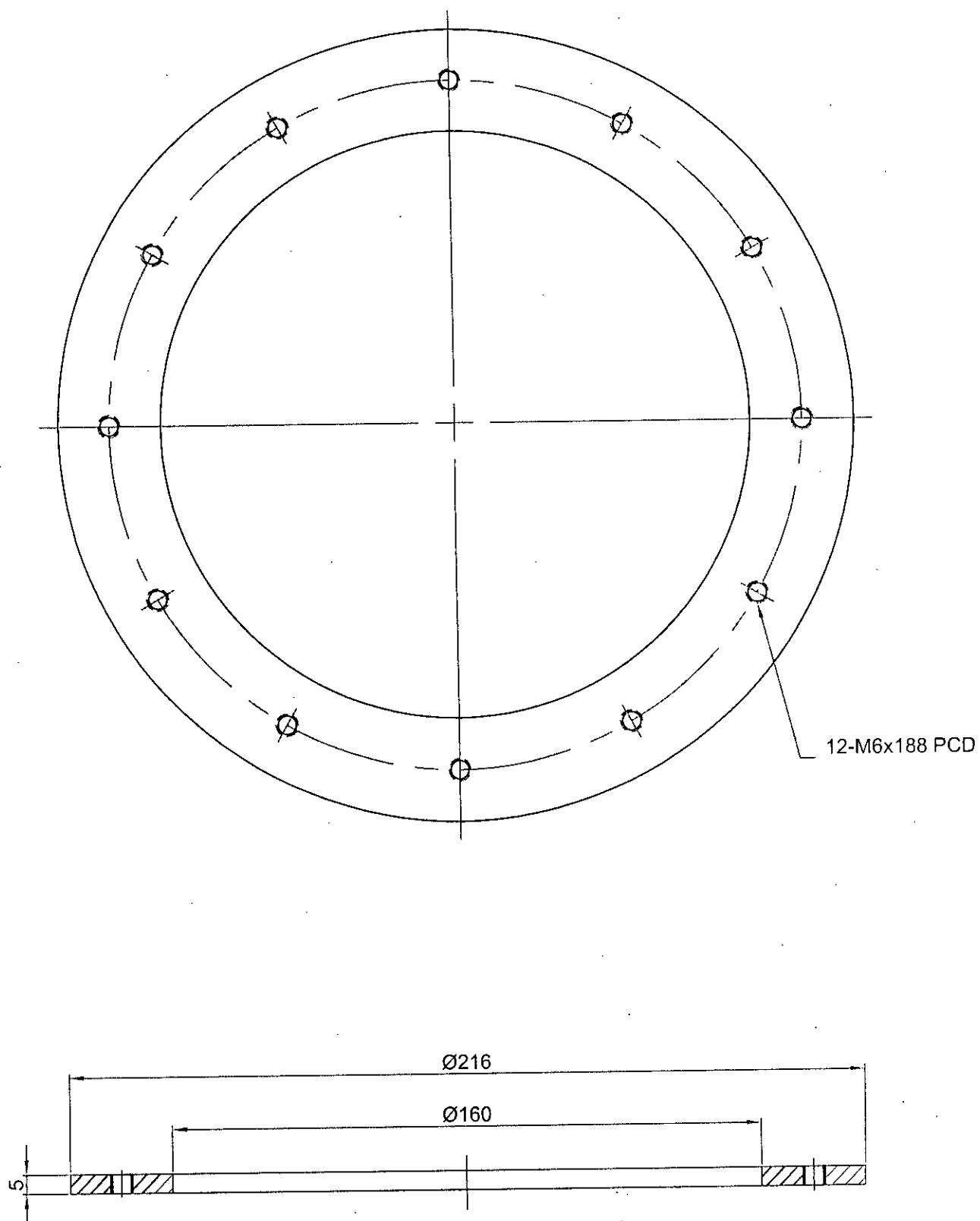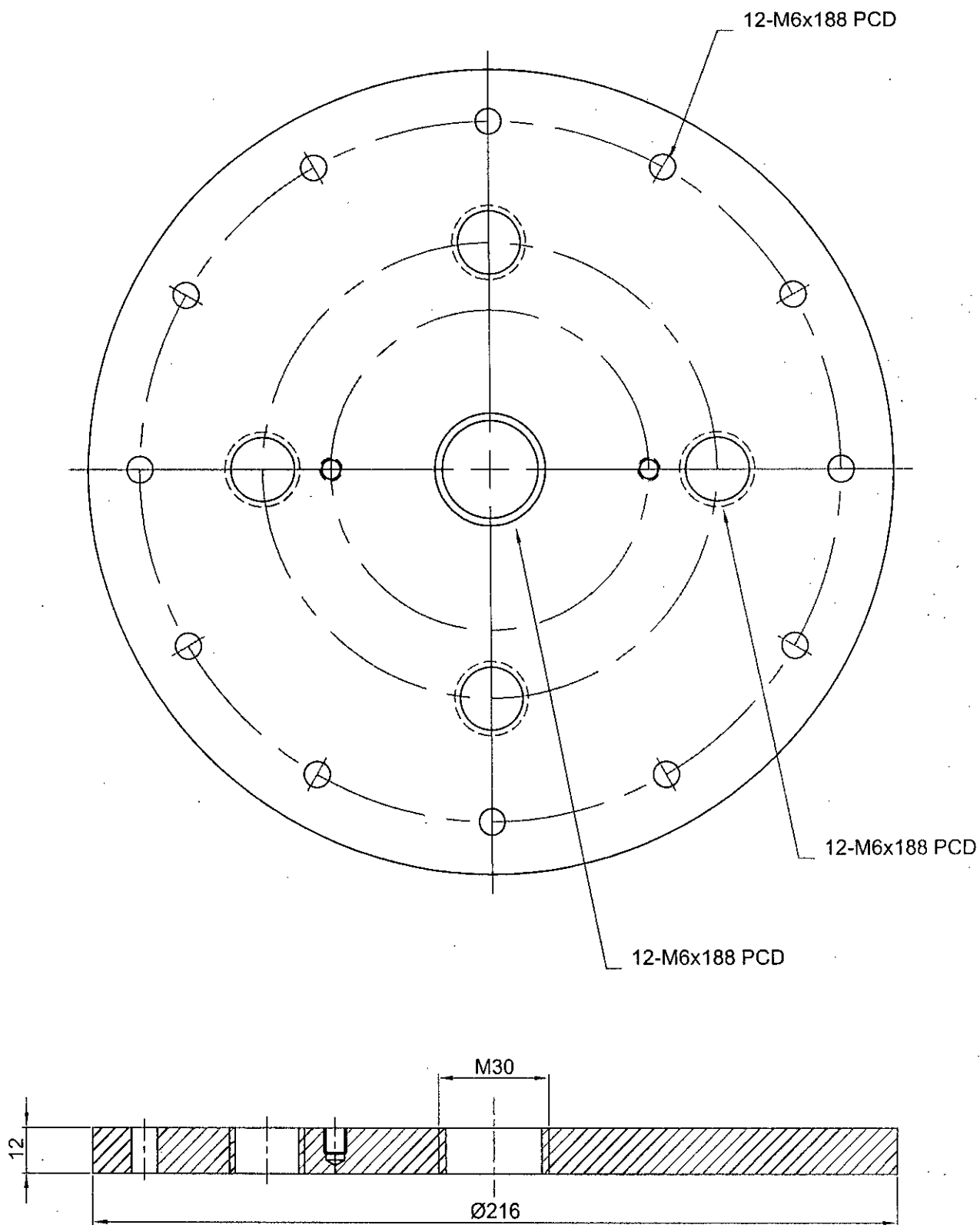
Fig. 3.4.5c. Bottom Plate
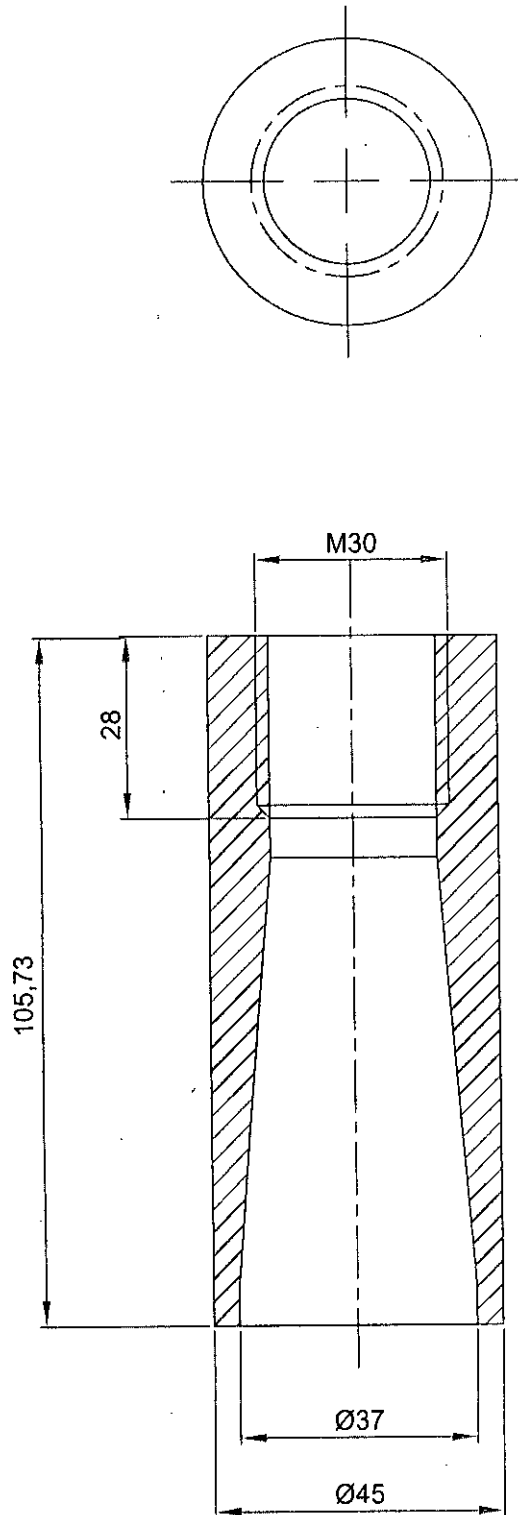
Fig. 3.4.5d. Internally Threaded Hollow Pipe
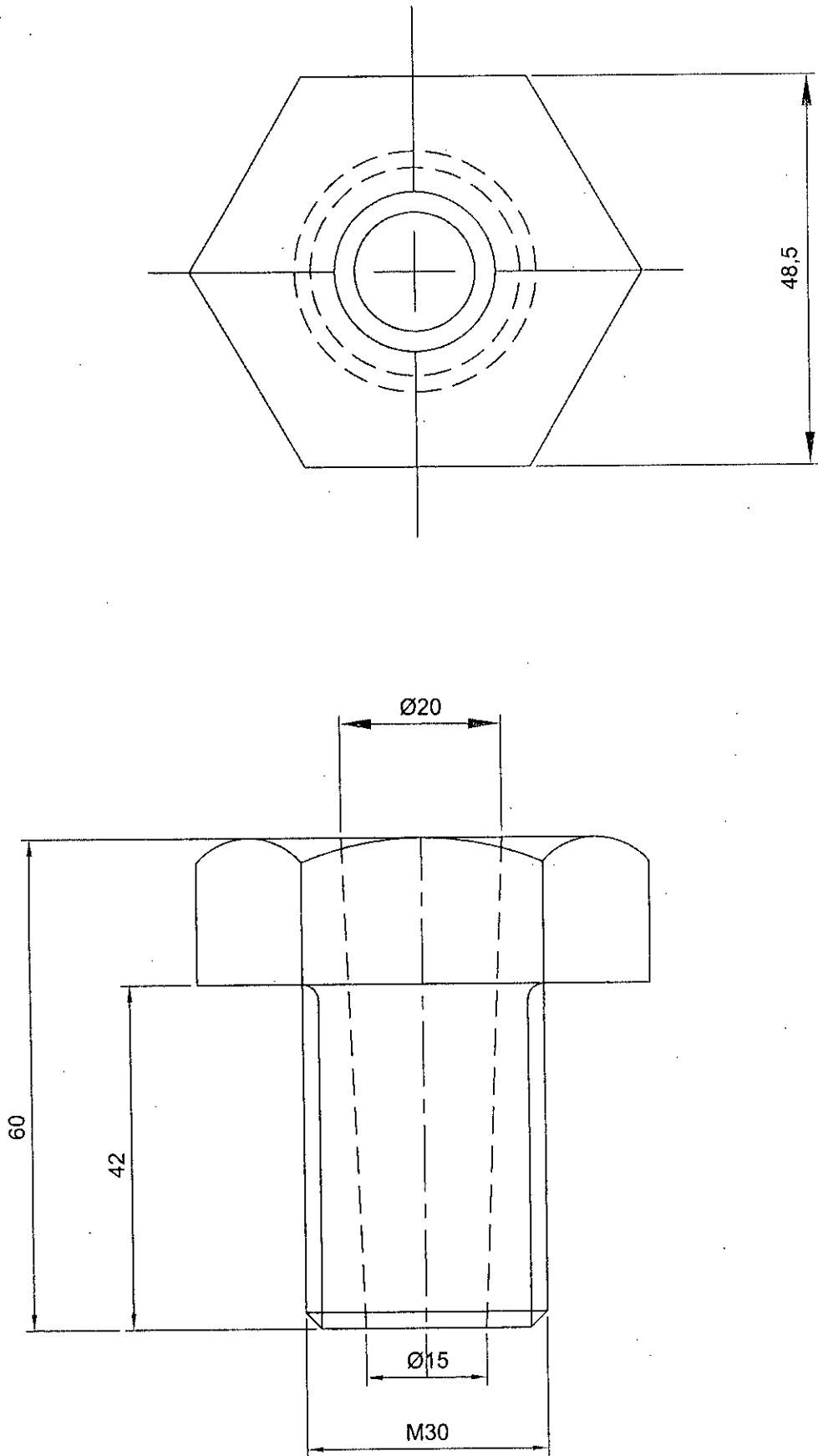
Fig. 3.4.5e. Hollow Bolt

M20

Ø9,65

9.5

17

27

Ø8

Ø30
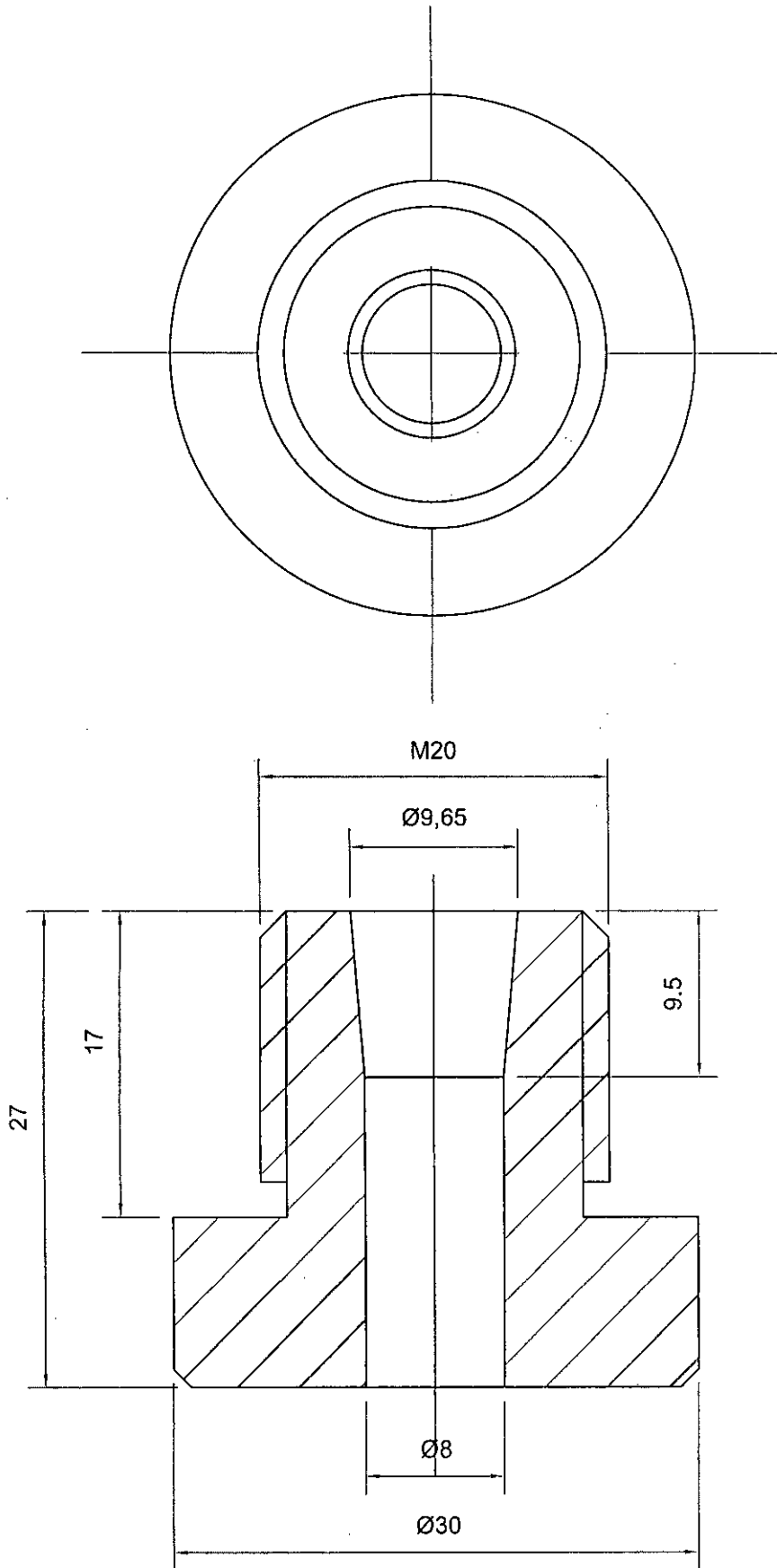
Fig. 3.4.5f. Teflon Bolt
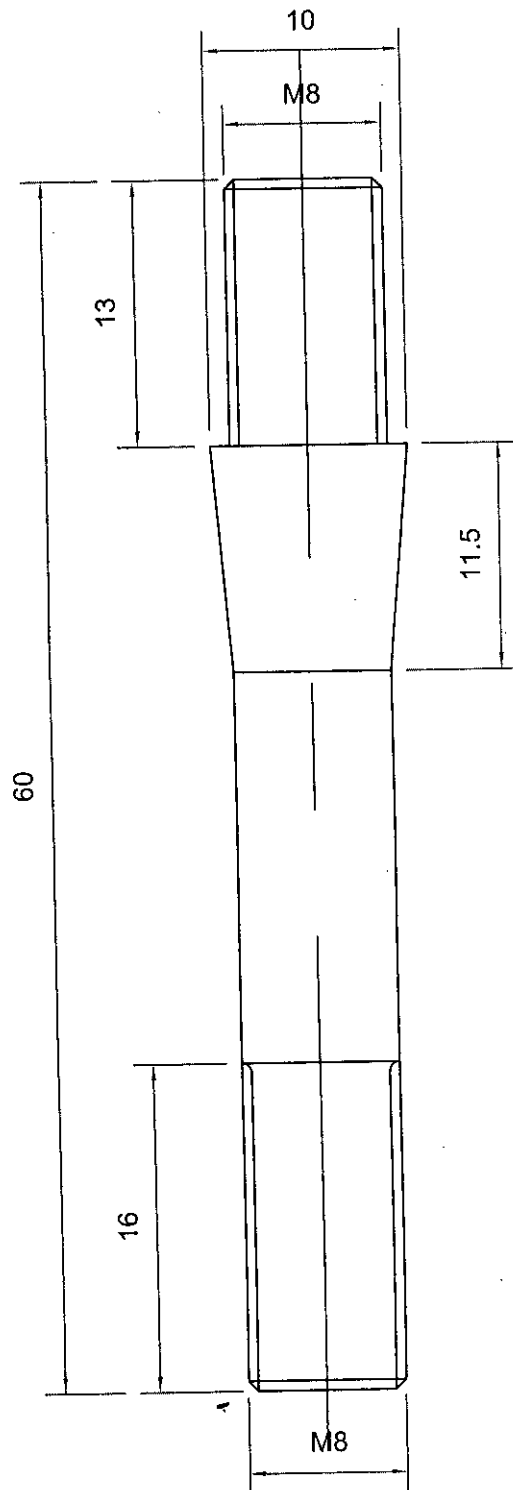
Fig. 3.4.5g. Connector Rod

Fig. 3.4.5f. Metalic Washer

a) Connector rod

b) Teflon Nut

c) SS washer

d) Bush

a

b

c

d
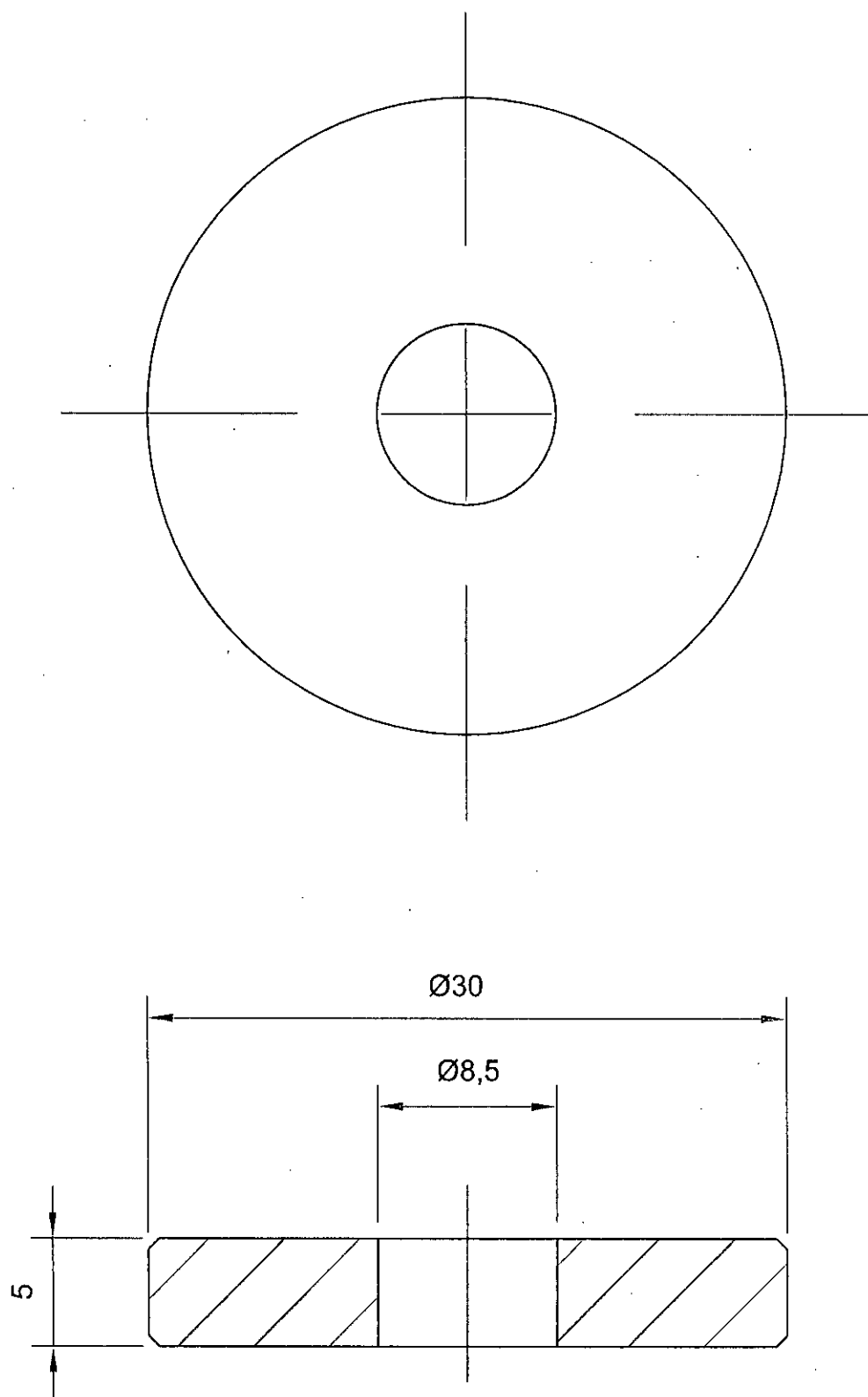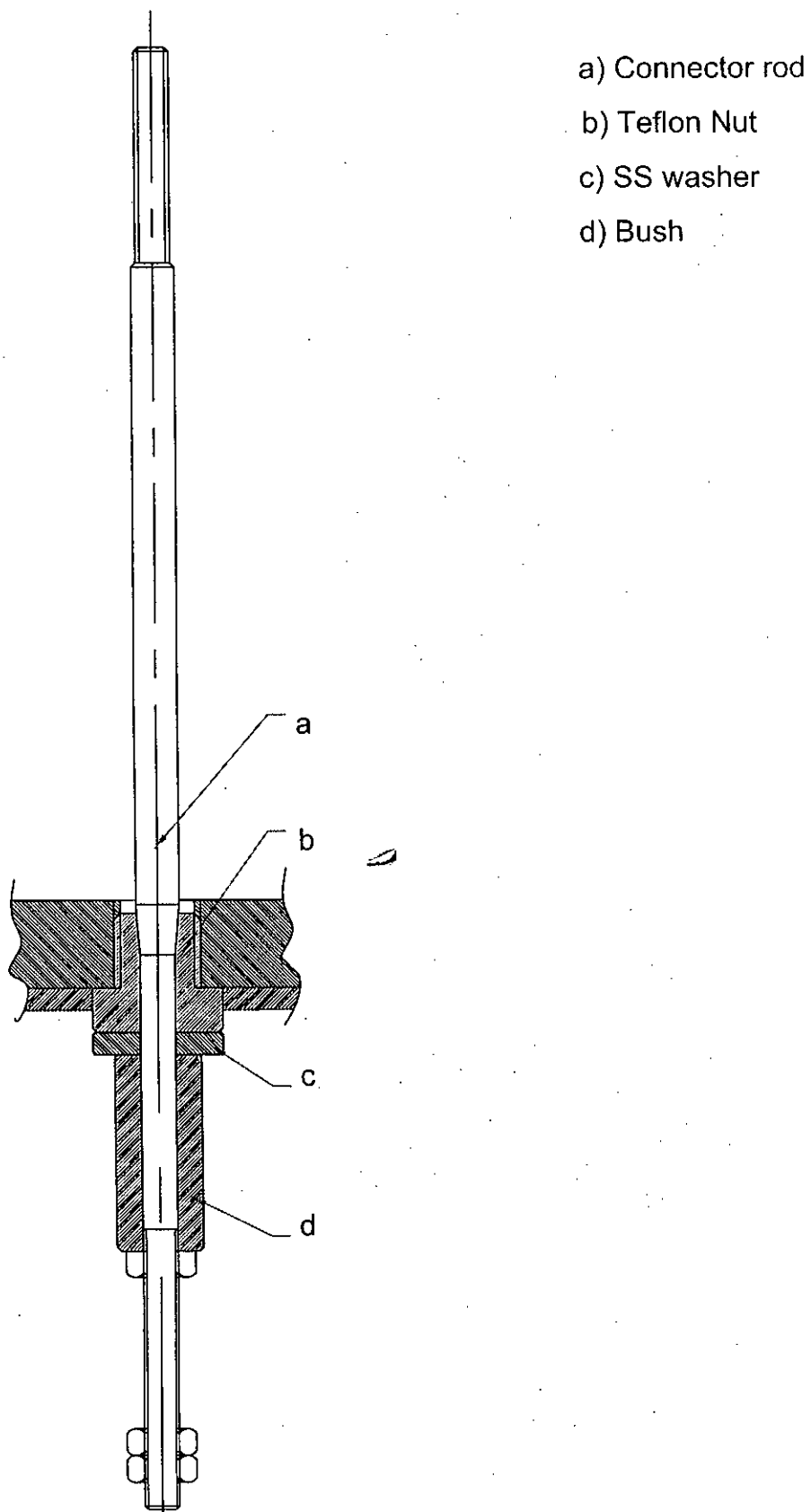
Fig. 3.4.6. Connector for Activatation Heater
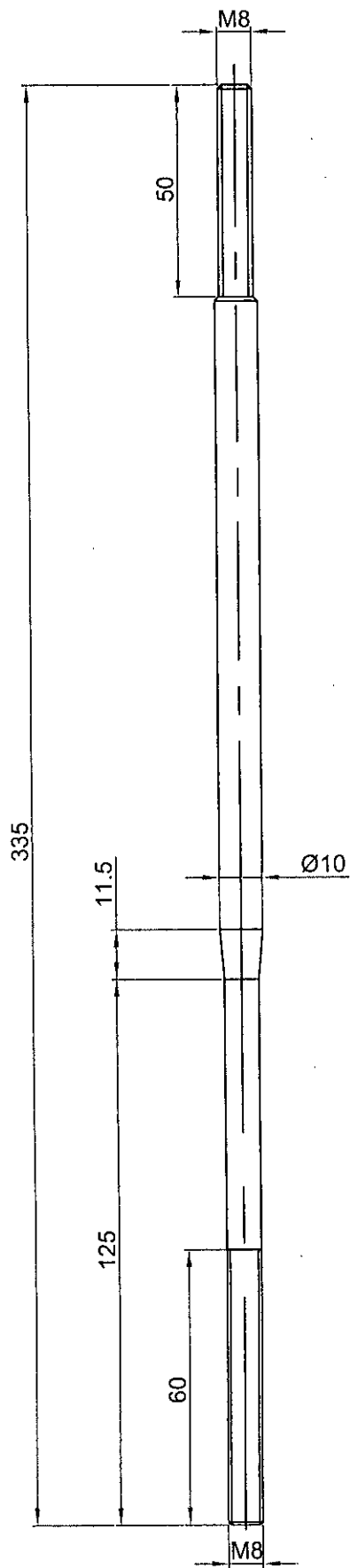
Fig. 3.4.6a. Connector rod
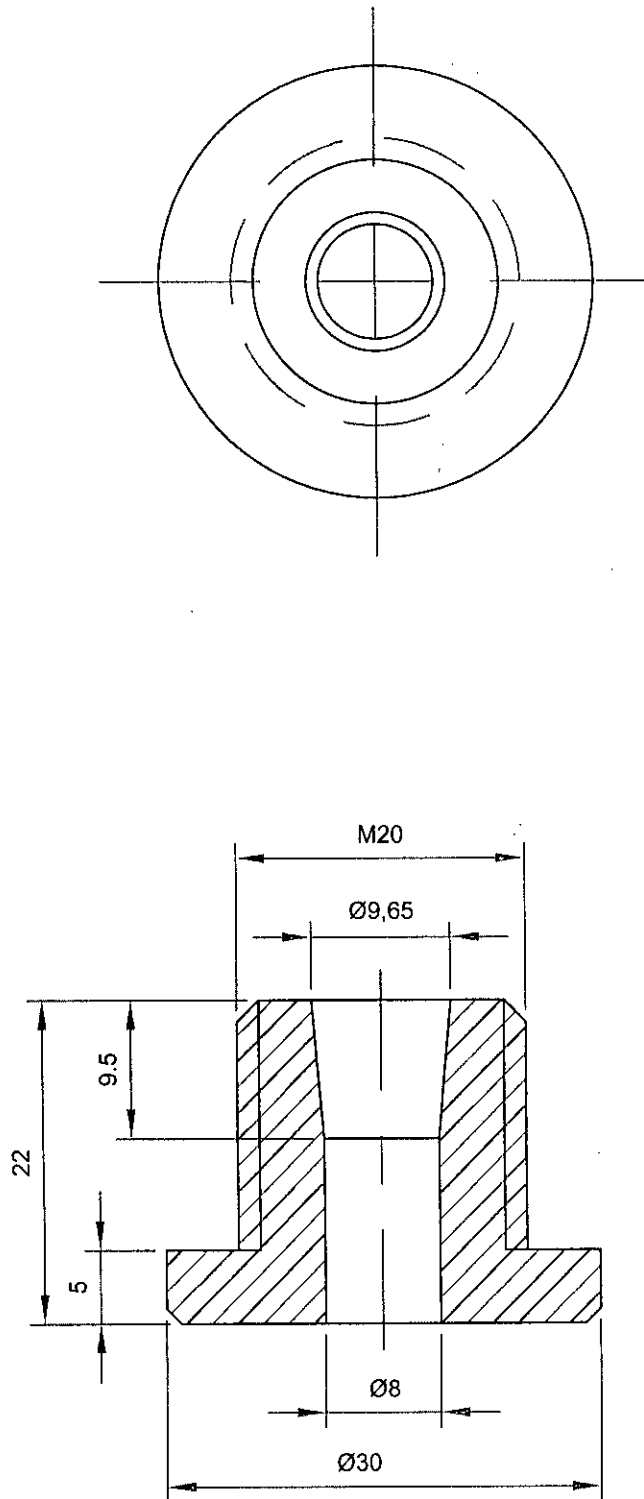
Fig. 3.4.6b. Teflon Nut
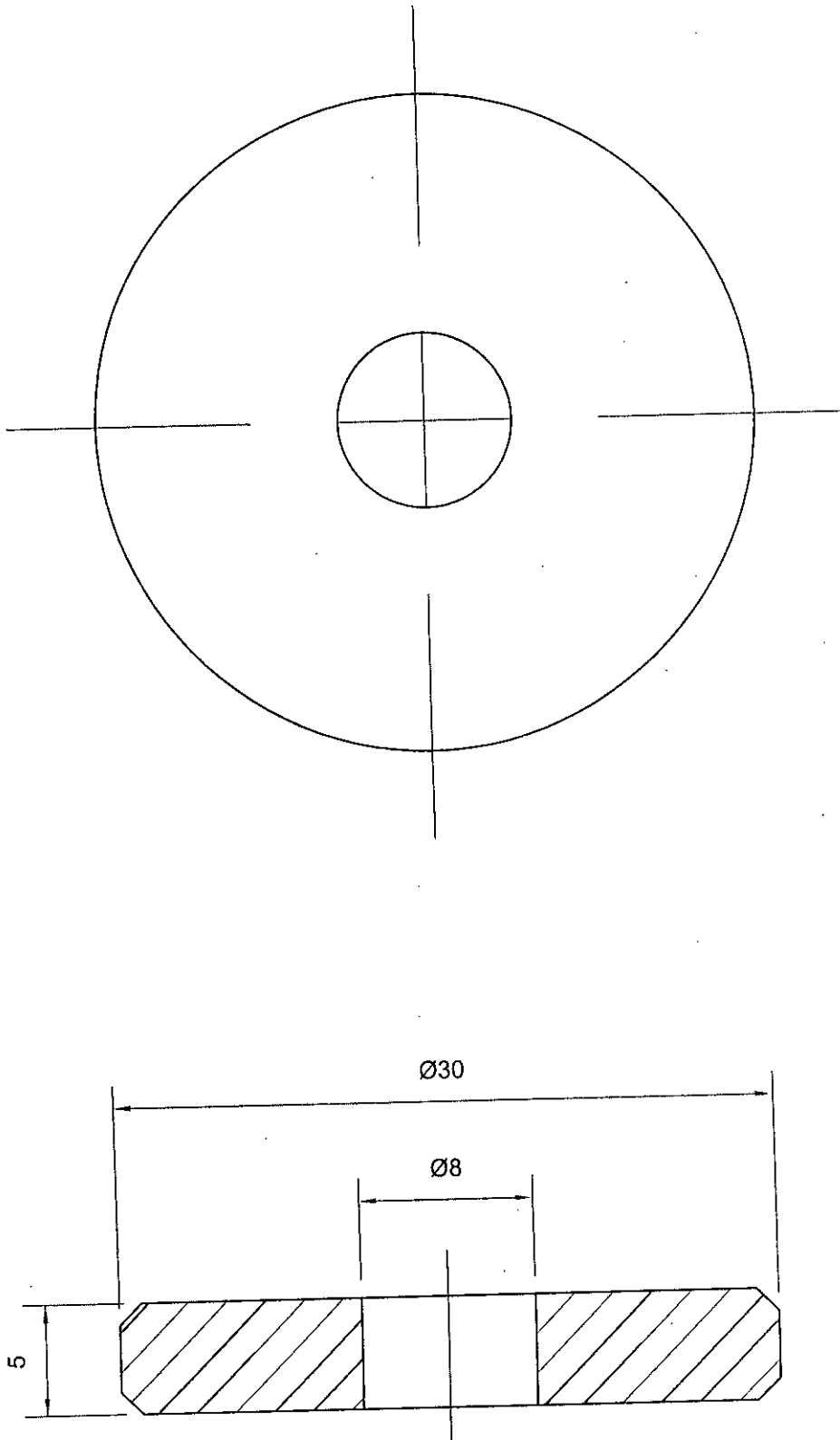
Fig. 3.4.6c. SS Washer

Fig. 3.4.6d. Bush

a) Connector rod

b) Teflon Nut

c) SS washer

d) Bush

a

b

c

d
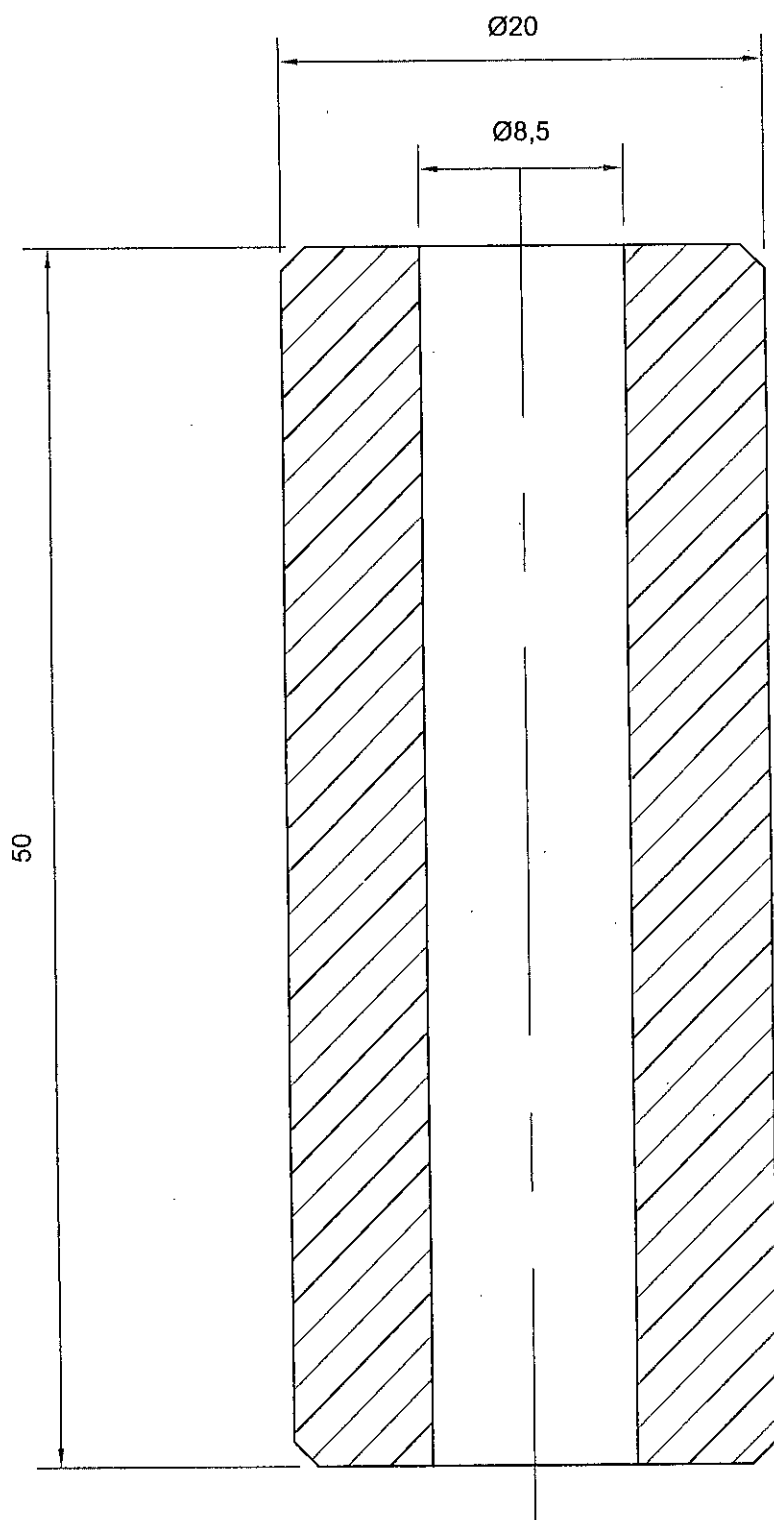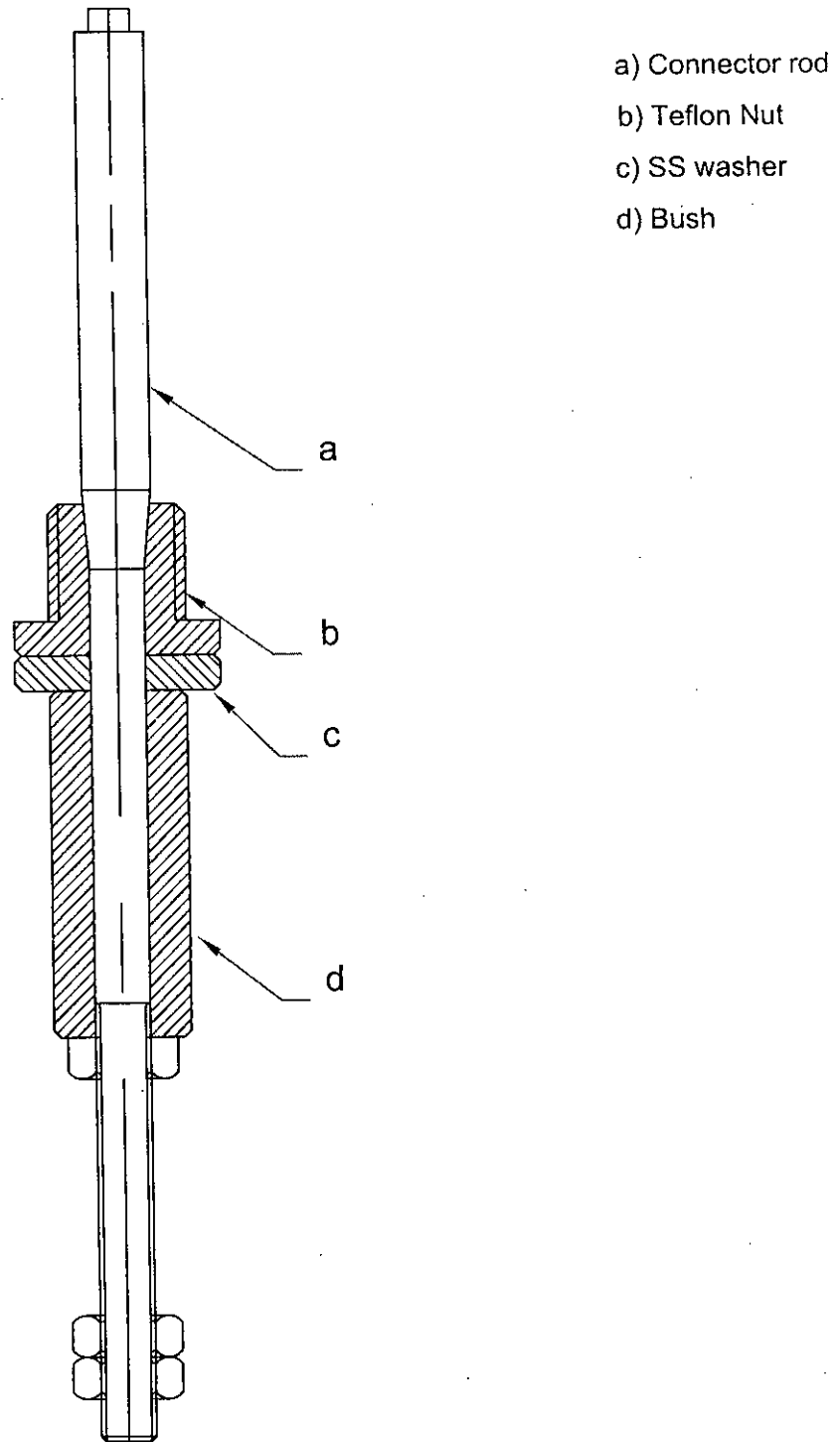
Fig. 3.4.7. Connector for Substrate Heater
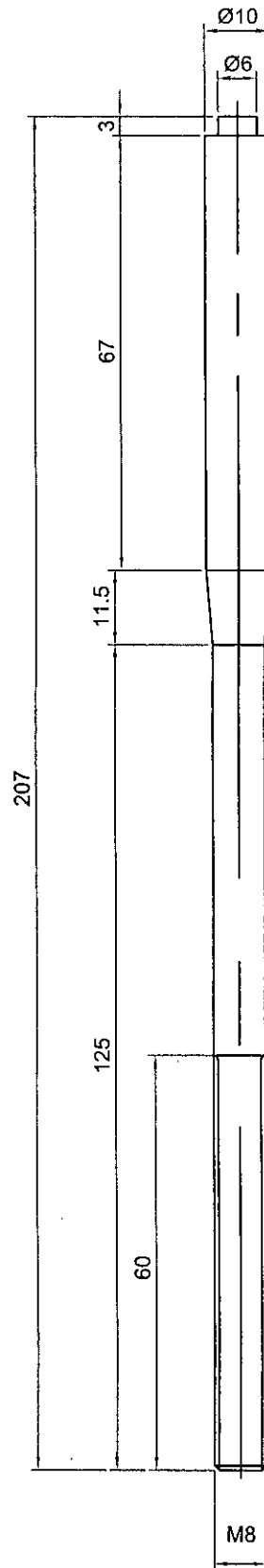
Fig. 3.4.7a. Connector rod
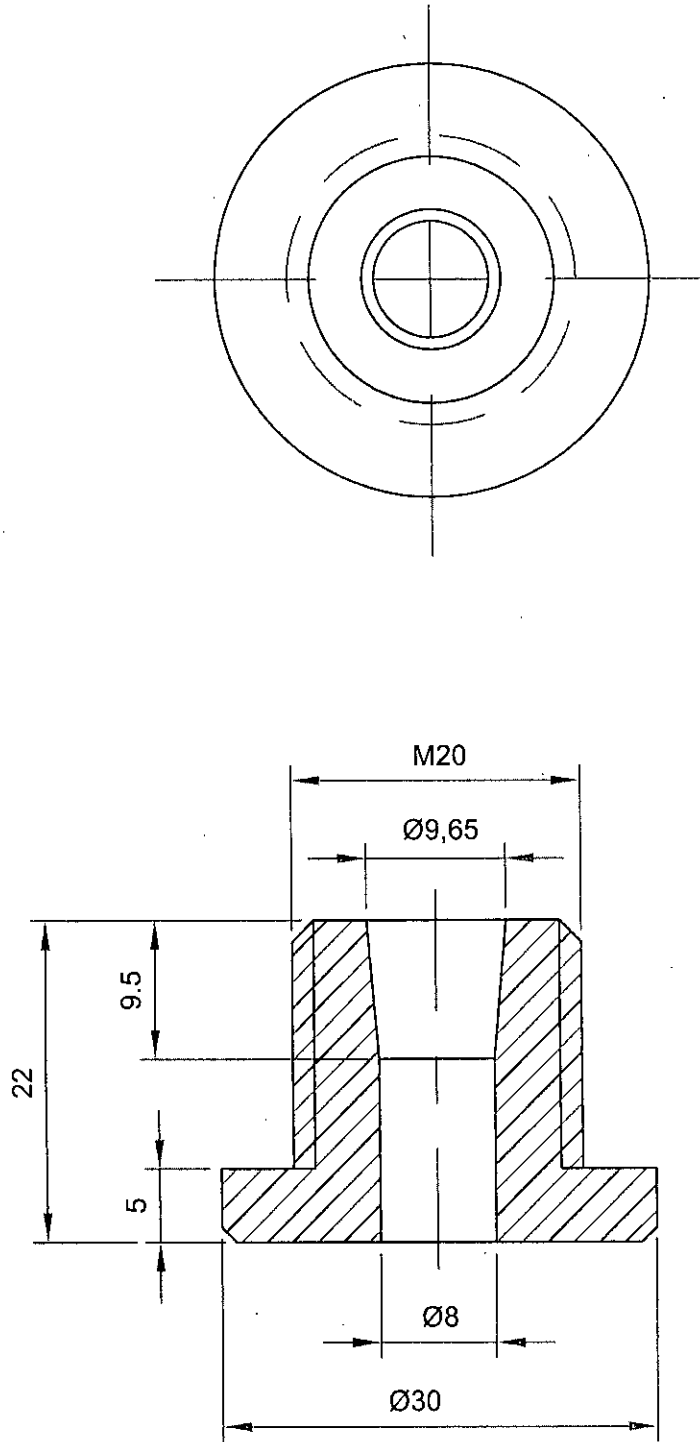
Fig. 3.4.7b. Teflon Nut
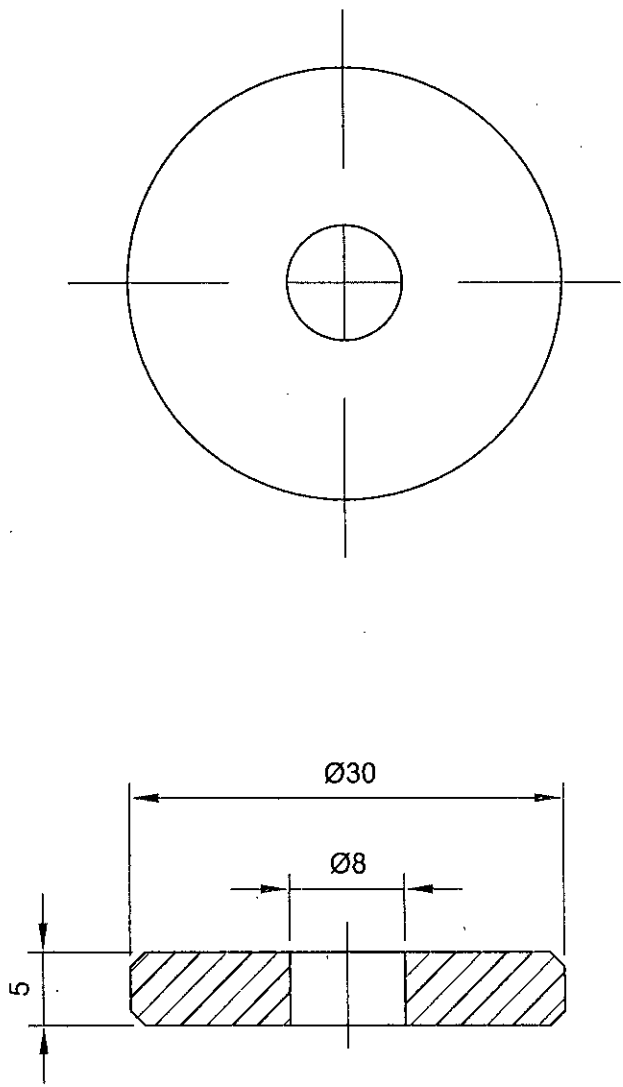
Fig. 3.4.7c. SS washer
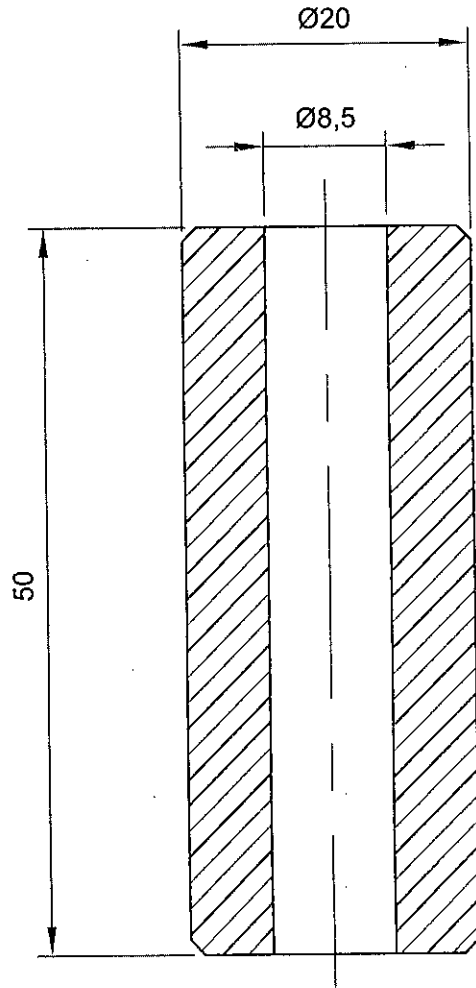
Fig. 3.4.7d. Bush
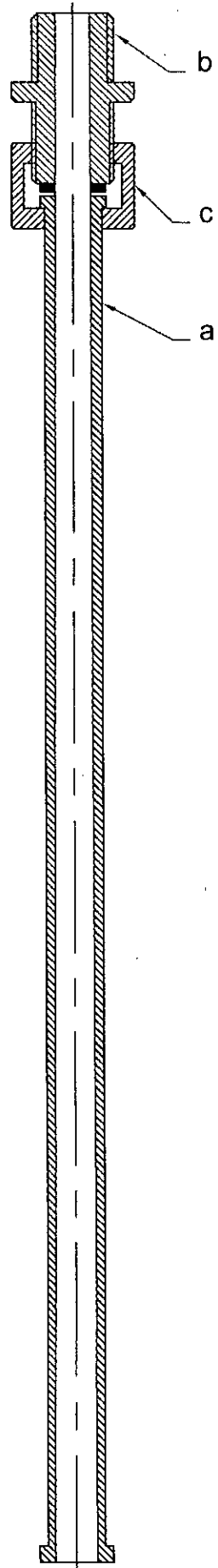
a) Connector Pipe

b) Nut

c) Coupling

Fig. 3.4.8. Connector for Vacuam Pump
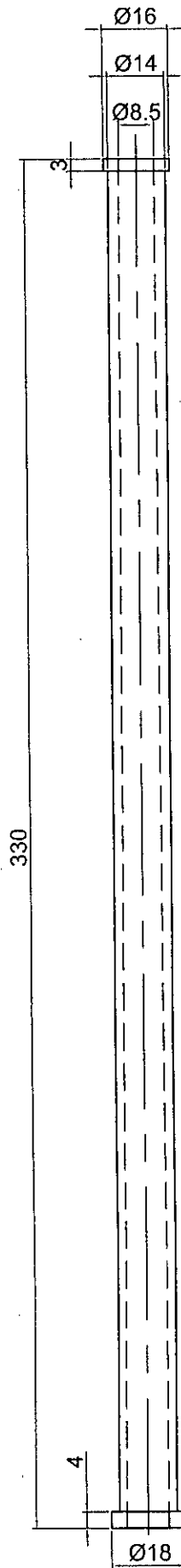
Fig. 3.4.8a. Connector rod

Ø30

M20

Ø8

17

5

20

42
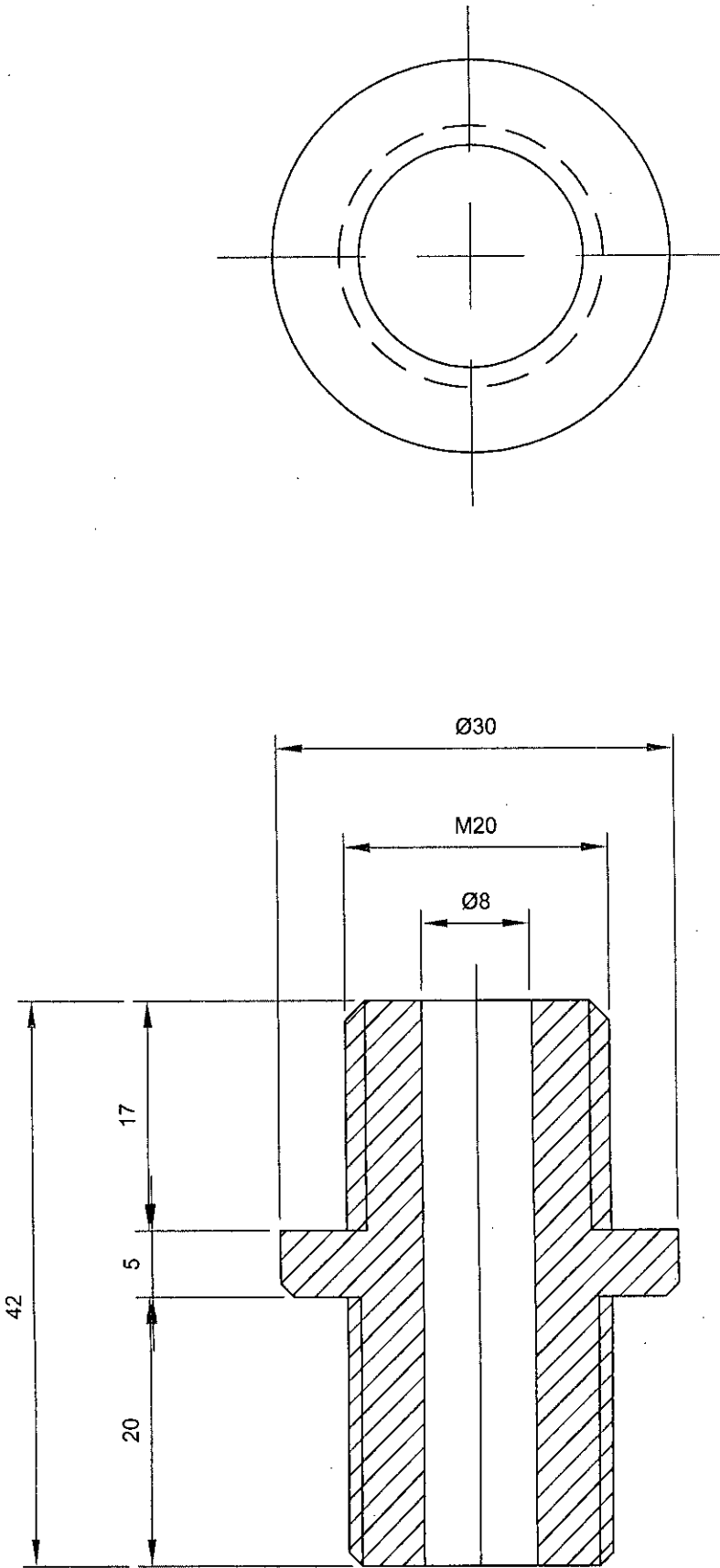
Fig. 3.4.8b. Nut

Fig. 3.4.8c. Coupling

a) Connector Pipe

b) Nut

c) Coupling

Gas regulator
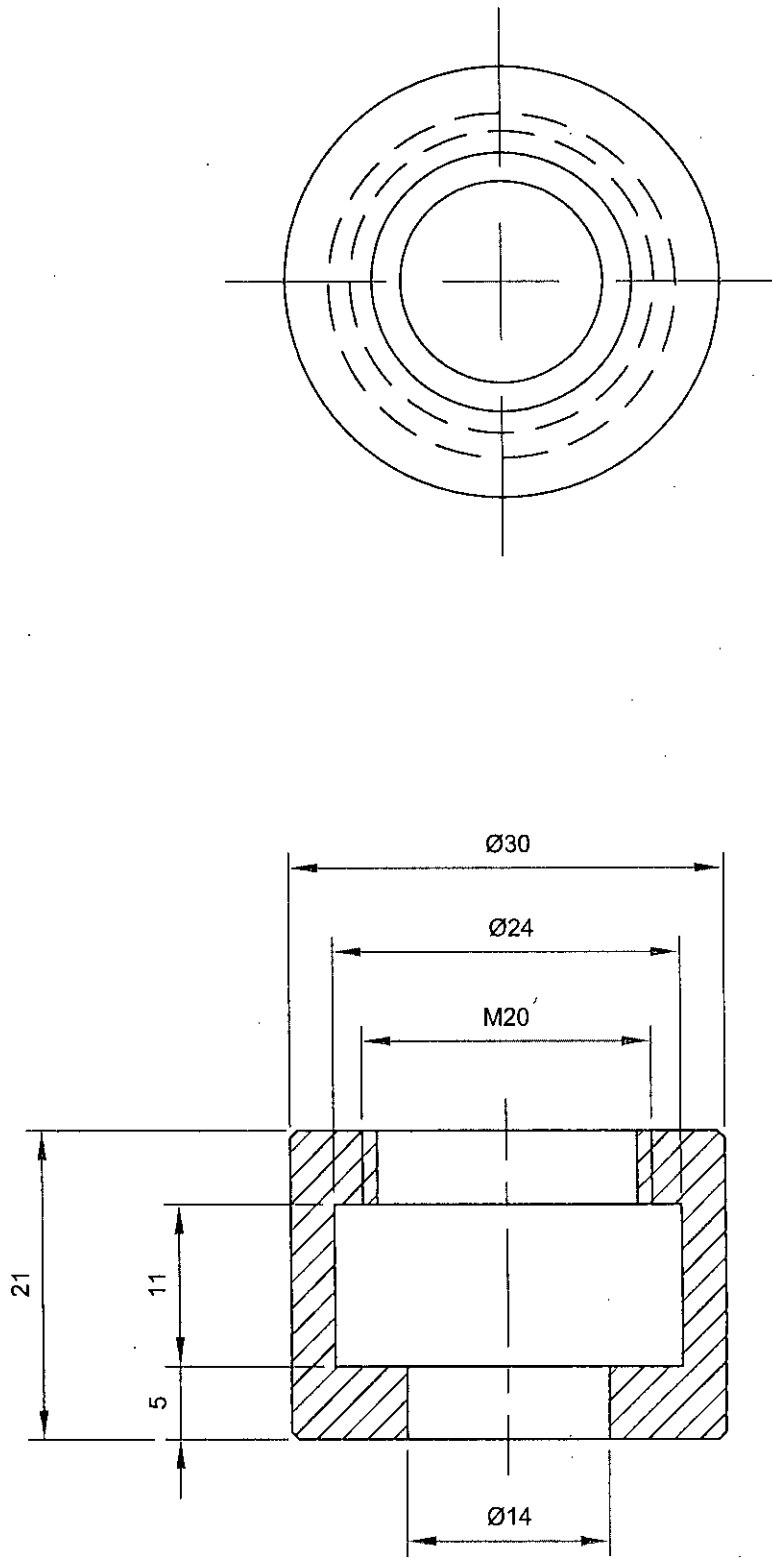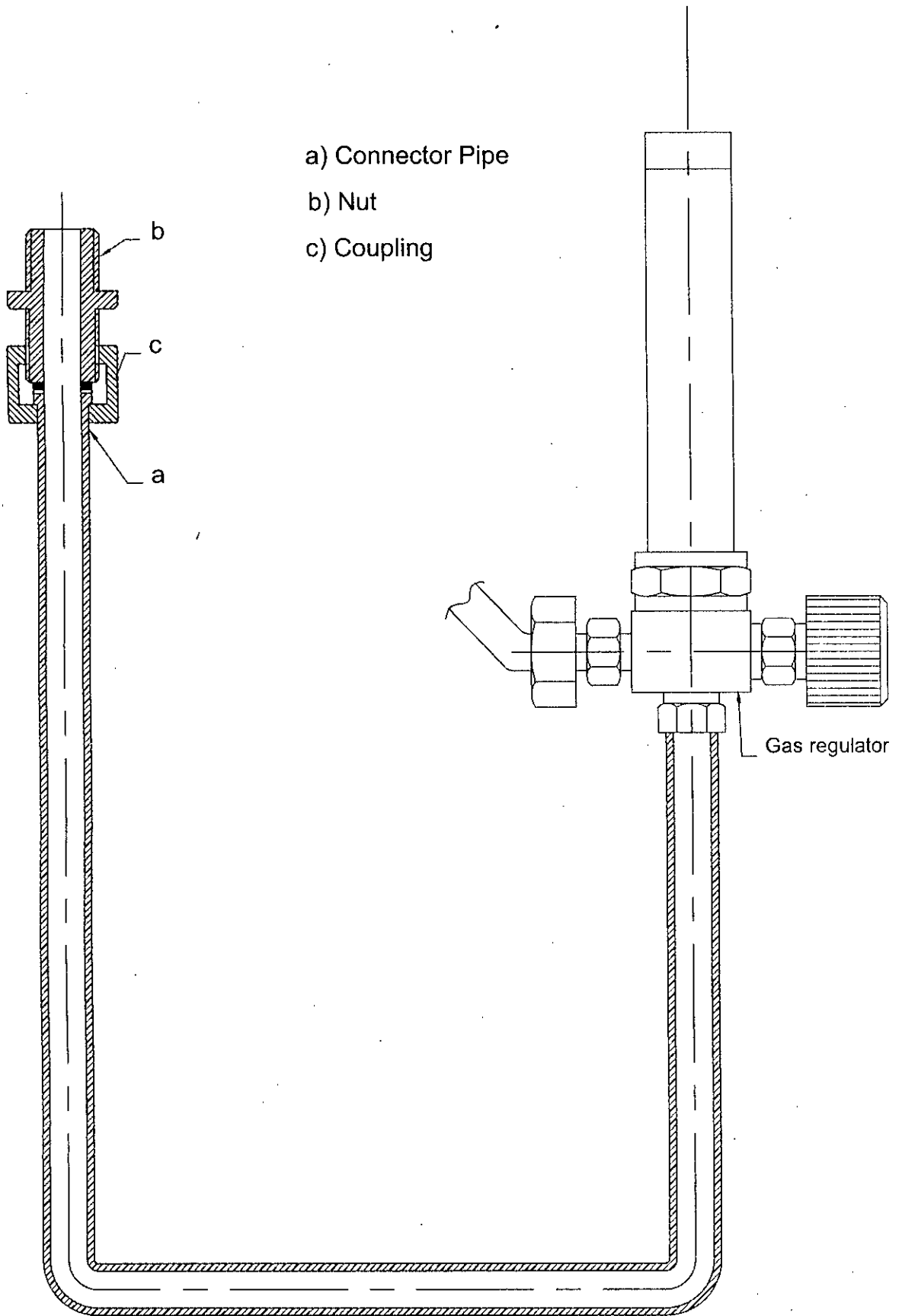
Fig. 3.4.9. Connector for Gas Inlet
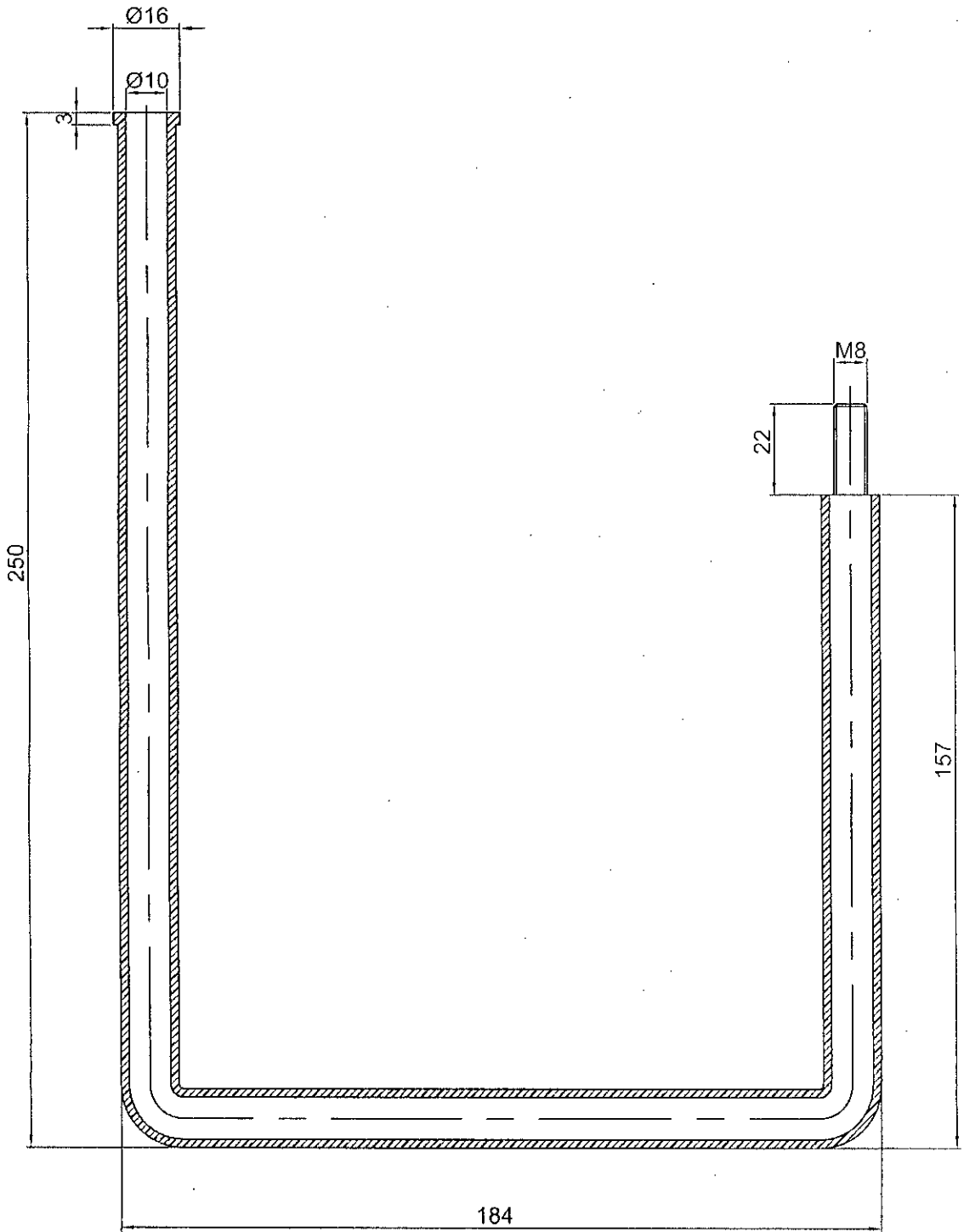
Fig. 3.4.9a. Connector Pipe

Ø30

M20

Ø9

17

5

42

20
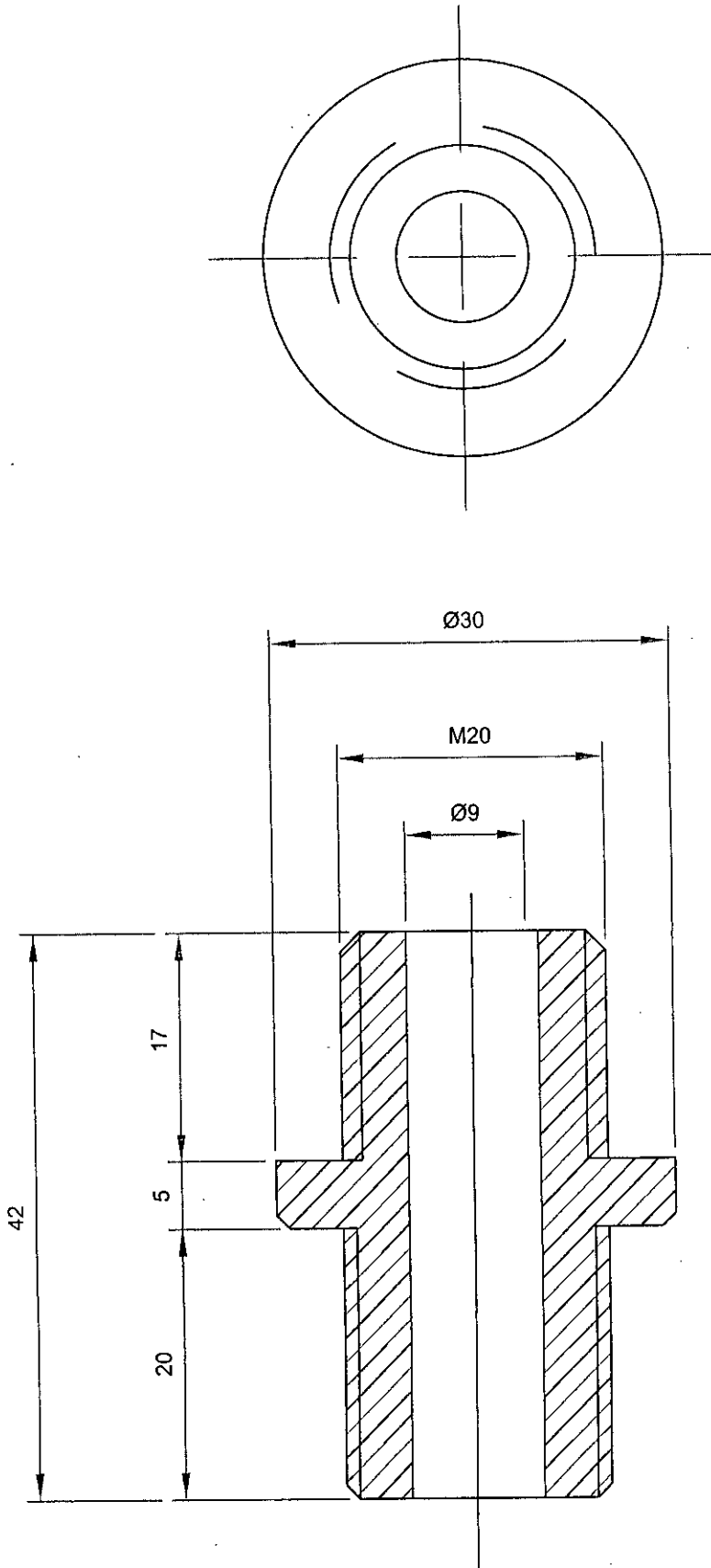
Fig. 3.4.9b. Nut

Fig. 3.4.9c. Coupling

a) Copper Tube Coil

b) Nut

c) Coupling

Copper Tube Coil

Gauge Sensor
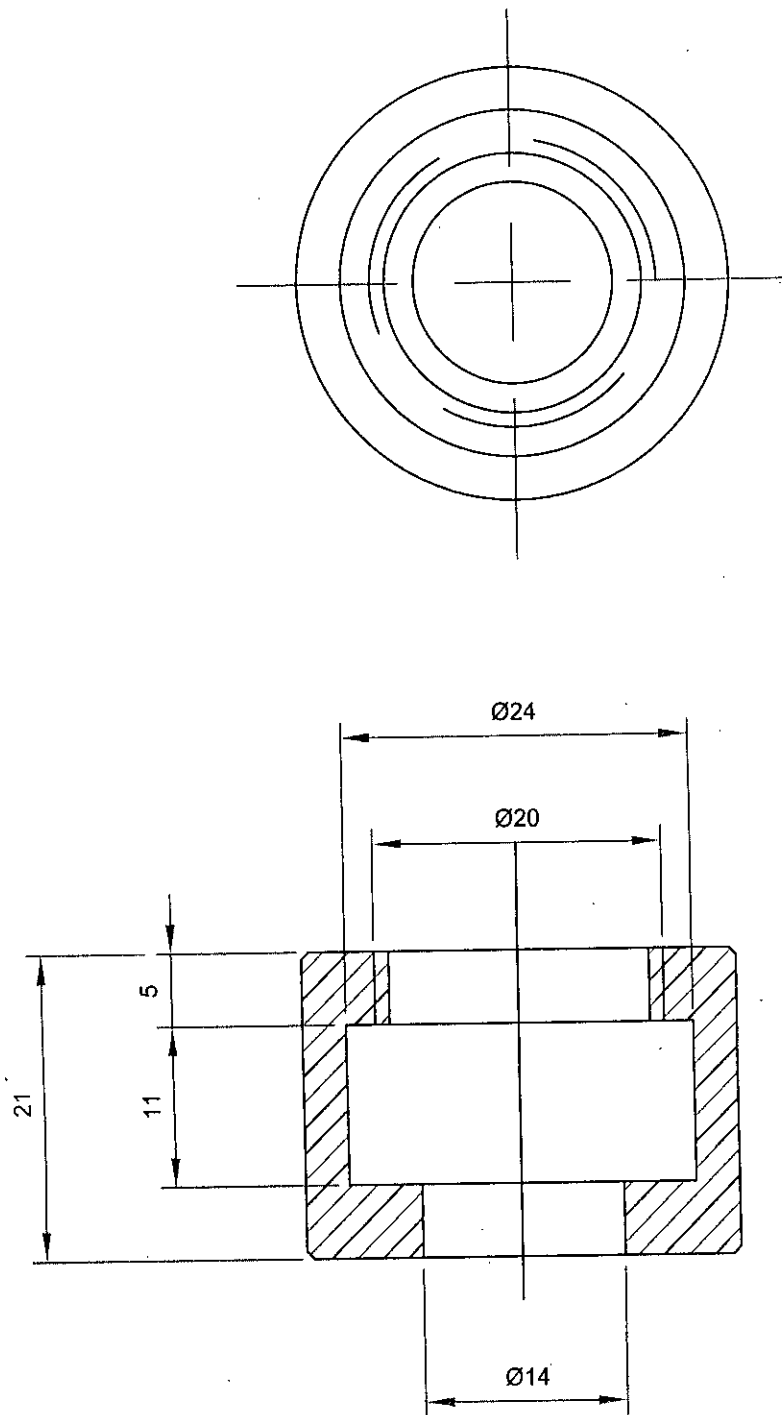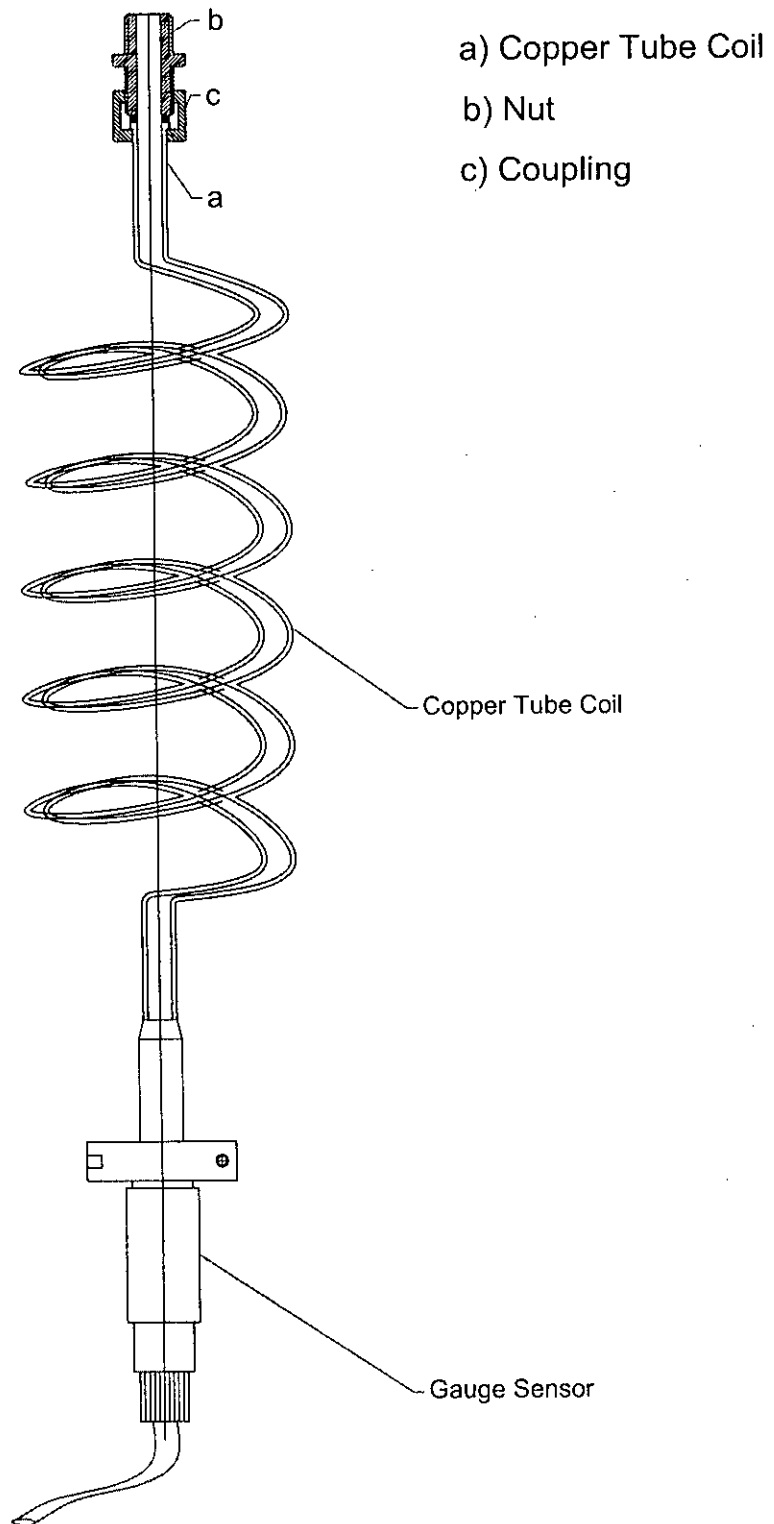
Fig. 3.4.16. Connector for Vacuum Gauge
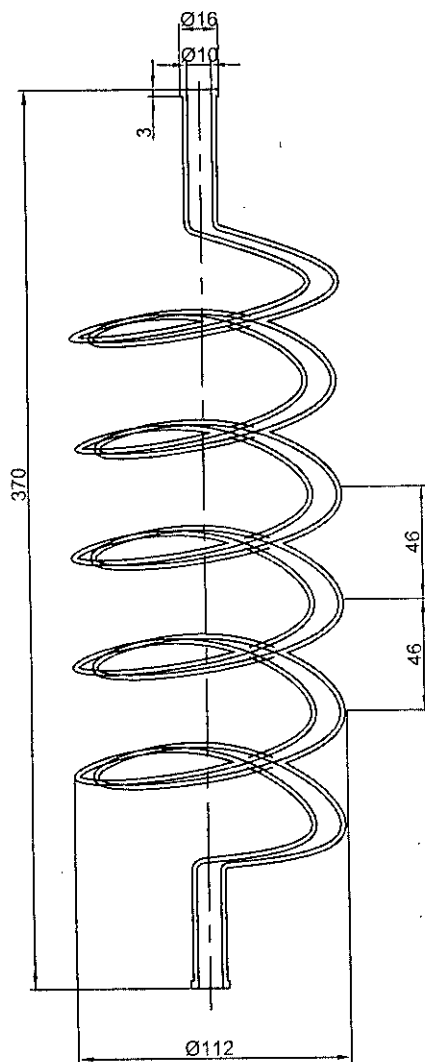
Fig. 3.4.16. Copper Tube Coil
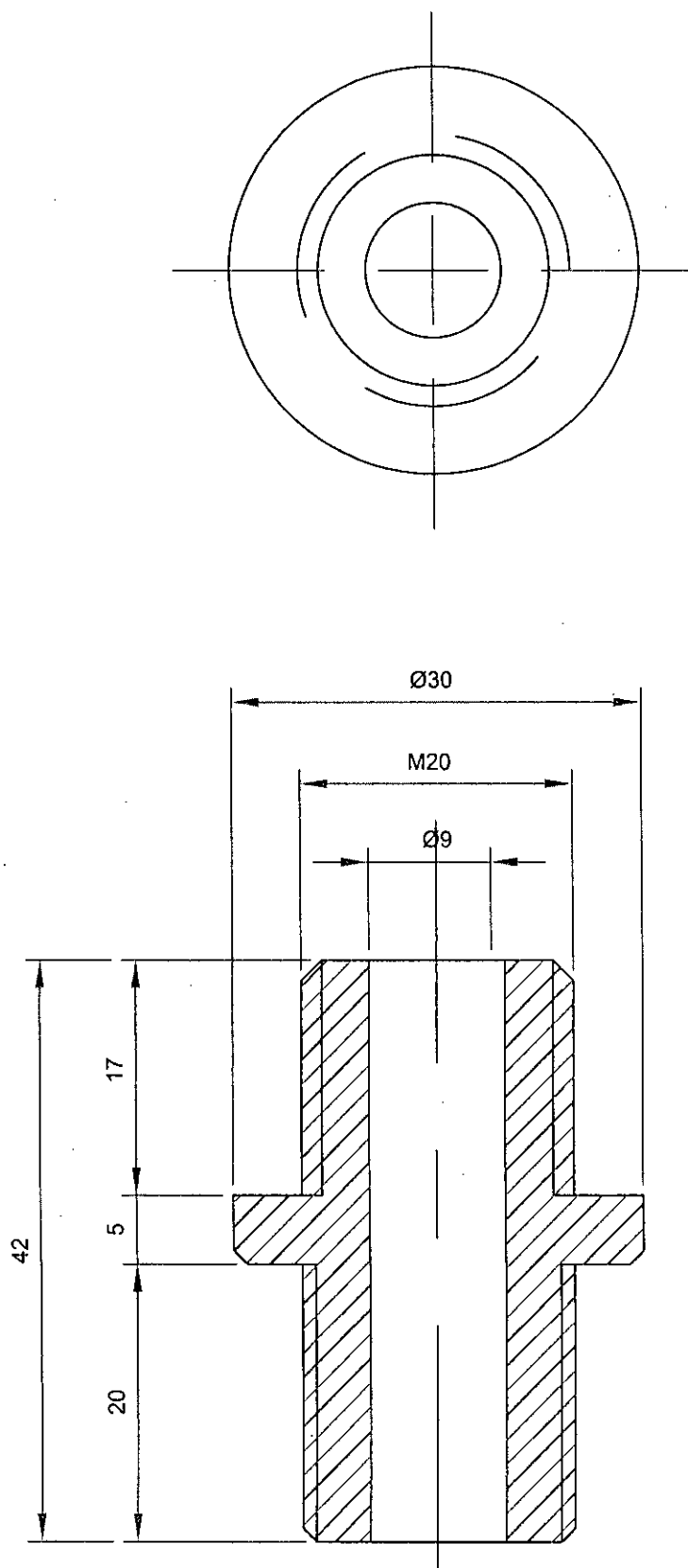
Fig. 3.4.16b. Nut
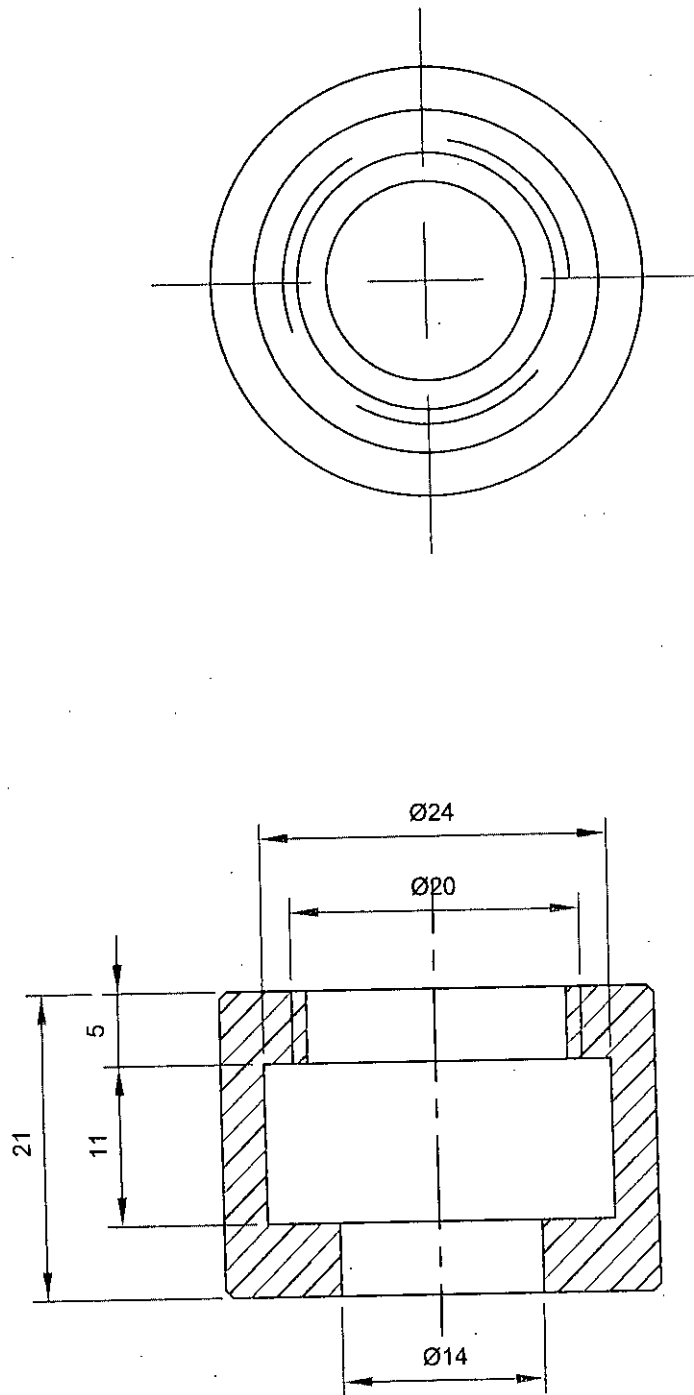
Fig. 3.4.16c. Coupling
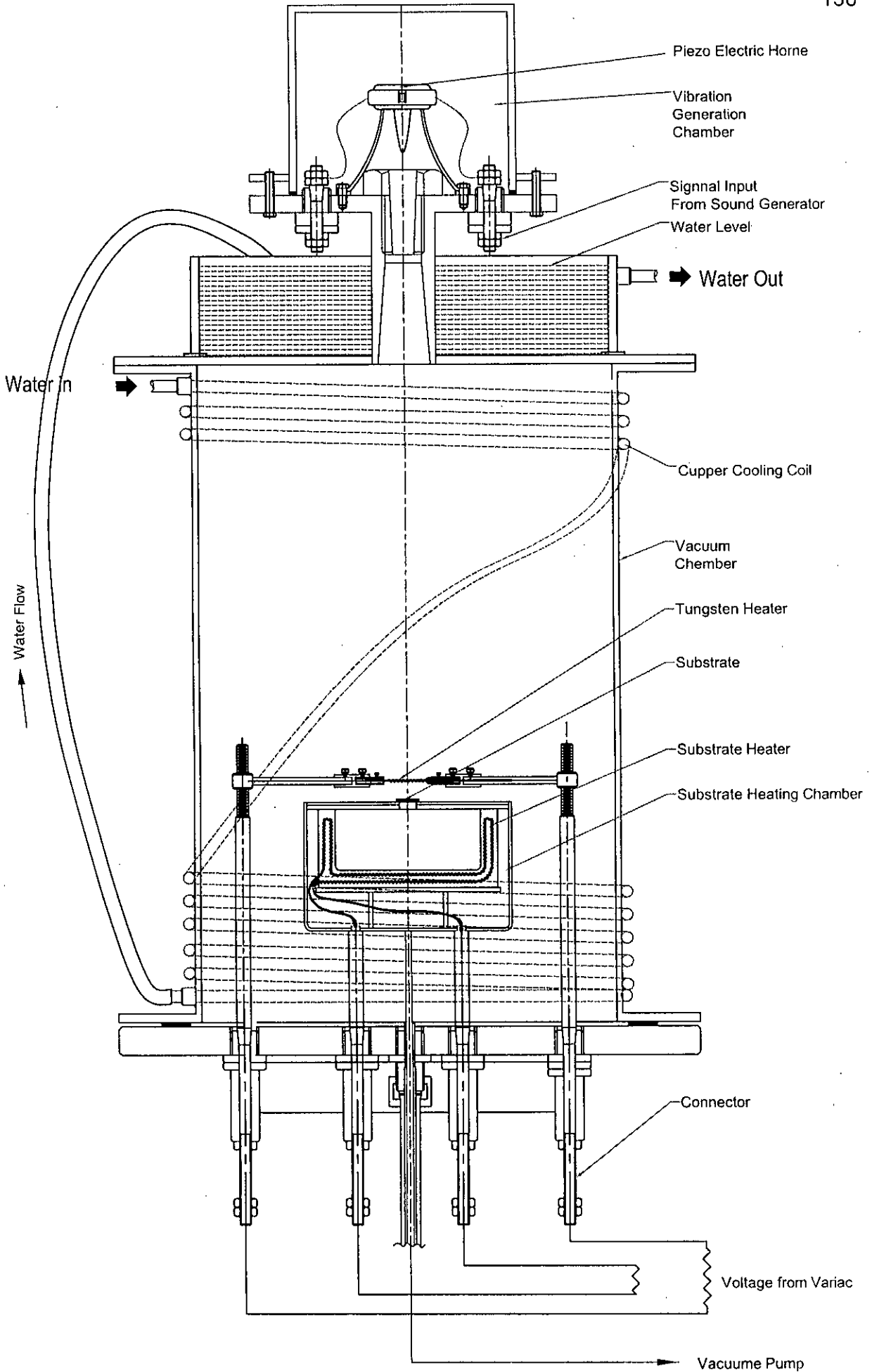
Fig 3.5. Schematic Diagram of CVD Set-up Showing
Differant System Working During Experiment.
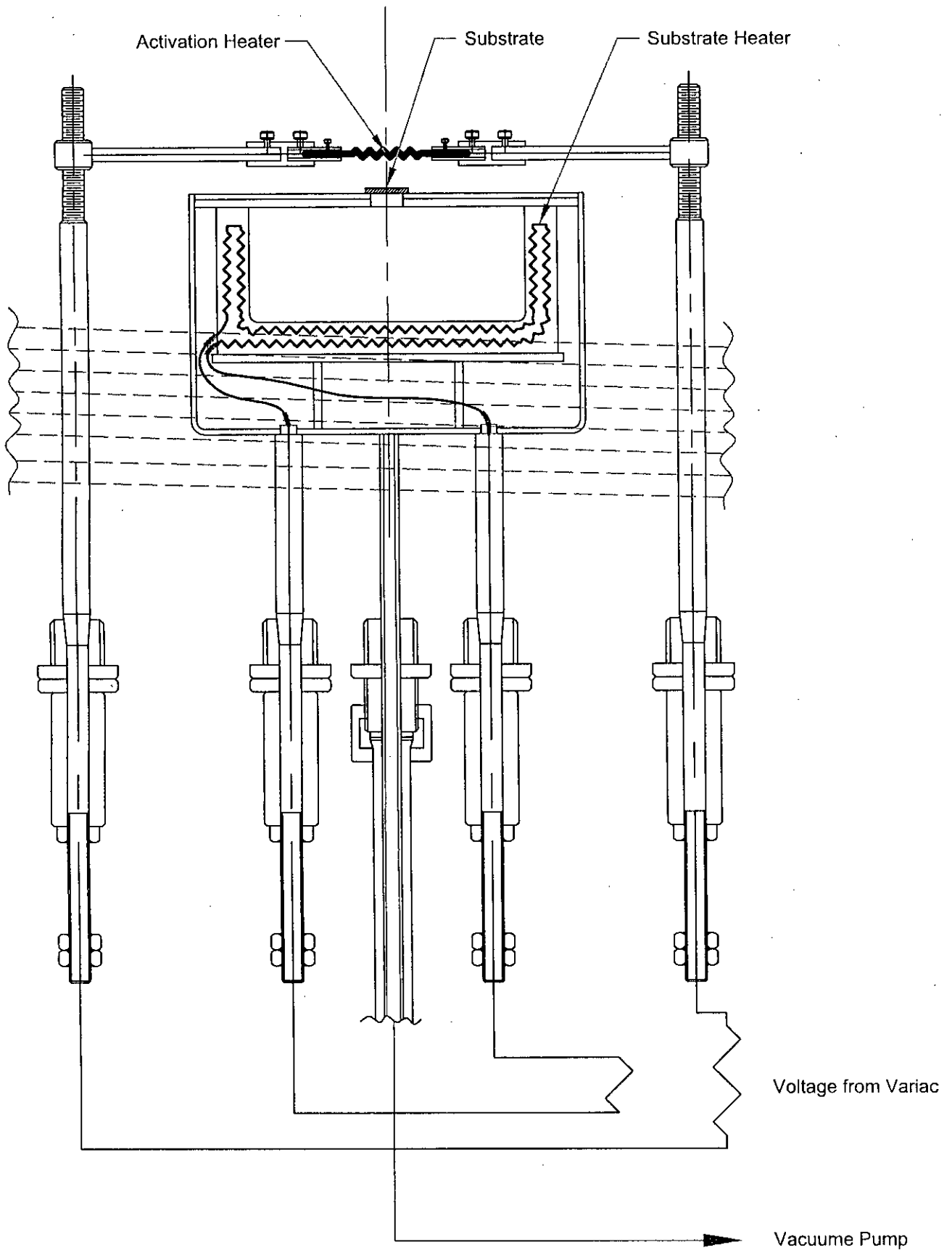
Fig. 3.4.6. Schematic Diagram of Heating System

Water Out

Water In

Water Flow

Air Flow
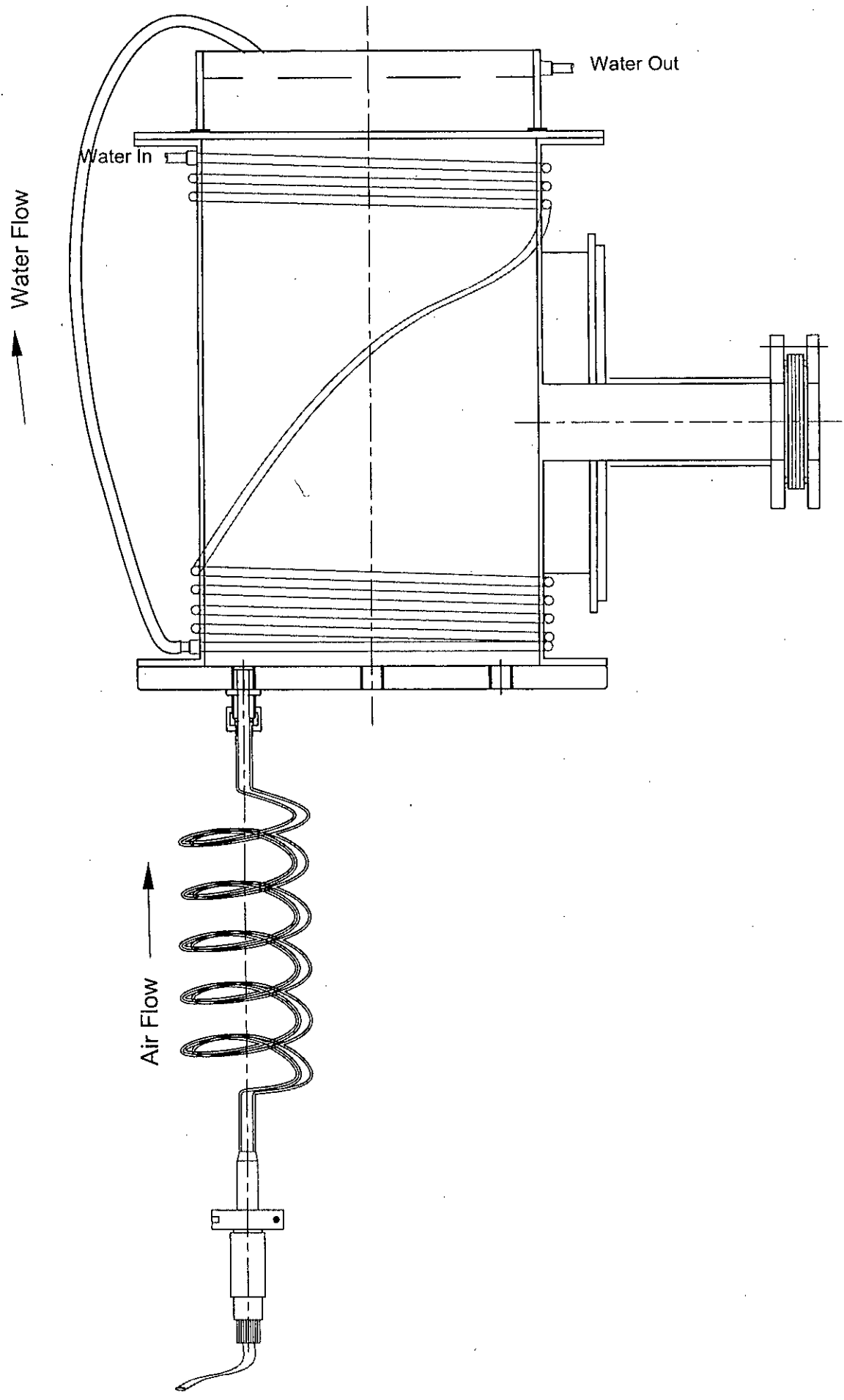
Fig. 3.7. Schematic Diagram of Cooling System
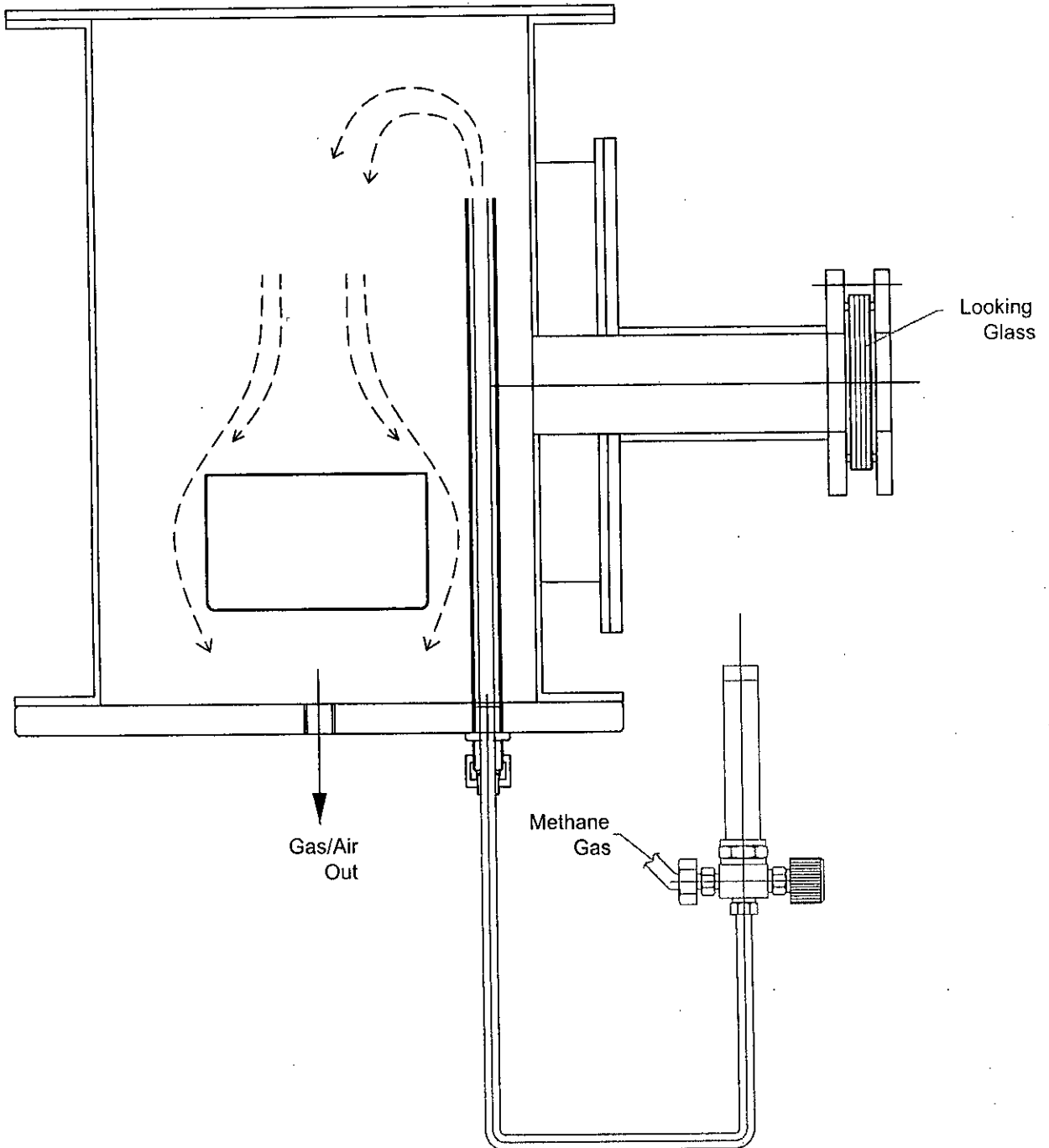
Fig. 3.8. Schematic Diagram of Gas Flow System
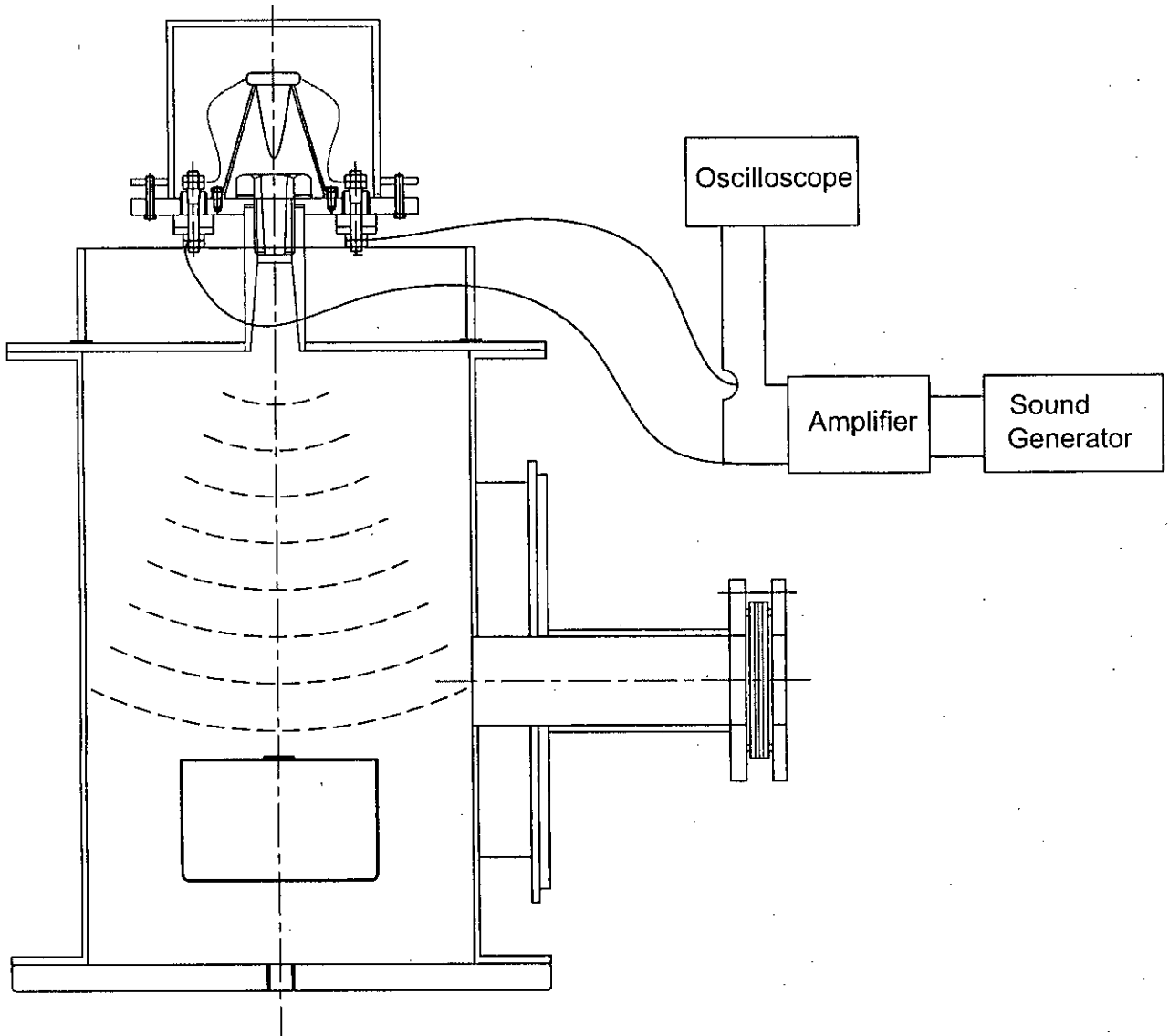
Fig 3.9. Schematic Diagram of Sound Generation System

Oscilloscope

AC 220 V

Sound Generator Amplifier

Piezoelectric Horn

AC 220 V

Activation Heater

AC 220 V

Substrate Heater

AC 220 V

Motor

Vacuum Pump

Gauge

AC 220 V
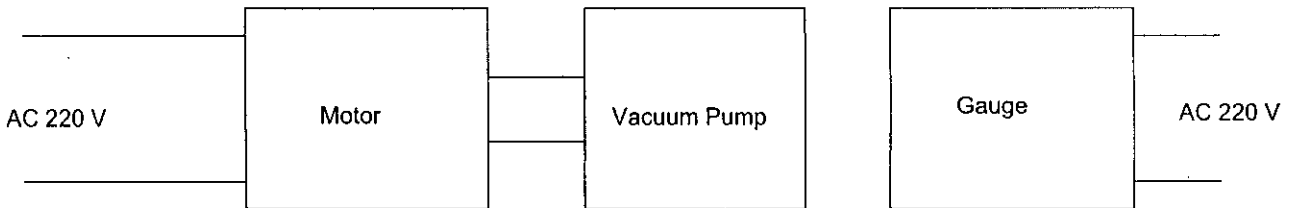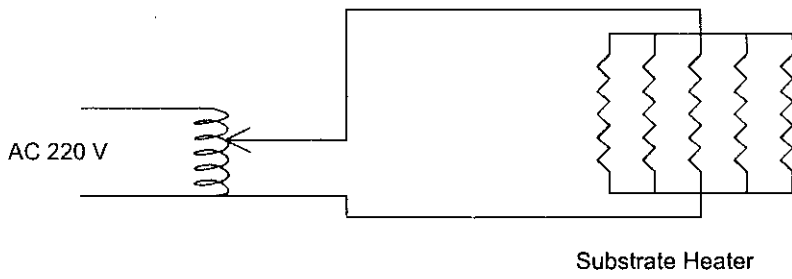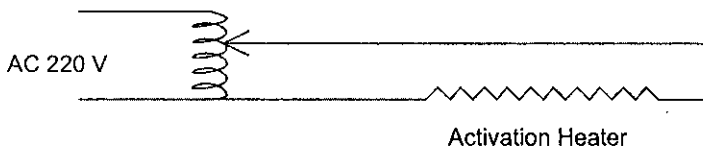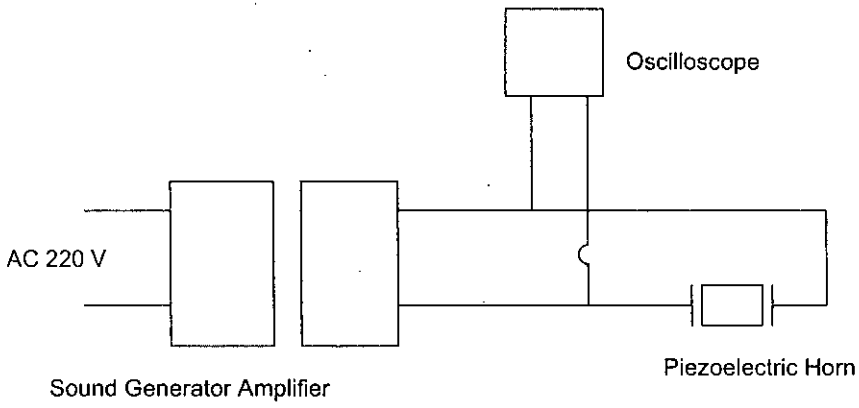
Fig 3.10. Schematics of Circuit Diagram
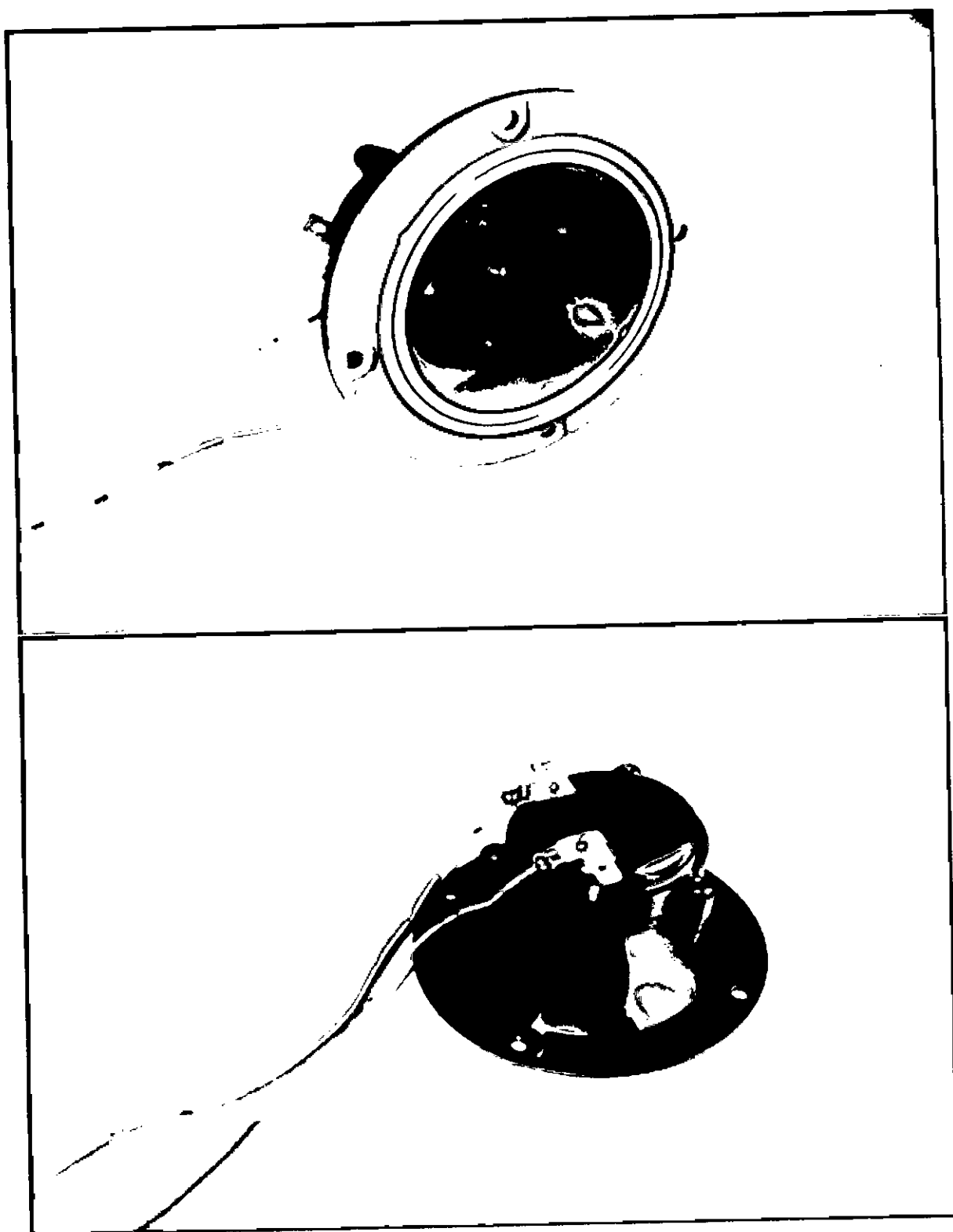
Fig. 3.11: Photograph of piezoelectric horn
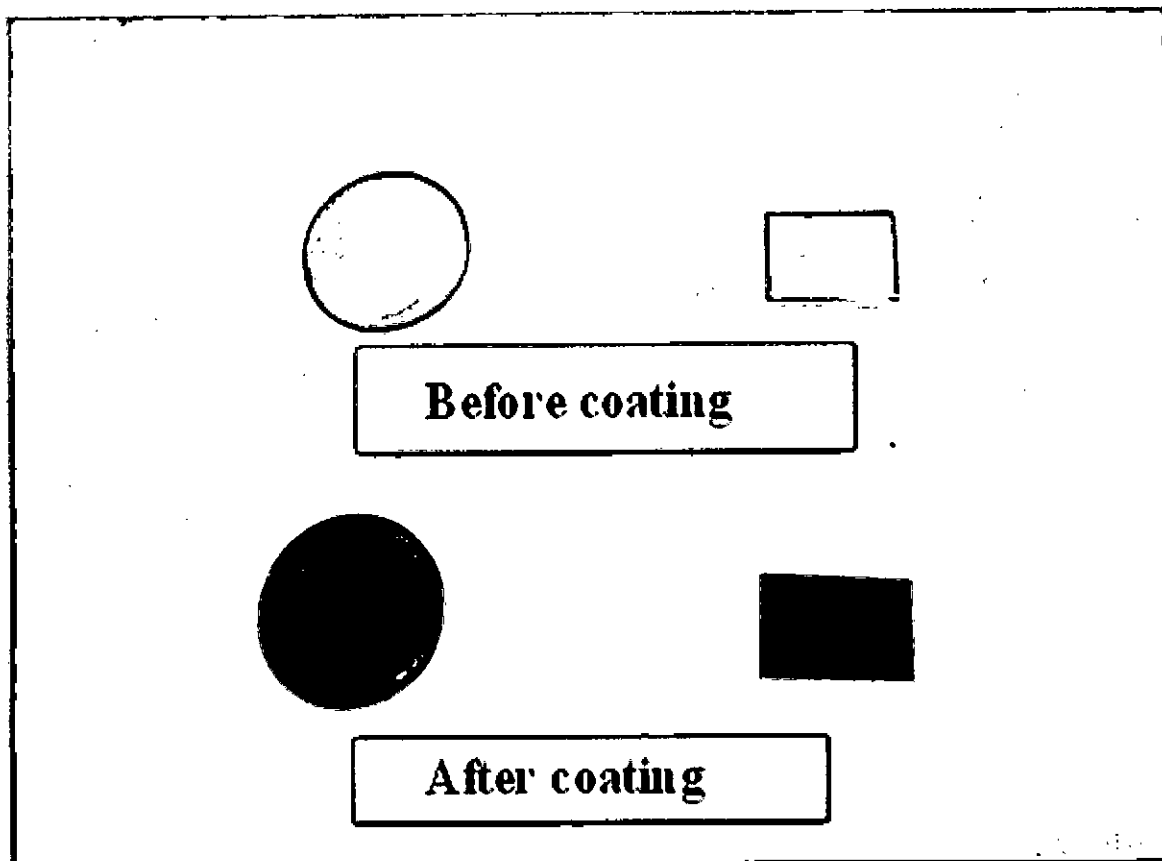
Fig. 3.12. Test sample before and after coating

(substrate = stainless steel 304, substrate temperature = 1000°C, activation heater temperature =1800-2000°C, gas used = CH4, pressure of reaction chamber = 25 Torr, frequency of sound= 30 KHz)

Table 3.1: Analysis of natural gas (CH_4)

	Parameters	Unit	Results	Remarks
A.	**Chemical Composition**			
01.	Methane (CH_4)	% (v/v)	97.14	
02.	Ethane ($C_2 H_6$)	% (v/v)	1.69	
03.	Propane ($C_3 H_8$)	% (v/v)	0.04	
04.	i-Butane ($C_4 H_{10}$)	% (v/v)	0.10	
05.	n-Butane ($C_4 H_{10}$)	% (v/v)	0.08	
06.	i-Pentane ($C_5 H_{12}$)	% (v/v)	0.04	
07.	n-Pentane ($C_5 H_{12}$)	% (v/v)	0.02	
08.	Higher Hydrocarbon (C_6 and above)	% (v/v)	0.39	
09.	Nitrogen (N_2)	% (v/v)	0.19	
10.	Carbon dioxide (CO_2)	% (v/v)	0.29	
B.	**Calorific Values**			
11.	Gross Calorific Value	K.cal/Nm^3	9772.96	
12.	Net Calorific Value	K.cal/Nm^3	8818.51	
C.	**Specific Gravity (density)**			
13.	Relative density		0.578	With respect to air

Source: Training Institute for Chemical, Industries (TICI), Ghorasal. Instruments used: Gas Chromotograph, Precision Calorimeter etc.

Table 3.2: Detailed Specification of the Accessories Used in the Experiment:

S. No.	Name of the Accessories	Specification	Application
1.	Vacuum Pump	Brand: vacuubrand, Germany Model: RZ 2 Capacity: 2.2 m^3/h	To pump out inside gas of the reactor chamber.
2.	Vacuum Gauge	Brand: vacuubrand, Germany Model: VAP 5 Capacity: 10^{-3} Torr	To measure the level of vacuum.
3.	Audio Signal Generator	Brand: GW brand, England Model: 808G Capacity: 1 MHz	To generate the signal of vibration.
4.	Oscilloscope	Brand: Yokohama, Japan Model: AL310	To measure the vibration parameters.
5.	Optical Pyrometer	Brand: Foster, England Model: AJ/ON/19.5 Capacity: 1950^0C	To measure the inside temperature of the reactor

Table 3.3: Chemical Composition of SS 304 (wt %)

C	Si	Mn	P	S
%	%	%	%	%
0.0968	0.83	2.11	<0.0014	<0.0011

Cr	Mo	Ni	Al	Co
%	%	%	%	%
16.069	0.1302	8.90	<0.0004	0.4148

Cu	Nb	Ti	V	W
%	%	%	%	%
0.63	0.1173	0.0186	0.2744	0.2826

Pb	Sn	Ce	B	Fe
%	%	%	%	%
>0.0360	<0.0021	0.1380	<0.0010	<69.951

Source: Spectro analysis, Bangladesh Industrial Technical Assistance Center (BITAC)

Table 3.4: Experimental Conditions

S. no.	Parameters	Range
1.	Pressure	20-30 Torr
2.	Substrate (Nicrom) temperature	$800\text{-}1000^0$ C
3.	Activation (Tungsten) heater temperature	$1800\text{-}2000^0$ C
4.	Substrate (Nicrom) heater power	1000 watt
5.	Substrate (Nicrom) heater voltage	80-100 V
6.	Substrate (Nicrom) heater current	7-10 amp
7.	Activation (Tungsten) heater power	200 watt
8.	Activation (Tungsten) heater voltage	5-7 V
9.	Activation (Tungsten) heater current	25-35 amp
10.	Flow rate (CH_4 gas)	0.1-1.5 l/min
11.	Gap between substrate and Tungsten heater	2.5-8.0 mm
12.	Sound frequency	0-110 kHz
13.	Deposition duration	3-10 minutes
14.	Substrate size	22mmX14mmX1.15mm

CHAPTER 4
RESULTS AND DISCUSSIONS

4.1 INTRODUCTION

Experiments are carried out with and without vibration under different operating conditions. In this chapter, the effects of vibration on vapor deposited coating are discussed and then results of vibration are compared with those of without vibration.

4.2 CHARACTERIZATION OF THE DEPOSITED COATING WITHOUT VIBRATION

The surface morphologies of the deposited coatings were investigated by a scanning electron microscope (SEM) equipped with energy dispersive X-ray spectrometry (EDX). X-ray diffraction (XRD) analysis was also carried out to identify the compound of the deposited coating. Also, the cross-sectional view of the coated sample was investigated under SEM and optical microscope.

4.2.1 SEM & EDX Investigation

SEM study revealed that a dense and rough layer was deposited on the stainless steel substrate illustrated in figure 4.1. The EDX analyses of coated and uncoated samples are shown in figure 4.2 and 4.3, respectively. Figures show the carbon peak along with the peaks of chromium, iron etc. It is clear that peaks other than carbon come from the substrate stainless steel. It is also observed that the amount of carbon particles in coated sample is higher as compared with the uncoated sample (compare figure 4.2 and 4.3). This indicates that a layer of carbon is deposited on the substrate.

4.2.2 XRD Analysis

XRD spectra of the sample of base substrate stainless steel 304 without coating and with coating are shown in figures 4.4, and 4.5, respectively. Peaks of the carbon for graphite and diamond along with the peaks of austenite of austenitic stainless steel are observed in the X-rays. This indicates that graphite and diamond/diamond like

carbon are deposited on the stainless steel substrate. But this layer is very thin because the XRD pattern shows the austenite peaks of the substrate stainless steel. The d-spacings determined from XRD patterns of the coated layer without sound vibration are shown in table 4.1. They are compared with the standard d-spacings for graphite, diamond and austenite of austenitic stainless steel. The table 4.1 shows that the measured value of d-spacings peaks are almost similar with the standard d-spacings values of graphite, diamond and austenite of austenitic stainless steel. It is known that if methane is pyrolyzed at 1100 ^{0}C or above, and within the pressure range of about 1 Torr to 1 atm, graphite is formed. As in the present case the deposition was conducted at activation temperature 1800-2000^{0}C, the presence of some graphite peaks confirmed the deposition of graphite on the substrate stainless steel. Formation of some diamonds is also possible because the deposition and morphology of diamond growth are function of temperature (generally 2000^{0}C) and distance (1 cm) between substrate and activation heater (1). By maintaining this condition, plasma is generated which is obtained by resistance-heated wire of tungsten. As atomic hydrogen is formed and the carbon species become activated in the vicinity of activation heater and transformed into diamond, and deposited on the substrate. Although XRD pattern shows peaks of carbon for graphite and diamond at the same position, the presence of diamond in the deposited coating can be confirmed by further analysis by Raman spectroscopy which identifies the characteristic C-C diamond bond.

Since, by XRD analysis the peaks of graphite and diamond are found, it may have the possibility of existence of Diamond like Carbon (DLC) within the coating also. The DLC, due to its amorphous microstructure, can be analyzed by Raman spectroscopy analysis.

4.3 COATING UNDER SOUND VIBRATION

To observe the effect of sound vibration on deposited coating, a sound generating system has been incorporated with this CVD system.

To generate sound, a laboratory sound generator was selected. This sound generator can provide sub-sonic, sonic and ultra-sonic sound. In this case,

piezoelectric horn was used instead of magnetic horn due to its oversize and possibility of disturbance in magnetic field from possible over heating during experiment. To install this, a special arrangement was made at the top of the reactor chamber, described in section 3.4.

The functionality of the process parameters were also re-checked including the sound vibration. During investigation, it was found that the process pressure during coating had a great effect when sound vibration system is included, since the density of the media affects the transportation of sound vibration. To optimize the value of process pressure during coating, several experiments were performed. Figure 4.13 shows that, at pressure below 25 Torr (approximately) the deposition curves with and without vibration tends to coincide each other, that means the effects of vibration become negligible, on the other hand bonding is better in low vacuum range. S that it was justified to assume the optimum value of deposition pressure is 25 Torr.

The sound was mainly introduced from the top of the reactor chamber that is, normal to the substrate surface. The experiment was also performed by introducing sound vibration horizontally, parallel to the substrate surface. The deposition rate was found by visual inspection of SEM analysis to be approximately 50% lower when parallel than when normal. The nature of the surface of the coated samples under perpendicular direction shows smoother surface than that of the surface of the deposited sample under parallel direction by visual observation (figure 4.6).

To observe the effect of sound vibration on coating, the other parameters were kept constant as much as possible. For this reason, the experimental conditions were designed in such a way that the exhaust system by vacuum pump and as well as the supply of reactant gas (methane) into the reaction chamber was stopped during the deposition time of experiment.

After investigating all the process parameters including the optimization of the process pressure with sound vibration, successful coatings were deposited on the substrates which were further characterized.

4.3.1 Characterization of Deposited Coating under Sonic Vibration

In this section, characterization of deposited coating under sound vibration and comparison of coating under vibration and without vibration are discussed.

4.3.1a SEM and EDX Investigation

Figure 4.8 shows the comparison of micrographs of coated surface under vibration and without vibration at 200 magnifications. The left side view of this figure is the coated surface deposited under vibration (40 kHz) and right side view is the coated surface deposited without vibration. By observing the morphologies of the coated surfaces (figure 4.7), it is shown that the deposited coating under vibration are more compact, smooth as compared to the coating deposited without vibration. The EDX analysis also shows that the coating on the substrate have considerable amount of carbon particles (figure 4.8). Comparing this figure with figure 4.2 of without sound vibration shows that the percentages of carbon with vibration and without vibration are 13% and 11% respectively by computerized SEM analysis display. This indicates that vibration of sound creates mechanical and pressure wave propagation, which influences the mass transport towards the substrate. As a result better coating is obtained under sound vibration compared to that without vibration.

4.3.1b XRD Analysis

XRD analysis of specimen is shown in figure 4.9 for coating under sound vibration. The d-spacings determined from XRD patterns of the existing crystals within the coated layer under vibration is shown in table 4.2. They are compared with the standard d-spacings for graphite, diamond and austenite of austenitic stainless steel. It is found that the values of d-spacings calculated from the observed peaks and from XRD analysis are almost similar with the standard d-spacings values of graphite, diamond and austenite of austenitic stainless steel.

For comparison of data of area under the significant peaks of figures 4.2, 4.3 and 4.9 indicating the intensity are summarized and presented in table 4.3. The

peaks 1, 3 and 6 of figures indicate the presence of austenite of austenitic stainless steel, and the other peaks of the figures indicate graphite and diamond. The intensity of the peaks 1, 3, and 6 of austenite of austenitic stainless steel substrate without coating are 38, 16, and 13 units, while for coated substrate without sound vibration are 30, 17, and 11 units, and for coated substrate with vibration are 17, 12, and 10 units. From these data, it is observed that, the intensity of the peaks of austenite of austenitic stainless steel decreases in the coated layer due to deposition of carbon. This intensity of the peaks of austenite of austenitic stainless steel with the coated layer under vibration reduces more as compared with the coated layer under no vibration. On the other hand, the intensity of the peaks 2, 4, 5, and 7 of graphite and diamond under no vibration are 12, 8, 4, and 4 units and for coating with sound vibration are 9, 11, 5, and 5 units. It is seen from these data that the intensity of the peaks of graphite and diamond for the sample coated under vibration increases in the average compared with the coated layer under no vibration that means deposition rate under vibration is better as compared to without vibration.

.4.3.2 Effects of sound vibration on deposition rate

The deposition rates of the coating in gram per unit area per unit time were calculated from the weight difference of substrate before and after deposition, divided by the substrate surface area and deposition time. The deposition rate by weight on unit area for both coated substrate were measured for without and with vibration. A considerable increase in deposition rate on unit area is observed for deposition under vibration compared to that no vibration.

Figure 4.10 shows the variation of deposition rate under vibration and without vibration in the range of frequency 0 to 110 KHz at a distance of 5 mm between substrate and activation heater. At each frequency, at least five experiments were conducted to get an average deposition rate. All these data are presented in the figure. From these data a considerable increase in deposition rate on unit area is observed for deposition under vibration compare to that under no vibration.

From this figure, it is observed that deposition rate increases from 0 at no to approximately 6 KHz. Between these frequency range no data were taken due to

the limitation of our sound generating system. From 6 KHz the deposition rate increases linearly up to approximately 20 KHz and after that the steepness of the curve shows higher deposition rate and finally increment rate reduces to almost negligible amount up to the observed range. The higher deposition rate under vibration might be due to the fact that mechanical and pressure wave of propagated sound towards the substrate enhances the mass transfer rate of depositing carbon species. The variation of the rate of increment of deposition at different frequency ranges might be due to the change of resultant vibration of carbon particles which depends on the wave length of the sound at different frequency and the particle size and the mass of the species. It is observed that deposition rate under sonic range of sound vibration does not vary significantly with frequency of vibration. But the rate of deposition under ultrasonic vibration increase significantly with frequency of vibration.

The corresponding linear fit of the curve of deposition rate versus vibration for zones a and b are shown also in figure 4.10.

Figure 4.11 shows the variation of deposition rate with the distance between substrate and activation heater under vibration and no vibration. From this figure it is observed that deposition rate under vibration is higher than that under no vibration at identical conditions within the observed range. Curves 1, 2, 3 and 4 of figure 4.11 are drawn for 4 mm to 8 mm distance between substrate and activation heater and under the vibration of 0, 40, 70, 90 and 110 kHz, respectively. From this figure, it is shown that the deposition rate decreases linearly with the increase of distance between substrate and activation heater up to 6 mm and after that it remains almost constant. This may be due to the numbers of activated carbon species and atomic hydrogen are more near the activation tungsten heater. It is observed that the decreasing deposition rate with distance (up to a certain distance) is higher for high frequency in comparison to lower frequency. This is because the higher the intensity, the higher is the variation of energy with respect to distance. For a particular distance, the deposition rate is high for higher frequency. This is because, at higher frequency, the intensity of sound is higher and thus the energy transmitted from sound to the particle is higher. For all frequencies, when the distance is more than 5.5 mm the deposition rate is almost constant. That means, beyond this distance, the

effect of frequency on deposition rate is negligible. This may be due to the dissipation of sound energy to the environment reaches to a mean value (for any intensity) at a distance more than 5.5 mm.

Figure 4.12 is drawn at a frequency of vibration 0 and 40 kHz showing the effects of activation heater temperature on deposition rate. From this figure it is observed that deposition rate increases almost linearly with the increase of activation heater temperature. This figure also shows that deposition under vibration condition is more than that of under no vibration condition and the difference of deposition also increases with the increase of activation heater temperature. The increase of deposition with the increase of temperature with and without vibration of sound might be due to the activation of carbon species increases as the temperature increases and thus increases the deposition rate.

Figure 4.13 is drawn for 0 and 30 kHz to observe the effect of deposition pressure on deposition rate. From this figure it is shown that deposition rate increases almost linearly with the increase of deposition pressure under 0 and 30 kHz. The nature of these two curves indicates that the difference of deposition rate between 0 and 30 kHz increases with the increase of deposition pressure. This might be due to the fact that, the higher the deposition pressure the higher the density of the sound transmitting media which increases the sound transmission as well as the mechanical and pressure wave of sound.

Figure 4.14, shows the deposition by weight on unit surface area of the substrate at different duration of deposition time under 0 and 6 kHz. From this figure it is shown that deposition by weight increase almost linearly with the increase of duration of deposition. This is obviously due to the fact that, for a particular condition of deposition; it is the function of time. In this figure, curve shown for vibration is steeper than the curve for no vibration.

4.4 POSSIBLE CAUSES OF HIGHER DEPOSITION UNDER SOUND VIBRATION

Possible causes of higher deposition rate, compactness and smoothness of the deposited coating under sound vibration condition can be explained as follows.

It is already explained in the literature that the complex chemical and physical processes, which occur during diamond CVD, comprise several different but interrelated features. The process gases of the chamber before diffusing toward the substrate surface pass through an activation region (a hot filament), which provide energy to the gaseous species. This activation causes molecules to fragment into reactive radicals and atoms, creates ions and electrons, and heats the gas up to temperatures approaching a few thousand Kelvin. Beyond the activation region, these reactive fragments continue to mix and undergo a complex set of chemical reactions until they strike the substrate surface. At this point the species is adsorbed and entrapped within the surface, some portions is desorbed again back into the gas phase, or diffuse around close to the surface until an appropriate reaction site is found. If a surface reaction occurs, one possible outcome, if all the conditions are suitable, is diamond. During this process, the addition of sound vibration shown in figure 4.15 might increase the energy level of the depositing species. The increase of deposition rate and the surface quality of the deposited coating might be due to elimination or reduction of the potential barrier [17] during the chemical activity by adding some extra sound energy. This extra sound energy may work on the deposition process in the following ways:

- According to the potential energy as a function of interatomic distance between two charged atoms or ions [70], as media particles vibrate back and forth, for equilibrium condition, some extra energy remains in the process, during the introduction of extra vibration into the system.

- Deposition increases due to increase of pressure. At constant temperature, the amount of adsorption depends on pressure [71-73].

- As movement of the particles increase, the concentration of diffusing carbon elements increase [74-75]. Therefore the diffusion rate of the coating may increase.

- Extra vibration of sound may increase the momentum difference of carbon and hydrogen due to their atomic mass difference in methane (CH_4) molecule [70]. This might enhance the chemical reaction in CVD process, and ultimately the deposition rate may increase.

The results obtained under this study shows that sound vibration increases deposition rate with more compact and smoother surface finish. Similar study is conducted in the formation of thin film produced by thermal vaporization process with ultrasonic vibration by Severdenko, V P et all [15] and the effects of ultrasonic vibrations on the localized electrochemical deposition (LECD) process by S H Yeo, J H Choo and K H A Sim [16]. According to their results ultrasonic vibrations increase the rate of deposition and improve the concentricity of the fabricated micro-columns. Ultrasonic vibrations perpendicular to the deposition plane improved the uniformity of vapor-deposited films by intensifying diffusion. The effect increases with increasing intensity. Ultrasonic vibrations normal to the deposition surface increase the film thickness. These results confirm our findings in the present study.
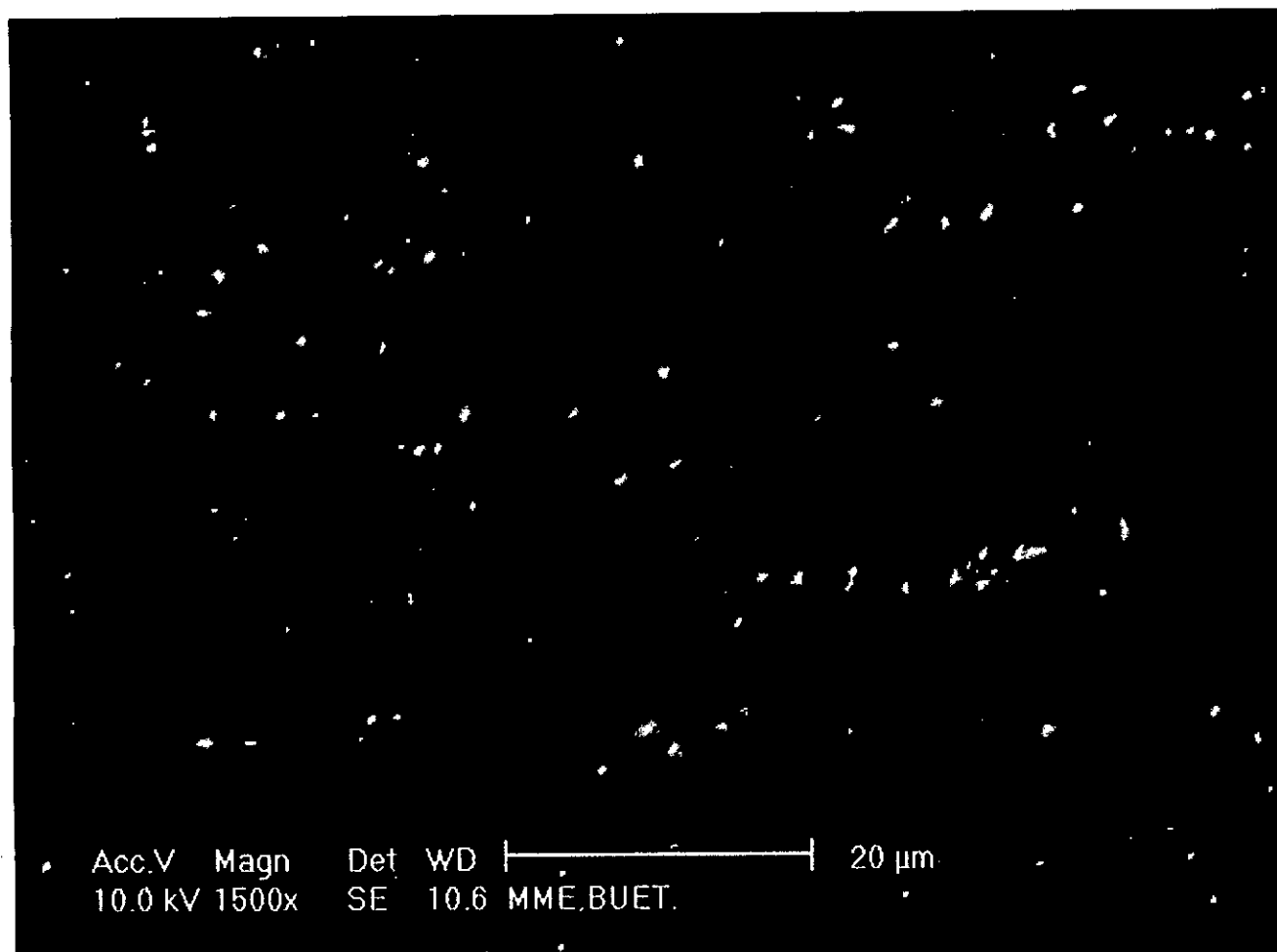
Fig. 4.1: Surface Morphology of the coated layer (substrate = stainless steel 304, substrate temperature = 1000°C, activation heater temperature =1800-2000°C, gas used = CH4, pressure of reaction chamber = 25 Torr)
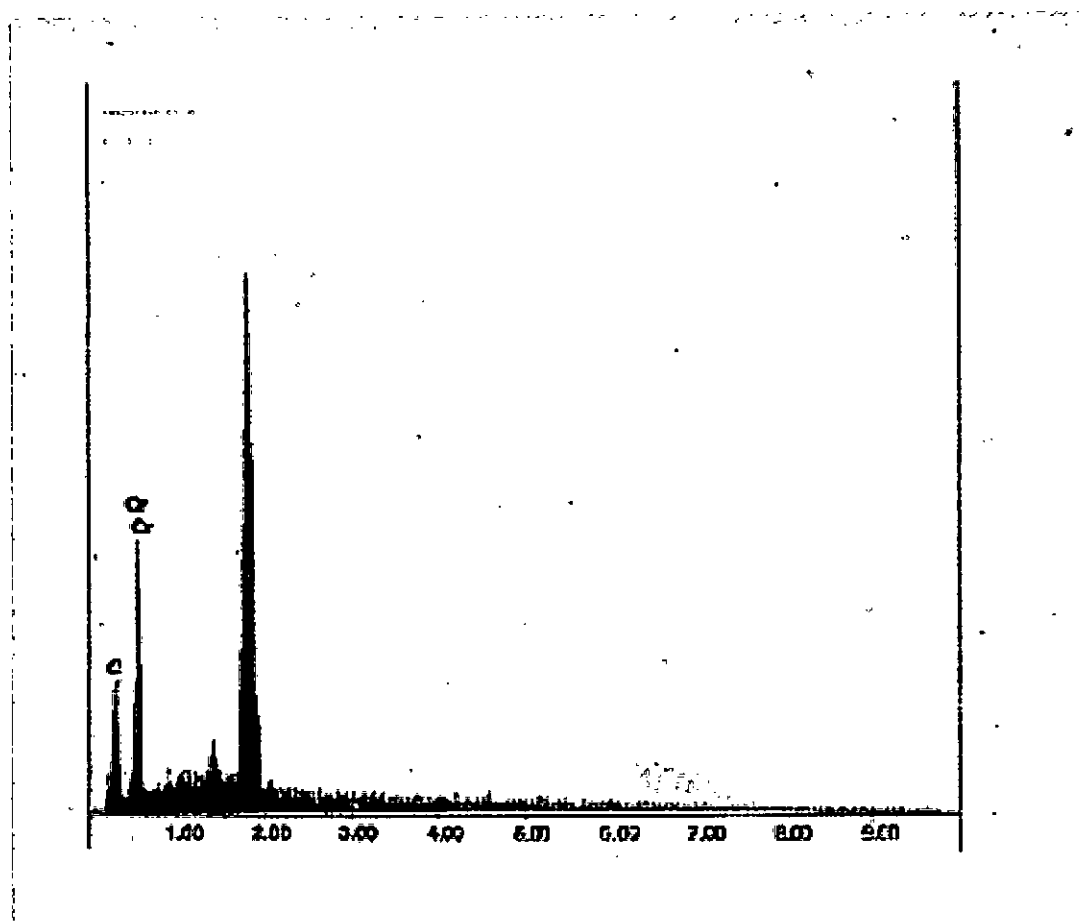
Fig. 4.2: EDX analysis of coating on substrate with no sound vibration (substrate = stainless steel 304, substrate temperature = 1000°C, activation heater temperature =1800-2000°C, gas used = CH4, pressure of reaction chamber = 25 Torr)
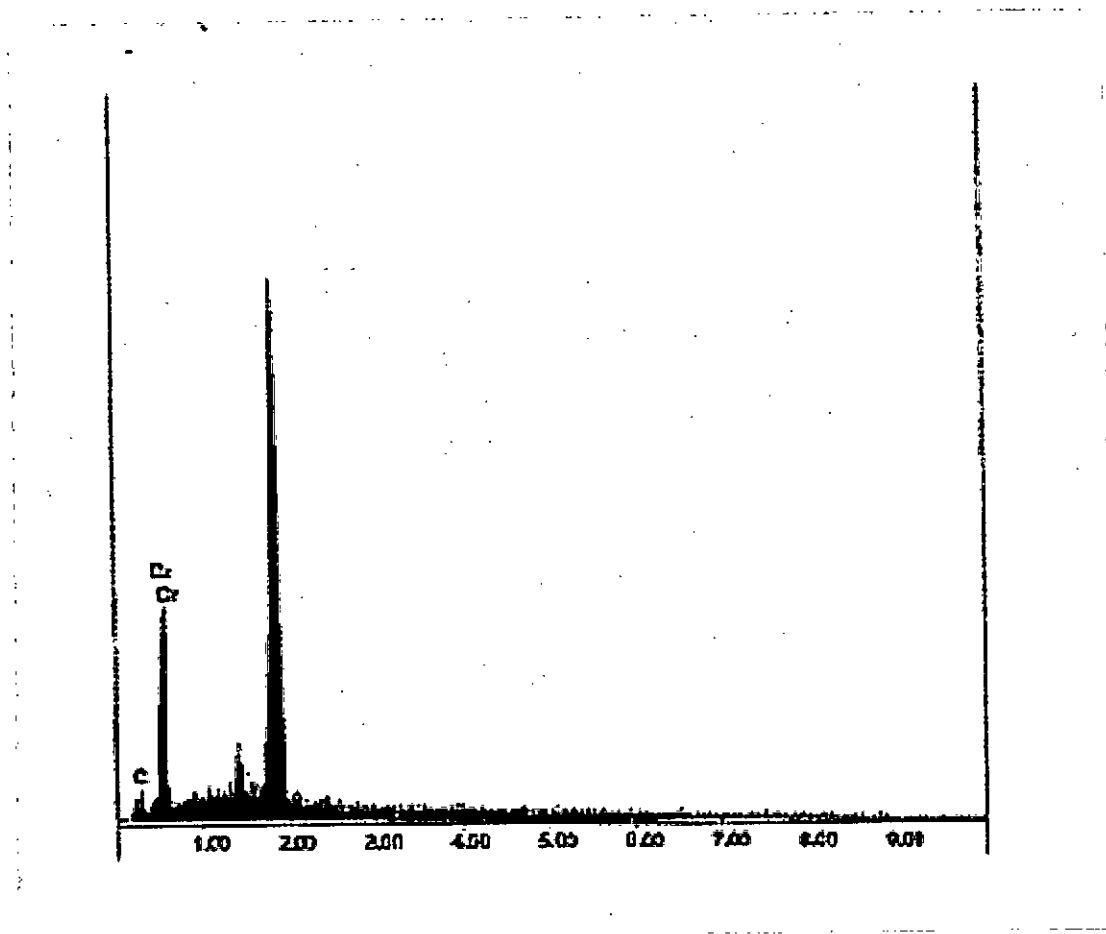
Fig. 4.3: EDX analysis of coating on SS 304 substrate
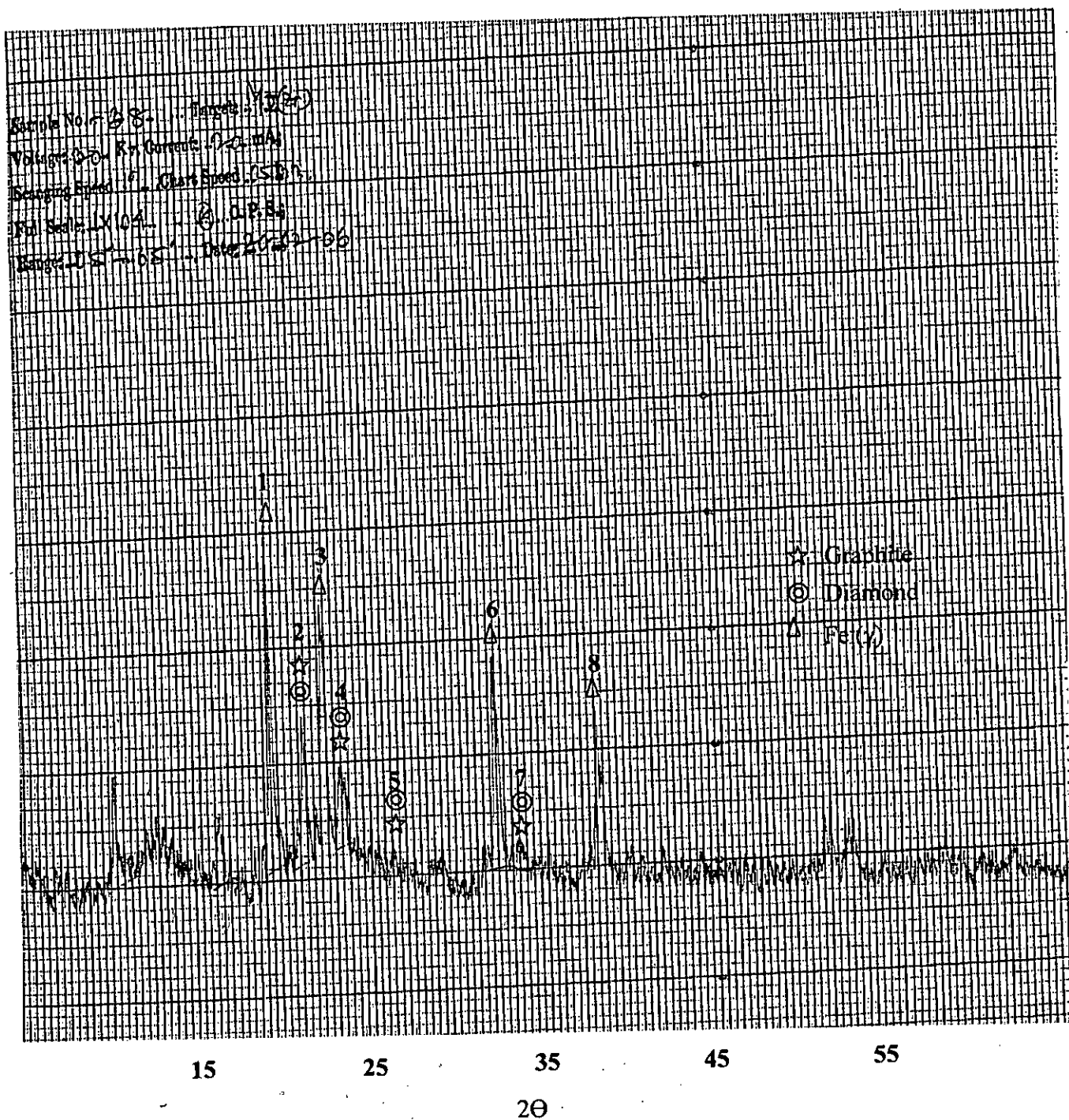
Fig. 4.4: XRD analysis of coated surface without sound vibration (substrate = stainless steel 304, substrate temperature = 1000°C, activation heater temperature =1800-2000°C, gas used = CH4, pressure of reaction chamber = 25 Torr)
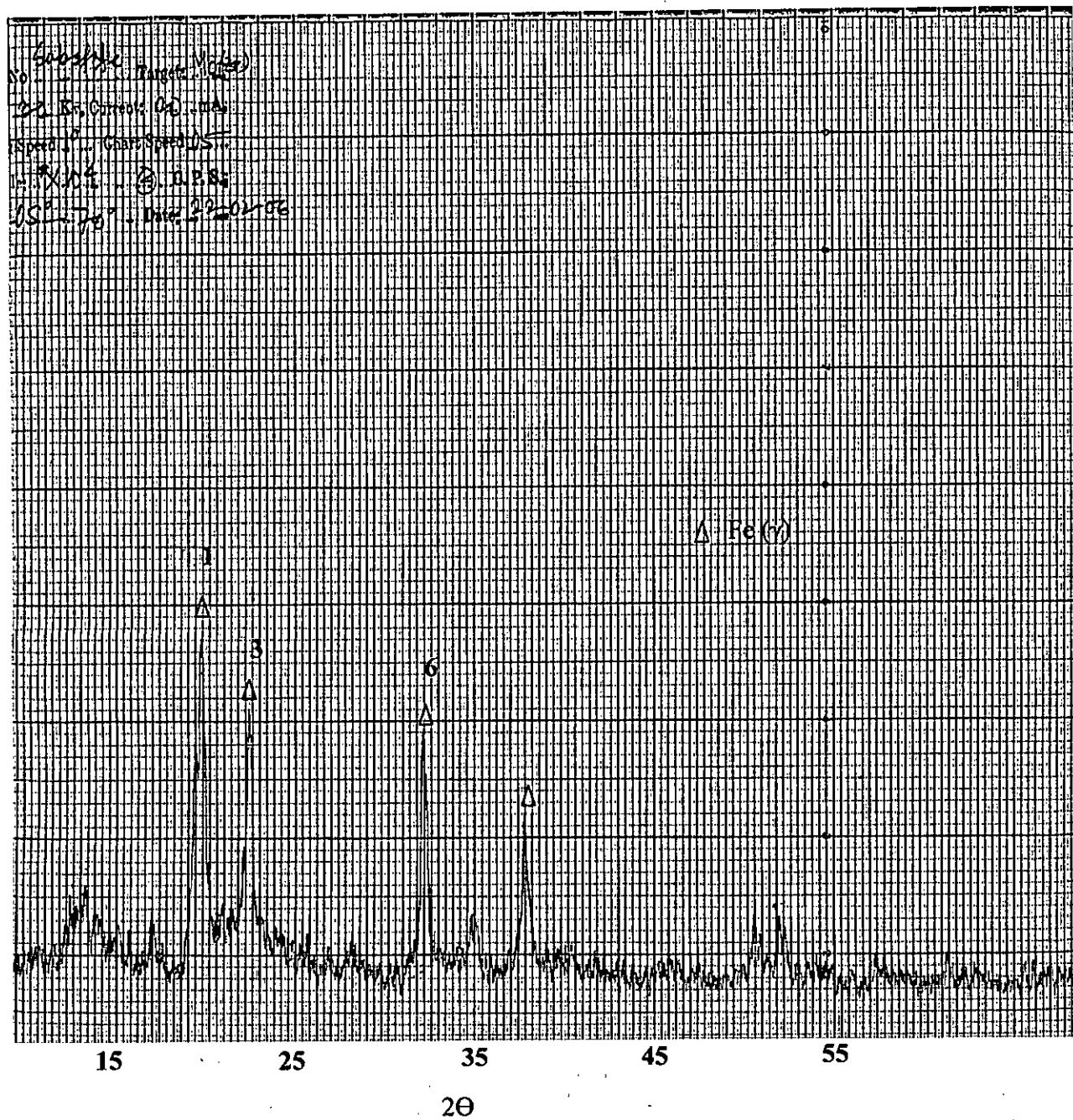
Fig. 4.5: XRD analysis of the substrate without coating
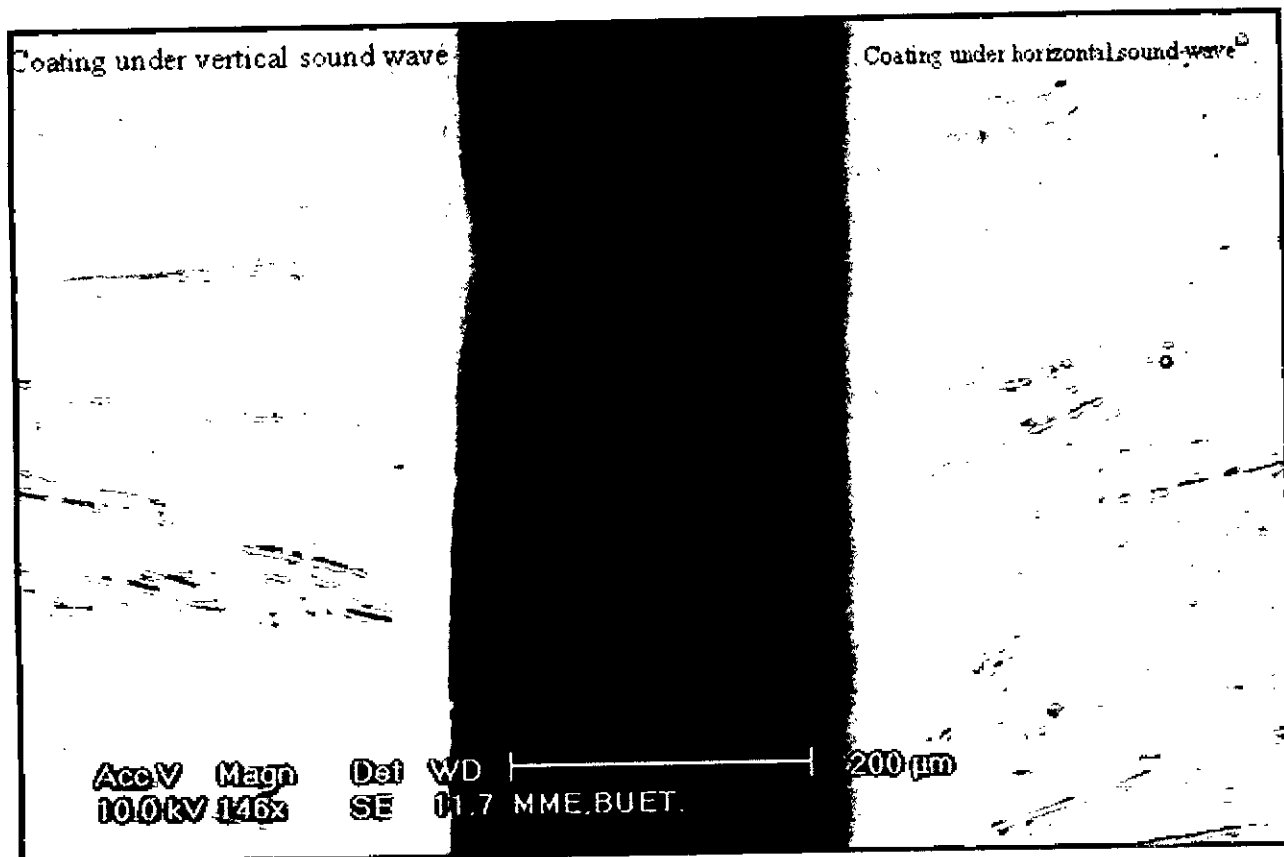
Fig. 4.6: Comparison of morphology of coated surface between vertical and horizontal sound vibration (substrate = stainless steel 304, substrate temperature = 1000°C, activation heater temperature =1800-2000°C, gas used = CH4, pressure of reaction chamber = 25 Torr, frequency of sound= 30 KHz)

with vibration
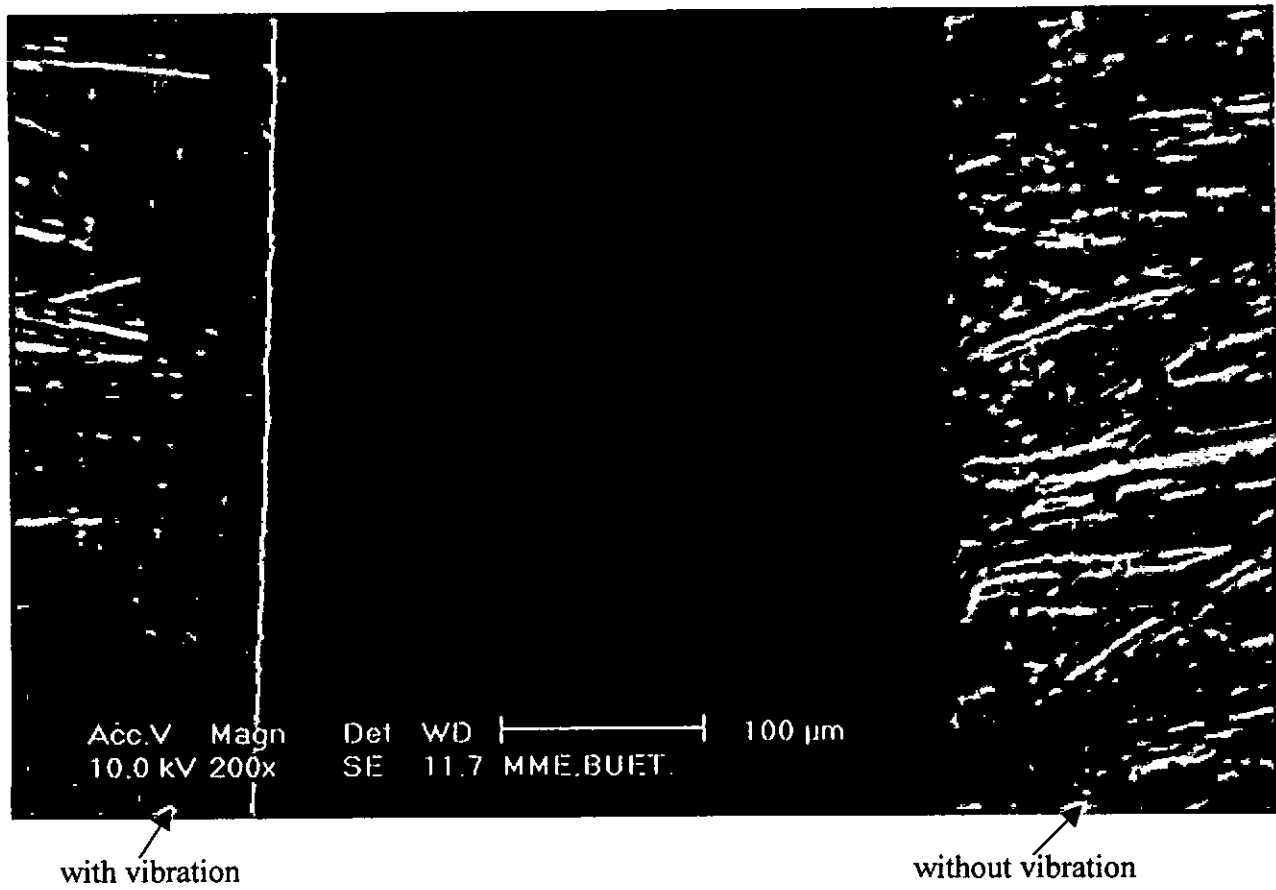
without vibration

Fig 4.7: Microstructure (under SEM) of deposited coating under vibration (left side view) and without vibration (right side view) condition at different resolutions.
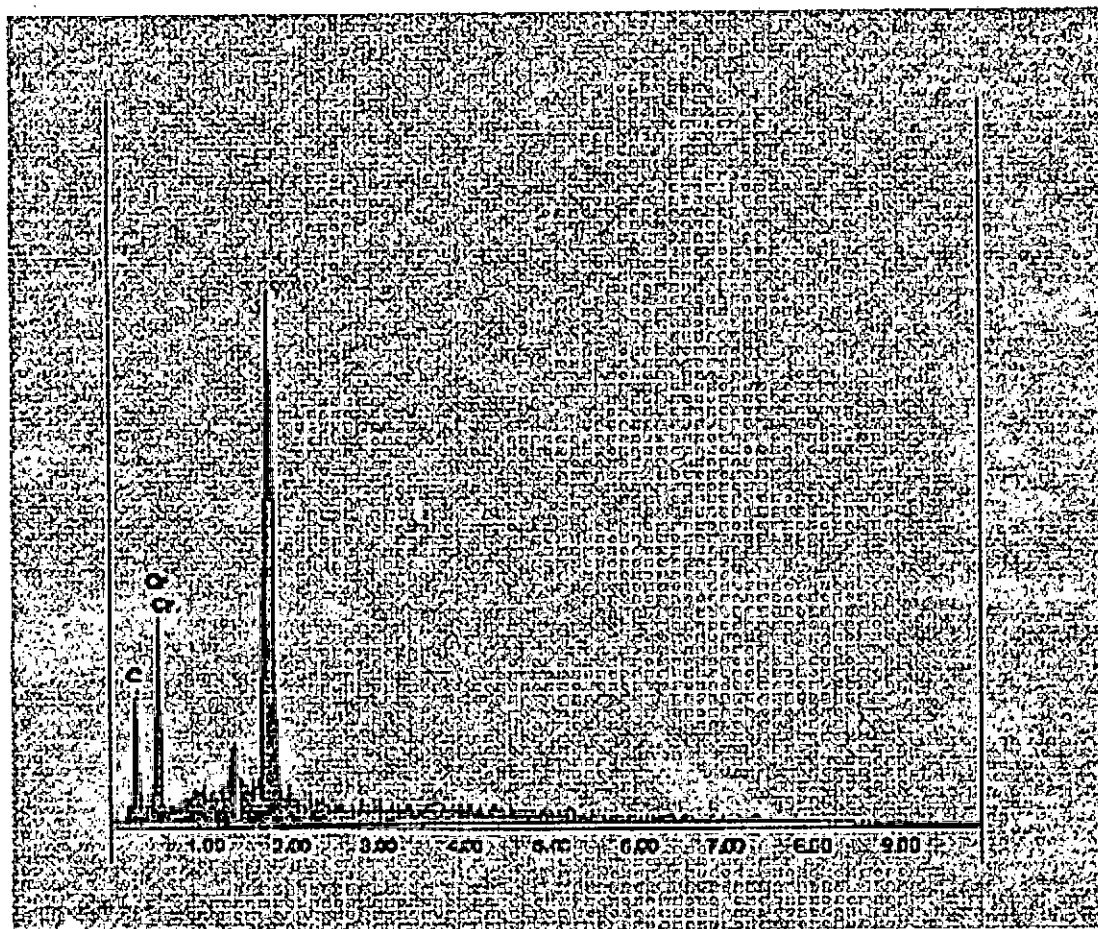
Fig. 4.8: EDX analysis of coating on substrate with sound vibration (substrate = stainless steel 304, substrate temperature = 1000°C, activation heater temperature =1800-2000°C, gas used = CH4, pressure of reaction chamber = 25 Torr, frequency of vibration= 40 kHz)
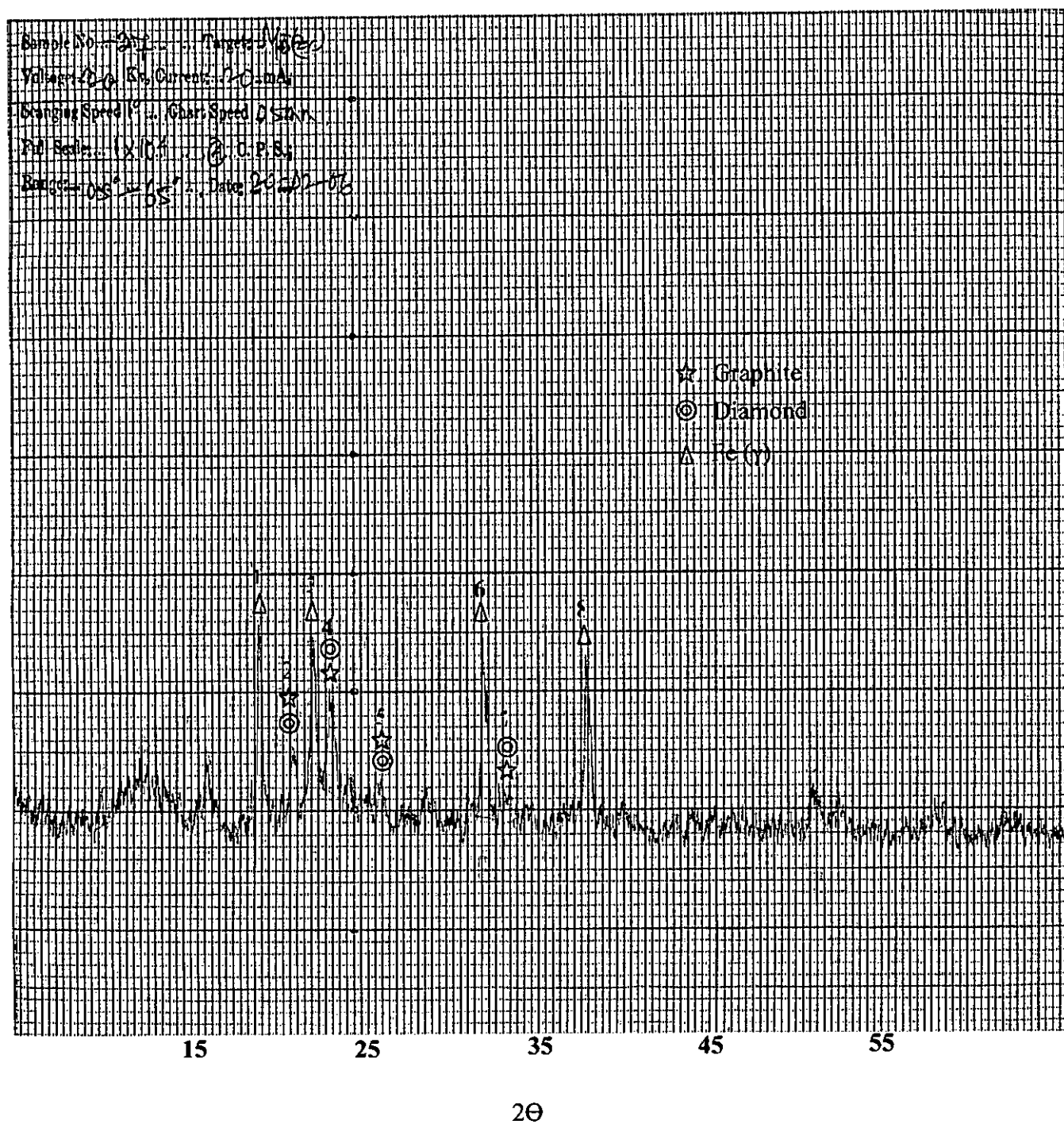
Fig. 4.9: XRD analysis of coated surface under sound vibration (substrate = stainless steel 304, substrate temperature = 1000°C, activation heater temperature =1800-2000°C, gas used = CH4, pressure of reaction chamber = 25 Torr, frequency of sound= 90 KHz)
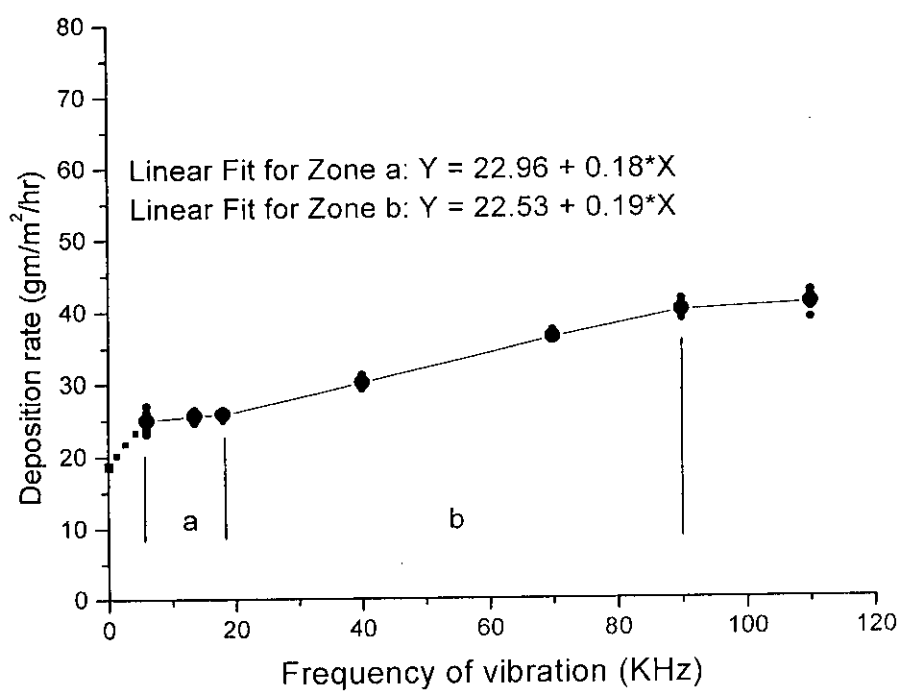
Fig.4.10. Deposition rate as a function of frequency of vibration
(T_{sub}=1000^{0}C, T_{act}=1900^{0}C, P_{ch}=25 Torr, d=5mm)
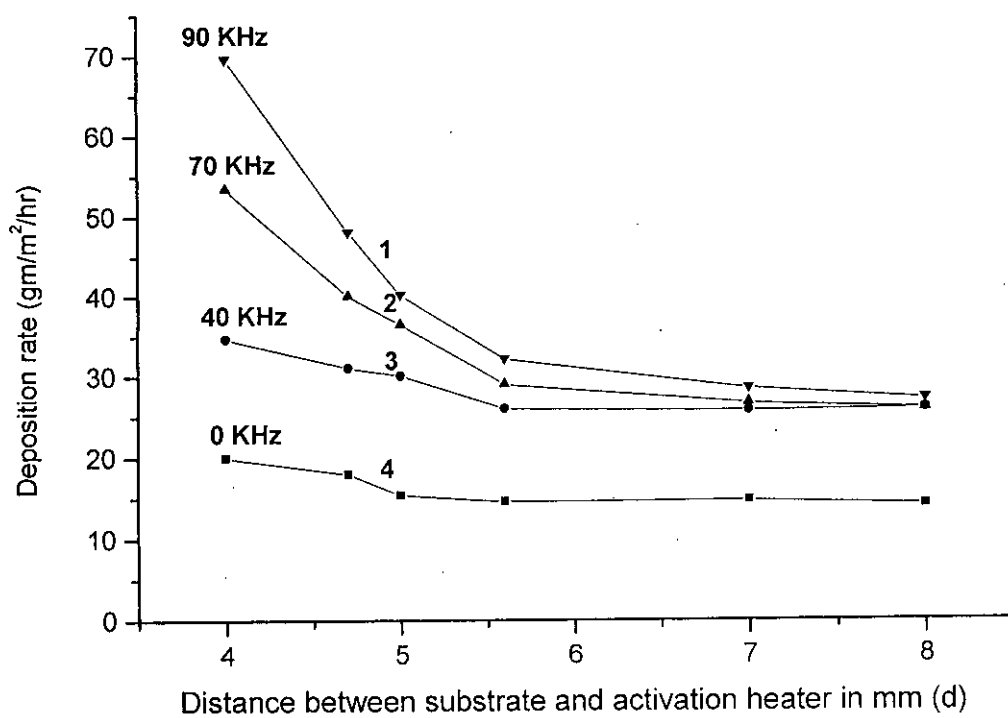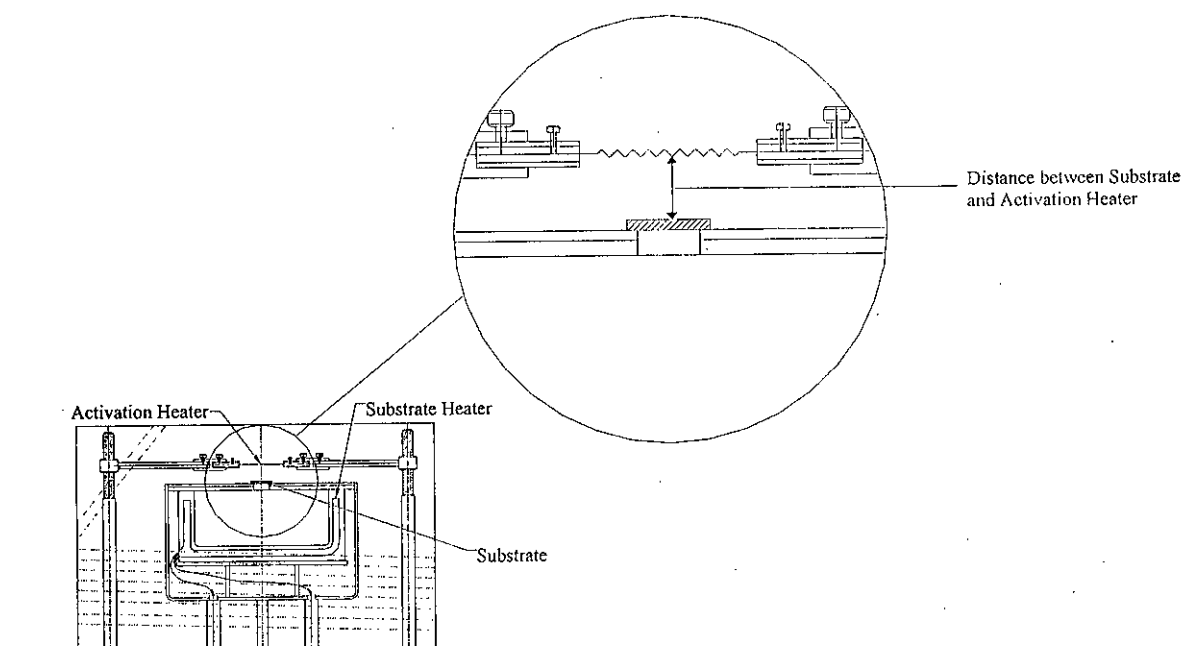
Fig.4.11: Effect of vibration on deposition rate with respect to distance between substrate and activation heater

$(T_{sub}=1000^{0}C,\ T_{act}=1900^{0}C,\ P_{ch}=25\ Torr)$
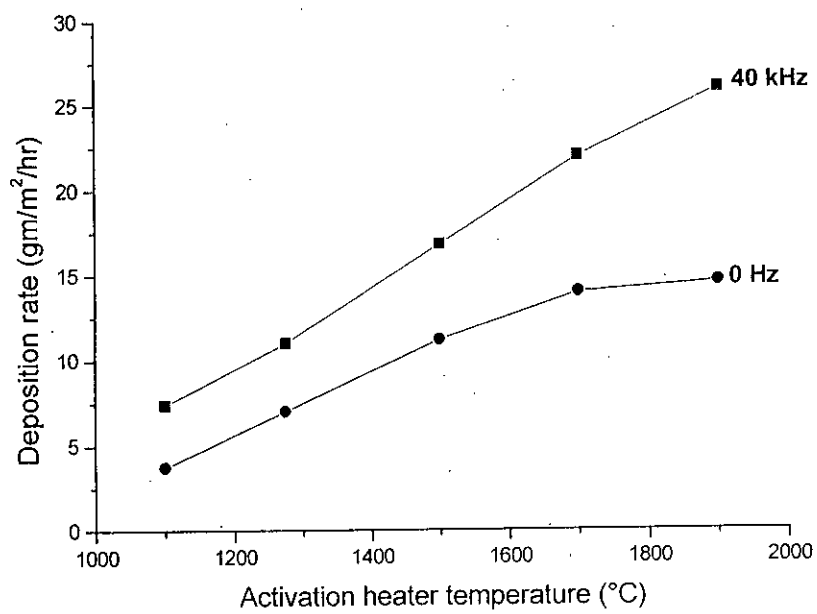
Fig.4.12: Deposition rate vs activation heater temperature

$(T_{sub}=1000^0C, P_{ch}=25 \text{ Torr, } d=5mm)$
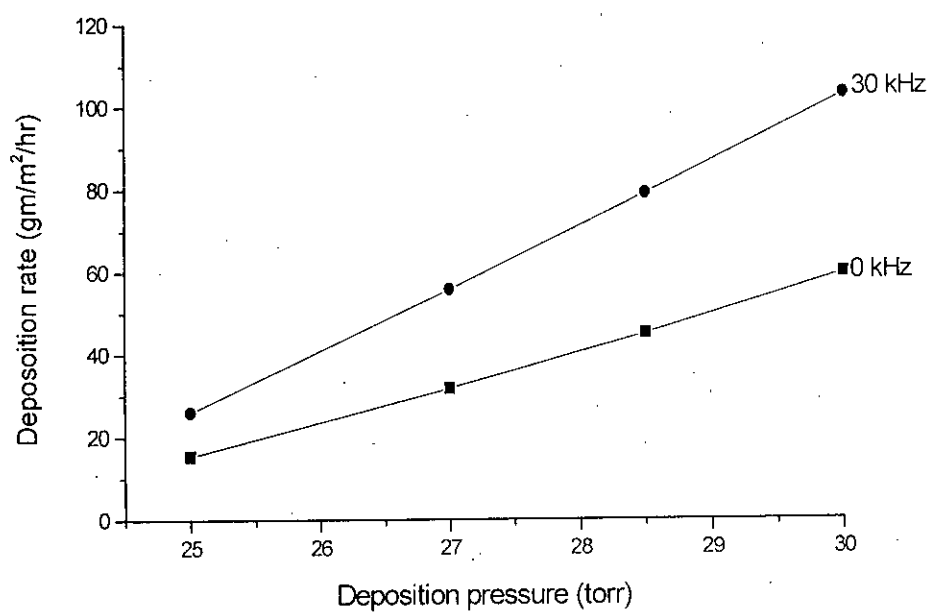
Fig. 4.13:Deposition pressure vs deposition rate

$(T_{sub}=1000^0C, T_{act}=1900^0C, d=5.6mm)$
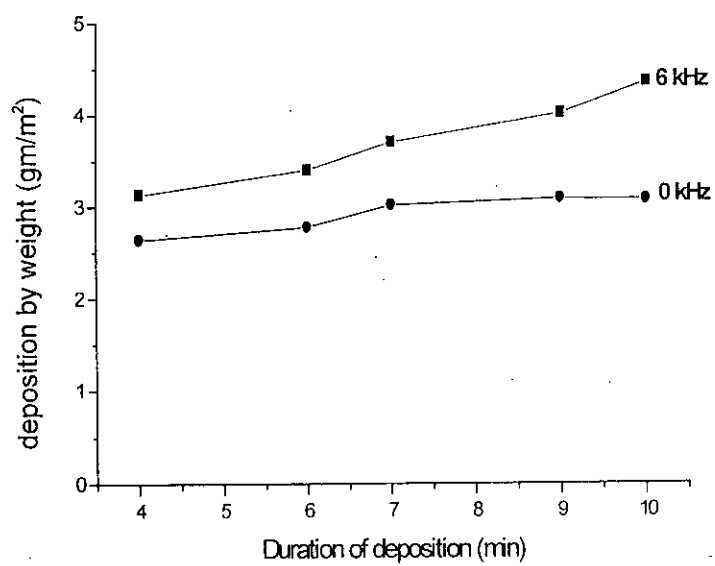
Fig. 4.14: Duration of deposition vs deposition by weight
(T_{sub}=1000^{0}C, T_{act}=1900^{0}C, P_{ch}=25 Torr, d=5mm)
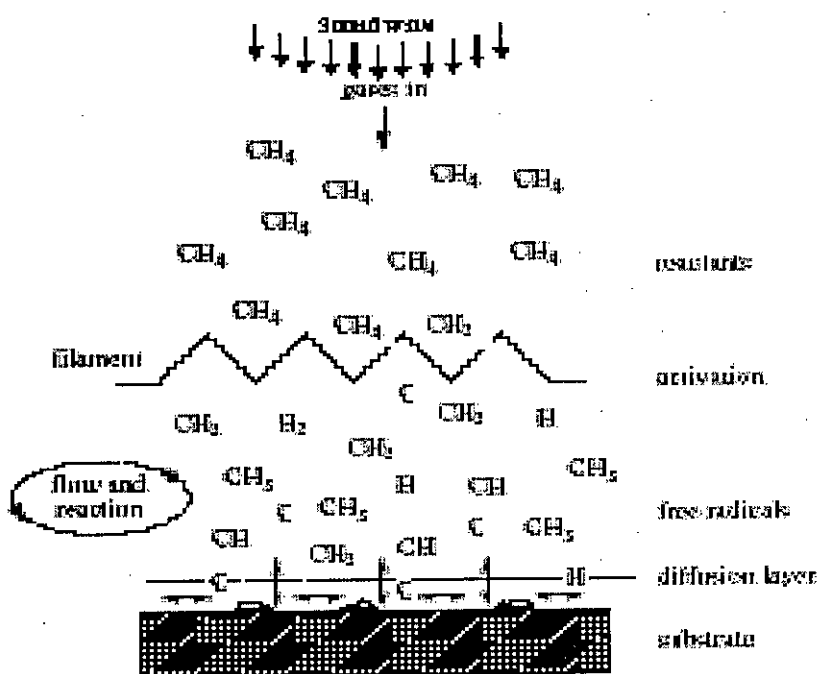
Fig. 4.15: Schematic of physical and chemical process occurring during diamond CVD under sound vibration

Table 4.1: Comparison of the d-spacings of XRD spectrum of the deposited crystal with the actual d-spacings for graphite, diamond and Fe (γ) without sound

Peak no.	2θ	Measure d d (A)	i/i₀	Diamond (h k l)	d (A)	Graphite (h k l)	d (A)	Fe (γ) (h k l)	d (A)
1	19.5	2.0982	89					111	2.095
2	21.2	1.9317	64	105	1.930	103	1.9200		
3	22.5	1.8214	86					200	1.8214
4	23.3	1.7597	53	108	1.6650	104	1.7950		
5	26.0	1.5796	14	109	1.5800	106	1.5400		
6	32.6	1.2660	100					220	1.283
7	33.4	1.2365	14	101$\underline{4}$	1.2200	110	1.2280		

Table 4.2: Comparison of the d-spacings of XRD spectrum of the deposited crystal with the actual d-spacings for graphite, diamond and Fe (γ) with sound

Peak no.	2θ	Measure d d (A)	i/i₀	Diamond (h k l)	d (A)	Graphite (h k l)	d (A)	Fe (γ) (h k l)	d (A)
1	19.5	2.0982	92					111	2.095
2	21.2	1.9317	42	105	1.930	103	1.9200		
3	22.5	1.8214	100					200	1.8214
4	23.3	1.7597	83	108	1.6650	104	1.7950		
5	26.0	1.5796	17	109	1.5800	106	1.5400		
6	32.6	1.2660	75					220	1.283
7	33.4	1.2365	21	101$\underline{4}$	1.2200	110	1.2280		

Table 4.3: Comparison of intensity among substrate without coating, coating without sound vibration and coating with sound vibration

Serial no.	1	2	3	4	5	6	7
2Θ	19.5 Fe (γ)	21.2 Diamond /Graphite	22.5 Fe (γ)	23.3 Graphite /Diamond	26.0 Diamond /Graphite	32.6 Fe (γ)	33.4 Graphite /Diamond
Conditions	Intensity (I)						
Substrate without coating	38		16			13	
Substrate with coating without sound vibration	30	12	17	8	3.5	11	4
Substrate with coating with sound vibration	17	9	12	11	5	10	5

CHAPTER 5
CONCLUSIONS

5.1 CONCLUSIONS

The following can be concluded from this study:

1. Deposition rate increases significantly (about 18% higher) under sound vibration condition than that of no sound vibration condition.

2. With the increase of chamber pressure the deposition rate increases. This rate of increase is more at higher pressure.

3. With the increase of activation heater temperature the deposition rate increases. This rate of increase is more at higher temperature.

4. The deposition rate under sonic vibration increases slightly with the frequency of vibration.

5. The deposition rate under ultrasonic vibration increases significantly with the frequency of vibration upto a certain value and after that value, the deposition rate remains almost constant.

6. For a particular frequency of vibration the deposition rate decreases with the distance upto certain value and after that the deposition rate remains almost constant (upto observed distance).

7. Percentage of Diamond/Graphite in the deposited coating increases about 10% with the addition of sound vibration.

8. The surface morphology under SEM analysis of the deposited coatings under sound vibration condition are observed more compact and smoother surface finish than that of without vibration condition.

Therefore by maintaining an appropriate level of frequency of vibration, temperature of the activation heater and pressure of the chamber, deposition rate of Carbon (diamond/graphite) may be maintained to higher value.

5.2 RECOMMENDATIONS FOR THE FUTURE STUDY

This work will lead to a better understanding of the effects of sound vibration on deposition. In the present study, the effects of sound vibration on deposition were investigated. The directions of sound vibration were mainly vertical.

1. The future study can be carried out under multidirectional sound vibration to observe the effect of multidirectional vibration on deposition by maintaining particular amplitude and frequency of vibration at different directions.

2. The effect of amplitude of vibration on deposition can also be investigated.

3. Experiments can be carried out to find out the optimum condition.

4. Similar experiments can also be conducted to observe the effect of above mentioned vibration on different functional properties such as bonding strength, coating thickness, wear resistance, hardness of deposited coating on substrate materials.

References

References

1. Huge, O. Pierson., Handbook of Chemical Vapor Deposition, second edition, Noyes publications, 1999, Norwich, New York, U.S.A.

2. Bunshah, R.F., Handbook of Deposition Technologies for films and Coatings, second edition, Noyes publications, 1994, New Jersey, U.S.A.,.

3. Regel, L.L., and Wilcox, W.R., "Diamond film Deposited by Chemical Vapor Transport," Acta Astronautica, 2001, vol. 48, pp. 129-144.

4. Atul Pant, T. W. F., and Russell, Marylin C. Huff., Department of Chemical Engineering University of Delaware, Newark DE 19716, Roger Aparicio, Robert. W., Birkmire, Institute of Energy Conversion, University of Delaware, Newark, DE 19716, "Hot-Wire Chemical Vapor Deposition of Silicon from Silane: Effect of Process Conditions," Journal of Crystal Growth, 1995, vol. 121, pp. 29-52.

5. Stannowski, B., C, H.M., van der Werf., and R, E.I., Schropp., "Hot-Wire Chemical-Vapour Deposition For Low-Temperature Deposition Of Silicon-NitrideLayers," Proc. of the 3rd Intern. Conf. on Coatings on Glass, Oct 29 - Nov 2, 2000, Maastricht, pp. 387-394.

6. William, N., Shafarman., and Jie, Zhu., "Effect of Substrate Temperature and Deposition Profile on Evaporated Cu(Inga)Se2 Films And Devices," paper reference: 0-624 Institute of Energy Conversion University of Delaware, Newark, DE 19716 USA, 1998.

7. Corata, E. J., and Goodwin, D. G., "Temperature dependence of species concentrations near the substrate during diamond chemical vapor deposition," Journal of Applied Physics, 1993.

8. Mark, C., McMaster, I., Wen, L., Hsuap, Michael. E., Coltrin, B., David, S. Dandy., Ciaran Fox, D., "Dependence of the gas composition in a microwave plasma-assisted diamond chemical vapor deposition reactor on the inlet carbon source: CH, versus & Hz," Diamond and Related Materials 4, 1995, pp. 1000-1008.

9. Yongqing Fu., Chang Q., Sun, Hejun Du., Bibo Yan., "From diamond to crystalline silicon carbonitride: effect of introduction in CH$_4$/H$_2$ gas mixture using MW-PECVD," Surface & coating Technology, 2002, vol. 160, pp. 165-172.

10. Regel, L. L., Wilcox, W. R., "Deposition of Diamond on Graphite and Carbon Felt from Graphite Heated in Hydrogen at Low Pressure," Journal of Materials Science Letters, 2000, vol. 19, pp. 455-457.

11. Weijun, Mohsen., Regel, L.L., Wilcox, W.R., "The Effect of Vertical Vibration of the Ampoule on the Directional Solidification of InSb-GaSb Alloy," Journal of Crystal Growth, 1995, vol. 151, pp. 235-242.

12. Chowa, L., Zhoub, D., Hussainb, A., Kleckleya, S., Zollingera, K., Schultea, A., Wang1, H., "Chemical vapor deposition of novel carbon materials," Thin Solid Films, 2000, vol. 368, pp. 193-197.

13. David S., Michael E., "Relationship between Diamond growth rate and Hydrocarbon Injector Location in Direct-Current arcjet Reactors," Applied Physics Letter, 1995, vol. 66 (3), pp. 391-393.

14. Sushil Kumar., Dixit, P. N., "High rate deposition of diamond like carbon films by very high frequency plasma enhanced chemical vapor deposition at 100 MHz," Journal of Applied Physics, 2003, vol. 93, pp. 6361-6369.

15. Severdenko, V. P., Labunov, V. A., Leshchenko, I. N., Danilovich, N. I., "Effect of Ultrasonic Vibrations on the Formation and Structure of Thin Films Produced by Thermal Vaporization in Vacuo," Prochn.-Plast. Mater. Ul'trazvuk. Pole, Tezisy Dokl. Nauchno-Tekh. Konf, 1973; vol. 2, pp. 60-62.

16. Yeo, S. H., Choo J. H., and Sim K. H. A., "On the effects of ultrasonic vibrations on localized electrochemical deposition," J. Micromech. Microeng, 2002, vol. 12, pp. 271-279.

17. Tadeusz, Burakowski., & Tadensz, Wierzchon., Surface Engineering of Metal, CRC Press, 2000, New York, USA.

18. Bhushan, B., and Gupta, B. K., Handbook of Tribology, Mcgraw Hill, 1991, New York.

19. Helali, M.M., "Spray Forming of Thin Walled Net-Shaped Components of Hard Materials by High Velocity Oxy-Fuel Thermal Spraying Process," Ph. D. Thesis, 1994, Dublin City University, Uk.

20. Burakowski, T., Rolinski, E., and Wierzchon, T., "Metal Surface Engineering," Warsaw University of Technology Publications, Warsaw, 1992.

21. Joint Report, "Engineering Manual: Heat Treatment of Ferrous Alloys," WNT, Warsaw, 1977.

22. Janowski, S., "Changes in Residual Stress State in Elements with Hardened Superficial Layers, as a result of Subsequent Heat Treatment," Metallurgy, Heat Treatment, Surface Engineering, No. 99-100, 1989, pp. 54-58.

23. Janowski, S., "Effect of Residual Stresses on Mechanical Properties of Structural Steels," Metallurgy, Heat Treatment, Surface Engineering, No. 79, 1986, pp. 6-12.

24. Svecev, V. D., "Measurement of Residual Stresses in Investigations Carried Out on the SMC-2 Friction Machine," Zavodskaya Laboratoria, No. 4, 1977, pp. 500-502.

25. Rehbinder, P. A., and Liktman, V. I., "Effect of Surface Active Media on Strains and rupture in Solids," Proceeding of second international congress on surface activity, London, 1957, vol. 3, pp. 563-580.

26. Przybylowicz, K., "Diffusion in Surface Treatments," Proceedings: Summer School on Surface Engineering, Kielce, 6-9 September, 1993, pp. 31-40.

27. Wesolowski, K., "Metallurgy," PWT, Warsaw, 1982.

28. Dobrzanski, L. A., "Metallurgy and Heat Treatment of Metal Alloys," Silesian Technical University Publications, Gliwice, 1993.

29. Jarzebski, Z., "Diffusion in Metals," Publ. Slask Katowice, 1975.

30. Przybylowicz, K., "Theoretical Metallurgy," 5th Edition, Mining Academy, Krakow, 1985.

31. Collection of Lectures: Summer School on Diffusion in Solids, Krakow-Mogilany, Published by the Mining Academy Publications, no 113, 1985.

32. Joint Report, "Metallurgy," Publ. Slask, Katowice, 1979.

33. Rudnik, S., "Metallurgy," PWN, Warsaw, 1980.

34. Wesolowski, K., "Metallurgy and Heat treatment," WNT, Warsaw, 1972.

35. Halling, J., "Introduction, Recent Development in Surface Coating and Modification processes," MEP, London, 1985.

36. Rickerby, D. S., and Matthews, A., Advance Surface Coating: A Handbook of Surface Engineering. Blakie and Son Ltd, London. 1991.

37. Bunshah, R.F., Handbook of Deposition Technologies for films and Coatings, Noyes publications, 1982, New Jersey, U.S.A.

38. Sundgren, J. E., and Hentzril, T. G., "A Review of Present State of art in Hard Coatings Grown from the Vapour Phase," J.Vac. Sci. Technol., 1986.

39. Kola etal., "Magnetron Sputtering of TiN protective Coatings," Proc. Of the Int. Conf. on Advances in Materials and Processing Technologies. 1993. pp 1323-1332.

40. Nakahara, S., "Microporosity Induced by Nucleation and Growth Process in Crystalline and Non-Crystalline Films," Thin Solid Films, 1993, Vol-45, pp 421-432.

41. Kawan etal., "Study on Elastic Contact and Residual Stress Measurements During Ceramic Coatings," Proc. Third National Thermal Spray Conf. Long Beach, CA, 1990, pp. 339-342.

42. Pan, A., and Green, J. E., "Residual Compressive Stress in Sputter Deposited TiC films on steel Substrate," Thin Solid Films, 1994, vol-78, pp 25-34.

43. Spear, K. E., "Thermochemical Modeling of Steady-State CVD Process," Proc. 9th. Int. Conf. on CVD, (M. Robinson, et al., eds.), Electrochem. Soc., Pennington, NJ 08534, 1984, pp. 81-97.

44. Sherman, A., Chemical Vapor Deposition for electronics, Noyes Publications, Park Ridge, NJ , 1987.

45. Stinton, D. P., Bessman, T. M., and Lowden, R., "Advanced Ceramics by Chemical Vapor Deposition Techniques," Cer. Bul., 1988, vol. 67(2), pp. 350-355.

46. Thorpe, M., "Plasma Energy, The Ultimate of Heat Transfer," Chem. Eng. Progress, July 1989, pp. 43-53.

47. Bachmann, P. K., Gartner, G., and Lydtin, H., "Plasma-Assisted Chemical Vapor Deposition," MRS Bulletin, Dec. 1988, pp. 52-59.

48. "Pyro-tech PT-101," Technical Brochure, Ultra Carbon Corp., Bay City, MI 48707, 1991.

49. Beavan, A., "LTI Pyrolytic Carbon," Material Engineering, Feb. 1990, pp 39-41.

50. "Graphite, Refractory Material," Bulletin from LeCarbone-Lorraine, Gennevilliers, France 92231. 1999.

51. "Products for the Semiconductor Industry," Bulletin from Ringsdorff, D-5300 Bonn-2, Germany, 1988.

52. Lucas, P., and Marchand, A., "Pyrolytic Carbon Deposition from Methane," Carbon, 1990, vol. 28(1), pp. 207-219.

53. Pierson, H. O., and Lieberman, M. L., "The Chemical Vapor Deposition of Carbon on Carbon Fibres," Carbon, 1975, vol. 13, pp. 159-166.

54. Guy, A. G., Elements of Physical Metallurgy, Addition-Wesley Publishing, Reading, MA, 1959.

55. Cullity, B. D., Elements of X-Ray Diffraction, Addition-Wesley Publishing, Reading, MA, 1956.

56. Pierson, H. O., Handbook of Carbon, Graphite, Diamond and Fullerenes, Noyes Publications, Park ridge, NJ, 1993.

57. "Norton CVD Diamond" Technical Bulletin from Norton Co., Northboro, MA, 1992.

58. "Diamond Coating, A World of Opportunity," Technical Brochure, Genasystems Inc., Worthington, OH, 1991.

59. Graebner, J. E., and Herb, J. A., "Dominance of Intrinsic Photon Scattering in CVD Diamond," Diamond Films and Technology, MY Tokyo, 1992, vol. 1(3), pp. 155-164.

60. Yasuda, T., Ihara, M., Miyamoto, K., Genchi, Y., and Komiyama, H., "Gas Phase Chemistry Determining the Quality of CVD Diamond," Proc. 11th. Conf. on CVD, (K. Spear and G. Gullen, eds.), 1990, pp. 134-140, Electrochem. Soc., Pennington, NJ.

61. Hsu, W. L., "Chemical Erosion of Graphite by Hydrogen Impact: A summary of Database Relevant to Diamond Film Growth," J. Vac. Sci. Technol. A, May/June 1988, vol. (6)3, pp. 1811.

62. Patterson, D. E., et al., "Thermochemical Vapor Deposition of Diamond in a Carbon-Halogen-Oxygen and/or Sulfur Atmospheric Hot-Wall Reactor," in Application of Diamond Films and Related Materials, (Y. Tzeng, et al., eds.), Elsevier Science Publishers, 1991, pp. 569-576.

63. Schafer, L., Sattler, M., and Klages, C. P., "Upscaling of the Hot-Filament CVD Process for deposition of Diamond Films on Large Area Substrate," in Applications of Diamond Films and Related Materials, (Y. Tzeng, et al., eds.), Elsevier Science Publishers, 1991, pp. 453-460.

64. Aisenberg, S., and Kimock, F. M., "Ion Beam and Ion-assisted Deposition of Diamond-Like Carbon Films," Materials Science Forum, Transtech publications, Switzerland ,1989, vol. 52,53, pp. 1-40

65. Grill, A., Patel, V., and Meyerson, B. S., "Applications of Diamond-Like Carbon in Computer Technology," in Application of Diamond Films and Related Materials, (Y. Tzeng, et al., eds.), Elsevier Science Publishers, 1991, pp. 683-689.

66. Ishaq, M., Talukder, N., Physics, Ideal Library, Bangladesh, 2005.

67. Subramanyam, N., A Textbook of Physics, Third Edition, Vikas Publishing Ltd., India, 2005.

68. Sears, F. W., Mechanics, Heat, and Sound, Addision-Wesley Publishing Company, pp 485-558, USA, 1958.

69. Ghosh, M., A Textbook of Sound, S. Chand & Company Ltd., India, 1996.

70. Bhushan, Bharat., Principles and Applications of Tribology, A Wiley-Interscience Publication, New York, 1999.

71. Oscik, J., Adsorption, PWN, Warsaw, E. Horwood Lim., Chichester 1982.

72. Tompkins, F.C., Chemisorption of Gases on Metals, PWN, Warsaw 1985.

73. Joint Report, Physical Chemistry, 2nd Edition, PWN, Warsaw 1965

74. Mrowec, S., "Selected Topics from the Chemistry of Defects and Theory of Diffusion in the Solid State", Geological publication, Warsaw, 1974.

75. Joint Report, "Warmebehandlung der Bau- und Werkzeuugstahle", BAZ Buchverlag Basel, 1978.

76. Paul, W. M., "CVD Diamond-a New Technology for the Future," Endeavour Magazine, 1995, vol. 19(3), pp.101-106.

77. Chow, L., Zhoub, D., Hussain, A., Kleckleya, S., Zollinger, K., Schulte, A., and Wang, H., "Chemical Vapor Deposition of Novel Carbon Materials," Thin Solid Films, 2000, vol. 368, pp. 193-197.

78. Fox, N. A., Youh, M. J., Steeds, J. W., and Wang, W. N., "Patterned Diamond Particle Films," Journal Of Applied Physics, 2000, vol. 87, pp. 8187-8192.

79. Paul, W. M., "Diamond thin films: a 21st-century material," Phil. Trans. R. Soc. Lond., 2000, vol. 358, pp. 473-495.

80. Goodwin, D. G., "Scaling Laws for Diamond Chemical-Vapor Deposition. IL Atomic Hydrogen Transport" J. Appl. Phys., 1993, vol.74(11), pp. 6895-6906.

81. Status and Applications of Diamond and Diamond-Like Materials: An Emerging Technology, 1990, Report of the Committee on Superhard Materials, National Materials Advisory Board, Commision on Engineering and Technical systems, National Research Council, National Acdemy of Science, USA.

82. Morshed, M. M., "Stress and Adhesion in DLC Coatings on 316L Stainless Steel Deposited by a Neutral Beam Source, " Ph. D thesis, National Centre for Plasma Science and Technology, Dublin City University, Glasevin, Dublin 9, Ireland, 2003.

APPENDIX-A

EXPERIMENTAL DATA SHEET

Sl. no.	S.V. kHz	Gap (mm)	Temp. (Subs.) ^{0}C	Temp. (Acti.) ^{0}C	Vacu. Torr	Depo. Durati. (Min.)	Initial Wt. (gm)	Final Wt (gm)	Wt Diff. (gm)	% deposition	Deposition rate gm/m²/hr
18	40	4	900	2000	25	10	3.1410	3.1430	.002	.0637	0.347
19	50	4	900	2000	25	10	3.1059	3.1081	.0022	.0708	0.386
20	70	4	900	2000	25	10	3,0634	3.0664	.003	.0979	0.534
21	90	4	900	2000	25	10	3.133	3.1370	.004	.1277	0.696
22	110	4	900	2000	25	10	3.110	3.1150	.005	.1608	0.877
23	6	5	900	2000	25	3	2.905	2.906	.001	.0344	0.188
24	8	5.6	900	2000	25	10	3.003	3.006	.003	.0999	0.545
25	13.5	5.6	900	2000	25	10	2.999	3.0004	.00143	.047	0.260
26	40	5.6	900	2000	25	10	2.969	2.9705	.0015	.05	0.276
27	60	5.6	900	2000	25	10	2.912	2.9138	.0018	.062	0.337
28	90	5.6	900	2000	25	10	2.981	2.9825	.0015	.05	0.274
29	00	5.6	900	2000	25	10	2.9760	2.9767	.0008	.027	0.146
30	110	5.6	900	2000	25	10	3.051	3.0526	.0016	.052	0.286
31	90	3.3	900	2000	25	10	3.0354	3.0383	.0029	.0955	0.52
32	90	8.05	900	2000	25	10	3.0135	3.0150	.0015	.0498	0.272
33	00	8.02	900	2000	25	10	3.0636	3.0644	.0008	.026	0.142
37	90	4.8	900	2000	25	10	2.8449	2.8479	.003	.1054	0.575
38	00	5	900	2000	25	10	2.9560	2.9570	.001	.035	0.184

39	30	5	900	2000	30	10	3.1628	3.1688	.006	.19	0.01
40	40	5	900	1100	25	10	2.9611	2.9615	.0004	.0135	0.0737
41	6	5	900	2000	25	10	2.9253	2.9267	.0014	.048	0.26
42	18	5	900	2000	25	10	2.9213	2.9227	.00139	.047	0.259
43	00	5	900	2000	30	10	2.9222	2.9254	.0032	.11	0.597
44	40	8	900	2000	25	10	2.9254	2.9268	.0014	.048	0.26.
45	00	4	900	2000	25	10	2.9234	2.9245	.0011	.039	0.2
46	50	5.6	900	2000	25	10	2.9258	2.9274	.0016	.055	0.298
47	70	5.6	900	2000	25	10	2.9211	2.9226	.0015	.053	0.28
48	30	5	900	2000	27	10	2.9290	2.9320	.003	.104	0.558
49	00	5	900	2000	27	10	2.9240	2.9257	.0017	.058	0.317
50	40	5	900	1500	25	10	2.9251	2.9260	.0009	.031	0.168
51	00	5	900	1500	25	10	2.9270	2.9276	.0006	.021	0.112
52	00	5	900	1100	25	10	2.9289	2.9291	.0002	.0087	0.0372
53	70	8	1000	2000	25	10	3.0620	3.0635	.0015	.049	0.26
54	90	4.7	1000	2000	25	10	3.0250	3.0277	.0027	.091	0.48
55	00	4.7	1000	2000	25	10	2.9360	2.9370	.001	.033	0.18
56	40	4.7	1000	2000	25	10	2.9400	2.9417	.0017	.058	0.31
57	70	4.7	1000	2000	25	10	2.9354	2.9376	.0022	.074	0.40
58	00	5	1000	2000	28.5	10	3.0146	3.0166	.002	.0849	0.45
59	30	5	1000	2000	28.5	10	2.9501	2.9544	.0043	.147	0.79
60	00	5	1000	2000	25	4	3.1006	3.1015	.0009	.028	0.16
61	6	5	1000	2000	25	6	2.9434	2.9445	.0011	.038	0.20

b

62	00	5	1000	2000	25	6	2.9378	2.9387	.0009	.031	0.17
63	6	5	1000	2000	25	7	2.9469	2.9481	.0012	.0412	0.22
64	00	5	1000	2000	25	7	3.0146	3.0156	.001	.033	0.18
65	6	5	1000	2000	25	9	2.9506	2.9519	.0013	.045	0.24
66	00	5	1000	2000	25	9	2.9424	2.9434	.001	.034	0.18
67	40	5	1000	1275	25	10	2.9506	2.9512	.0006	.022	0.11
68	00	5	1000	1275	25	10	3.0286	3.0290	.0004	.015	0.07
69	40	5	1000	1700	25	10	2.9506	2.9518	.0012	.041	0.22
70	00	5	1000	1700	25	10	3.0286	3.0294	.0008	.028	0.14
71	40	5	1000	2000	25	10	2.9306	2.9320	.0014	.048	0.26

APPENDIX-B

Publication on this Study

(1) Karim, S. M. I., Helali, M.M., "Effect of Sound Vibration on Vapor Deposited Coating," Thin Solid Film (under review)

Table A1 : Reactor designs and typical production applications [1].

Coating Type	Application	Reactor Type	Pressure
BPSG (boro-phopho-silicate glass)	passivation of semiconductors	cold wall	ca. 1 Torr
Silicon epitaxy	semiconductors	cold wall	80 Torr to 1 atm
SiO_2	passivation of semiconductors	cold wall	1 atm
TiC, TiN, Ti(CN)	cutting tools	hot wall	1 Torr
Doped silicon	semiconductors	hot wall	1 Torr
TiO_2	solar cells	cold wall	1 atm
Tungsten silicide	gates & inter-connections of semiconductors	cold wall	1 Torr

Table A2 : Properties of CVD graphite at 25^0 C [48]-[51].

Crystalline form: hexagonal
Lattice parameters: $a_o = 0.246$ nm, $c_o = 0.671$ nm
Color: Black
Sublimation point at 1 atm (estimated): 4000 K
Density, g/cm^3: 2.10–2.24

Flexural strength (c direction) , MPa: 80–170
Tensile strength (ab direction), MPa: 110
Young's modulus of elasticity, GPa: 28–31

Thermal conductivity, W/m•K:
        c direction: 1–3
        ab directions: 190–390
Thermal expansion 0-100°C, mx10^{-6}/m•K:
        c direction: 15–25
        ab direction: -1 to 1
Electrical resistivity, $\mu\Omega$m: c direction: 1000–3000
        ab directions: 4–5

Table A3 : Properties of single-crystal and CVD diamond [56]-[59].

	CVD Diamond	Single-Crystal Diamond
Density, g/cm^3	3.51	3.515
Specific heat, C_p, J/mol (at 300K)	6.195	6.195
Thermal conductivity at 25°C, W/m·K	2100	2200
Thermal expansion (10^{-6}/°C @ 25–200°C)	2.0	1.5–4.8
Index of refraction at 10 μm	2.34–2.42	2.40
Bandgap, eV	5.45	5.45
Electrical resistivity, ohm·cm	10^{12}–10^{16}	10^{16}
Dielectric constant (45 MHz–20 GHz)	5.6	5.70
Dielectric strength, V/cm	10^6	10^6
Loss tangent (45 MHz–20 GHz)	<0.0001	
Saturated electron velocity	2.7	2.7
Carrier mobilities (cm^2/V·s)		
electron (n)	1350–1500	2200
positive hole (p)	480	1600
Young's modulus, GPa	910–1250	1250
Compression strength, GPa	8.68–16.53	16
Vickers hardness range,* GPa	50–100	57–100
Coefficient of friction	0.05–0.15	0.05–0.15

*Varies with crystal orientation